Tampere University

STEFAN SÖDERHOLM

Methods for Improving Performance in Consumer Grade GNSS Receivers

Tampere University Dissertations 863

Tampere University Dissertations 863

STEFAN SÖDERHOLM

Methods for Improving Performance in Consumer Grade GNSS Receivers

ACADEMIC DISSERTATION
To be presented, with the permission of
the Faculty of Information Technology and Communication Sciences
of Tampere University,
for public discussion in the Lecture Room TB109
of the Tietotalo, Korkeakoulunkatu, Tampere,
on 13 October 2023, at 12 o'clock.

ACADEMIC DISSERTATION
Tampere University, Faculty of Information Technology and Communication Sciences
Finland

Responsible supervisor and Custos	Professor Jari Nurmi Tampere University Finland	
Pre-examiners	Doctor Anna Jensen AJ Geomatics Denmark	Professor Fabio Dovis Politecnico di Torino Italy
Opponents	Doctor Anna Jensen AJ Geomatics Denmark	Professor Emeritus Terry Moore University of Nottingham United Kingdom

The originality of this thesis has been checked using the Turnitin OriginalityCheck service.

Cover design: Roihu Inc.

ISBN 978-952-03-3059-0 (print)
ISBN 978-952-03-3060-6 (pdf)
ISSN 2489-9860 (print)
ISSN 2490-0028 (pdf)
http://urn.fi/URN:ISBN:978-952-03-3060-6

Carbon dioxide emissions from printing Tampere University dissertations have been compensated.

PunaMusta Oy – Yliopistopaino
Joensuu 2023

I would like to dedicate this thesis to a person that has supported me the whole of my life, never pushed me into doing something I did not choose myself, and always been nothing but proud of my achievements. During my 20 years of writing this she was so looking forward to seeing me graduate. It is my biggest regret that I could not give that to you, my mother, but I hope you are watching from somewhere.

ACKNOWLEDGEMENTS

Personally, I would first like to express my gratitude to my wife Ulrika, who has suffered the consequences of me writing on this thesis for almost 20 years and several other theses before that. This would obviously not have been possible without your support, and I promise I will not write any more theses.

Professionally first and foremost I would like to express my sincere gratitude to Professor Jari Nurmi from Tampere University, you supported me in finally getting this done without pushing me too hard when I had not progressed as planned and allowing me to do things my way (which probably not always was the best way).

I would also like to give a special thank you to Heidi Kuusniemi who convinced me to join FGI many years ago and pick up my PhD work again after a long break and supported me in any way possible during my years at Finnish Geospatial Research Institute (FGI). Sorry we could not finish this work already then.

For the support of my research and publications at the FGI I would like to thank my colleagues and co-publishers in the SARANA group: Zahid, Sarang, Laura, Martti and Salomon. I also want to mention Hannu and Sonja from the Geodesy department for their support in my RTK and PPP work. Hannu always had his door open and always made time for my questions.

I would also like to thank the great team we had at Fastrax that made it possible to publish next to developing the world's first GPS watch and GPS enabled mobile phone. Timo, Kim, Hanna and Heidi as my co-authors of course, but also everyone else at Fastrax. A special thank you here goes to Timo, whom I have had the privilege to work with for more than 15 years and still counting.

Finally, I would like to extend my gratitude to the team at CGI, Netherlands, for the joint work in the two General Support Technology Programme (GSTP) projects we had together. A special thanks to Axel who always had the right questions to challenge me and Timo at FGI.

ABSTRACT

For the last three decades, satellite navigation has evolved from being a technology for professional and military users to a technology available for everyone. Especially during the last 15 years, since the receivers started getting smaller and cheaper, there has been an increasing number of companies delivering Global Positioning System (GPS) enabled devices for hundreds of different kind of applications. Typical for any modern technology, there has also been an enormous amount of money spent on research and accompanied receiver development resulting in an immense increase in receiver performance.

In addition to the development efforts on GPS receivers the introduction of new global navigation satellite systems such as the Russian Globalnaja Navigatsionnaja Sputnikovaja Sistema (GLONASS), the Chinese BeiDou, and the European Galileo systems offers even more opportunities for improved performance. Both GPS and these new systems have also introduced new types of signal structures that can provide better quality observations and even further improve the performance of all receivers.

Finally, methods like Precise Point Positioning (PPP) and Real Time Kinematic (RTK) that earlier were reserved for professional users have entered into the consumer market enabling never before seen performance for every user of satellite navigation receivers.

This thesis will assess the impact of this development on both performance as well as on receiver architecture.

The design of the software defined receiver developed at FGI, the FGI-GSRx, is presented in detail in this thesis. This receiver has then been used to assess the impact of using multiple constellations as well as new novel signal processing methods for modern signals. To evaluate the impact of PPP and RTK methods the FinnRef Continuously Operating Reference Station (CORS) network has been used together with several different types of receivers including consumer grade off the shelf re-

ceivers.

The results show that when using more constellations and signals the accuracy of the positioning solution improves from 3 meters to 1.4 meters in open sky conditions and by more than a factor 10 in severe urban canyons. For severe urban canyons the available also increases by a factor 2 when using three constellations. When using new modern modulation techniques like high order BOC results show an accuracy improvement for a Galileo solution of almost 25 % and the presented new signal processing method increase the availability of such an accuracy from 50 % to almost 100 %. Finally, results from precise point positioning methods show that an accuracy of 15 cm is achievable, which is a significant improvement compared to an accuracy of 1.4 m for a standalone multi constellation solution.

To achieve these improvements, it is essential that the receiver itself is adapted to make use of these new signals and constellations. This means that the design of modern consumer market receivers is challenging and in many cases a software defined receiver would be a better and cheaper choice than developing new Application Specific Integrated Circuit (ASIC)'s.

TIIVISTELMÄ

Viimeisten kolmen vuosikymmenen aikana satelliittinavigointi on kehittynyt ammatti- ja sotilaskäyttäjien tekniikasta kaikkien saatavilla olevaksi tekniikaksi. Varsinkin viimeisen 15 vuoden aikana, kun vastaanottimet alkoivat pienentyä ja halpenivat, on lisääntynyt määrä yrityksiä, jotka toimittavat GPS-laitteita satoihin erilaisiin sovelluksiin. Kaikille moderneille tekniikoille on myös tyypillistä, että tutkimukseen ja siihen liittyvään vastaanottimien kehittämiseen on käytetty valtavasti rahaa, mikä on johtanut huomattavaan parantumiseen vastaanottimen suorituskyvyssä.

GPS-vastaanottimien kehitystyön lisäksi uusien maailmanlaajuisten satelliittinavigointijärjestelmien, kuten venäläisen GLONASS, kiinalaisen BeiDou- ja eurooppalaisen Galileo-järjestelmien käyttöönotto tarjoaa entistä enemmän mahdollisuuksia suorituskyvyn parantamiseen. Sekä GPS että nämä uudet järjestelmät ovat myös ottaneet käyttöön uudentyyppisiä signaalirakenteita, jotka voivat tarjota parempilaatuisia havaintoja ja siten parantaa kaikkien vastaanottimien suorituskykyä.

Lopuksi menetelmät, kuten PPP ja RTK, jotka aiemmin olivat varattu ammattikäyttäjille, ovat tulleet kuluttajamarkkinoille mahdollistaen ennennäkemättömän suorituskyvyn jokaiselle satelliittinavigointivastaanottimien käyttäjälle.

Tässä opinnäytetyössä arvioidaan tämän kehityksen vaikutusta sekä suorituskykyyn että vastaanottimen arkkitehtuuriin.

Työssä esitellään yksityiskohtaisesti FGI:ssä kehitetyn ohjelmistopohjaisen vastaanottimen, FGI-GSRx:n. Tämän vastaanottimen avulla on työssä arvioitu miten sekä uudet konstellaatiot että uudet nykyaikaiset signaalit ja niitten seurantamenetelmät vaikuttavat suorituskykyyn ja vastaanotin arkitehtuuriin. Tämän lisäki on arvioitu PPP- ja RTK-tarkkuuspaikannusmenetelmien vaikutus FinnRef CORS-verkkoa käyttäen useiden erityyppisten vastaanottimien kanssa, mukaan lukien kuluttajalaatuiset vastaanottimet.

Tulokset osoittavat, että enemmän konstellaatioita ja signaaleja käytettäessä paikannusratkaisun tarkkuus paranee 3 metristä 1,4 metriin hyvissä olosuhteissa ja yli 10-

kertaiseksi tiheästi rakennetuissa kaupungeissa, jossa käytettävissä olevien signaalien määrä kasvaa kertoimella 2 käytettäessä kolmea konstellaatiota. Uusia moderneja modulaatiotekniikoita, kuten BOC-modulaatiota, käytettäessä tulokset osoittavat Galileo-ratkaisun tarkkuuden paranevan lähes 25%:lla ja esitelty uusi signaalinkäsittelymenetelmä lisää tällaisen tarkkuuden saatavuutta 50%:sta lähes 100%:iin. Lopuksi tarkkuuspaikannusmenetelmien tulokset osoittavat, että 15 cm:n tarkkuus on saavutettavissa, mikä on merkittävä parannus verrattuna 1,4 metrin tarkkuuteen.

Näiden parannusten saavuttamiseksi on olennaista, että itse vastaanotin on mukautettu hyödyntämään näitä uusia signaaleja ja konstellaatioita. Tämä tarkoittaa, että nykyaikaisten kuluttajamarkkinoiden vastaanottimien suunnittelu on haastavaa ja monissa tapauksissa ohjelmistopohjainen vastaanotin olisi parempi ja halvempi valinta kuin uusien mikropiirien kehittäminen.

ABSTRAKT

Under de senaste tre decennierna har satellitnavigeringen utvecklats från att vara en teknik för professionella och militära användare till en teknik som är tillgänglig för alla. Speciellt under de senaste 15 åren, sedan mottagarna började bli mindre och billigare, har det uppstått ett ökande antal företag som levererar GPS-aktiverade enheter för hundratals olika typer av applikationer. Typiskt som det är för all modern teknik, har det också investerats en enorm mängd pengar på forskning och åtföljande produktutveckling, vilket resulterat i en enorm ökning av mottagarens prestanda.

Utöver utvecklingsinsatserna för GPS-mottagare erbjuder introduktionen av nya globala satellitnavigeringssystem såsom ryska GLONASS, kinesiska BeiDou och de europeiska Galileo-systemen ännu fler möjligheter till förbättrad prestanda. Både GPS och dessa nya system har också introducerat nya typer av signalstrukturer som kan ge observationer av bättre kvalitet och förbättra prestandan för alla mottagare.

Slutligen har precision navigerings metoder som PPP och RTK, som tidigare var reserverade för professionella användare, introducerats på konsumentmarknaden och möjliggjort aldrig tidigare skådad prestanda för varje användare av satellitnavigeringsmottagare.

Detta examensarbete kommer att bedöma effekten av denna utveckling på både mottagarens prestanda och dess interna arkitektur.

Designen av en mjukvarumottagare utvecklad vid FGI, FGI-GSRx, presenteras i detalj i denna avhandling. Denna mottagare har sedan använts för att bedöma effekten av att använda flera konstellationer såväl som nya signalbehandlingsmetoder för moderna signaler. För att utvärdera effekten av PPP- och RTK-metoder har FinnRef CORS-nätverket använts tillsammans med flera olika typer av mottagare, inklusive mottagare för vanliga konsumenter.

Resultaten visar att när man använder fler konstellationer och signaler förbättras positioneringslösningens noggrannhet från 3 meter till 1,4 meter under öppen himmel och med mer än en faktor 10 i svåra urbana miljöer. I urbana miljöer ökar också

tillgången av signaler med en faktor 2 när man använder tre konstellationer istället för bara GPS. Vid användning av nya moderna tekniker som BOC modulering visar resultaten en noggrannhetsförbättring för en Galileo-lösning på nästan 25 % och den presenterade nya signalbehandlingsmetoden ökar tillgängligheten för en sådan noggrannhet från 50 % till nästan 100 %. Slutligen visar resultat med precision navigerings metoder att en noggrannhet på 15 cm kan uppnås, vilket är en betydande förbättring jämfört med en noggrannhet på 1,4 m för den fristående lösningen.

För att uppnå dessa förbättringar är det väsentligt att själva mottagaren är anpassad för att använda dessa nya signaler och konstellationer. Detta innebär att arkitekturen av moderna konsumentmottagare blir komplicerad och i många fall skulle en mjukvarumottagare vara ett bättre och billigare val än att utveckla nya integrerade kretsar.

CONTENTS

List of Tables

SYMBOLS

A	Signal amplitude
A_{LO}	Signal amplitude of locally generated signal
BW	Bandwidth
B_c^{rx}	Receiver code bias
B_c^{sv}	Satellite code bias
B_p^{rx}	Receiver phase bias
B_p^{sv}	Satellite phase bias
C/N_0	Carrier to noise
DD_i	Double difference observation
D_{Code},D_{Freq},D_{Phase}	Code, frequency and phase discriminators
E_i	Sum of errors for observation i
Ele	Elevation angle of the satellite
G	Gain
I	Ionospheric delay
IF_{Nom}	Nominal IF frequency
I_E, I_L, I_P	Early, Late and prompt fingers for in-phase signal
I_f	Ionospheric delay for frequency f
K	TCXO multiplier in RF front end
L	Local displacement errors
M_c	Code multipath error
M_p	Carrier Phase multipath error

N_0	Noise power for one Hz bandwidth
N_B	BOC order
N_T	Thermal noise
O_{rx}	Antenna offset for receiver
O_{sv}	Antenna offset for satellite
P_0	Surface pressure in hPa
P_E, P_L	Power for early and late fingers
P_S	Signal power
Q_E,Q_L, Q_P	Early, Late and prompt fingers for quadrature phase signal
R_i	True range to satellite i
S	Signal
T	Length of any period
T_{chip}	Length of one code chip
T_{epoch}	Length of one code epoch
Tr	Tropospheric delay
$\Delta X, \Delta Y, \Delta Z$	Local vector between base station and user receiver
Δf^{L1}	Frequency step for GLONASS L1 channels
Δf^{L2}	Frequency step for GLONASS L2 channels
Δf_i	Doppler shift for satellite i
Δt_{rx}	Receiver clock offset
Δt_{rx}^{B}	Receiver clock offset in Beidou time domain
Δt_{rx}^{E}	Receiver clock offset in Galileo time domain
Δt_{rx}^{G}	Receiver clock offset in GPS time domain
Δt_{sv}	Satellite clock error
Δt_{sv}^{Rel}	Relativistic clock error
$\Delta x, \Delta y, \Delta z$	Change in user position
Λ	Electron density

ϵ_c	Receiver code noise
ϵ_p	Receiver phase noise
λ	Carrier signal wavelength
$\mathbf{A}$	Design matrix
$\mathbf{W}$	Observation weight matrix
$\hat{\mathbf{e}}$	Residual vector
$\hat{\mathbf{x}}$	State vector that minimizes the residuals
$\mathbf{b}$	Observation vector
$\mathbf{t_{rx}}$	Receiver time vector
$\mathbf{x}$	State vector
μ	Earth universal gravitational constant
ω	Phase windup delay
ϕ	Ellipsoidal latitude
ρ^N	Pseudo range at epoch N
ρ_c	Code pseudo range
ρ_i	Pseudo range for satellite i
ρ_i^k	Pseudo range for satellite i and system k
ρ_p	Carrier phase pseudo range
ρ_s^N	Smoothed pseudo range at epoch N
ρ_{BS}^i	Pseudo range measured at base station for satellite i
ρ_{BS}^{ref}	Pseudo range measured at base station for reference satellite
ρ_U^i	Pseudo range measured at user receiver for satellite i
ρ_U^{ref}	Pseudo range measured at user receiver for reference satellite
σ^2	Observation variance
c	Speed of light
f	Frequency
f_0^{L1}	Center frequency for GLONASS L1

f_0^{L2}	Center frequency for GLONASS L2
f_c	Code frequency
f_i	Measured frequency or satellite i
f_k^{L1}	Frequency of GLONASS L1 channel k
f_k^{L2}	Frequency of GLONASS L2 channel k
f_{LO}	Locally generated frequency in RF front end
f_{sc}	Sub carrier frequency / frequency of the modulation
f_{tcxo}	TCXO frequency
h	Height in km
k	Boltzmans constant
t	Time
t_{rx}^B	Receiver time in Beidou time domain
t_{rx}^E	Receiver time in Galileo time domain
t_{rx}^G	Receiver time in GPS time domain
t_{rx}^{true}	True receiver time vector
t_{sv}	Transmission time
t_{sv}^N	Transmission time for satellite N
t_{sv}^i	Transmission time for satellite i
toc	Reference time for clock model in the navigation data
tow	Time of week number from navigation data stream
v_{rx}	Receiver velocity
v_{sv}	Satellite velocity
x, y, z	Unknown user coordinates
x_0, y_0, z_0	Last known user coordinates
x_i, y_i, z_i	Satellite coordinates for satellite i

ORIGINAL PUBLICATIONS

Publication I S. Söderholm, T. Jokitalo, K. Kaisti, H. Kuusniemi and H. Naukkarinen. Smart positioning with Fastrax's software GPS receiver solution. *Proceedings of the 21st International Technical Meeting of the Satellite Division of The Institute of Navigation*. 2008, 1193–1200.

Publication II S. Söderholm, M. Z. H. Bhuiyan, S. Thombre, L. Ruotsalainen and H. Kuusniemi. A multi-GNSS software-defined receiver: design, implementation, and performance benefits. *Annals of Telecommunications* 71 (2016), 399–410.

Publication III M. Z. H. Bhuiyan, S. Söderholm, S. T. L. Ruotsalainen and H. Kuusniemi. Overcoming the challenges of BeiDou receiver implementation. *Sensors* 14 (2014), 22082–22098.

Publication IV S. Thombre, S. Söderholm, M. Z. H. Bhuiyan and M. Kirkko-Jaakkola. Investigating the Indian regional navigation satellite system using a software multi-GNSS receiver in Europe. *Proceedings of 2015 European Navigation Conference*. 2015, 22082–22098.

Publication V S. Söderholm, J. Nurmi, A. Berg and H. Kuusniemi. Optimal Signal processing of the Galileo PRS Signal In a Snapshot Receiver. *IEEE Sensors Journal* (2023). Submitted.

Publication VI M. Kirkko-Jaakkola, S. Söderholm, S. Honkala, H. Koivula and S. Nyberg. Low-cost precise positioning using a national GNSS network. *Proceedings of the 28th International Technical Meeting of the Satellite Division of The Institute of Navigation*. 2015, 2570–2577.

Publication VII S. Söderholm, H. Koivula, H. Kuusniemi, S. Lahtinen and M. Kirkko-Jaakkola. Performance assessment of single frequency Precise Point Positioning using the SSR model from the Finnish National GNSS Network. *European Journal of Navigation* 14 (2016), 39–40.

Author's contribution

This chapter summarizes the publications that are a part of this thesis. A short description of each publication is given together with a description of the author's contribution to the publication. The co-authors of each paper have seen and approved these descriptions and contributions.

Publication I The publication gives an overview of different receiver architectures and then describes a new type of software-based GPS receiver developed for consumer grade devices in more detail. In this software-based receiver part of or all the receiver functionalities can be hosted on the main processor in the device and the only additional hardware needed is a small and cheap RF module that converts the GPS signal to a digital signal.

The complete software architecture for this new receiver type is presented including functional blocks, flexible configuration, various system features and interfaces. Performance results, such as navigation accuracy, sensitivity and cold/hot start characteristics are also provided.

Finally, some requirements for the host processor in terms of Central Processing Unit (CPU) load and memory usage are presented both for the purely software-based and for an accelerated version of this receiver.

In the work presented in this paper the author has been responsible for writing the paper, and he was the team leader for the team that developed the software receiver. He also participated in the development of some key algorithms in the receiver. The co-authors have participated in the implementation and reviewed

the paper before submission.

Publication II — The publication describes the design of a Multi-GNSS receiver and present test results where the performance of a GPS only solution is compared to a multi GNSS solution. The design includes a parameter system, assisted GNSS and multi GNSS signal acquisition and tracking. The presented multi GNSS tracking architecture is highly configurable and enables easy implementation of different tracking modes. Using these modes, it is, for example, possible to add support for weak signal tracking and high dynamic tracking. Finally, the design describes in detail how the position, velocity and time solutions are obtained in a multi GNSS receiver.

Based on the design in the paper a complete Multi GNSS receiver has been developed in Matlab, the FGI-GSRx, and this receiver has been used to evaluate the performance of a GPS only receiver versus a multi GNSS receiver.

Experimental results from two test cases are presented. A static open sky and an urban canyon test case. It is shown that both accuracy and fix availability is improved when combining signals from multiple GNSS. Especially in the urban canyon test case the multi GNSS outperforms the GPS only case significantly.

In the work presented in this paper the author has been responsible for writing the paper and implementing the multi GNSS Matlab receiver. The co-authors have helped in the implementation and reviewed the paper before submission.

Publication III — The publication focuses on topics specific to the Beidou B1 signal and implementation issues related to this in a software defined GNSS receiver. The Beidou signals have many similarities to the GPS Coarse/Acquisition (C/A) signal, the major differences being the signal modulation and data rate. The Beidou D1 signal transmitted from the Inclined Geosynchronous Orbit (IGSO) and Medium Earth Orbit (MEO) satellites has the same data rate as GPS C/A signal, but in addition the signal is modulated with

an extra Neumann–Hoffman (NH) modulation with a modulation rate of one kHz. The Beidou Geostationary (GEO) satellites transmit the D2 signal which does not have the NH modulation, but the data rate is 500 bps, i.e. the same as for Space Based Augmentation Systems (SBAS) signals. For both signals the high modulation and data rate need to be considered both in signal acquisition and tracking. The paper presents a novel new acquisition technique for the D1 and D2 signals and elaborates on the differences in signal tracking. A two-quadrant arctan Frequency Locked Loop (FLL) discriminator is proposed for the carrier tracking and a narrow correlator discriminator for code tracking. Differences in bit edge detection and C/No calculation compared to the GPS C/A signal are also discussed.

In the work presented in this paper the author has been responsible for designing and implementing the multi GNSS Matlab receiver used in the paper. The author has also provided support for the implementation of the Beidou algorithms and reviewed the paper.

Publication IV

The publication present the Indian Regional Navigation Satellite System (IRNSS) and it's signals and how to configure the used radio frequency front end to capture the L5 signals.

The multi GNSS Matlab receiver described in Publication II is then presented with its innovative, flexible and modular state-based tracking architecture, and it is shown that adding support for IRNSS signals is straight forward. This tracking architecture allows for having multiple types of tracking loops for different tracking states and the best loop filter implementation parameters for the IRNSS L5 signal tracking are presented. Finally, some results from IRNSS satellite signal acquisition and tracking are presented. Some details on the navigation data structure for IRNSS are also provided and the positioning engine of the software receiver and utilization of IRNSS observations is described.

In the work presented in this paper the author has been respon-

sible for designing and implementing the multi GNSS Matlab receiver and its tracking architecture used in the paper. The author has also provided support for the implementation of the IRNSS tracking loops and participated in writing and reviewing the paper.

Publication V

The publication presents a new method to process the Galileo Public Regulated Service (PRS) signal in a snapshot receiver. Various tracking techniques used previously for high order Binary Offset Carrier (BOC) signals are presented together with a new novel method that can provided a better accuracy and more robustness than previously used methods. The PRS signal was generated with a GNSS simulator and short digital Radio Frequency (RF) samples were stored and later processed in the receiver. A total of eight different processing methods was used, and the results compared.

In the work presented in this paper the author was responsible for implementing the snapshot receiver, logging and analyzing data, developing a new novel tracking method and writing the paper. The co-authors have helped in reviewing the paper before submission.

Publication VI

The publication presents results from an RTK solution using a single frequency GPS consumer grade receiver and the FinnRef Network. The FinnRef network provides the receiver with either single base station data or Network RTK data. Three different types of receivers were used: a consumer grade single frequency receiver, a geodetic grade dual frequency receiver and a commercial smartphone internal receiver. The receivers provide raw carrier phase and pseudo range observations. A software was developed for processing data from the Network and from the receivers and calculating the RTK solutions. The results presented in the paper show that it is possible to achieve even sub meter accuracy with consumer grade receivers.

In the work presented in this paper the author was the main ar-

chitect for the software developed in the project and used for testing RTK algorithms. The author has also helped in reviewing and analyzing test results as well as reviewing the paper before submission.

Publication VII

The publication presents a PPP solution utilizing an State Space Representation (SSR) model of the GNSS observation errors. The SSR model parameters are provided by the Finnish National GNSS Network, FinnRef. Three different kind of receivers were used: a consumer grade single frequency receiver, a geodetic grade dual frequency receiver and a commercial smartphone internal receiver. The single frequency PPP solution was calculated in the FGI-GSRx receiver, and the performance of the solution assessed.

In the work presented in this paper the author has been responsible for implementing the SSR and PPP support in the FGI-GSRx receiver and writing the paper. The co-authors have helped in reviewing the paper before submission.

List of Acronyms

ACF Auto Correlation Function

ADC Analog to Digital Converter

AGC Automatic Gain Control

ANTEX Antenna Exchange Format

API Application Programming Interface

ARNS Aeronautical Radio Navigation Service

ARP Antenna Reference Point

ASIC Application Specific Integrated Circuit

BDS Beidou Navigation System

BOC Binary Offset Carrier

BPSK Binary-Phase-Shift-Key

C/A Coarse/Acquisition

CBOC Composite BOC

CC Chip Counter

CDDIS Crustal Dynamics Data Information System

CDMA Code Division Multiple Access

CLAS Centimeter Level Augmentation Service

CORS Continuously Operating Reference Station

CPU Central Processing Unit

CRC Cyclic Redundancy Check

CS Commercial Service

DCB Differential Code Biases

DGPS Differential GPS

DGNSS Differential GNSS

DLL Delay Lock Loop

DoD Department of Defence

EC Epoch Counter

EDAS EGNOS Data Access Service

EGNOS European Geostationary Navigation Overlay Service

ESA European Space Agency

EXOR Exclusive OR

FDE Fault Detection and Exclusion

FDMA Frequency Division Multiple Access

FEC Forward Error Correction

FFT Fast Fourier Transform

FGI Finnish Geospatial Research Institute

FLL Frequency Locked Loop

FOC Full Operational Capability

GAGAN GPS-Aided GEO Augmented Navigation

GCC Galileo Control Centers

GEO Geostationary

GETR Galileo Experimental Test Receiver

GIOVE Galileo In-Orbit Validation Element

GLONASS Globalnaja Navigatsionnaja Sputnikovaja Sistema

GNSS Global Navigation Satellite Systems

GPS Global Positioning System

GSA European GNSS Agency

GSS Galileo Sensor Stations

GSTB Galileo System Test Bed

GSTP General Support Technology Programme

HAS High Accuracy Service

HW Hardware

I In-Phase

ICD Interface Control Document

IF Intermediate Frequency

IGS International GNSS Service

IGSO Inclined Geosynchronous Orbit

IOC Initial Operational Capability

IONEX Ionosphere Exchange Format

IOV In-Orbit Validation

IR Infra Red

IRNSS Indian Regional Navigation Satellite System

ITU International Telecommunications Union

LAMBDA Least-squares Ambiguity Decorrelation Approach

LEO Low Earth Orbit

LFSR Linear Feedback Shift Registers

LNA Low Noise Amplifier

LORAN Long Range Navigation system

LSE Least Square Estimator

MBOC Multiplexed BOC

MCS Master Control Station

MEO Medium Earth Orbit

ML Maximum Length

MS Monitoring Station

MSAS Multi-functional Satellite Augmentation System

NAVSTAR Navigation System with Timing and Ranging

NH Neumann–Hoffman

NMEA National Marine Electronics Association

NNSS Navigation Satellite System

NSL Nottingham Scientific Limited

NTRIP Networked Transport of RTCM via Internet Protocol

OS Open Service

PC Phase Counter

PCO Phase Center Offset

PCV Phase Center Variation

PLL Phase Locked Loop

PPP Precise Point Positioning

PPP-AR Precise Point Positioning with Ambiguity Resolution

PPP-RTK Precise Point Positioning with Real Time Kinematic

PRS Public Regulated Service

PSD Power Spectral Density

PVT Position, Velocity and Time

Q Quadrature

QMBOC Quadrature Multiplexed BOC

QZSS Quasi-Zenith Satellite System

RAF Royal Air Force

RAIM Receiver Autonomous Integrity Monitor

RDF Radio Direction Finder

RF Radio Frequency

RINEX Receiver Independent Exchange Format

RMS Root Mean Square

RNSS Radio Navigation Satellite Services

RTCM Radio Technical Commission for Maritime Services

RTK Real Time Kinematic

SAR Search And Rescue

SBAS Space Based Augmentation Systems

SDCM System for Differential Corrections and Monitoring

SDR Software Defined Receiver

SINEX Solution Independent Exchange Format

SLAS Sub-Meter Level Augmentation Service

SLR Satellite Laser Ranging

SNR Signal-to-Noise Ratio

SPI Serial Peripheral Interface

SPS Standard point Positioning Service

SSC System Control Center

SSR State Space Representation

STEC Slant Total Electron Count

TCXO Temperature Controlled Crystal Oscillator

TEC Total Electron Count

TECU Total Electron Count Unit

TMBOC Time Multiplexed BOC

TTC Telemetry, Tracking and Control

UART Universal Asynchronous Receiver Transmitter

ULS Up Link Stations

WAAS Wide Area Augmentation System

WWII World War 2

XOR Exclusive OR

ZHD Zenith Hydrostatic Delay

1 INTRODUCTION

The first chapter will give a brief introduction to the history of navigation, the objectives for the thesis, and a description of the thesis structure.

1.1 History

The art of surveying, or measuring positions of points and distances and angles between them, is believed to date back to ancient Babylonia [Har87]. One of the drivers for developing surveying methods was of course the need for more accurate maps for navigation and easier definition of boundaries between countries and properties. The methods used by these surveyors are not very well documented, but it is believed that in many cases the positions of towns with respect to each other were based on traveler's tales and the surveying part consisted of drawing geometrical models of the earth based on these tales.

1.1.1 Concept of triangulation and trilateration

The concept of triangulation can be defined as determining points of interest and distances between them by forming triangles. Some claim that triangulation was invented by Arab mathematicians, but in the literature the concept was first introduced in the mid-sixteenth century by the Flemish mathematician Gemma Frisius [Fri33]. Triangulation commonly uses a known distance between two points and the measured angle from these two points to an unknown third point. An example is shown in figure 1.1.

The two known points + the unknown point form a triangle and if the baseline and two angles are known the angle-side-angle triangle congruence theorem can be used to find the other unknowns in the triangle. By repeating this process, it was possible to build whole networks of triangles and determine the relative locations

Figure 1.1 Example of triangulation

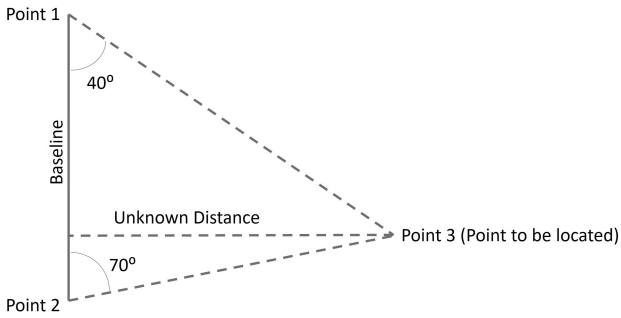

between each observation point. In some strict definitions triangulation is defined as only using measured angles.

The instrument used for triangulation is called a theodolite [Dau89]. It can measure very accurately both the horizontal and vertical angle between two sides in the triangle. Quite often points in the triangles were located at a high altitude, which is beneficial since a point at a high altitude is visible for long distances, and it was possible to make the triangles bigger. Therefore, the vertical angle was also needed to account for differences in height.

In the 1950's new methods were developed to measure long distances using the travel time of reflected electromagnetic waves. The Tellurometer [Wad57] used microwaves and the Geodimeter [Ber52] used light waves that reflected from an object at the unknown location and travel time multiplied by the speed of light gave the distance to the object. The process of obtaining the positions was the same as for triangulation, building networks of triangles. The difference was that now the distances were measured instead of the angles and the triangles were determined by measuring the length of the three sides without angles - the concept of trilateration was born.

In many cases triangulation and trilateration were used as complementary methods, also called triangulateration, improving accuracy and reliability of the result.

1.1.2 Early days of navigation

The above-mentioned methods and instruments are primarily intended for surveying, or determining the relative distances of points by using geometrical means, and

not suited for navigation.

Navigation is usually defined as the art of determining the current position, course, and speed of an object. The latin word *navis* means ship, and in the early days this was also the main use case for navigation. The reason these methods were first developed for use at sea is that when moving on land there were roads and identifiable landmarks, but out at open sea this was not the case. The same principles that had been developed in surveying could also be used in navigation, but since the surveying work already had been done and sea charts and maps were available, the methods were simplified.

The perhaps most widely used method was to measure the bearing to multiple known points on the map that were visible. These points could be islands or identifiable points on the coastline and later man-made constructions like buildings and lighthouses. The method consisted of measuring the bearing, or the angle between the direction of an object and that of true north, using a compass to at least two of these objects. You can then draw the lines from the objects on the map with the measured angle with respect to north and your position will then be at the crossing of all these lines as is shown in figure 1.2

Figure 1.2 Determining location using bearings.

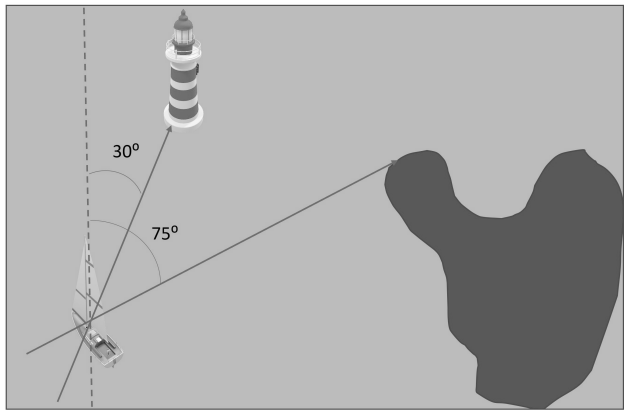

Another version of the same method is to measure the bearing to the same object at two different times and estimating the travelled distance by measuring time and speed of the ship. The distance the ship has travelled then become our baseline and the two bearings our two measured angles, and it is easy to see the resemblance with the concept of triangulation.

1.1.3 Radio Navigation Systems

The first radio navigation systems were built during the 1930's. The principle of these were to have a set of radio transmitters, for example along the coastline and a receiver onboard the vessel with a directional antenna. By turning the antenna and finding the angle that gave the best reception, you could determine the bearing to the radio transmitters. The position could be determined by finding the intersection point between the bearing lines to two transmitters. An example of such a system was the Radio Direction Finder (RDF) [Wat71]. Another example was the Lorenz system [Dia30].

Land based radio navigation systems had their golden age during the 40's and 50's driven by the World War 2 (WWII). The DECCA [Bla15] system and the GEE [Bla91] system were the first ones to be developed almost in parallel, starting in the 30's. Both systems were so-called hyperbolic navigation systems, a well-known idea at the time, and the major difference was that GEE was based on timing differences and DECCA based on phase differences. The principle used in the GEE system was originally proposed as a landing system for airplanes, but since the range of the system was much longer than expected, it quickly evolved into a navigation system used for aiding Royal Air Force (RAF) bombers during night missions in WWII. The use of the system continued after the war, both in civil and military aviation.

The basic GEE setup consists of one master and two or three secondary stations. The master stations send out a pulse and when the secondary stations detect it, they will transmit their own pulse. The stations are thus synchronized with each other, and the user can measure the time difference between signals from two stations. This time difference is constant on a hyperbolic curve between the stations, and by finding the intersection point of multiple such curves, the user could determine its position. The stations were often placed in an L shape with the master station in the corner of "L" and the curves formed almost perpendicular grid lines. The name GEE originates from "G" in Grid. The GEE could offer an accuracy of a few hundred meters and ranges up to 560 km.

The DECCA system was first used during WWII by the British Royal Navy and further developed by the newly formed company Decca Navigator Co. Ltd. after the war. Decca was a radio navigation system based on measuring phase differences between signals transmitted from multiple stations at different frequencies. The sta-

tions were synchronized, or phase locked, using the same technique as in the GEE system. By using different multiples of the same base frequency, the phase difference between any two stations was constant on a hyperbolic curve or on multiple hyperbolic curves. The range of the DECCA system was 400-800 km and accuracy were from a few meters to more than one km depending on the weather conditions.

The Long Range Navigation system (LORAN) [Dic59] was essentially a version of the GEE system, using much lower frequencies. It was developed in the United States and when the team developing it became aware of the work done in the UK with the GEE system, they realized that the benefit with the LORAN is the longer range. When the focus for LORAN was switched to long range, the demand for high timing accuracy was reduced and even lower frequencies could be used that reflected from the atmosphere and could even be used beyond the horizon. This enabled the use of radio navigation also at areas where no base stations could be placed, like the Atlantic and Pacific Oceans. The range of the LORAN system could be up to 2600 km, but as for all hyperbolic navigation systems, the accuracy decreases with increasing range to the stations. LORAN later evolved into LORAN-B and LORAN-C [Hef72] (the original system was renamed to LORAN-A), and LORAN-C was still used in the 1990's in China. LORAN-C has been shown to achieve positioning accuracies of about 100 m.

The Omega [Asc72; Sco69] system can be considered as the final step towards a truly global satellite navigation system. In the existing systems at that time all stations needed to synchronize to a signal from the master station and this became increasingly difficult to do with increasing distances between the stations since the radio signal were reflected from the atmosphere and could arrive via multiple paths. Omega was the first system using atomic clocks for synchronization between the stations. This meant that the stations no longer needed to detect the signal from the master stations, enabling much longer distances between the stations. Omega consisted of eight active base stations distributed over the whole globe and the position of the user was still estimated using the intersection of hyperbolic curves and the accuracy was in the order of 7-8 km. The difference compared to GEE and LORAN was that Omega was a truly global system. The Omega signal was also much more complicated than its predecessors. It consisted of fixed pulses at four different frequencies in a patter that repeated itself every 10 seconds. One of the frequencies was unique for each base station. The resemblance to the Global Navigation Satellite

Systems (GNSS) signal is apparent. The last Omega station was shut down in 1997.

1.2 Objectives of the thesis

The main objective of this thesis is to assess the impact of the evolution of GNSS technology on the performance and design of consumer grade GNSS receivers. There are five main research questions to be addressed in the thesis:

How should a receiver be designed to allow for maximum flexibility when it comes to new signals and methods? This question becomes increasingly relevant as more GNSS signals become available and new methods must be applied to successfully handle all the signals and provide robust performance under varying conditions for different types of GNSS applications. Switching from one constellation to another, handling of multiple clock domains, tracking a large variety of modulation types, decoding many different types of data at different data rates and selecting between data and pilot signals are only some examples of functionality that did not exist when only GPS was used. How to design a receiver to allow for maximal flexibility is therefore a very relevant question.

What is the impact of having more satellite navigation systems and signals available? The number of available signals will certainly improve the availability of a positioning solution especially in more challenging environments where many of the signals are blocked by buildings or other obstacles. More signals will, up to some limit, also provide better accuracy, but there is not necessarily a simple relationship between number of used satellites and accuracy. More satellite systems will provide better robustness due to their independent nature. To better understand how multiple systems and more signals impacts the performance is therefore an interesting challenge.

What kind of new receiver algorithms are needed to process new signals, in particular from the Beidou and IRNSS systems? In many cases the new signals are designed to be as compatible as possible with legacy GPS signals, but in order to benefit from higher data rates, pilot signals and more complex modulation schemes new algorithms for signal processing and navigation are needed. What is somewhat unclear is how much benefit these new algorithms will bring to mass market receivers compared to the effort to implement them. The types of new algorithms needed is therefore worth exploring.

What will the impact be of more accurate observations from high frequency codes? Modern GNSS signal often uses higher code rates and should in theory also provide better measurement accuracy, but what kind of improvements can really be expected keeping in mind that also the signal processing algorithms are not the same as for legacy signals. Even if the signals are more accurate the receiver also needs to be able to utilize this properly. Looking at the best possible signals available and understanding what the maximum benefit could be is therefore a very valid research question.

How well does methods like RTK and PPP work in consumer grade receivers? High accuracy navigation methods like RTK and PPP using mass market receivers is not a new thing, but with the new chipsets supporting dual frequency and some of the new modulation techniques these methods are becoming increasingly popular and results today look very promising. The balance between receiver and algorithm complexity versus benefit for the end user is an interesting challenge to address for many receiver manufacturers. Understanding what can be achieved today is therefore also a very relevant research question.

1.3 Thesis structure

The thesis is divided into seven chapters. This chapter provides a short historical background to navigation systems, starting from ancient Babylonia to the early days of radio navigation. The next chapter provides an overview of Global Navigation Satellite systems, including a description of all signals transmitted from the satellites. Chapter three describes the fundamental elements and principles used in GNSS positioning, and chapter four provides an overview of carrier phase positioning methods like PPP and RTK. In chapter five, the focus is on receiver design and the main tool used in this work, the FGI-GSRx. Finally, chapters six and seven provides discussing on the results and some conclusions. The seven scientific papers referred to in this thesis are provided at the end.

2 GLOBAL NAVIGATION SATELLITE SYSTEMS

This chapter will give an overview of the different satellite navigation systems that exists today. The chapter will describe the history of each system, the architecture of the systems, the different types of satellites that have been launched and the different signals that are and have been transmitted in the past.

2.1 The beginning of GNSS

GNSS refers to any system used for navigation, is global, and utilizes satellites. The story of Satellite Navigation Systems began in the 1960's with the United States Navy Navigation Satellite System (NNSS), that used the TRANSIT [Dan98] satellite system, and the Russian Parus and Tsikada [Dal86] systems. These were later replaced by the United States GPS, and the Russian counterpart GLONASS. Later China and Europe have followed and have developed the Beidou Navigation System (BDS), and Galileo system, which are both also truly global systems.

Local navigation systems like the IRNSS in India and Quasi-Zenith Satellite System (QZSS) in Japan also exist and satellite augmentation systems like the European Geostationary Navigation Overlay Service (EGNOS), Wide Area Augmentation System (WAAS), Multi-functional Satellite Augmentation System (MSAS), System for Differential Corrections and Monitoring (SDCM) and GPS-Aided GEO Augmented Navigation (GAGAN) have been deployed.

All GNSS uses trilateration as their principle of operation. So, they are measuring the distance between the user and the satellites. They do not use any angle measurements. Measuring the distance to the satellites is done by measuring the time it takes for a known signal to travel from the satellites to the user. For this to work, accurate clocks and suitable signals are needed, and the invention of both of these

have driven the development of GNSS.

Atomic clocks are the heart of GNSS, like in the Omega system. Each satellite has these accurate clocks on board, and the satellites are all synchronized to a common time system. The invention of Code Division Multiple Access (CDMA) signals is the second enabler, since that made it possible for all satellites to transmit at the same frequency and minimizing interference between the signals.

2.2 Overview of GNSS systems

This section will provide a brief overview of each of the operational navigation and augmentation systems. The total number of operational satellites per system as of November 2022 is shown in table 2.1.

Table 2.1 Current status of navigation and augmentation systems

System	Operational Satellites
GPS	31
GLONASS	22
Compass/Beidou	44
Galileo	24
IRNSS	7
QZSS	4
EGNOS	4
WAAS	3
MSAS	2
SDCM	3
GAGAN	3
Total	147

2.2.1 GPS

One of the starting points for the development of GPS is sometimes considered to be the TRANSIT system or the NNSS, that was developed in the United States during

the late 1950's and early 1960's. This system had ground stations tracking the signals from the satellites, and the transmitted signals contained data about the satellite orbits. The positioning was, however, based on measuring Doppler shifts instead of distances and the main use case was positioning United States submarines. The NNSS was operational until 1991 until it finally was made obsolete by the GPS.

The United States Department of Defence (DoD) had realized in the late 1960's that a more robust and stable satellite navigation system than NNSS will be needed in the future, and in 1978 the first satellites were launched in the Navigation System with Timing and Ranging (NAVSTAR) system. In these satellites, synchronized timing signals were used for the first time. The system was primarily developed for the United States military, but in the 1980's the system was opened for civil users and the first handheld GPS receiver was introduced in 1989 by Magellan [Xia02]. In 1999 the first mobile phone with a GPS receiver was introduced by the Finnish company Benefon [Ben99]. Today, few people in industrialized countries can imagine a life without GPS.

2.2.1.1 System

The GPS consists of three so-called segments: the control segment, the space segment and the user segment [Hof92]. The control segment consists of a network of ground stations with different tasks related to operation of the system. The Master Control Station (MCS) is located at Schriever Air Force Base in Colorado, United States, and an alternate MCS is located at Vanderberg Air Force Base in California. In addition to the MCS, the control segment also includes sixteen monitoring stations, of which four are equipped with dedicated uplink antennas.

Monitoring stations are equipped with geodetic grade GNSS receivers, and their main task is to collect GNSS observations and data and feed that to the MCS. The MCS can compute the precise location of each satellite and continuously monitor the quality of each signal and health of every satellite, as well as the accuracy and integrity of the whole system. The MCS also manages, via the uplink antennas, control of the satellites and uploading of the data that are transmitted to the users. Commands can also be given to reposition the satellites and perform maintenance and software upgrades on the satellites.

The GPS space segment consists of a maximum number of 36 MEO satellites in six orbital planes with an inclination angle of 55 degrees with respect to the equato-

rial plane. The nominal period of the satellites is slightly less than 12 hours. Since the launch of the first satellite in 1978 seven different types of satellites have been deployed. Every new type of satellite has introduced both new and improved features, as well as significantly increased the time of operation. The newest satellites have an expected lifetime of 12 years. Information on the different types of satellites can be found in table 2.2

Table 2.2 GPS satellites

	Launched	Operational	Launch Period
Block I	11	0	1978-1985
Block II	9	0	1989-1990
Block II-A	19	0	1990-1997
Block II-R	13	7	1997-2004
Block IIR-M	8	7	2005-2009
Block II-F	12	12	2010-2016
Block III	5	5	2018-
Total	75	31	1978-

The user segment consists of all the receivers utilizing the signals from the space segment. In 2021 there was estimated to be about seven billion GNSS enabled devices [EUS22] in use and GPS is enabled in most of them for calculating position, time, and velocity.

2.2.1.2 Satellite Signals

The oldest signals transmitted by the GPS satellites are the open L1 C/A signal (1575.42 MHz) and the military L1 and L2 P signals (1227.60 MHz). They have been transmitted starting from the Block I satellites, and they are still transmitted from the newest satellites.

Starting from the Block IIR-M satellites a new civil signal was added on the L2 band, the L2C signal, enabling the development of civil dual frequency GPS receivers. Two new military signals, the M-signals, were also added to both the L1 and L2 bands and with the Block II-F satellite a third civil signal was added on the L5 band (1176 MHz), the L5C. This signal is compatible with other GNSS systems and

is transmitting at a higher power and have a wider bandwidth than the other signals.

Finally, in 2018 the first satellites (Block III) were launched that broadcasted the newest civil signal L1C. A signal that has been developed together with Europe and China to ensure maximum inter-operability between the different satellite navigation systems. The L1C is still backwards compatible with the legacy L1 signal.

The signals transmitted by the GPS satellites are shown in table 2.3.

Table 2.3 GPS signals

	Signals
Block I	L1 C/A,L1P(Y),L2 P(Y)
Block IIR-M	+ L2C, L1-M, L2-M
Block IIF	+ L5
Block III	+ L1C

The new generation Block III-F are being built.

2.2.2 GLONASS

Satellite navigation system development was started in the Soviet Union in the 1960's with the Tsiklon (Cyclone) satellites that were intended for positioning of their ballistic missile submarines. The system was suffering from extremely poor accuracy and was not declared operational until 1972, just two years prior to the first launch of its successor, the Tsiklon-B. The biggest problem Tsiklon faced was modelling the Earth's gravitational field for accurate orbit determination.

Tsiklon-B was deployed by the Parus (Sail) satellites, 99 Low Earth Orbit (LEO) satellites that were launched 1974-2010. The primary task of these satellites was Tsiklon-B, but they also carried other payloads. This system was very similar to the United States TRANSIT system. The constellation included six satellites flying in circular orbits at a height of 1000 km. The inclination was 82.6 degrees and each plane was separated by 30 degrees. A Doppler based navigation method was used and satellites had to be tracked for 5–15 minutes before an accuracy of 100-300 m could be reached.

The concept of GLONASS was presented already in the 1960s, but its actual development started in 1976 and the first launch took place in 1982. When the Soviet

Union fell apart in 1991 the system consisted of 12 satellites. The Russian Federation continued to develop the system, declaring it being operational in 1993 and reaching a full constellation of 24 satellites in 1995. The economic crisis at the end of the 1990's effectively stopped any new launches, and the GLONASS system degraded slowly. When the Russian economy recovered 10 years later, a new era started in Russian satellite navigation and a total of 4.7 Billion Dollars were invested over the next 10 years into renewing GLONASS.

2.2.2.1 System

The GLONASS system consists, like GPS, of three segments, the space segment, the control segment and the user segment. The control segment includes a control center, three uplink stations, a network of monitoring stations, a network of tracking stations, two laser ranging stations and a system clock.

The System Control Center (SSC) is located in Krasnoznamensk 25 km southwest from Moscow. The three uplink stations are distributed over the country in the West-East directions and the central clock is located in Schelkovo 25 km northeast from Moscow. Three Monitoring Stations are co-located with the uplink stations, and a fourth station is located in Yakutsk (northeast Russia). A separate network of five Telemetry, Tracking and Control (TTC) stations and two Satellite Laser Ranging (SLR) Stations are also included in the control segment. More MS are being built that also has SLR capability.

The space segment or the satellites in GLONASS are located in three orbital planes with eight slots in each. All the planes have an inclination of 64.8 degrees with respect to the equatorial plane and the satellites are flying at an average height of 19100 km (MEO satellites). The nominal period is slightly shorter than for GPS, about 11 hours 15 min. The first and second generation of satellites were launched between 1982 and 2005 and all of these have been decommissioned since then. The GLONASS constellation thus consists of only third generation satellites, of which the last type, the first GLONASS-K2 satellites, was launched end of 2022. Information on the different types of satellites can be found in table 2.4

GLONASS is, like GPS, primarily a military system and because of the deterioration of the system in the beginning of the century the commercial adaptation of the signals was much slower than for GPS. In 2001 the Russian government started demanding that all vehicles transporting dangerous goods need to be tracked using

Table 2.4 GLONASS satellites

	Launched	Operational	Launch Period
Block I	10	0	1982-1985
Block IIa	9	0	1985-1989
Block IIb	12	0	1987-1988
Block IIv	56	0	1988-2005
Block III	1	0	2001-
GLONASS-M	50	21	2003-2020
GLONASS-K (K1)	2	1	2011-
Total	140	22	1982-

GLONASS and from 2011 there is a requirement that all Russian made cars need to be equipped with GLONASS receivers. In 2011 the first GLONASS capable mobile phone was also released, the MTS 945 from ZTE [Qua11]. This was made possible by the new Qualcomm chipset, the Snapdragon MSM7x30, that supported both GPS and GLONASS signals [Ins11]. For Geodetic reference stations, especially on high latitudes, GLONASS was also quickly adapted because its satellite orbits are located higher in the sky offering better signal availability and therefore also better robustness and, in some cases, even better accuracy [EWD11].

2.2.2.2 Satellite Signals

All the satellites in the GLONASS system are transmitting three different signals. The civil L1OF (L1 frequency, Open Signal, Frequency Modulated) and the obfuscated military L1SF and L2SF signals. These signals are all so-called Frequency Division Multiple Access (FDMA) signals, which means that every satellite is transmitting the same code on a unique frequency. For GLONASS the transmitting frequency on L1 and L2 are defined by equations 2.1

$$f_k^{L1} = f_0^{L1} + k\Delta f^{L1},\ where\ f_0^{L1} = 1602\,MHz\ and\ \Delta f^{L1} = 562.5\,kHz, \quad (2.1a)$$
$$f_k^{L2} = f_0^{L2} + k\Delta f^{L2},\ where\ f_0^{L2} = 1246\,MHz\ and\ \Delta f^{L2} = 437.5\,kHz, \quad (2.1b)$$

where f_k^{L1} and f_k^{L2} are the carrier frequencies for channel k in the $L1$ and $L2$ bands, f_0^{L1} and f_0^{L2} are the center frequencies for the $L1$ and $L2$ bands, Δf^{L1} and Δf^{L2} are the frequency steps for the $L1$ and $L2$ bands, and the channel number k in both the above equations spans from -7 to 6 in steps of one. In 2003 when the first GLONASS-M satellite was launched a new civil L2 signal, the L2OF, was added. The frequencies were the same as defined in equation 2.1a. The signals transmitted by the GLONASS satellites are shown in table 2.5.

Table 2.5 GLONASS signals

	Signals
Block I	L1OF, L1SF, L2SF
GLONASS-M	+ L2OF, (L3OC)
GLONASS-K (K1)	+ L3OC

Already, the later M satellites started to transmit a CDMA test signal at the L3 band, but the K satellites are the first ones to officially support the new signal. GLONASS L3OC will be centered at 1202.025 MHz. The GLONASS-K2 satellites will add four more CDMA signals. Two civil signals at L1 and L2 and two encrypted signals at L1 and L2. The transmitting frequencies will be 1600.995 MHz for L1 and 1248.06 MHz for L2.

2.2.3 Beidou

Satellite navigation in China started in 1967 as an idea by the Chinese Navy and a conceptual navigation satellite, Denga 1, was developed and ready for testing in 1970. This project continued for almost 10 years until it was cancelled by the government in 1980. A new idea of a local navigation system utilizing two GEO stationary satellites was presented in 1983 and the development of that started in 1986. The concept was finally demonstrated using two in-orbit DFH-2/2A Chinese communications satellites in 1989 showing an accuracy comparable to GPS. A program to develop a Chinese satellite navigation system was officially accepted in 1993.

The Beidou-I system is based on this same two-satellite concept and the first satellites were launched in 2000 providing a positioning service one year later. A third satellite was launched in 2003 and the system became commercially available in 2004.

This third satellite also included test payloads for the next generation of satellites. Beidou-I covered a region between 70 and 140 degrees East longitude and 5 and 55 degrees North latitude. The ground segment included a control station, three tracking stations and several ground correction stations.

The positioning concept in Beidou-I was based on two-way communication. The control station sent out a signal via the two satellites to the user terminal, and the user terminal responded with its own signal. The control station could then estimate the user position based on the time it took to get the signals back and an estimation of the user's altitude from regional maps. The resulting position was returned to the user. The two-way communication resulted in relatively large user terminals and a limited number of simultaneous users (150). An important feature of the system was the capability to actively communicate with the terminals enabled by the two-way communication. The accuracy was estimated to be around 20 meters by the United States DoD.

In 2006 China announced that they will start developing a global navigation system similar to that of the other existing and planned systems (GPS, GLONASS, Galileo). The same principles would be used, and the signals were defined based on input from other nations to ensure compatibility and inter-operability of the systems. The new system would transmit civil and military signals on three different frequencies. The development was planned to be done in two phases. In the first phase (Compass or Beidou-II) the focus would be on developing a regional system for China and the second phase (Beidou-III) the system would become a truly global system.

2.2.3.1 System

Like the other systems, Compass and Beidou-III also consists of three segments. Not many details are known about the ground segment of Beidou, but it includes one master control station that monitors the system using data from the monitoring stations, controls the constellations and generates the navigation data. Currently, there are a total of 30 monitoring stations. The segment also includes two separate uplink stations for uploading data to the satellites. Because of the initial target to develop a local system for China, the space segment looks different compared to the other systems. It is essentially a mixture of a local and a global system, as can be clearly seen from the ground tracks shown in figure 2.1

Figure 2.1 Beidou ground track for GEO satellites, one IGSO and one MEO satellite

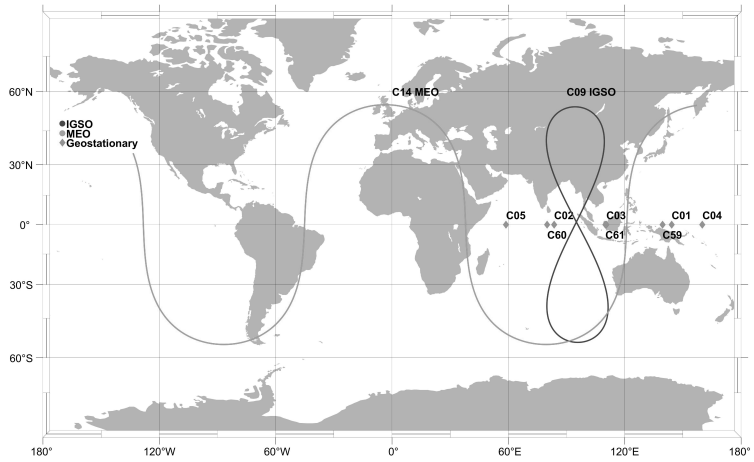

Beidou was designed to have five GEO satellites, five IGSO satellites and four MEO satellites. During the years 2007-2012 a total of 16 satellites were launched, completing the first version of the system. Since then, the system has been modernized and there are already a total number of 30 new Beidou 3 generation satellites in addition to the 15 still operational Compass satellites. The constellation today is a mixture of Compass and Beidou-III satellites. Information on the different types of satellites can be found in table 2.6

Table 2.6 Beidou satellites

	Launched	Operational	Launch Period
Beidou-1	4	0	2000-2007
Compass-M	4	3	2007- 2012
Compass-G	8	5	2009-2019
Compass-IGSO	7	7	2010-2018
Beidou-3 M	24	24	2017-2019
Beidou-3 G	3	2	2018-2020
Beidou-3 IGSO	3	3	2019
Total	53	44	2000-2020

Compass and Beidou terminals have mostly been developed and used in China

up until 2015. The Interface Control Document (ICD) of the Beidou system was released in late 2012 marking the starting point for international receiver manufacturers to start adding Beidou support to their receivers. Septentrio [De 07] was one of the first to announce support for Beidou signals, already in 2012, but the first commercial receivers started to become available in 2013. Consumer grade receivers like those in mobile phones have added Beidou much later, and it is not until recent years that Beidou support has become a must-have in most receivers.

2.2.3.2 Satellite Signals

Compass satellites transmit on three frequency bands, B1, B2 and B3. The signals are split into In-Phase (I) and Quadrature (Q) parts, where the I parts are provided as an open service and the Q parts are part of an authenticated service. The Beidou-3 satellites still transmit the same B1 and B3 signals, but the B2 signal is replaced by new signals. For the new signals in the B1 band, the B1C signal is open and provide both a data and a pilot channel and the B1A signal is authenticated. In the B2 band, the new signals provide only the open service signals B2a and B2b, which are both split into a data and a pilot channel. A new authenticated service signal with a data and pilot channel is introduced in the B3 band. The signals transmitted by the Beidou satellites are shown in table 2.7

Table 2.7 Beidou signals

	Signals
Compass Open Service	B1I,B2I, B3I
Compass Authenticated Service	B1Q, B2Q, B3Q
Beidou-3 Open Service	-B2I + B1C, B2a, B2b
Beidou-3 Authenticated Service	+ B1A, B3A

2.2.4 Galileo

In the 1990's the European Union identified the need for a civilian satellite navigation system controlled by the member states. The name Galileo shows up in a communication from the European Commission in the beginning of 1999 [The99] and the

financing decision was taken in the early 2000's. The development of Galileo was divided into three phases, the In-Orbit Validation (IOV) phase, the Initial Operational Capability (IOC) phase, and the Full Operational Capability (FOC) phase.

The Galileo System Test Bed (GSTB)-V1 was designed to validate planned algorithms for Orbit Determination and Time Synchronization [Pír06]. No satellites were launched in this test bed. The second version, GSTB-V2 included two test satellites, the GSTB-V2/A and GSTB-V2/B. They were later renamed to Galileo In-Orbit Validation Element (GIOVE)-A [Gat06] and GIOVE-B. GIOVE-A was launched in 2005 and GIOVE-B followed almost three years later. Already, GIOVE-A could transmit all the signals planned for Galileo, although it could only transmit either E1+E5 or E1+E6. GIOVE-B had greatly improved hardware onboard, and it could transmit for the first time also the navigation message.

The Galileo Experimental Test Receiver (GETR) was built by Septentrio, and it was used to validate the signals from GIOVE-A [Sim06]. After the signals had been validated, the first two operational satellites were launched in 2011 and one year later two additional satellites were launched. With four satellites in the constellation, it was now possible to obtain a position solution, and the first time that happened was in 2013. Three out of these four satellites are still usable.

2.2.4.1 System

Galileo is, like all the other systems, divided into a ground segment, a space segment and a user segment. Galileo also introduces different types of services for the user. The IOC Phase included the initial commissioning of the ground and space infrastructure and the definition of the three first services: The Open Service (OS), Search And Rescue (SAR) Service and the PRS. During the FOC phase, the rest of the ground and space infrastructure was deployed. The ground segment consists of two Galileo Control Centers (GCC) located in Germany (Oberpfaffenhofen) and Italy (Fucino), 14 Galileo Sensor Stations (GSS), five Up Link Stations (ULS) and five TTC. All stations are shown in figure 2.2

The full Galileo space segment consist of 30 satellites, 10 in each of the three equally spaced orbital planes with an orbital inclination of 56 degrees. Each plane will have nine operational and one spare satellite. The Galileo satellites are so called W class satellites with a mass of 700 kg and a peak power capacity of 1600 W. Lifetime is expected to be 12 years. The satellites will have two passive hydrogen masers and

Figure 2.2 Galileo ground segment

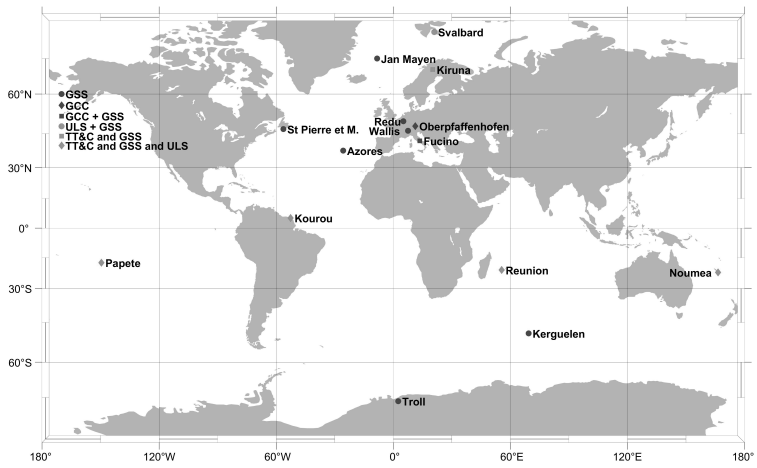

two rubidium backup clocks onboard. The satellites also have several antennas, an Infra Red (IR) Earth Sensor, a sun sensor, a laser retro-reflector and space radiators.

The two first satellites in the space segment were launched in 2014, but injection into orbit failed, and these satellites are in test mode and will probably never be part of the constellation. A total of six satellites were launched in 2015 and an additional six in 2016. A total of 14 additional satellites had been launched when IOC was declared end of 2016. Out of these, 11 are operational.

Since the declaration of IOC 10 more satellites have been launched, the last one in 2021. A total of 24 satellites are currently included in the active constellation, three IOV, 11 IOC and 10 FOC satellites. In 2017 European Space Agency (ESA) handed over the operational responsibility for the Galileo Constellation to the European GNSS Agency (GSA). Information on all the launched satellites can be found in table 2.8

Receiver manufacturers started the development of Galileo support long before Galileo became operational, but the support was often not released for the users. It was not until 2016, when ESA authorized Galileo for Early Operational Capability, that manufacturers also released the support publicly. A new firmware for the uBlox M8 receiver with Galileo support was released early 2017 [Bag16] and Qualcomm announced in June 2016 that they will add support for Galileo to their Snapdragon processors [Qua16]. Soon after that, the first Galileo ready smartphone was announced to hit the market late 2016, the Aquaris X5 Plus Phone from BQ. In 2023

Table 2.8 Galileo satellites

	Launched	Operational	Launch Period
GSTB-V2	2	0	2005-2008
IOV	4	3	2011-2012
IOC	14	11	2014-2016
FOC	10	10	2017-2020
Total	30	24	2005-2020

it was estimated that more than 3.9 billion smartphones on the market were Galileo compatible [EUS23].

2.2.4.2 Satellite Signals and Services

All Galileo Satellites transmit on three frequency bands, E1, E5 and E6. The E5 band is further split into E5a and E5b bands. The E1 frequency is actually a sum of three signals: A, B and C. E1-B and C are part of the Open Service, and the only difference is that E1-C does not contain any data (Pilot Channel). The E1-A signal is part of the PRS and access to this signal is restricted. The E5 signals are all part of Open Service, thus enabling dual frequency civil receivers. There are four signals in total transmitted, the I and Q channels on E5a and I and Q channels on E5b. I channels are data channels and Q channels are Pilot channels. The E6 band also consist of the A, B, and C part. E6-B and E6-C are the data and pilot components of the Commercial Service (CS) and E6-A is a PRS signal. A complete list of Galileo signals are shown in table 2.9

Table 2.9 Galileo signals

	Data Signals	Pilot Signals
OS	E1-B, E5a-I, E5b-I	E1-C, E5a-Q, E5b-Q
CS	E6-B	E6-C
PRS	E1-A, E6-A	

2.2.5 Other navigation systems

There are two additional satellite navigation system that are not truly global systems. IRNSS or Navic is developed by India and QZSS is developed by Japan. The IRNSS Ground Segment consist of centers for Control, Navigation and Timing, Uplinking Stations, Range and Integrity Monitoring Stations, Laser Ranging Stations and a data communication network. The space segment is designed to cover India [Maj17] and consists of GEO satellites and IGSO satellites with 29 degrees inclination, much like Compass. So far nine satellites have been launched and seven are operational, out of which three are GEO satellites. India has plans to extend the constellation to 11 satellites.

The satellites transmit three signals on both L5 and S band. The system provides two types of service: An open Standard point Positioning Service (SPS) and a restricted PPP service [Ind17]. The restricted signals are split into a data and a pilot signal on both bands. A new L1 signal is planned for IRNSS in 2022. A complete list of IRNSS signals are shown in table 2.10

Table 2.10 IRNSS signals

	Signals
Open SPS Service	L5-SPS, S5-SPS
Restricted PPP Service	L5-RS Data, L5-RS Pilot, S5-RS Data, S5-RS Pilot

The QZSS is a four-satellite regional navigation system developed by Japan. It is often defined only as a time transfer and augmentation system, since four satellites is barely enough to obtain an independent position solution. The ground segment includes a Monitoring Station (MS) in Okinawa, and several TTC and SLR stations. Many of the stations are located outside Japan (India, Guam, Australia, Thailand, and Hawaii). The uplink station is the TTC station in Okinawa. The space segment consists of one GEO and three IGSO satellites with a high inclination of around 43 degrees. The first satellite was launched in 2010 and the last in 2021. Japan has plans to extend the system to seven satellites within the next two years.

The primary purpose of QZSS is to add high elevation satellites to the GPS constellation to improve performance in the deep urban canyons in Japan's big cities, and also to augment the GPS signals by providing observation corrections. The

QZSS satellites are also different to the other constellation satellites since there are no atomic clocks on the satellites. Instead, the onboard crystal clocks are constantly synchronized to ground clocks, making the satellites much smaller and cheaper. QZSS offers in addition the standard positioning service also a Sub-Meter Level Augmentation Service (SLAS) and a Centimeter Level Augmentation Service (CLAS).

The QZSS satellites transmits signals very similar to GPS [Qua21a] on the L1, L2 and L5 bands. An additional LEX signal is also transmitted on the L6 band. The L1 band includes the L1 C/A and L1C codes like GPS, but also the L1SAIF signal. On the L2 band the data and pilot signals L2CM and L2CL are transmitted, and on the L5 band the L5I and L5Q data and pilot signals are transmitted. The LEX data and pilot signals on the L6 band are unique for QZSS and uses an exotic type of codes. The SAIF and LEX signals contain the data for the SLAS and CLAS services, respectively. SAIF (SLAS) is compatible with the GPS SBAS service and LEX (CLAS) will be compatible with the Galileo CS.

Table 2.11 QZSS signals

	Signals
Open Service	L1 C/A, L1C, L2C, L5
SLAS	L1SAIF
CLAS	LEX

2.2.6 Augmentation systems

SBAS are satellite systems that contain 1-3 GEO satellites and are designed to provide augmentation to the true navigation systems. SBAS satellites can in theory be used also for navigation, but in practice they are very seldom used in that capacity. Typically, transmitted data are differential corrections, integrity information and ionospheric correctional models. The satellites used are often commercial television or telecommunication satellites, where the SBAS part is a small separate payload.

Currently, there are six operational SBAS systems and a few more are planned for 2021-2022. A complete list is shown in table 2.12 and the status of the systems are shown in table 2.13

Table 2.12 SBAS systems

	System	Region
WAAS	Wide Area Augmentation System	USA
EGNOS	European Geostationary Navigation Overlay Service	Europe
SDCM	System for Differential Corrections and Monitoring	Russia
MSAS	Michibiki Satellite Augmentation System	Japan
GAGAN	GPS-aided GEO-Augmented Navigation	India
BDSBAS	BeiDou SBAS	China
KASS	Korea Augmentation Satellite System	South Korea
ASECNA	SBAS for Africa and Indian Ocean	Africa
SPAN	Southern Positioning Augmentation Network	Australia and New Zealand

Table 2.13 SBAS signals

	Constellation	Signals
WAAS	3 GEO	L1
EGNOS	4 GEO	L1
SDCM	3 GEO	L1
MSAS	2 GEO	L1, L5
GAGAN	3 GEO	L1, L5
BDSBAS	3 GEO	L1, L5
KASS	In development	
ASECNA	In development	
SPAN	In development	

3 FUNDAMENTALS OF GNSS POSITIONING

This chapter describes the fundamental concepts involved in GNSS positioning in more detail. Starting from the signal structure and continuing via the concept of auto correlation to the functions of the GNSS receiver all the way to the final Position, Velocity and Time (PVT) solution calculated by the receiver.

3.1 GNSS signals

Understanding the GNSS signal is the starting point for understanding the concept of GNSS positioning. The GNSS signal consists essentially of three components: The carrier, the spreading or ranging code, and the data bits. The spreading code may be a simple so-called pseudo random noise code, or it may be a more complex combination of multiple such codes. The data bits are not present in all signals.

3.1.1 Carrier Signal

In our world today more and more services are becoming wireless and for those services to work signals need to be transmitted and received over the air. To handle the increasing number of services and users and make sure that the signals do not interfere with each other, the International Telecommunications Union (ITU) [Int22] was founded already in 1865 to supervise the allocation of radio frequencies for all types of wireless services. Today, ITU is an agency with 193 member states within the United Nations.

For GNSS, there are two services defined. The Aeronautical Radio Navigation Service (ARNS) is defined by the ITU as «A radionavigation service intended for the benefit and for the safe operation of aircraft.» [Int16b]. This service is classified as a safety-of-life service, and it is therefore more protected against interference. The frequency bands reserved for ARNS are the upper L-Band 1559-1610 MHz and the

lower L-Band 1151-1214 MHz. The upper L-band includes all the GPS L1 signals, GLONASS L1 OF, Beidou B1, Galileo E1 signals and QZSS L1 signals and the lower L-band includes GPS L5, GLONASS L3OC, Beidou B2, Galileo E5, IRNSS L5 and QZSS L5 signals.

The Radio Navigation Satellite Services (RNSS) [Int16c] was introduced at the World Radiocommunication Conference in 2000 by the ITU and is defined as "a radiodetermination-satellite service used for the purpose of radionavigation. This service also includes the uplinks to the satellites necessary for their operation". The RNSS bands are partly overlapping with the ARNS bands: 1559-1610 MHz (same) and 1164-1215 MHz (ARNS is 1151-1214). In addition, the three bands 1215-1260 MHz, 1260-1300 MHz and 5010-5030 MHz were introduced.

The 1215-1260 MHz band contains the GPS, GLONASS and QZSS L2 signals and the 1260-1300 MHz band contains the Galileo E6, QZSS L6, and Beidou B3 signals. Mathematically, a GNSS carrier signals can be described as a sinusoidal signal with a frequency that falls into one of the bands allocated for GNSS. The bands are shown in figure 3.1 and the actual used carrier frequencies in GNSS are listed in table 3.1

Figure 3.1 GNSS frequency bands

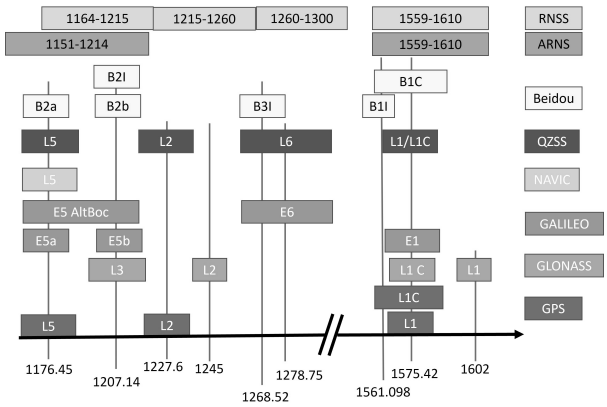

3.1.2 Ranging codes

Ranging codes are used to provide the accurate timing needed for calculating the ranges to the satellites. The ranging code is sometimes called a spreading code, since

Table 3.1 GNSS carrier frequencies. G:GPS, R:GLONASS, E:Galileo, C:Beidou, I:IRNSS, J:QZSS, D: Data, P: Pilot.

Frequency	Signals
1176.45	G: L5 I, Q; C: B2a D, P
	E: E5a I, Q;J: L5 I, Q; I: L5-SPS
1202.025	R: L3 OC D, P
1207.14	E: E5b I, Q; C:B2I
	C: B2b I
1227.6	G: L2 CM, CL; J: L2 CM, CL
	G: L2 P(Y)
	G: L2-M
1242-1249	R: L2 OF
1268.52	C: B3 I
1278.75	E: E6 B, C
1561.098	C: B1 I
1575.42	G: L1 C/A; E: E1 B, C
	C: B1C D, P; J: L1 C/A
	G: L1C D, P; J: L1C D, P
	G: L1 P(Y)
	G: L1-M
1598-1605	R: L1OF
2492.028	I: S5-SPS

the second purpose is to spread out the signal power over a larger frequency bandwidth making it less sensitive to narrowband interference and to mitigate interference from other GNSS signals. The spreading codes used to be simple sequences of -1 and 1 (so-called chips) in a seemingly random fashion, but in the modern signals they are often more complex.

Every satellite uses a unique spreading code that enables the receiver to identify from what satellite it originates. The exception is GLONASS FDMA signals where all satellites use the same code, but the carrier frequency is different for every satellite. The codes are generated in the satellites either by using suitable hardware or by prestoring the codes in memory and reading from there. The spreading codes need to

be selected so that the cross correlation between any two codes is minimized. A few different so-called families of codes are used in the different GNSS signals.

The most popular is the Gold Code [Gol67] family that was the one used already in the first GPS satellites. But the same family of codes is also used in the new GPS L5 signals, the Beidou B2 and B3 signals and the IRNSS signals. Gold codes are generated by Exclusive OR (EXOR):ing or modulo-2 adding two Maximum Length (ML)- or m-sequences [Zie59] of the same length. In the GNSS satellites the m-sequences are generated by two Linear Feedback Shift Registers (LFSR) and the outputs are modulo-2 added together. If the shift registers are designed in the right way the resulting Gold Codes have even better cross correlation properties than the original m-sequences.

M-sequences are used as such in for example the Galileo E5 signals and the GLONASS FDMA L1 and L2 open signals. The Kasami codes [Kas66] used in the new GLONASS L3 CDMA signals are also constructed from an m-sequence. A Kasami code is generated by combining a single m-sequence with a decimated and shifted version of the original sequence. For the Galileo E1 and E6 B and C signals, randomly generated codes are used. For longer code sequences it has been shown that the Weil codes [Rus06], which are based on a Legendre sequence, have better cross-correlation properties than the Gold codes [Rus07]. Weil codes are used in the new GPS L1C signal and Beidou's B1C signal.

There are a handful of ranging code lengths. A length of 1023 chips are perhaps the most common, but we also see lengths of 511, 2046, 4092, 5111, and 10230 chips. The duration varies between the most common one ms to one week for some of the signals intended for authorized users only. The Weil and Random codes are generated in software and the rest in hardware. The chipping rate and code length for each family of codes used for the different GNSS signals are listed in table 3.2

3.1.3 Secondary Codes

Many of the new GNSS signals have introduced so-called secondary codes or overlay codes. Such signals are for example the GPS L1C and L5, the GLONASS L3OC, several of the new Beidou signals and the Galileo's E5 signals. Secondary codes consist of chips that are a multiple of code lengths long, so they are always synchronized with the ranging code. Lengths range from one code epochs in the GPS L1C D signal

Table 3.2 GNSS spreading codes. G:GPS, R:GLONASS, E:Galileo, C:Beidou, I:IRNSS, J:QZSS, D: Data, P: Pilot.

Family	Length (chips/ms)	Rate (ms)	Signals
Gold	511.5	1.5	G: L2 CL
Gold	511.5	20	G: L2 CM
Gold	1023	1	G: L1 C/A ;I: L5-SPS;S5-SPS; J: L1 C/A
Gold	2046	1	C: B1I,B2I
Gold	10230	1	G: L5 I, Q; C: B2a D, P;B2b I;B3I
Random	4092	4	E: E1 B, C
Random	5115	1	E: E6 B, C
m-sequence	511	1	R: L1 OF;L2 OF
m-sequence	511.5	1.5	J: L2CL
m-sequence		20	J: L2 CM
m-sequence	10230	1	E: E5a I, Q; E5b I, Q; J: L5I
Kasami	10230	1	R: L3 OC D, P
Weil	1023	10	G: L1C D, P
Weil	10230	10	C: B1C D, P; J: L1C D, P

to 1000 code epochs for the GPS L5 signals.

There are three reasons for why secondary codes have become so popular. They make receivers more robust against narrowband interference, they make it easier to find the data bits, and they reduce the cross-correlation power between different signals. Unfortunately, secondary codes also result in more complex signal processing in the receiver. The types of secondary codes used in GNSS are listed in table 3.3

For the GPS L1C signal, the overlay codes are either truncated m-sequences or truncated Gold Codes selected to have the best possible performance [Rus07]. Each bit is 10 ms long and the codes are 1800 bits, giving a total length of 18 seconds. The codes are generated using Hardware (HW) shift registers.

For the GPS L5 signals, the NH codes are used. The length is either 10 or 20 bits and the code rate is one kHz. That means that each NH bit includes 1000 code epochs. Similar kind of approaches are used for the GLONASS L3 OC P, Beidou B1I, B2I, B3I, and the QZSS L5 signals. For the GLONASS L3 OC Data signal, a

Table 3.3 GNSS secondary codes. G:GPS, R:GLONASS, E:Galileo, C:Beidou, I:IRNSS, J:QZSS, D: Data, P: Pilot.

Type	Length (bits)	Rate (bits/s)	Signals
HW	1800	100	G: L1C D, P;J: L1C P
NH	10	1000	G: L5I; R: L3OC P; J: L5 I, Q
NH	20	1000	G: L5Q;C D1: B1I;B2I;B3I
Weil	1800	100	C: B1C P
Weil	100	1000	C: B2a P
Barker Code	5	1000	R: L3OC D
Fixed	5	1000	C: B2a D
Memory	25	250	E: E1-C
Memory	20	1000	E: E5a-I
Memory	100	1000	E: E5a-Q; E5b-Q; E6-C
Memory	4	1000	E: E5b-I

Barker Code [Bar53] with a length of five bits and a rate of one kHz is used. Beidou B1C Pilot and B2a Pilot uses a Weil code as the overlay code and the B2a Data signal uses a fixed five-bit sequence of 00010 running also at a bit rate of one kHz. The Galileo secondary codes are all random memory codes defined in the ICD of Galileo. The L1C Overlay codes (L1CO) used in the QZSS L1C Pilot signal are generated by HW shift registers, and they are 1800 bits long transmitted at 10 kHz.

3.1.4 Navigation Data

All signals except the Pilot signals contain data bits, which are grouped together to form words, pages, and frames. The naming of these is different for different systems, but the basic concept is the same. These data bits can then be decoded by the receiver into useful information for each satellite and for the whole GNSS system. This decoded data is called the navigation data.

When the receiver decodes this navigation data, errors may occur. These so-called bit errors can cause severe errors in the receiver and to mitigate these, different kind of methods are used in the signals to protect against bit errors. The legacy GPS L1

signal for example includes a six bit parity number at the end of each data frame, but for modern signals techniques such as Cyclic Redundancy Check (CRC), block interleaving and Forward Error Correction (FEC) [Ham50] are used.

FEC means that one data bit is represented by multiple symbols. In GNSS typically two symbols equal one data bit and therefore the symbol bit rate is not the same as the data bit rate. The satellites need to transmit two symbols for each bit in this case. Block interleaving means that the data is separated into blocks and transposed before transmitted. If the data transmission is disrupted, the errors after deinterleaving will then be spread out over the data and not consecutive. Finally, a calculated CRC value is included in the data to allow for error correction and data validation.

Different signals transmit different types of navigation data, and sometimes they are referred to by a specific name, like CNAV or LNAV. The content is very similar, but exact representation may be different in the different types. The different types, symbol rates and error correction methods are listed in table 3.4

The navigation data can be divided into components. The smallest one is often called a data word, and several words makes a page, several pages make a frame etc. An example for the Galileo F/NAV message is shown in figure 3.2

Figure 3.2 Galileo F/NAV navigation message

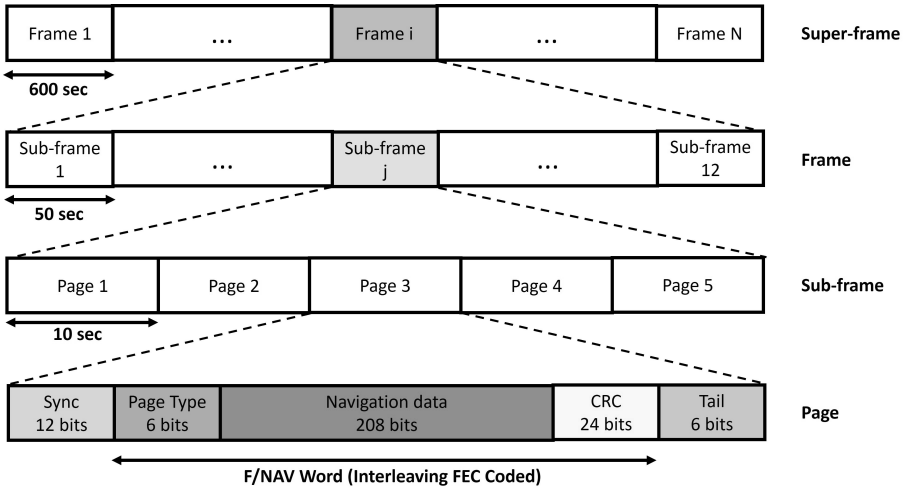

Once the navigation data has been obtained, it can be split into ephemeris data and almanac data. The ephemeris data is different for every satellite and updated every two to four hours. Ephemeris data contain satellite clock correction coefficients,

Table 3.4 GNSS navigation data. G:GPS, R:GLONASS, E:Galileo, C:Beidou, I:IRNSS, J:QZSS, D: Data, P: Pilot.

Msg Type	Rate (sps)	Signals
LNAV	50	G: L1 C/A; J: L1 C/A
CNAV	50	G: L2 CM; J: L2 CM
CNAV	100	J: L5I
CNAV-2	100	G: L1C D; J: L1C D
L5 CNAV	50	G: L5I
Nav Data	50	R: L1OF;L2OF
		I: L5-SPS;S5-SPS
Nav Data	100	R: L3OC D
B-CNAV1	100	C: B1C D
B-CNAV2	200	C: B2a D
B-CNAV3	1000	C: B2b I
D1	50	C: B1I;B2I;B3I
D2(GEO)	500	C: B1I;B2I;B3I
I/NAV	250	E: E1-B;E5b-I
F/NAV	50	E: E5a-I
C/NAV	1000	E: E6-B

orbital parameters, age of data, satellite accuracy estimates and health status for one satellite, and it is repeated every 12–30 seconds depending on constellation.

The almanac data contains less accurate orbital information for all the satellites in the constellation, and it is used for predicting where satellites signals can be found. This data is valid for months, and it is transmitted with a much lower rate by changing the bits in some of the subframes for every transmitted frame. Data needed for conversion between time domains and correcting for ionospheric delay may also be included in the almanac data. The exact implementation may differ between constellations.

The GNSS satellite orbits are defined by the six Keplerian elements included in the ephemeris data: Eccentricity, Semi Major Axis, Inclination, Longitude of the ascending node, Argument of periapsis and True anomaly. True anomaly is a function

of time and defines the position of the satellite on the orbit, so when time is known the satellite position can be calculated. The satellites are, however, disturbed in their orbits and therefore six additional perturbation parameters are also provided in the ephemeris data. The satellite clocks are highly accurate and adjusted from time to time, but there remains an error and to correct for this a simple correctional model with three parameters is broadcasted as part of the ephemeris data.

3.1.5 Modulation and Mixing

Mixing can be defined as an addition of any two signals into one single output signal, whereas modulation, which is a type of mixing, usually requires that one of the signals is a periodical carrier signal of some sort and the other signal carries some sort of information with it. The terms mixing and modulation are sometimes used incorrectly when describing GNSS signals.

Previously we have described that the GNSS signals consist of multiple components: The ranging code, the navigation data bits in the data signals, a possible secondary code, and the carrier signal itself. The codes and data bits are all mixed together by modulo-2 addition (or Exclusive OR (XOR)) of the 0's and 1's resulting in a pseudo random sequence similar to the original sequence. With no secondary code and no data bits, the result is simply the ranging code itself. This mixed code is then modulated on the carrier signal to form one single signal that is transmitted from the satellites.

There are hundreds of different types of mixing and modulation presented in communication theory, but in GNSS only six different main types are used. Binary-Phase-Shift-Key (BPSK), BOC, three variants of Multiplexed BOC (MBOC) and AltBOC. The simplest one, that also was the first one used in the legacy GPS L1 and L2 signals, is the BPSK modulation. BPSK is still used in two thirds of the GNSS signals, so it is still the most used modulation technique. The principle of BPSK is simple. The mixed code is modulated onto the carrier signal so that whenever the chip flips, the phase of the carrier signal is rotated 180 degrees. The process is illustrated in figure 3.3

Four different rates of BPSK are used in GNSS: BPSK(0.511), BPSK(1), BPSK(2) and BPSK(10) where the number simply indicates the chipping rate of the ranging code in multiples of the fundamental GNSS frequency of 1.023 MHz. BPSK(2) then

Figure 3.3 Mixing and modulation of the GPS L1 signal

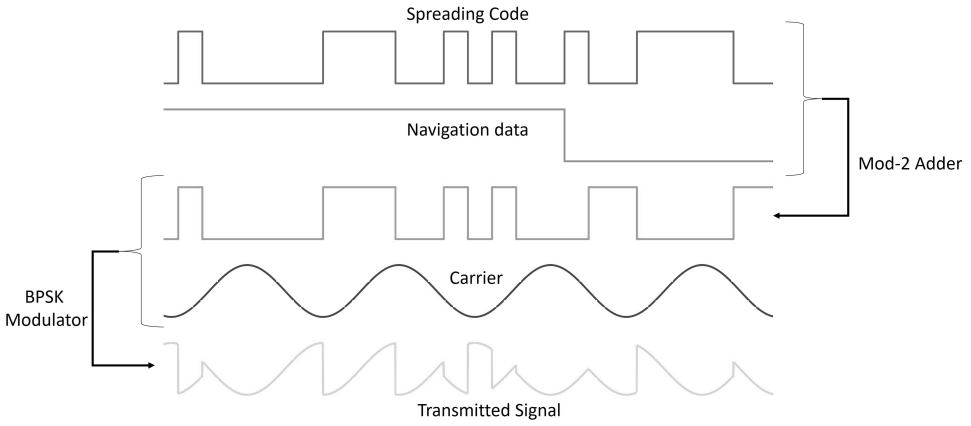

means that the chipping rate is 2 x 1.023 MHz = 2.046 MHz.

In addition to BPSK, five different types of BOC [Bet01; Gre06; Lo 06] techniques are used. BOC modulation was developed to improve inter-operability of the GNSS systems. The idea was to shift the Power Spectral Density (PSD) away from the center frequency to avoid overlapping signals. In the time domain, the principle of BOC modulation is to split each of the ranging code chips into a sequence of +1 -1 +1 -1 etc. The BOC signal can be considered as a sine or cosine waveform and the +1 and -1:s the sign of that waveform. The number of +1 and -1:s for each chip is defined by the two numbers m and n in the notation $BOC(m,n)$ and the order of the BOC modulation N_B is defined as:

$$BOC(m,n) \text{ order} = N_B = 2 * \frac{m}{n} \tag{3.1}$$

This BOC modulation is often referred to as the sub carrier with frequency f_{sc}. The number n then defines the frequency of the ranging code f_c and the number m the frequency of the sub carrier f_{sc} according to

$$f_c = n * 1.023MHz \tag{3.2a}$$

$$f_{sc} = m * 1.023MHz \tag{3.2b}$$

Depending on if we have cosine or sine BOC, the phase of the sub carrier is differ-

ent. The mathematical expressions for the $CosBOC$ signal $S_{CosBOC}(t)$ as a function of time t is

$$S_{CosBOC}(t) = sign\left(cos\left(\frac{N_B \pi t}{T_c}\right)\right) \tag{3.3}$$

where T_c is the length of one period of the subcarrier. The $CosBOC$ signal for N_B equal to 2,3 and 4 is shown in figure 3.4

Figure 3.4 CosBOC modulation for N_B equal to 2,3 and 4

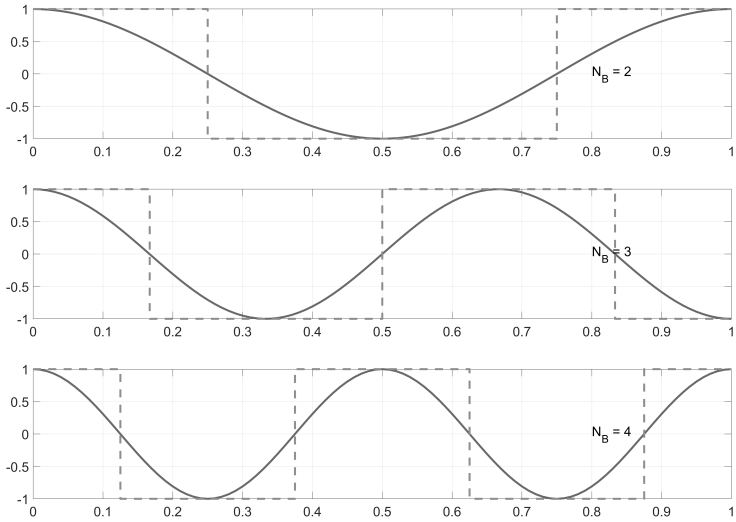

For $SinBOC$ the Cos function is just replaced by the Sin function. This extra BOC modulation will, when mixed with the spreading code and the carrier, result in a split of the PSD with lobes symmetrical placed on both side of the center frequency when it is modulated onto the carrier signal. An example of the GPS L1 BPSK(1) and Galileo E1 BOC(1,1) PSD is shown in figure 3.5

Three GNSS signals today use simple BOC modulation: GPS L1C Data, Beidou B1C Data and QZSS L1C Data. The other modulation types are derivatives of the BOC modulation. Time Multiplexed BOC (TMBOC), Composite BOC (CBOC) and Quadrature Multiplexed BOC (QMBOC) are all different types of MBOC.

MBOC [Hei06] is a technique where two different BOC signals are multiplexed, or combined, together in a pre-defined way. In GNSS the two BOC signals Sin-

Figure 3.5 PSD for GPS L1 BPSK and Galileo E1 BOC(1,1) signals

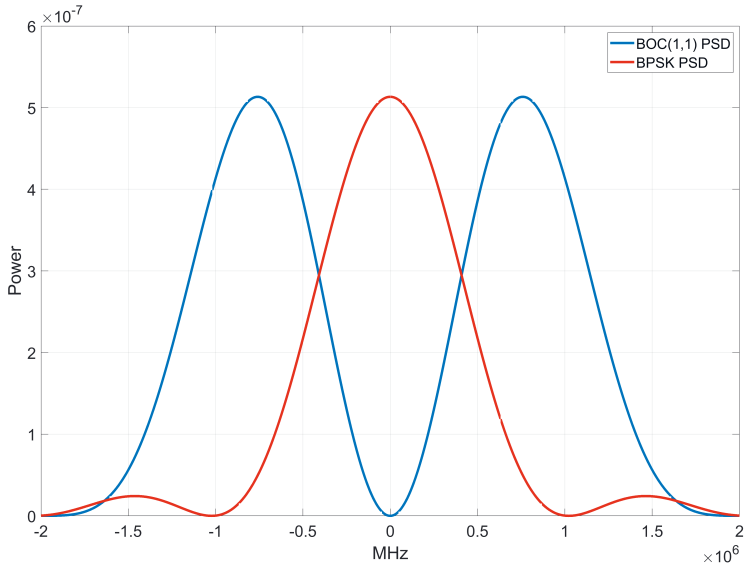

BOC(1,1) and SinBOC(6,1) are used in all MBOC modulation schemes. The reason for this is to firstly allow for a more accurate and multipath resilient tracking due to high frequency component, but still also being backwards compatible with the BOC(1,1) signal. Receivers can use only the BOC(1,1) replica signal for all operations if needed. The penalty from the power in the BOC(6,1) signal is relatively small.

For the CBOC [Avi06] that are used in the Galileo E1 OS they are combined by weighing their contribution so that 10/11 of the PSD is on the BOC(1,1) and 1/11 of the PSD in the BOC(6,1). The PSD as a function of frequency f of CBOC [Jul07] is given by

$$PSD(f) = \frac{10}{11} PSD_{BOC(1,1)}(f) + \frac{1}{11} PSD_{BOC(6,1)}(f) \tag{3.4}$$

where $PSD_{BOC(1,1)}(f)$ and $PSD_{BOC(6,1)}(f)$ is the PSD of $BOC(1,1)$ and $BOC(6,1)$. For the TMBOC [Avi07; Bet06] used in the GPS and QZSS L1C Pilot signal the same two SinBOC signal are used. On the Data signal only the BOC(1,1) component is used, but on the pilot signal BOC(1,1) is used for 29/33 part of the time and the higher frequency BOC(6,1) for 4/33 parts of the time. This approach is used since data demodulation does not benefit from the high frequency BOC(6,1), but

tracking does.

Finally, the QMBOC [Lu 10] used in the Beidou B1 Pilot signal is also part of the MBOC family. In QMBOC the same two BOC signals are used, but they are modulated on separate orthogonal I and Q components. The QMBOC signal $S_{QMBOC}(t)$ as a function of time t can be expressed as:

$$S_{QMBOC}(t) = \alpha S_{BOC(1,1)}(t) + \beta S_{BOC(6,1)}(t) \tag{3.5}$$

where $S_{BOC(1,1)}(t)+S_{BOC(6,1)}(t)$ are the $BOC(1,1)$ and $BOC(6,1)$ signals and α and β are coefficients. The AltBOC(15,10) modulation [Les08] that is used for the Galileo E5 signals is not an MBOC technique, and it is perhaps the most complex type of modulation used in GNSS. In short, the sub-carrier is here a complex signal, and it is multiplexed not with one single code, but with different codes for the two components. To further complicate it data and pilot components can also be introduced with different codes to generate four signals altogether. The signal $S_{AltBOC}(t)$ as a function of time t can be written as:

$$S_{AltBOC}(t) = \left(C_L^D + jC_L^P\right)c_s(t) + \left(C_U^D + jC_U^P\right)c_s^*(t) \tag{3.6}$$

where C_L^D and C_L^P are the codes for the lower band Data and Pilot signals, C_U^D and C_U^P are the codes for the upper band Data and Pilot signals and c_s is defined as a function of the subcarrier frequency f_{sc} as

$$c_s(t) = sign[cos(2\pi f_{sc}t)] + jsign[sin(2\pi f_{sc}t)] \tag{3.7}$$

and $c_s^*(t)$ the complex conjugate of that. The 4 components of the AltBOC(15,10) signals can be processed separately by the receiver as BPSK(10) modulated signals.

A list of signals and the modulation types are shown in table 3.5

3.1.6 Signal Power

The GNSS signals that were described in the previous chapter are transmitted by the satellites. For the GPS L1 C/A signal the transmission power depends on the satellite generation, but some sources list 27 W at the satellite antenna input for GPS satellites in 2005 and an Antenna gain of 12.9 dB for moderate satellite elevation angles [Mis06]. Converting the transmission power into a logarithmic scale using

Table 3.5 GNSS modulations. G:GPS, R:GLONASS, E:Galileo, C:Beidou, I:IRNSS, J:QZSS, D: Data, P: Pilot.

Modulation	Signals
BPSK(1)	G: L1 C/A;L2 CM/CL;I: L5-SPS;S5-SPS
	J: L1 C/A;L2 CL/CM
BOC(1,1)	G: L1C D; C: B1C D;J: L1C D
TMBOC(1,6,1/11)	G: L1C P
BPSK(10)	G: L5 I/Q; R: L3OC D/P; C: B2a D/P;B2b I;B3I
	J: L5 I/Q
BPSK(0.511)	R: L1OF;L2OF
BPSK(2)	C: B1I;B2I
QMBOC(6,1,1/11)	C: B1C P
CBOC(6,1,1/11)	E: E1-B/C
AltBOC(15,10)	E: E5a-I/Q;E5b-I/Q
BPKS(5)	E: E6-B/C
TMBOC	J: L1C P

equation 3.8

$$\text{Power in dBW} = 10 \times \log_{10}(\text{Power in Watt}), \tag{3.8}$$

and adding the antenna gain gives an antenna output power of 27.2 dBW. When the signal travels through space it will experience the free space path loss $FSPL$ in dB according to equation 3.9

$$\text{FSPL(dB)} = 10 \times \log_{10}\left(\left(\frac{4\pi d f}{c}\right)^2\right) \tag{3.9}$$

where d is the distance travelled, f is the frequency and c is the speed of light in vacuum. For GPS L1, where $f = 1575.42\ MHz$, $d = 20000\ km$, and $c = 2.99793e8\ \frac{m}{s}$ we get $FSPL = -182.4\ dB$. This gives the received signal power

$$\text{Received Signal Power} = 27.2\ dBW - 182.4\ dB = -155.2\ dBW \tag{3.10}$$

The thermal noise N_T at the antenna for a four MHz bandwidth at room temperature (290 K) can be calculated using

$$N_T(4MHz) = k \times T \times BW = 1.3803 \times 10^{-23} \times 290 \times 4 * 10^6 = 1.6 \times 10^{-14}\ W \quad (3.11)$$

where k is Boltzmans constant, BW is the bandwidth and T is the temperature. By using equation 3.8 we get $-138\ dBW$. By comparing to equation 3.10 we see that the received power is actually 17.2 dB below the thermal noise floor and not visible using any conventional spectrum analyzer.

The tasks of the receiver are then to amplify this very weak signal, lock onto it and its ranging code, decode the data embedded in the signal and from this information extract a PVT solution for the user. Next the fundamental elements of this process are described.

3.2 GNSS Receiver

Most GNSS receivers consist of an antenna, an analogue part, and a digital part. A GNSS antenna is needed to convert the received radio signal into an electrical signal at the input of the analogue part, often referred to as the receiver RF Front End. This RF Front End down converts the signal to an intermediate frequency and converts it into a digital signal. The digital signal is then processed by the digital part generating raw observations and a PVT solution is outputted to the user.

3.2.1 Receiver antenna

Antennas can be classified into active or passive antennas. An active antenna includes an integrated Low Noise Amplifier (LNA) and amplifies the signal significantly, but needs to be supplied with power in order to work. The benefit of an active antenna comes from the fact that the dominating component when calculating the system noise is the first element in the chain provided it has high gain and a low noise figure. With an active antenna, cable loss does therefore not impact the performance and the antenna does not have to be close to the RF front end. A passive antenna implies that it does not have an integrated LNA. Passive antennas therefore only have a so-

called passive gain, i.e., they will amplify the signal only because of their directivity. Passive antennas are often used only in devices where the antenna is very close to the RF front end. The most important parameters for an antenna are size, quality, bandwidth and antenna gain. The simplest antennas are dipole antennas, monopole antennas, helix antennas and loop antennas.

The optimal bandwidth of an antenna depends very much on what signals are planned to be received. For GPS L1 C/A receivers a bandwidth of 10-20 MHz is sufficient. Such an antenna can also receive the new L1C signal and Galileos E1 band. If you would need a single antenna that could receive all GNSS bands the bandwidth would need to be 450 MHz (from L5 1164 MHz to GLONASS 1610 MHz). This is, however, not practical since the noise will increase as a function of the bandwidth and there are several frequency areas that does not contain any signals. Multi signal antennas therefore often consist of several antenna elements instead of one single element, one for each GNSS frequency band.

The most common type of GNSS antenna is by far the patch antenna, which is a micro-strip antenna. The patch antenna is made up of a substrate with a high dielectric constant, a metallic ground plane at the bottom of the substrate, a patch element on top of the substrate and a feed line through the element. A cross-section of such an antenna is shown in figure 3.6

Figure 3.6 Cross-section of a patch antenna

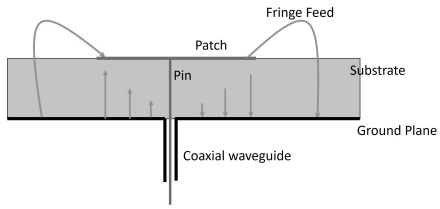

The thickness of the substrate, the size of the antenna, the size of the ground plane and the size and shape of the patch element impact such factors as bandwidth, impedance matching, radiation pattern and gain of the antenna. The most common size is 25 x 25 mm^2 with a thickness of 4-7 mm. More info on patch antennas can be found in [Ary15; Moe09; Orb09; Pan12; Yeg18]. Some typical patch antennas with and without casing are shown in figure 3.7

The gain of any antenna can be improved by introducing a ground plane beneath them. The ground plane will impact the radiation pattern of the antenna and increase

Figure 3.7 GNSS patch antennas

the gain in the upwards direction. For a passive dipole antenna, the gain can be increased from 2dB to around 5dB.

The antenna phase center is the point of the antenna where the electromagnetic signal is received. The location of this point may vary depending on the elevation and azimuth angle of the incoming signal and the received frequency. For high quality antennas this so-called antenna Phase Center Variation (PCV) is kept as small as possible. High quality antennas are also calibrated, and the location of the phase center is marked on the antenna. It is worth mentioning that the phase center may be outside the physical antenna and that for similar types of antennas the phase centers are not necessarily at the same point.

3.2.2 Receiver RF front end

The front end is divided into three parts. The RF part with amplifiers and filters, the Intermediate Frequency (IF) part or down converter that mixes the signal down from the GHz range to the MHz range and the baseband part converting the signal to a digital signal and splitting it into I and Q parts. An Automatic Gain Control (AGC) unit is often also added to increase the dynamic range of the front end. This Gain Control can be either analogue or digital. An overview of the antenna connected to the RF front end is shown in figure 3.8

The IF part uses a reference oscillator and a frequency synthesizer to generate a carrier signal close the incoming GNSS carrier signal. By multiplying this signal

Figure 3.8 GNSS antenna and receiver front end

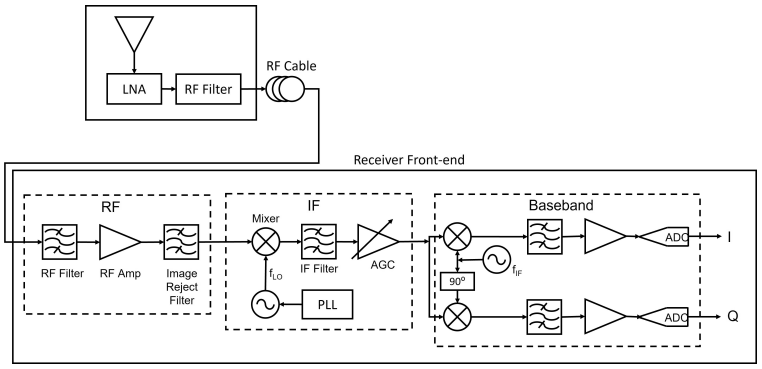

with the GNSS signal a delta signal S_{out} will be generated

$$S_{out} = \frac{A(t)A_{L0}}{2} \times (cos((f_{L0}+f)t+\phi(t)) + cos((f_{L0}-f)t+\phi(t))) \qquad (3.12)$$

where $A(t)$ is the incoming signal amplitude as a function of time t, A_{L0} is the amplitude of the locally generated signal, f_{L0} is the locally generated signal frequency, f is the incoming signal frequency and $\phi(t)$ is the phase difference between the two signals also as a function of time. A low pass filter is added to filter out the high frequency component from S_{out} and the IF is then $IF = (f_{L0}-f)$. In the baseband part the signal is mixed again with two signals generated from the reference clock with a phase shift of 90 degrees. The result is two signals, the I, and the Q signal. Both of these are then passed through an Analog to Digital Converter (ADC) generating a 1-16 bit output value as a function of the input voltage. Cheap consumer grade receivers often use two-bit ADC's whereas geodetic grade receiver may use eight bits or even 16-bit ADC's. In some receivers the AGC is implemented after the ADC. The digital signal is then passed on to the baseband processing unit that is purely digital.

3.2.3 Baseband processing

The last step in the processing chain in a GNSS receiver is often referred to as the baseband ASIC. In a traditional receiver the baseband ASIC is a chip consisting of an application processor, some memory, and some dedicated HW modules for commu-

nication (Universal Asynchronous Receiver Transmitter (UART), Serial Peripheral Interface (SPI)) and signal processing (correlators, acquisition engine). The tasks of signal acquisition, code and carrier tracking, decoding the navigation data, pseudo range calculations (measuring satellite-to-user distances) and a navigation filter to calculate the user position are all executed in the baseband ASIC. This is shown in figure 3.9.

Figure 3.9 GNSS receiver baseband tasks

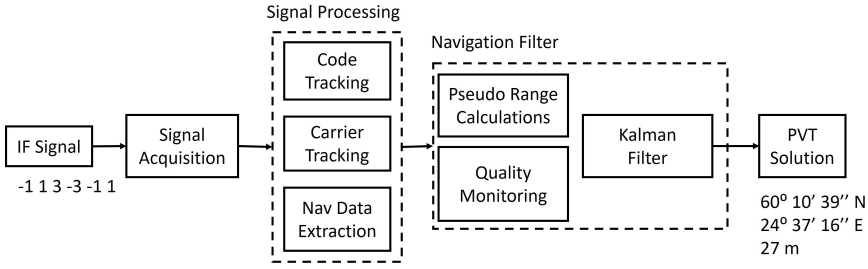

The interface between the HW on the ASIC and the software running on the application processor determines what type of receiver it is [Söd08]. In a traditional receiver the signal processing part is controlled by software on the application processor but performed by HW blocks. In a software defined receiver, the signal processing is also done in software eliminating the need for HW specific blocks for that. That also means that an ASIC is not strictly needed and the GNSS software part can be executed on any generic application processor. An intermediate solution would be to have an ASIC running only the signal processing blocks without any processor and all the software would instead be run on a generic application processor. This approach is usually referred to as a measurement frontend receiver. The motivator for not having a full GNSS ASIC is the reduced size and cost if an external host CPU can be utilized. The different types of receiver architectures are shown in figure 3.10

3.2.3.1 Auto correlation function

We have described what the GNSS signals look like, how they are mixed and transmitted from the satellites and how they are converted to a digital signal in the receiver. We have also described, in section 3.1.6, that the signal power at the input of the receiver is significantly lower than the thermal noise floor and not visible to the receiver. To solve this weak signal problem and to extract the observables in the

Figure 3.10 GNSS receiver types

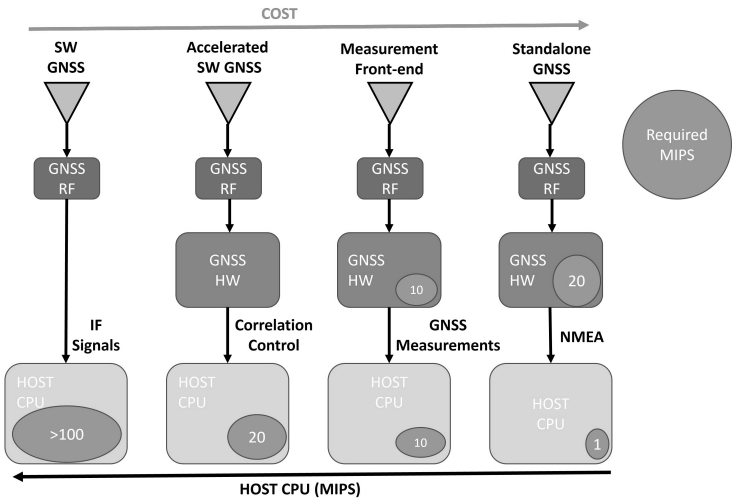

receiver the process of auto correlation is used.

To be able to do auto correlation the same signals are generated in the receiver as in the satellites with some differences: The frequency is now the IF and not in the GHz range and the navigation data and secondary codes are seldom generated. This so-called replica signal is then mixed or correlated with the incoming signal from the satellites and an Auto Correlation Function (ACF) is generated. The ACF for a generic GNSS signal with BPSK or BOC modulation can be defined by introducing the concept of DBOC [Loh06], a combination of two BOC modulated signals with orders N_{B_1} and N_{B_2}. The ACF then becomes

$$ACF(\tau) = \Lambda_{T_B}(\tau) \circledast \sum_{k=0}^{N_{B_2}-1} \sum_{j=0}^{N_{B_2}-1} \sum_{i=0}^{N_{B_1}-1} \sum_{l=0}^{N_{B_1}-1} (-1)^{k+i+j+l} \times \delta\left(\tau - iT_{B_1} + lT_{B_1} - kT_B + jT_B\right) \tag{3.13}$$

where $\Lambda_{T_B}(\tau)$ is the triangular pulse of support $2T_B$, and T_{B_1} is the period of the BOC modulation on signal 1. T_B is defined as

$$T_B = \frac{T_C}{N_{B_1} N_{B_2}} \tag{3.14}$$

where T_C is the chip period.

Depending on the factors N_{B_1} and N_{B_2} we can obtain the ACF for all SinBOC, CosBOC and BPSK signals as

$$\begin{cases} N_{B_1} = 1 \, and \, N_{B_2} = 1, \, BPSK \\ N_{B_1} > 1 \, and \, N_{B_2} = 1, \, SinBOC \\ N_{B_1} > 1 \, and \, N_{B_2} = 2, \, CosBOC \\ N_{B_1} > 1 \, and \, N_{B_2} > 1, \, Higher \, order \, BOC \end{cases} \tag{3.15}$$

The auto correlation provides a gain of up to 60 dB and that will bring the incoming signal above the noise floor (see equation 3.10 and 3.11).

3.2.3.2 Signal acquisition

The signal acquisition process in a receiver is the process to find the signals. The process includes configuring the replica signal (code, modulation, frequency, time, length, etc.), initializing proper hardware with this configuration, executing the auto correlation, and reading the output of the process. The acquisition process for GPS L1 C/A with a 20 ms long data bit normally uses a 1-20 ms long part of a signal and therefore in most cases the longer navigation data bits and the secondary code chips are not needed in the replica signal. For other signals with shorter navigation data bits the situation might be different.

Once the spreading code has been selected the process then reduces to defining the carrier frequency and the exact time or starting point of the code in the selected part of the signal, i.e., the code phase. For the carrier frequency there is a large uncertainty depending on satellite movement, user movement and uncertainty in the receiver clock drift. The signal transmitted by the satellites has the carrier frequency listed in table 3.1, but since the satellites are moving at a speed of up to 14000 km/hour or 3.8 km/sec the Doppler effect will shift the carrier frequency seen by the receiver according to equation 3.16

$$f' = \left(\frac{c \pm v_{rx}}{c \pm v_{sv}} \right) \times f, \tag{3.16}$$

where f is the transmitted frequency, f' is the received frequency, v_{rx} is the receiver velocity, v_{sv} is the satellite velocity, and c is the speed of light. The Doppler

shift Δf is defined by equation 3.17

$$\Delta f = f' - f, \tag{3.17}$$

of a typical GNSS signal is between -4 kHz and +4 kHz. In some cases, we can calculate the velocity of the satellites and therefore reduce the Doppler uncertainty assuming the user position and velocity is known.

One additional contributor to the uncertainty of the received frequency comes from the fact that the receiver clock frequency is not necessarily known. This clock is used to generate the signal in the radio front end that is used to down convert the incoming signal to the IF signal according to equation 3.18

$$IF = f - K \times f_{tcxo}, \tag{3.18}$$

where f is the frequency of the incoming signal, K is a constant and f_{tcxo} is the frequency of the Temperature Controlled Crystal Oscillator (TCXO) in the receiver. With a TCXO frequency of 16.368 MHz and a constant K of 96 the IF becomes:

$$IF = 1575.42 - 96 \times 16.368 = 4.092 MHz, \tag{3.19}$$

which is a very typical TCXO frequency and front-end configuration. The TCXO is, however, temperature dependent and the frequency might be off by as much as 0.5 ppm resulting in a frequency offset of eight Hz in either direction. Looking at equation 3.18 we see that the IF then will be shifted by $\pm$ 800 Hz. Even though the TCXO crystals have been artificially aged there is also still the fact that their frequency will slowly change over time resulting in an even bigger uncertainty window for the search process.

Fortunately the TCXO frequency can be calculated when we have a navigation solution, and we can even measure the temperature of the TCXO in some receivers and compensate for that so in the best case the uncertainty of the TCXO frequency can be reduced significantly. The resolution typically used for a carrier frequency search varies between 25-500 Hz.

To find the code phase the code needs to be known and for the open signals this is the case. The current phase is found by searching through all the code phases with a typical resolution of 0.5 chips. For each supported code, the receiver has to search through all possible combinations of carrier frequencies and code phases in order to

find that specific signal and this process is then repeated for every code. This three-dimensional search process for each signal is indicated in figure 3.11

Figure 3.11 Three-dimensional signal search

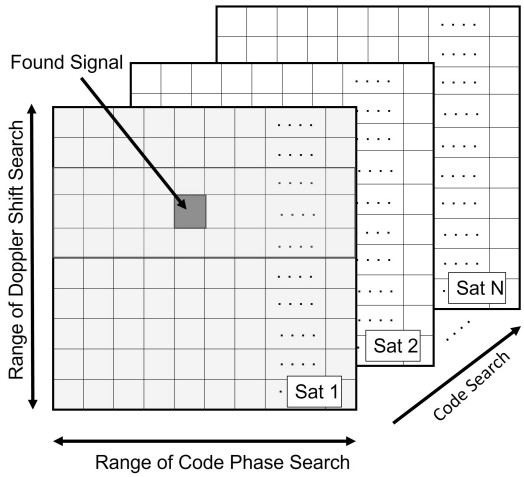

For a receiver supporting all the codes listed in table 3.2 that is a significant and time-consuming task.

In practice most ASICs have a hardware acquisition block that uses one full code epoch and all code delays are searched for automatically for a given carrier frequency. This is done using either Fourier Transforms or Matched Filter techniques. The output of the acquisition is then the correlation amplitude for every code chip value used in the process. If the amplitude for one code chip value exceeds a pre-defined threshold a signal is considered being found.

If only one full code epoch of the GPS L1 C/A signal or 1 ms is used the signal needs to be approximately 42 dBHz to ensure a detection probability of more than 50 % [Mer20]. To increase the receiver acquisition sensitivity multiple outputs from a one epoch correlation need to be added together. This can be done coherently or non-coherently. So-called coherent integration means the output from every correlation is added together directly and non-coherent integration means the results are squared before the addition. This is illustrated in figure 3.12

The more epochs that are added the higher the acquisition gain becomes, and weaker signals can be detected. The problem with coherent integration is the data bits and secondary codes. They are often not present in the replica signal, and they may both change from -1 to +1 or vice versa in the satellite signal and that means

Figure 3.12 Coherent and non-coherent integration in signal acquisition

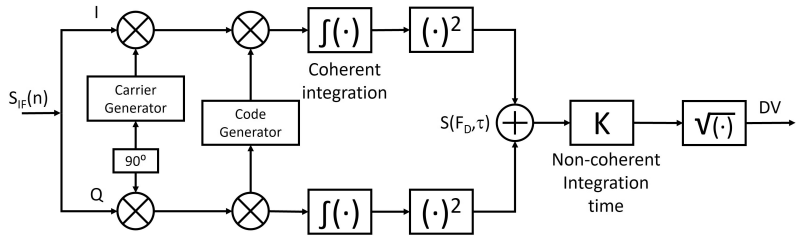

that the sign of the auto correlation result will also change and if we continue to add these together the total amplitude will start to decrease. It is therefore important that coherent integration is only done within one data bit and within one chip of a secondary code or that these are known.

The introduction of pilot signals with no data bits was partly done to mitigate this limitation of coherent integration time. For non-coherent integration, the result of the auto correlation is squared before the addition ensuring that the sign of the result is always positive. The penalty is that the noise will increase more from the squaring process than it does in the coherent integration. The number of coherent and non-coherent integration rounds are often configuration parameters for the signal acquisition block.

When all the integration rounds have been executed it is then up to the detection algorithm to compare the maximum value to some pre-defined baseline and decide if a signal has been found. The output from the signal acquisition is noisy and different kinds of detection logic have been proposed [Kap17]. The selected detection algorithm is often a compromise that minimizes the probability of a false alarm and the probability of a missed detection while providing a good sensitivity (weak signals can be detected).

3.2.4 Tracking the signals

Signal tracking also uses the concept of autocorrelation like acquisition. When the acquisition has found a signal, it will provide the carrier frequency and code phase to the tracker which will then try to keep the alignment between the signal and the replica by continuously updating these. This is done using a set of correlators. Each tracking channel has three or more correlators for both the I and the Q signals. These

correlators are often also referred to as fingers. Each finger in a tracking channel uses the same replica signal, but with a slightly different code phase. The difference in code phase between the fingers are typically 0.1 - 0.5 code chips and this is often referred to as the correlator finger spacing. In a three + three finger configuration the code phase from the acquisition is used to set the phase for the two middle fingers and the four other fingers are then set on both sides of these fingers. A typical six finger non-coherent tracking architecture is shown in figure 3.13

Figure 3.13 Six finger non-coherent tracking architecture

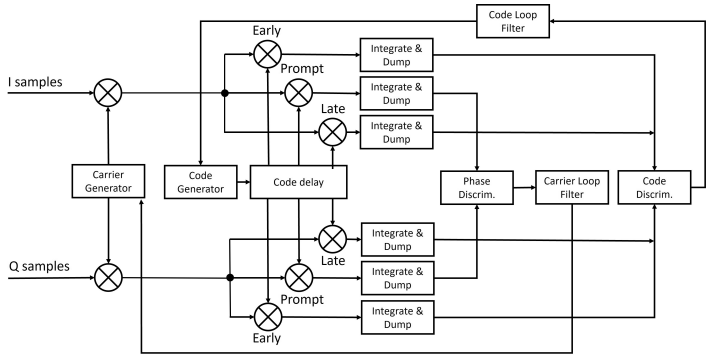

The fingers are often called Early, Prompt and Late (three fingers) or Very Early, Early, Prompt, Late, Very Late (five fingers). The correlators are traditionally implemented as hardware blocks and the control of these are implemented in software.

In a Software Defined Receiver (SDR) the correlators are implemented in software, and they are then also the most CPU intensive part of an SDR. The output of the fingers is typically generated 1–10 times per code chip and this output is accumulated in integrators to reduce the noise level. The output from the integrate and dump filters are typically generated once per code epoch, i.e. once every ms for GPS L1 C/A. The output is then the correlation amplitude for the I and Q signals of all fingers. In a three + three finger configuration this means six output values. For both I and Q the middle finger should be perfectly aligned with the signal and give the highest amplitude, whereas the other fingers with a slightly shifted code phase should give a lower amplitude since the signal and the replica are not perfectly aligned. The output from the correlator fingers is provided to several discriminators, that produces a signal that is proportional to the amount of adjustment needed to achieve optimal alignment between the satellite signal and the replica signal assuming the misalignment is small.

The discriminator output is very noisy so an additional low pass filter, or a loop filter, is often added between the discriminator and the feedback to the correlators. Sometimes the discriminators output can also be further integrated coherently or non-coherently to increase the sensitivity of the receiver. The correlator fingers, discriminators and loop filters are together often referred to as a tracking loop. There are often separate tracking loops for code tracking called a Delay Lock Loop (DLL), carrier tracking called an FLL and phase tracking called a Phase Locked Loop (PLL). All of these tracking loops together form a tracking channel.

3.2.4.1 Discriminators

For code tracking the most commonly used discriminator is the early-late discriminator defined in equation 3.20

$$D_{Code} = \frac{1}{2}\frac{P_E - P_L}{P_E + P_L}, \tag{3.20}$$

where D_{Code} is the output of the discriminator and the definition of P_E and P_L are

$$P_E = \sqrt{I_E^2 + Q_E^2} \tag{3.21}$$

$$P_L = \sqrt{I_L^2 + Q_L^2} \tag{3.22}$$

I_E, Q_E, I_L and Q_L are the early and late finger for the I and Q signal. The power values P_E and the P_L should be equal if the code is aligned with the prompt finger and thus the discriminator output, D_{Code}, should be zero. If D_{Code} gives a positive value, it means the code replica signal is ahead of the satellite signal and that can then be adjusted for by reducing the code frequency so that the satellite signal will catch up again.

For frequency tracking the perhaps most commonly used discriminator is the cross product of consecutive prompt finger outputs defined in equation 3.23

$$D_{Freq} = \frac{I_P^{N-1} \times Q_P^N - I_P^N \times Q_P^{N-1}}{t_N - t_{N-1}}, \tag{3.23}$$

where N and $N-1$ indicate the values for two consecutive epochs, I_P and Q_P are

the prompt fingers of the I and Q signal, and D_{Freq} is the discriminator output. This discriminator gives an output value proportional to the phase difference between epochs N and $N-1$, which in turn is a measure of the frequency error. For carrier phase tracking the most commonly used discriminator is the $Atan$ discriminator shown in equation 3.24

$$D_{Phase} = Atan\left(\frac{Q_P}{I_P}\right) \tag{3.24}$$

where I_P and Q_P are the prompt fingers of the I and Q signal, and D_{Phase} is the discriminator output. This discriminator gives an output value proportional to the phase error between the generated Q signal and the incoming signal. This means that the phase discriminator will drive all the power into the I part of the tracking channel. Other often used discriminators are listed in [Kap17] and many other books.

3.2.4.2 Loop Filters

As mentioned before the objective of the loop filter is to reduce the noise of the discriminator outputs by low pass filtering before the feedback is provided to the correlators. There are numerous different types of loop filter designs [Gar05; Kap17], but common for all is that the characteristic behavior of a loop filter is determined by its bandwidth and its order. These need to be selected based on expected signal dynamics and required accuracy of the receiver. The lower the bandwidth is the more filtering will occur and the better the accuracy will be. A lower bandwidth is, however, more sensitive to rapidly changing signals due to user movement for example. This can be partly mitigated by using higher order loops.

A first order loop simply filters the incoming discriminator signal using one simple integrator step that will keep adding the input values to the output value for every epoch. This type of loop is sensitive to large variations in the discriminator output that can be a result of a rapid change in user velocity. If the change is too big the adjustment of the replica signals can no longer compensate, and the signal will diverge from the replica in the receiver so much that the discriminator can no longer generate a valid error signal. The code tracking loop filter is often a first order loop filter, since the change in code frequency is very small even for large accelerations. For the same reason the bandwidth can be small.

A second order filter has two integrators. One that integrates the input directly like in the first order loop, but also one that integrates the change or derivative of the output from the first order integrator. The result is that if the velocity changes rapidly the loop can compensate better than the first order loop. However, a rapid change in acceleration can cause the second order loop to lose track of the signal. In an analogue way a third order loop adds yet another integrator and becomes less sensitive to change in acceleration. A frequency tracking loop filter is often a second order loop and a phase tracking loop filter is often a third order loop. A block diagram of the different loop filters are shown in figure 3.14

Figure 3.14 Block diagram of analog loop filters. a) First- b) Second- and c) Third-order.

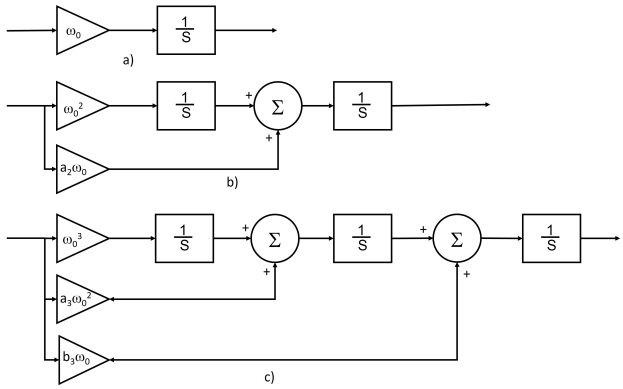

The ω_0 is the loop bandwidth and by selecting the coefficients a_i and b_i the behavior of the loop can be defined. The $\frac{1}{S}$ defines a delay.

3.2.4.3 Navigation data extraction

The incoming signal from the satellites contains the code, carrier and the navigation data bits, whereas the locally generated signal contains only the code and the carrier signal. As we can see from equation 3.24 the phase tracking will drive the Q_P value to zero and all the power into I_P. As we have seen in figure 3.3 the carrier phase in the incoming signal will rotate 180 degrees whenever there is a bit flip in the navigation data and this will also change the sign of the I_P value providing we have a phase lock, i.e., carrier signal and replica are perfectly aligned. The sign of I_P will then directly provide the navigation data bit value. These data bit values are passed on to a data decoder unit that will combine them into a continuous data stream and search for

a preamble in the data, i.e., a known bit pattern that each subframe or page starts with. When this is detected, the receiver knows that a new frame or page has started and after the full frame or page have been received additional checks and operation (parity, CRC, de-interleaving etc.) on the data can be done. Every data frame also contains the transmission time of the signal which is needed for the pseudo range calculations, and all the decoded frames and pages will be combined into ephemeris and almanac data needed by the navigation filter.

3.2.5 Navigation Observables

In this section we will describe a little bit in more detail what kind of observables are needed for the navigation filter and how these observables are obtained from the raw observation from the signal tracking.

3.2.5.1 Output from Tracking

As mentioned in section 3.2.4 the raw observables from the signal tracking is the carrier frequency and phase, code phase and transmission time. Carrier frequency and carrier and code phase are typically sampled simultaneously for all channels at regular intervals directly from the correlators. As described in the previous section the transmission time is obtained from the decoded navigation data and the number of full code epochs that has passed since the beginning of the previous navigation data frame. In addition to these observables other data like Signal-to-Noise Ratio (SNR), status bits and Doppler frequencies may be outputted.

3.2.5.2 Code pseudo range

The tracking channel is generating a replica of the spreading code and provides several output parameters. First of all the channel maintains an Epoch Counter (EC), i.e., a counter that counts exactly how many full code epochs has been generated. Secondly it also provides a Chip Counter (CC) for the number of chips that has been generated since the start of the last code epoch. This counter is reset at the beginning of a new code epoch. Finally, a third counter resets at the start of each code chip and increments to its maximum value before the next chip is generated. This Phase Counter (PC) provides the fractional chip value. The maximum value of

this counter then defines the resolution of the output. In a consumer grade receiver a typical counter run from 0 to 256 providing a resolution of approximately one meter if the chip length is one μs or approximately 300 meters.

When the preamble has been detected in the navigation bit stream described in section 3.2.4.3 the transmission time can be decoded. This transmission time refers to the start of the next data frame. Since we know how many bits one frame contains, and we know the EC at the time the frame started we can align the transmission time with the EC. Once this is known we can estimate the full unambiguous transmission time t_{sv} of the signal using:

$$t_{sv} = tow + EC \times T_{epoch} + CC \times T_{chip} + \frac{PC}{PC_{max}} \times T_{chip} \tag{3.25}$$

where EC, CC and PC are Epoch Counter, Chip Counter and Phase Counter values and the T values are the length of each of these. The tow is the decoded transmission time from the navigation bit stream and PC_{max} is the maximum value of the phase counter. If the receiver can maintain code tracking, we always have an unambiguous transmission time after we have decoded the tow. The concept of transmission time t_{sv} is illustrated in figure 3.15

Figure 3.15 Determining the transmission time

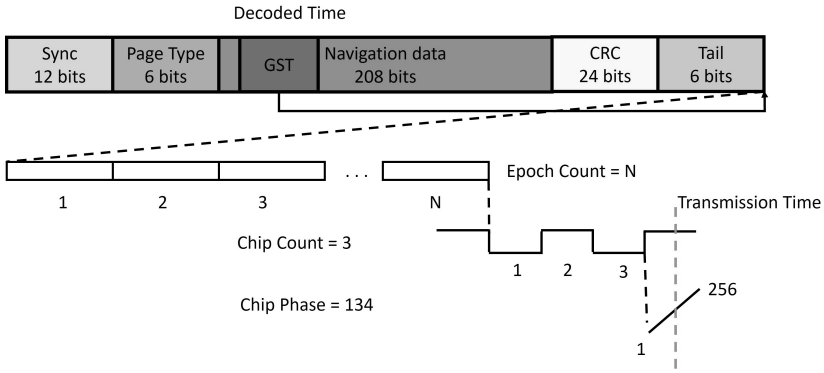

To calculate the pseudo ranges we also need the receiver time, and this is typically estimated initially by using an average travel time of the signal. A value of 60 or 70 ms is often used. The receiver time t_{rx} is thus estimated to:

$$t_{rx} = t_{sv}^{N} + 65ms \tag{3.26}$$

where t_{sv}^{N} is the transmission time for satellite N that can in principle be any of the available signals. Often the strongest one or the first one to obtain the transmission time is used. The pseudo range ρ_i for the satellite i is then simply given by

$$\rho_i = \left(t_{rx} - t_{sv}^{i}\right) \times c \tag{3.27}$$

where c is the speed of light. The receiver time estimated like this now contains an unknown offset with respect to correct time, and therefore it is called a pseudo range and not a true range or range. To obtain the pseudo ranges for all tracked signals sampling of the correlators are done simultaneously for all receiver channels at a predefined interval and the pseudo ranges are sent to the navigation filters. The predefined interval is typically anything from one sec (one Hz) to 10 ms (100 Hz) depending on the application the receiver is used for.

3.2.5.3 Phase Range

The correlators in a tracking channel are also generating a replica of the carrier signal and two output parameters are provided. The channel maintains a carrier cycle counter that calculates the number of full carrier cycles generated and a phase counter that starts from zero and increments to a maximum value during one carrier cycle. The resolution of the phase counter varies, but a typical value is that one carrier cycle is generated every 256 steps of the phase counters. The resolution is therefore much higher than for the code. One carrier cycle is approximately 19 cm for GPS L1, and the resolution is in that case 1/256*19 cm = 0.7 mm or 1.5 degrees in phase angle.

The phase range is then simply the sum of the integer carrier cycles and the fractional value from the phase counter times the length of one carrier cycle. To obtain the phase ranges for all tracked signals sampling of the correlators are done simultaneously for all receiver channels at a predefined interval and the phase ranges are sent to the navigation filters. The predefined interval is typically anything from one sec (one Hz) to 10 ms (100 Hz) depending on the application the receiver is used for. It is good to note that the phase range does not have any transmission time, so it is ambiguous.

3.2.5.4 Doppler

The carrier frequency can be calculated as the differences between two consecutive phase range measurements. This frequency then is a sum of the IF of the receiver and the Doppler frequency shift due to the satellite to user relative movement. If the Doppler shift, Δf, are to be provided the IF need to be removed. Typically, the nominal IF for the receiver is used for this and the Doppler shift Δf_i for the satellite i becomes

$$\Delta f_i = (f_i - IF_{Nom}) \tag{3.28}$$

where f_i is the measured carrier frequency and IF_{Nom} is the nominal IF in the receiver. This should be called pseudo Doppler shifts since it also contains an unknown frequency offset between the nominal IF and the actual IF based on the receiver clock drift. Doppler shift is also often converted to m/s instead of Hz like the carrier frequency since Doppler shift is used to determine user velocity that is expected to be in m/s.

3.2.5.5 C/N0 and SNR

The strength of the signal is one of the observables from the signal processing stage that can be used to eliminate weak signals or used to weight the observables for the navigation solution. Signal strength is provided either as a carrier to noise density, C/N_0, or a signal-to-noise ratio, SNR. The C/N_0 is independent of receiver implementation since it is normalized to a bandwidth of one Hz and can be defined as

$$C/N_0 = 10 \times \log_{10}\left(\frac{P_S}{N_0}\right) dBHz \tag{3.29}$$

where P_S is the signal power in W and N_0 is the noise power for a one Hz bandwidth in W/Hz. Typical values for a strong signal in GNSS receivers are 40-45 dBHz. The SNR provides the signal strength for a specific bandwidth, and it is a better indicator of receiver performance. The SNR is defined as

$$SNR = \left(\frac{P_S}{BW \times N_0}\right) dB \tag{3.30}$$

where BW is the bandwidth in Hz. SNR is measured in dB.

3.2.5.6 Others

The signal tracking part may also provide other kind of outputs like noise estimates of the observations or other quality indicators that may be used to aid the selection of the signals to be used in the navigation filter. The simplest quality indicators are the lock bits that give binary information of the tracking state. Typical such lock bits are code lock, carrier lock, phase lock, bit lock, frame lock and time decoded. Google have tried to standardize some of these lock bits in their Location Application Programming Interface (API), but every receiver manufacturer have their own output format that specifies the lock bits they are using.

Instead of lock bits the RINEX format [Rom20] defines a loss of lock indicator that gives information on how long the signal has been in lock. Some receivers also offer indicators for suspected multipath and observation noise estimates. In addition to the observation related outputs another sometimes useful output is the state of the AGC. This can be obtained in some receivers, and it can be useful for detecting abnormal signal levels in case of malicious signal jamming for example.

3.2.6 Satellite position calculations

In addition to the ranges to the satellites, or pseudo ranges, we also need the point of origin for the signal, i.e., the satellite positions. As mentioned before the information needed to obtain those are embedded in the navigation data transmitted by the satellites. This information is decoded by the receiver and converted into meaningful parameters and values. Part of those parameters are the orbit information parameters that determines the exact orbit parameters for the satellites. For every constellation except GLONASS these parameters are similar. They contain the six Keplerian elements and six correction parameters [Chi20; Eur21; Flo21; Ind17; Qua21a]. Once the transmission time is known we can use the equations described in the ICD's to calculate the exact position and velocity of the satellites at the time the signal was transmitted.

The GLONASS navigation data [Coo98] provides the position, velocity, and acceleration of the satellite at a given time and the satellite trajectory is then propagated forward or backward by numerical integration of a set of differential equations that

describes the satellite movement.

3.2.7 Positioning equations

As mentioned in section 2.1 GNSS position calculations are based on the concept of trilateration. The principle is simple, if we know the location of three points and the distance to these three points we can solve the user position x, y, z by solving the equation system

$$\begin{cases} \sqrt{(x_1-x)^2+(y_1-y)^2+(z_1-z)^2} = R_1 \\ \sqrt{(x_2-x)^2+(y_2-y)^2+(z_2-z)^2} = R_2 \\ \sqrt{(x_3-x)^2+(y_3-y)^2+(z_3-z)^2} = R_3 \end{cases} \tag{3.31}$$

where x_i, y_i and z_i are coordinates of the three satellites, x, y, z are the unknown user position and R_i is the true ranges to the satellites. The ranges to the satellites are measured using the time difference between transmission and reception. Unfortunately, both the satellite clock and the receiver clock have an error or time offset and these need to be accounted for. In addition, several different types of errors will cause an additional offset between real range and measured range. We need to define a so-called pseudo range ρ_i for satellite i as

$$\rho_i = \sqrt{(x_i-x)^2+(y_i-y)^2+(z_i-z)^2} + c\Delta t_{rx} + E_i \tag{3.32}$$

where Δt_{rx} is the receiver clock error, c is the speed of light and E_i is the sum of all errors for the satellite i. By replacing all the equations in 3.31 with the corresponding equations from 3.32 we get a highly nonlinear equation system that need to be solved with respect to x, y, z. The perhaps most common way to do this is to solve for the change in user position between two epochs instead of for x, y, z. By setting

$$\begin{cases} x = x_0 + \Delta x \\ y = y_0 + \Delta y \\ z = z_0 + \Delta z \end{cases} \tag{3.33}$$

where x_0, y_0, z_0 is the previous user position and $\Delta x, \Delta y, \Delta z$ are the change in user position and defining

$$R_i^0 = \sqrt{(x_i - x_0)^2 + (y_i - y_0)^2 + (z_i - z_0)^2} \tag{3.34}$$

we can write the first order Taylor expansion of equation 3.32 as

$$\rho_i = R_i^0 - \frac{x_i - x_0}{R_i^0}\Delta x - \frac{y_i - y_0}{R_i^0}\Delta y - \frac{z_i - z_0}{R_i^0}\Delta z + c\Delta t_{rx} + E_i \tag{3.35}$$

since the change in position is minor compared to the distance to the satellites. By rewriting this into vector form and rearranging the terms we can write

$$\begin{bmatrix} -\frac{x_i - x_0}{R_i^0} & -\frac{y_i - y_0}{R_i^0} & -\frac{z_i - z_0}{R_i^0} & 1 \end{bmatrix} \begin{bmatrix} \Delta x \\ \Delta y \\ \Delta z \\ c\Delta t_{rx} \end{bmatrix} = \rho_i - R_i^0 - E_i \tag{3.36}$$

3.2.8 Velocity calculations

Calculating the velocity is done with the same equations as the position with two differences. The observation vector consists of the Doppler frequency shifts instead of the pseudo ranges and the previous solution is often set to [0,0,0], which simplifies the equations. The clock error in equation 3.35 is also replaced by the clock drift. The error components in the Doppler shifts are also much smaller than for the ranges.

3.2.9 Navigation Filters

The Navigation filter in the receiver is the component that calculates the position and velocity according to the equations given in the previous sections. Several types of filters can be used. The simplest one being the Least Square Estimator (LSE) and the perhaps most common one being the Kalman Filter. Other types of filters that can be used in GNSS receivers are described in [Gib11]

The LSE requires that we have more observations than unknowns and finds the solution that minimizes the error vector. If a set of linear equations can be written

as

$$\mathbf{A}\mathbf{x} = \mathbf{b} \tag{3.37}$$

it can then be shown that the optimal solution is

$$\hat{\mathbf{x}} = (\mathbf{A}^T\mathbf{A})^{-1}\mathbf{A}^T\mathbf{b} \tag{3.38}$$

and the error vector becomes

$$\hat{\mathbf{e}} = \mathbf{b} - \mathbf{A}\hat{\mathbf{x}} \tag{3.39}$$

In case of GNSS we quickly see that equation 3.36 can be written in the same form as equation 3.37 where

$$\mathbf{A} = \begin{bmatrix} -\frac{x_1 - x_0}{R_1^0} & -\frac{y_1 - y_0}{R_1^0} & -\frac{z_1 - z_0}{R_1^0} & 1 \\ -\frac{x_2 - x_0}{R_2^0} & -\frac{y_2 - y_0}{R_2^0} & -\frac{z_2 - z_0}{R_2^0} & 1 \\ \cdots & \cdots & \cdots & 1 \\ -\frac{x_n - x_0}{R_n^0} & -\frac{y_n - y_0}{R_n^0} & -\frac{z_n - z_0}{R_n^0} & 1 \end{bmatrix} \tag{3.40}$$

$$\mathbf{x} = \begin{bmatrix} \Delta x \\ \Delta y \\ \Delta z \\ c\Delta t_{rx} \end{bmatrix} \tag{3.41}$$

$$\mathbf{b} = \begin{bmatrix} \rho_1 - R_1^0 - E_1 \\ \rho_2 - R_2^0 - E_2 \\ \cdots \\ \rho_n - R_n^0 - E_n \end{bmatrix} \tag{3.42}$$

for satellites 1,2,3,...n. **A** is often called the design matrix, **x** the state vector and **b** the observation vector. One additional challenge with the LSE is that some of the errors are dependent on the estimated position and therefore an iterative approach is often used. This is also true when we do not know the previous position. By

iterating three or more times or until the error vector does not change anymore this challenge can be overcome. A LSE is not a filter, since the solution does not contain any historical information. Therefore, the LSE solution is often quite noisy since all the errors and all the noise in the observables will be directly visible in the solution.

The so-called weighted LSE is also sometimes used. In this approach each observation is given a weight based on the estimated error in the observation. A weak signal with high noise is given less weight in the LSE and will have a smaller impact on the solution. The solution for the weighted LSE can be written as

$$\hat{\mathbf{x}} = (\mathbf{A}^T \mathbf{W} \mathbf{A})^{-1} \mathbf{W} \mathbf{A}^T \mathbf{b} \tag{3.43}$$

where W is the weight matrix that can be written as

$$\mathbf{W} = \frac{\mathbf{I}}{\sigma^2} \tag{3.44}$$

where $\mathbf{I}$ is the identity matrix and σ^2 the variance of the observable. The Kalman filter is the perhaps most common filter used in GNSS receivers and the steps and equations used are significantly more complex than for the LSE. When the LSE typically just uses the previous solution, or state, as the starting point and calculates the updated state by minimizing the new residuals, the Kalman filter uses a model to first predict the new state from the previous state and then updates the state with the new observations. This means that the Kalman filter has a much better starting point than the LSE and the output will be much smoother or filtered. The Kalman filter also estimates the uncertainties in the model (process noise) and the uncertainties in the observations (measurement noise) as part of the prediction and update step. Depending on these the filter calculates a gain value that determines how much weight the predicted state has versus the observations. The steps in a Kalman filter is shown in equation 3.16. The Kalman filter state is often initialized by the LSE solution.

3.2.10 Support functions

So far, we have focused on the straight forward tasks in the receiver: Observations, Satellite positions and Navigation Filters. These are tasks needed to obtain a PVT solution, but there are also a lot of supportive tasks in a receiver that determines the quality of the solution and provides extra output to the user.

Figure 3.16 Kalman filter steps

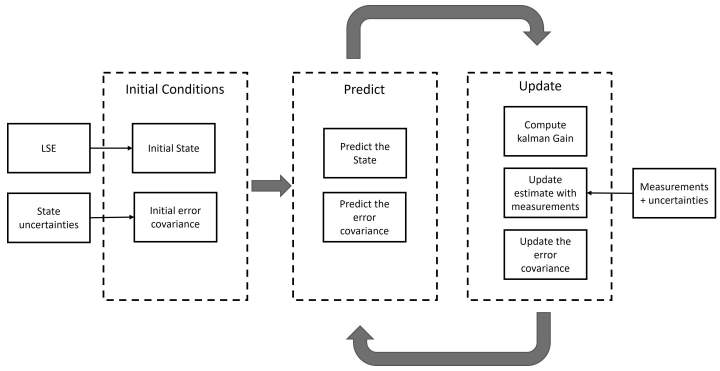

3.2.10.1 RAIM/FDE

Receiver Autonomous Integrity Monitor (RAIM) was first introduced in aviation applications where the integrity of a solution is essential. Integrity here referring to the capability to detect if the solution should not be used for navigation. In the early days of satellite navigation RAIM was in fact more used to detect satellite failure. The basic principle of RAIM is simple, to use an over determined solution to detect if one observation deviates from the rest of the observations. Some traditional RAIM methods are described in [Kuu05].

In consumer grade receivers the purpose of RAIM has changed. Integrity is no longer the only important output and the errors in the observations are mostly related to weak signals, interference, or signal reflections and not as much to satellite failure. Therefore, the name Fault Detection and Exclusion (FDE), are more suitable than RAIM.

The FDE uses the residuals of the observations after a solution has been obtained as input. The challenge is that if one or more erroneous observations were used to obtain the solution it will be itself erroneous, and the residuals are not correct. Instead, the erroneous solution will influence all residuals, and it is difficult to detect the observations that are erroneous.

Traditional FDE methods are based on a global test and local tests. Local tests are simply solutions where observations are excluded one by one and the subset that provides the best global test result and the largest number of observations will be selected.

A more advanced method is to use weighting of observation instead of eliminat-

ing observations. If the magnitude of the residual are larger than a defined threshold the weight for that observation will be reduced and the solution re calculated. The iteration will continue until the weights no longer changes. The a priori weights are often obtained using signal strength or elevation angle of the satellites.

3.2.10.2 Carrier Smoother

As described in section 3.2.5.3 the carrier signal is tracked with a much higher accuracy than the code signal. The code signal that is used to obtain the position often has an accuracy of no more than 0.5 m and in practice the Root Mean Square (RMS) tracking noise can be as much as 10 meters. If this is used to calculate a PVT solution the noise in the solution would be in the order of meters in most cases.

The carrier signal is much more accurate, and we can obtain observables with noise levels of centimeters, but they are ambiguous since we do not know the number of full carrier cycles. The carrier phase rate or carrier frequency is however known if carrier lock has been maintained and this can be used to smooth the pseudo range using

$$\rho_s^{N+1} = (1-K) \times (\rho_s^N + PRR^{N+1}\Delta t) + G \times \rho^{N+1} \tag{3.45}$$

where ρ_s is the smoothed pseudo range, G is the gain, PRR is the carrier phase range rate in m/s, Δt is the time between two epochs in seconds, and ρ is the unsmoothed new pseudo range. N and $N+1$ indicate the epoch number. The range rates are not the same in the carrier and in the code since some of the errors in the signals are different, but in most cases the differences are very small and can be neglected. When such a carrier smoother is applied the noise level in the PVT solution can be reduced to approximately 10 cm.

3.2.10.3 Error Corrections

The GNSS signals are impacted by several different types of phenomena on the path from the satellites to the receiver. These will result in errors in the observables. Some errors are small, and some are large. In consumer grade receivers only the largest errors are corrected for, but if a more precise solution is required also the smaller errors need to be accounted for. The smaller errors will be described more in section

4, but in consumer grade receivers at least the atmospheric delays, satellite clock errors, relativistic correction and the earth rotation correction need to be accounted for.

The atmospheric delay can be divided into ionospheric and tropospheric delay. The ionospheric delay is caused by the signal interacting with the free electrons in the ionosphere and the total amount of free electrons, the Total Electron Count (TEC), defines the magnitude of the error. The TEC value depends on how strong the radiation from the sun is and this again depends on where you are on the globe, the time of day, the time of year and the 11-year sunspot cycle [ESA20] shown in figure 3.17

Figure 3.17 Number of sunspots

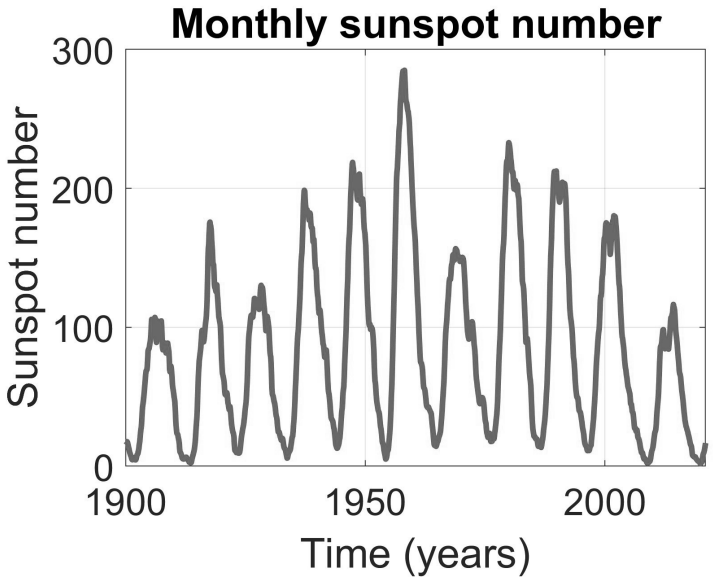

A rule of thumb is that the TEC is highest in the direction of the sun and thus the equatorial region is affected the most. An exception is the polar regions where also magnetic storms may cause large gradients in the TEC counts that are hard to model. To reduce the impact from the ionosphere the GNSS signals transmits an ionospheric correction model that can be used in the receiver to estimate the TEC and thus the impact on the signals. The ionospheric signal delay, I, as a function of the TEC count is given in equation

$$I = \int \Lambda \, dl = \frac{40.3}{f^2} \, \mathrm{TEC} \, [m] \tag{3.46}$$

where Λ is the electron density along the path l of the signal, and f is the frequency of the signal. The magnitude of the ionospheric delay can be as much as 30 meters, and it impacts the carrier and the code signal with an opposite sign. As can be seen from equation 3.46 the ionospheric delay is frequency dependent and this fact can be used in a dual frequency receivers to eliminate most of the delay.

To correct for the ionospheric delay in single frequency consumer grade receivers the different GNSS transmit model parameters in the navigation data that can be used to estimate the delay. GPS and Beidou uses a so-called Klobuchar model [Klo87] with eight parameters and Galileo uses a more precise NeQuick model [Eur16]. These models will account for 50-70 % of the ionospheric error.

The tropospheric error can be divided into the hydrostatic part and the wet part. The hydrostatic part depends mostly on the atmospheric pressure and can be quite accurately modelled inside the receiver. The wet delay depends on the amount of water vapor in the troposphere, and it is quite small (< 0.2 meters) so in most cases in can be neglected. Both delays are estimated using a model for the zenith delay and a mapping function that adjusts the error according to the path length through the troposphere.

Figure 3.18 Troposphere slant delay

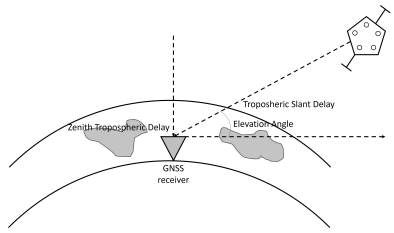

The Zenith Hydrostatic Delay (ZHD) is often estimated using the Saastamoinen model [Saa72].

$$\mathrm{ZHD} = \frac{0.0022767 \times P_0}{1 - 0.00266 \times cos(2\phi) - 0.00028 \times h} \, [m] \tag{3.47}$$

where P_0 is the surface pressure in hPa, h is the height in km and ϕ is the ellipsoidal latitude. A simple mapping function that assumes a flat earth surface is often

used to calculate the Slant delay, SHD

$$\text{SHD} = \frac{1.001}{\sqrt{0.002001 + sin(Ele)^2}} \text{ ZHD } [m] \tag{3.48}$$

where Ele is the elevation of the satellite. Other models exist also for mapping the tropospheric delay [Sch00]. Satellite clock corrections are always applied using the three-parameter polynomial model transmitted in the navigation data and the relativistic corrections can also be calculated from the parameters in the navigation data. The clock correction term Δt_{sv} at time t is estimated using [Flo21]

$$\Delta t_{sv} = a_{f0} + a_{f1}(t - toc) + a_{f2}(t - toc)^2 \tag{3.49}$$

where a_{f0}, a_{f1} and a_{f2} are the three terms transmitted in the navigation data and toc is the reference time for the clock data also transmitted in the navigation data. The correction term for the relativistic effect Δt_{sv}^{Rel} on the time is given by

$$\Delta t_{sv}^{Rel} = Fe^{\sqrt{A}} sin(E_k) \tag{3.50}$$

where the orbit parameters e, A and E_k are provided in the navigation data and F is a constant defined as

$$F = \frac{-2\sqrt{\mu}}{c^2} \tag{3.51}$$

where μ is the earth universal gravitational constant and c is the speed of light. The signal travel time is approximately 70 ms and during this time the earth will rotate and when the signal received the user is no longer at the same location as when the signals were transmitted. This Earth rotational correction is estimated in an iterative way with the user position since they depend on each other. The size of this correction can be several meters.

4 CARRIER PHASE POSITIONING METHODS

As is described in section 3 the GNSS signals consists of a carrier signal and a code signal, where the code signal includes a timestamp that can be used to measure the traveling time of the signal and thus the distance to the satellites. The code signal is unambiguous after the transmission time has been decoded from the navigation data and the position of the receiver can be calculated.

The carrier signal does not contain any timing information like the code signal, and it was never intended to be used as a ranging signal. However, in the 1980's the first papers [Bos80; Par79] were published where the carrier signal actually was used to measure the range to the satellites and calculate the position from these ranges. The advantage with using the carrier signal is that the accuracy of the carrier phase observations in a receiver is several orders of magnitudes better than the code. The phase tracking loop can determine the exact phase within a few degrees and since the carrier wavelength is 10-20 cm the accuracy can be as good as 0.1 cm.

The problem in these carrier phase positioning methods is the ambiguous nature of the carrier cycle. To reach the accuracy mentioned above the user also needs to know the total number of carrier cycles between the satellite and the user. Otherwise, an error of $\Delta N \times \lambda$ will be introduced into the ranges, where ΔN is the difference between true and estimated number of carrier cycles and λ is the wavelength of the signal. The task of estimating the number of cycles or the carrier ambiguity as it is sometimes called requires first that as much as possible of the signal propagation errors are removed. This is best illustrated by writing out the range to the satellite including all error components. The measured code range can be written as:

$$\rho_c = R + c(\Delta t_{rx} - \Delta t_{sv}) + Tr + I + B_c^{rx} + B_c^{sv} + M_c + L + O_{rx} + O_{sv} + \epsilon_c \quad (4.1)$$

and the corresponding phase range as

$$\rho_p = R + c(\Delta t_{rx} - \Delta t_{sv}) + Tr - I + B_p^{rx} + B_p^{sv} + \lambda\omega + M_p + L + O_{rx} + O_{sv} + \epsilon_p \quad (4.2)$$

In the equations above R is the true range, c is the speed of light, Δt_{rx} is receiver clock error, Δt_{sv} satellite clock error, Tr tropospheric error, I ionospheric error, B is code and phase hardware biases in the satellite and the receiver, M is multipath error, L are local site displacement errors, O are antenna phase center offsets, ω is the phase windup delay, λ is the wavelength and ϵ is receiver noise. The indexes c stand for code, p stands for phase, rx stands for receiver and sv stands for satellite. The sign of the ionospheric error depends on if we measure code range or carrier range.

4.1 Error Sources

The key to understanding carrier phase positioning methods is to understand the different types of errors that impact our position calculations in a GNSS receiver. These errors, if not eliminated, will result in an error of several meters in our position and the basic principle for all carrier phase based positioning methods is to eliminate the errors before calculating the position. Next, we will describe some of the main error sources in GNSS and how they can be removed.

4.1.1 Space segment errors

We have learned from section 3.2.7 that we need to know the exact time of transmission for every GNSS signal, and we need to know the exact position of the satellites when the signal was transmitted. The satellite clocks are very accurate and stable and clock correction terms are also transmitted to the user in the navigation data, but even so there will still be a small error left in the time stamp of the signals. This remaining satellite clock error can be 1-5 ns, or 1–2 meters in the range domain.

The satellite orbit parameters are also transmitted in the navigation data and used to calculate the satellite positions at any given time. These orbit parameters are also not precise and contain a remaining error and therefore the location of the satellite will include an error of about the same magnitude as the clock error. The clock error

will directly impact the ranges, whereas the position error can be in any direction and will impact the ranges differently if it is in the direction of the orbit (along track error) or perpendicular to the orbit (cross track or radial error).

For post-processing purposes the satellite's precise orbits and clocks can be retrieved for example from Crustal Dynamics Data Information System (CDDIS) and used instead of the broadcasted navigation data in the position calculations. For real time operations a correctional service that transmits clock and orbit corrections is required. Broadcast orbit parameters always refers to the coordinates of the antenna phase center, whereas precise orbit information may refer to the center of mass of the satellites. This so called Phase Center Offset (PCO) are known for every satellite and can be retrieved from IGS for example. Broadcasted clock corrections are always given with respect to a specific type of signal or signal combination and when using precise clock corrections, the signal or combination of signal may be different.

In addition to the signal transmission times having an error the signals will be further delayed when passing through all the hardware in the satellite electronics. This delay is frequency dependent, and it will impact the carrier signal and code signal differently. These code and phase biases also needs to be corrected for properly.

The Phase windup effect is caused by the rotation of the satellite around the axis between user and satellite. This rotation is a result of the satellite trying to point the solar panels towards the sun. Since the transmitted signals are circularly polarized electromagnetic waves, this rotation will be seen as a change in range by the receiver and this is different and time dependent for all satellites. Phase windup can be estimated in the receiver if the position of the sun is known.

4.1.2 Propagation errors

As described in section 3.2.10.3 the GNSS signal interacts with the atmosphere causing an apparent delay in the signal before it reaches the user and this will cause also an error in the user position unless corrected for. Some simple models are typically applied in the receiver to account for part of these errors, but these models are not good enough for carrier phase usage. For post-processing, it is possible to download both precise ionospheric and tropospheric models that can be used to calculate the propagation delay for each signal. The accuracy of these models are however very dependent on the density of the base station network. The troposphere is stable and

quite often the tropospheric residual is just added as a state in the solution, but the ionosphere is much more dynamic and therefore much more difficult to model. The ionospheric delay I_f for frequency f in meters can be written as

$$I_f = \alpha_f STEC \tag{4.3}$$

where Slant Total Electron Count (STEC) is the total integrated electron density in so-called TEC units (1 Total Electron Count Unit (TECU) $= 10^{16} electrons/m^2$) over the path from the satellite to the receiver and α_f is defined as

$$\alpha_f = \frac{40.3 * 10^{16}}{f^2} \tag{4.4}$$

This is the so-called first order term that accounts for 99.9 % of the ionospheric error. The dependency on the frequency means that if we have observations from multiple frequencies from one satellite, we can directly calculate the ionospheric delay for that observation. The ionosphere is also the reason why dual frequency receivers outperform single frequency receivers when using the carrier phase. Some real time correction services also offer ionospheric correctional models either as grid points or functions.

4.1.3 Receiver Errors

The receiver itself also generates errors in the observations. The receiver will receive the signals in one unique point called the antenna phase center. This phase center is not necessarily the same point as the geometrical center of the antenna. In high quality antennas the PCO is always provided with the antenna, and it is then with respect to a given physical Antenna Reference Point (ARP). An example is shown in figure 4.1

To further complicate things this phase center is a function of the direction of the signal and the frequency of the signal. To account for all these a calibration file is often used. For cheaper antennas there are typically no information on the PCO which means we do not know what point the solution refers to and the phase center variations will also decrease the accuracy of the solution if not accounted for.

When the signal passes from the antenna through the front end all the way to the baseband processing an additional delay will occur the same way as in the satellites

Figure 4.1 Antenna phase center offset for Tallysman VSP6037L triple band antenna.

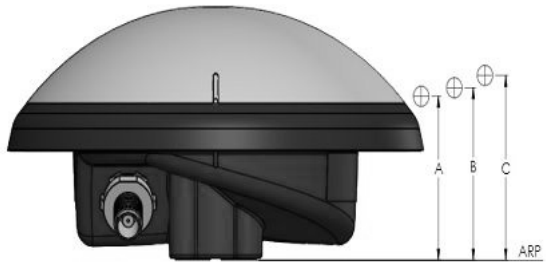

Label	Frequency	PCO (mm)
A	L1 / G1	48.82
B	L2 / G2	51.36
C	L5 / G5	55.04

and these signal biases are frequency dependent. When using only one frequency the delay will be the same for all signals and absorbed by the receiver clock error in the solution, but for multi frequency receivers this is not the case. In some cases, this error is absorbed by the ionospheric models when dual frequency observations are used. GLONASS is a special case since every signal has its own frequency and therefore the delay will be different and not observed by the clock. Base stations often transmit the estimated GLONASS front end biases for the receiver at the base station, but for the rover they might need to be estimated or calibrated away [Sle12].

4.1.4 Site Displacement effects

There are three different site displacement effects that will impact the measurement site where the rover is placed [Li 23]. The solid earth tides are a result of the gravitational forces from the moon and the sun deforming the ground much like the ocean tides. This effect can cause up to 30 cm of error in the radial direction and five cm in the horizontal direction. The effect has a periodical part with a period of approximately 24 hours and a permanent displacement part that depends on the latitude.

The second effect is the polar tides caused by the change of the orientation of the earths spin axes with respect to the earth's crust. This also causes a change in the earths gravitational field which in turn will cause a deformation of up to 25 mm in the vertical and seven mm in the horizontal direction. This effect is slowly oscillating

with a period of approximately 430 days.

The third effect is the ocean loading, i.e., the weight of the water in the oceans that presses down the earth's crust because of the ocean tides. This effect is one order of magnitude smaller than the solid earth tides, but it needs to be considered especially in coastal areas. The effect is periodic and does not have a permanent part like the solid earth tides. All three site displacement effect can be modelled quite accurately and estimated without any input data to the receiver.

4.2 Removing Errors

There are two different ways of removing errors. Differential methods, like RTK, and PPP methods. Differential methods use reference stations and provide as a solution the local vector between user and base station whereas PPP does not need a base station and provides absolute coordinates to the user. For differential methods, the assumption is that the base station and the rover experiences the same errors and by using the differenced observations the errors are eliminated. PPP does not need a base station, but instead uses corrections and models to estimate every error component, removes them and then calculates the position. If enough of the errors are removed it is possible to also use the carrier phases and fix the unknown cycle ambiguities like in RTK. But it can be much more challenging.

4.3 Differential methods

The easiest way to remove the observation errors is by using differential methods. The basic principle of a differential method is to use observations or error estimates from a base station at a known location that also has a GNSS receiver. If error estimates are provided from the base station the user receiver adjusts its own observations with these before attempting to calculate the position. If observations are provided the user receiver calculates the difference between these and its own observations and uses those instead as input to the positioning calculations.

Since the mean of the observation errors is almost identical for the user receiver and the base station receiver providing that the user receiver is close to the base station the advantage of the differentiation is that it will remove the errors almost completely. The disadvantage is that the method increases the residual errors in the ob-

servations and therefore good quality receivers should be used at least at the base station. The principle of a differential system is shown in figure 4.2

Figure 4.2 Principle of differential GNSS

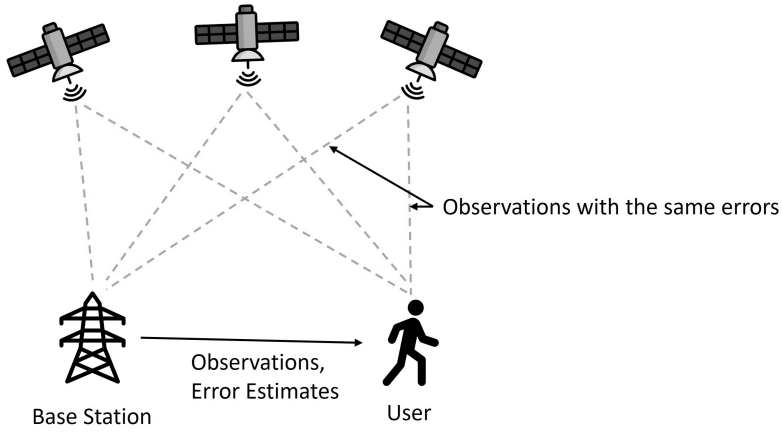

When the difference between the observations of one satellite from two receivers are calculated the only remaining error is the clock offset between the base receiver and the user receiver. Therefore, this single difference will still not have integer ambiguities. This clock offset is therefore often eliminated by forming a double difference DD according to equation 4.5

$$DD_i = (\rho_{BS}^i - \rho_{BS}^{ref}) - (\rho_U^i - \rho_U^{ref}) \tag{4.5}$$

where subscript BS refers to the base station, subscript U to the user receiver, i is the observation from satellite i and ref indicates the selected reference satellite that need to be the same for the base station and the user receiver. Taking the difference between two observations in the same receiver will effectively remove the receiver clock error for both the base station and the user receiver. The penalty is that one extra observation is needed, and we cannot solve for the clock error, so there are only position and velocity obtained.

When calculating the position from double difference observations your solution will be the relative vector from the base station, i.e., ΔX, ΔY, and ΔZ. To obtain absolute coordinates you therefore need to know the exact location of the base station. These coordinates can be found from databases, and they are also transmitted by the base station for real time operation. Today most of the systems transmitting only

error estimates are being replaced by system that transmit the observations directly.

4.3.1 DGNSS

Differential GPS (DGPS) or Differential GNSS (DGNSS), as it should be called if more constellations are used, is strictly speaking not a carrier phase positioning method, but still worth mentioning here. DGNSS uses double differenced code observations or applies error corrections from a base station to its code observations, so the principle is the same as in any differential method, but the achievable accuracy is only around 0.5 meters due to the limited resolution of the code ranges. It has been, however, the de facto standard used in many national systems for coastal navigation and for larger ships it is a strict requirement that they are equipped with DGNSS receivers. These systems are slowly being de commissioned and replaced by more modern methods.

4.3.2 Real Time Kinematic Solution

RTK is the carrier phase version of DGNSS. It is a differential solution utilizing the carrier phase as a range measurement.

4.3.3 Sources for base station data

For the reasons explained above any differential system requires a so-called base station in order to work. For post-processing solutions the data from the base station need to be logged and saved for later processing and for real time operations the user receiver or rover needs access to the base station data in real time.

There are three different types of operators of base stations. A local operator that sets up his own base station for himself only, a public entity or institution that operates a base station and provides access to the data for free, and a commercial operator like Novatel and Trimble who provides access to a base station for a license fee. For the commercial operators the service often also requires the use of the operator's own receiver as the user receiver. The institutional and commercial operators often maintain a whole network of base stations and the user can simply select the closest one. Some of these networks are global and some only cover a limited area like one

country for example.

4.3.3.1 Local base stations

A differential system requires a minimum of two receivers, and anyone can in principal use any pair of receivers and setup their own RTK or DGNSS system. This system is then centered around the receiver selected to be the base station. Such systems are often used in farming applications or with drones where the area that needs to be covered is small. These kinds of local systems can operate both in post-processing and real time mode. If real time operation is required, some sort of radio link is often utilized to transmit the base station data to the rover which then can calculate a differential solution.

4.3.3.2 Base station Networks and services

Several base station networks exist today, and they are connected to one or more different service provider. These networks consist of so called CORS distributed over a service area. The CORS receivers are continuously providing data that are stored in standard data formats that can be downloaded and used by anyone with access to it. Some of the providers also offer a real time streaming service. Some of them are commercial, some of them are free to use, and most of them require at least some sort of registration.

The perhaps most known and widely used database for post-processing data today is the one provided by the International GNSS Service (IGS). The IGS is a federation of more than 200 agencies, universities, and research institutions in more than 100 countries that provides free and open access to many different types of GNSS and other products for scientific purposes from more than 400 GNSS reference stations [IGS21b; Teu17]. In early 1992 CDDIS [NAS21] was selected to be the global data center for IGS.

Most countries also have their own base station network like FinnRef in Finland, and they also often offer data from their base stations [Nat21b]. On the commercial side companies like Hexagon offer their HxGN service [Hex21a]. The data is provided with a delay of 1–5 days typically, but for post-processing applications this is acceptable. This kind of approach eliminates the need for the user to set up a base station. All of the above service providers also offer real time services like

the FinnRef DGNSS service [Nat21a], the IGS RTS products [IGS21a], Hexagons TerraStar correction service [Hex21b] and the RTX service by Trimble [Tri21].

4.3.4 Correctional Data Formats

The data format depends on if we do real time or post-processing.

4.3.4.1 Post Processing RTK

For post-processing RTK solutions the common standard is the Receiver Independent Exchange Format (RINEX). The RINEX format is a simple ascii file format that already has had four major versions. Version 1 was release in 1989 [Gur89], but was quickly replaced by version 2 in 1993 already. Version 2 evolved over one decade and the final version, version 2.11, was released in 2004. RINEX 2.11 is still today used for older base stations and even new receivers and software still support it. The first version 3 release in 2007 introduced the new signals from GPS, GLONASS and Galileo and has evolved since then to the latest version 3.05 release [Rom20] end of 2020. The latest RINEX version already supports Beidou and IRNSS and all the new signals introduced over the years. Most base stations and service providers today offer RINEX 3.XX files for downloading and post-processing.

The RINEX format support three different files types. Observation data, Navigation data and Meteorological data. The observation files contain carrier phase, pseudo ranges, signal strength and Doppler observations from the GNSS receiver at the base station. The number of epochs and the update rate may vary. The header may also include information of the antenna used and general information on how the observations has been pre-processed before they are written into the file. The navigation data file contain the navigation data received from all satellites and the meteorological file contain information about air pressure, temperature, humidity etc., but also the total zenith delay of a specific signal. The navigation data file may also contain broadcast ionospheric model parameters.

For post-processing the minimum requirement is that you have the observation file from both the base station and the rover and a navigation data file from somewhere. Using this input data, a post-processing RTK software may calculate the RTK solution. In some case, especially if the baseline is long, satellite orbit and clock corrections and ionospheric corrections may also be applied.

Many receiver manufacturers like uBlox, Septentrio, Novatel and Trimble have also published the description of their proprietary binary output format and most post-processing software also support these formats. In this case the option is then to use RINEX files from the base stations and a proprietary file format from the rover. For local systems, the base station data may also be in a proprietary format.

4.3.4.2 Real Time RTK

In a real time RTK system the rover receiver needs access to a continuous near real time stream of observations. The common standard for this is Networked Transport of RTCM via Internet Protocol (NTRIP) and the Radio Technical Commission for Maritime Services (RTCM) protocol. RTCM is a data format developed for Maritime Services in general, but it also includes well-defined messages for GNSS that can be streamed in real time. Both the version 2 and version 3 of RTCM is still used, but version 3 is becoming more and more the de facto standard. The latest version for GNSS is RTCM 10403.3 that was released in April 2020 [RTC20]. The format of the NTRIP transfer protocol is given in the RTCM 10410.1 and RTCM 10410.0 standards. Many receivers support the RTCM messages so that they can be input directly into the receiver and the receiver can calculate the RTK or DGNSS position. Geodetic grade receivers are also often equipped with so called NTRIP clients and can connect directly to the internet and an NTRIP caster. Some receivers may also have their own built-in NTRIP server. A typical such system is shown in figure 4.3

RTCM provides similar observations like RINEX, carrier phase, pseudo ranges, Doppler and signal strength plus some additional information on the observations. RTCM can also provide navigation data, although most receivers will decode that themselves from the signals.

4.4 Precise Point Positioning

The concept of PPP was first mentioned by Malus [Mal90] in 1990 and later described by Zumberge [Zum97] in 1997. Before that several applications had emerged where a network of receivers was used to monitor deformation of the earth's surface due to earthquakes, motion of tectonic plates, changing earth rotation, and also for atmospheric monitoring. These applications used observations from all receivers

Figure 4.3 User receiver connecting to base stations using NTRIP

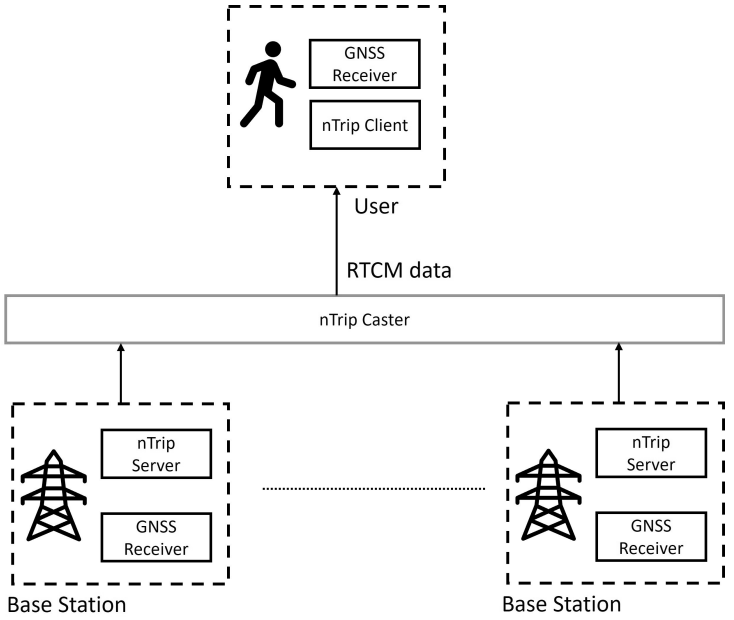

and estimated errors and parameters both in the receivers and in the GNSS as a single mathematical problem. The challenge was the large computational burden that grew rapidly with the number of receivers.

The PPP method introduced by Zumberge used a subset of receivers to estimate the unknown errors in the system first and after that the rest of the receivers could be processed one by one using these estimates. This reduced the complexity of the computations significantly. PPP methods of today are variants of this method. The principle of PPP is shown in figure 4.4

A network of base stations is receiving signals from all visible satellites and data is sent to a central data server that models each error component separately. The information about these error components can then be used by all user receivers within the area covered by the base stations. Like for RTK the PPP methods were in the beginning often used in post-processing mode, but lately also real time PPP solutions have emerged, and several service providers can provide also PPP corrections to the user.

The acronym PPP was originally used when the user applied precise orbit and clock corrections and the ambiguities were not fixed. Later the code and phase biases

Figure 4.4 Principle of PPP

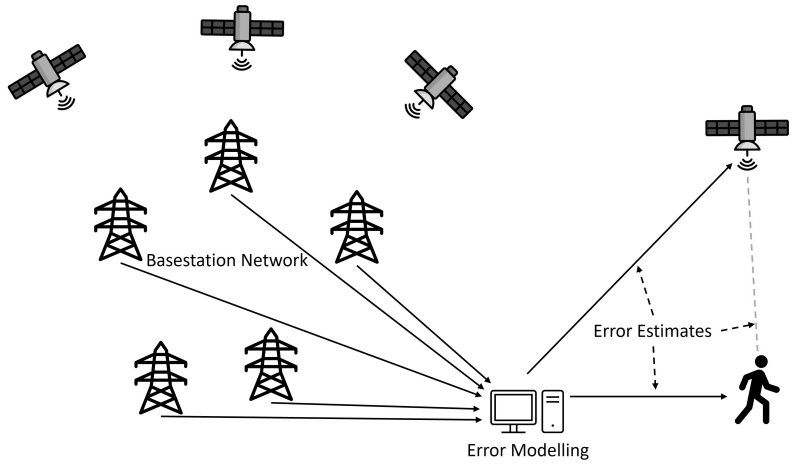

were applied and for the first time it was possible to also fix the ambiguities and the concept of Precise Point Positioning with Ambiguity Resolution (PPP-AR) was born [Ge 08]. Later also ionospheric corrections were applied, and the new method was named Precise Point Positioning with Real Time Kinematic (PPP-RTK) [Teu14; Wüb05].

4.4.1 Correctional Data Formats

The data format depends on if we do real time or post-processing.

4.4.1.1 Post Processing PPP

As mentioned before calculating a PPP solution is much more challenging since in that case, we need to remove all the individual errors one by one. The sp3 [Spo89] file format has been developed since 1989 and the latest version *d* was released in 2020 [Hil16] and this file includes precise orbit and clock information. Satellite clock offsets can also optionally be provided in a RINEX clock file [Ray17] that enables higher clock update rates. The Antenna Exchange Format (ANTEX) [Rot10] file format is based on the RINEX format, but developed for exchanging antenna information for both satellites and receivers. It includes the PCO and PCV values for all satellites and for most geodetic antennas.

The Ionosphere Exchange Format (IONEX) format [Sch89] was developed to have a common standard format for providing TEC maps that can be used to calculate the ionospheric delay for all observations and the Solution Independent Exchange Format (SINEX) [Pac20] developed by IGS for tropospheric Zenith Path Delay can be used to calculate the tropospheric delay.

The SINEX [Int16a] file format contains information about the base station and the models used for various types of calculations at the base station. Typical examples are models for the gravity field, ocean loading and solid earth tides, but also values for used constants like the speed of light and earths gravitational constant. The SINEX format can also be used to provide the so called Differential Code Biases (DCB)'s in Bias SINEX files [Sch16]. The file extension used for these are often bsx.

The Phase Biases are needed when ambiguity resolution is attempted since they are not integer wavelengths. In many cases only the fractional phase biases are used since the integer part will be absorbed by the ambiguities. Phase bias is also not an issue in differential solutions since they are eliminated in the subtraction. For PPP post-processing there are currently no reliable sources for phase biases. Corrections and input formats are listed in table 4.1

Table 4.1 Input data for post-processing PPP

Corrections	Input Format
Precise Orbits	sp3 files
Precise Clocks	sp3 or RINEX Clock files
Antenna PCO	ANTEX
Ionosphere	IONEX file
Satellite Code Biases	Bias SINEX
Troposhere	Tropo SINEX

4.4.1.2 Real Time PPP

Real Time PPP is becoming increasingly popular also in the consumer segment and there are an increasing number of service providers offering GNSS corrections today. uBlox, Fugro, Hexagon, and Trimble are just some examples. SBAS systems discussed in section 2.2.6 are also offering PPP corrections in the form of improved

ionospheric models and clock corrections and in some cases even orbit and other corrections like QZSS's CLAS service [Qua21b] and Galileos High Accuracy Service (HAS) [Eur20].

There are today three ways to receive real time PPP corrections: Over the internet, from a communication satellite over L-Band and from the GNSS satellites or their augmentation systems. The data from these are content wise similar, the formats are different and sometimes proprietary and the means for transportation is different.

When data is provided over an internet connection NTRIP and RTCM is often used like in RTK. The RTCM standard already includes messages for orbit, clock and code bias corrections and additional messages for ionosphere and phase biases have been proposed [Sch12]. Sapcorda was a consortium that tried to push their own open standard into the automotive market and several versions of the format were released [u-B21b], but in 2020 the Intellectual Property and services of Sapcorda was acquired by one of the consortium members, uBlox, who released their own service PointPerfect based on that. RX Networks [RX 12], GMV, Geo++ [Geo20] have also proposed their own formats which are all similar to the RTCM format with some differences.

The main challenge for using a real time network service is that the receiver needs to have a network connection and there need to be a good network available which is not necessarily true in all areas of the world. Utilizing communication satellites and the L-Band (1525-1559 MHz) for transmitting corrections is not a new thing. Several service providers like Hemisphere, Omnistar, Novatel and Fugro have provided this for the professional market for years and geodetic receivers are often equipped with L-Band receivers. Today also consumer grade receivers are entering into this market with uBlox and its NEO-D9S [u-B21a] as a good example. The benefit of L-Band is that no network connection is needed, and the service is truly global. Most of these services are using proprietary data format and comes with a cost for the user. A non-exhaustive list of providers, their services and the format used is provided in table 4.2

The augmentation offered by SBAS satellites also include corrections and the format is open, and it can be used for free. The receiver also does not need a separate radio for receiving the signals since they are GNSS like signals. The American WAAS and the European EGNOS offer ionospheric models and various types of differential

Table 4.2 Input data for real time PPP

Provider	Service	Format
uBlox	PointPerfect	SPARTN
QZSS	CLAS	Compact SSR
Galileo	HAS	Not Specified
RX Networks	TruePoint.io	RTCM SSR
Geo++	GNSMART Software	Geo++ SSR (SSRZ)
GMV	magicGNSS	RTCM SSR
Hemisphere	Atlas Service	Proprietary
Fugro	StarFix/SeaStar etc	Proprietary
Trimble	Omnistar	Proprietary
John Deere	Starfire	Proprietary
Swift Navigation	Skylark	RTCM SSR / 3GPP
Hexagon	TerraStar	Proprietary

corrections whereas as the Japanese QZSS already offers a centimeter level augmentation services, CLAS, that offers corrections in a format very similar to RTCM including orbit and clock corrections and code and phase biases. The Galileo HAS will offer something similar than CLAS but has not yet been specified.

4.5 Ambiguity Resolution

In order to find the integer ambiguities some sort of ambiguity search method, like the Least-squares Ambiguity Decorrelation Approach (LAMBDA) [De 96] method for example, is typically used. The ambiguity search will find the carrier ambiguities that minimize the observation residuals. This ambiguity search benefits from the fact that when the ranges change due to the satellite and user movements, the receiver can maintain a counter of the changing number of carrier cycles. That means that the exact number of added or subtracted carrier cycles are known, and the number of unknown carrier cycles are the same before and after a change in the ranges. Every new set of observations thus provides a new input for the search algorithm. The better we can estimate the errors and remove them initially the faster this ambiguity

search will go.

In theory the ambiguities should be integer numbers or so-called fixed ambiguities since we are counting the number of cycles, but in practice the ambiguities that minimizes the residuals are almost always non integers or float values. The ambiguity search typically forces the ambiguities to fixed values and the remaining unknown error are often managed as an additional state in the Kalman filter. When the ambiguities have been fixed to the correct integers the solution should in theory be more accurate. The time it takes to find the optimal fixed ambiguities is often referred to as convergence time.

In the early days of carrier phase positioning almost all solutions were done in post-processing and only using geodetic grade geodetic receivers. Still today in many applications where the best possible accuracy is needed the actual solution is calculated offline based on logged data. The benefit with such methods is that all the data is available and can be processed multiple times and both in forward and backward direction. This makes it easier to eliminate errors and fix the ambiguities. Lately carrier based positioning has also been introduced for consumer grade receivers [Kir15; Söd05] and mobile phones [Agg20; Ban16; Dar19; Rob19] and that has made real time operation more popular.

5 MULTI GNSS RECEIVER DESIGN

This chapter addresses the factors to take into account when designing a modern Multi GNSS receiver. The first section describes briefly the different types of receivers, the second section describes the different factors impacting the design of a receiver and the third sector describes in more detail the design of the main tool that has been used for the experimental part of the thesis, the FGI-GSRx Matlab receiver. In the fourth and final section some information is given on the snapshot receiver version of FGI-GSRx used in [Söd23].

5.1 GNSS receiver types

In section 3.2 some introduction was already given to the different types of GNSS receivers that exist and more details can be found from Publication I [Söd08] in this thesis. These types are also shown in figure 3.10. As is described in the paper most commercial receivers utilizes a GNSS ASIC and executes only the PVT calculations on a CPU integrated into the chip itself, whereas a SDR approach has been more used for research purposes.

A SDR gives a unique opportunity for testing new algorithms and adding support for new signals without the need to make a new ASIC. Therefore, this type of receiver is by far the best platform to use for the work done for this thesis. Publication I [Söd08] present a real commercialized SDR that was developed to be a product, but for the work in this thesis the Matlab FGI-GSRx SDR presented in Publication II [Söd16a] was used.

5.2 Receiver design considerations

Consumer grade receivers were for a long time only using the GPS L1 C/A code and limited to receiving 12 channels. For geodetic receiver the L2 signal was used to be able to do dual frequency solutions. The GLONASS signals were also first very early in geodetic receivers. When the Chineses Beidou system and the European Galileo system became operational more and more consumer grade receivers also started to support multiple constellations and frequencies. This has had a big impact on the receiver design since there are more and more frequencies, channels and modulations that need to be supported. These different signals require different types of signal processing algorithms. Also, the selection of which signals to use has changed significantly since we now have much more signals to choose from.

The PVT algorithms have also been modified to support multi constellation signals. Multiple constellations and frequencies and handling of a constantly changing set of these requires that Navigation Filters are much more configurable than before. The introduction of RTK and PPP to the consumer segment also means that one navigation filter is no longer enough. Instead, you may have several types of filters and the receiver need to select the best one. Again something that will impact the design of the receiver itself. A list of the most important factors requiring significant changes in receiver design are listed in table 5.1

Table 5.1 Factors impacting receiver design

Multiple Constellations
Multiple Frequencies
Different modulations
Large number of signals
Multiple navigation filters
Input of correctional data

5.3 The FGI-GSRx Matlab receiver

The FGI-GSRx receiver is loosely based on an open-source software receiver platform developed by [Bor07]. The original receiver by Borre was GPS only with limited support for GLONASS, but it was not a multi GNSS receiver. Also, the receiver configuration was rather complicated, and it would not have been easy to add new features and signals. Therefore, the receiver was re-designed completely utilizing only some algorithmic parts of the original receiver. The main features for this FGI-GSRx receiver is listed in table 5.2

Table 5.2 Main features of the Matlab FGI-GSRx SDR

Multi GNSS Support
Multi Frequency support
Parameter system
Kalman Filter
Support for observations from HW receivers (Novatel, uBlox, Lumia Phone)
Support for RINEX Observation files Support for RINEX Navigation files
Assisted GNSS
Support for RTCM-SSR
Support for precise orbits and clocks
PPP Solution
RTK solution including ambiguity resolution
SBAS
National Marine Electronics Association (NMEA) output
neQuick Iono model
Carrier Smoother
Several tropospheric models

The top level architecture is shown in figure 5.1

Figure 5.1 Top level architecture of the FGI-GSRx SDR

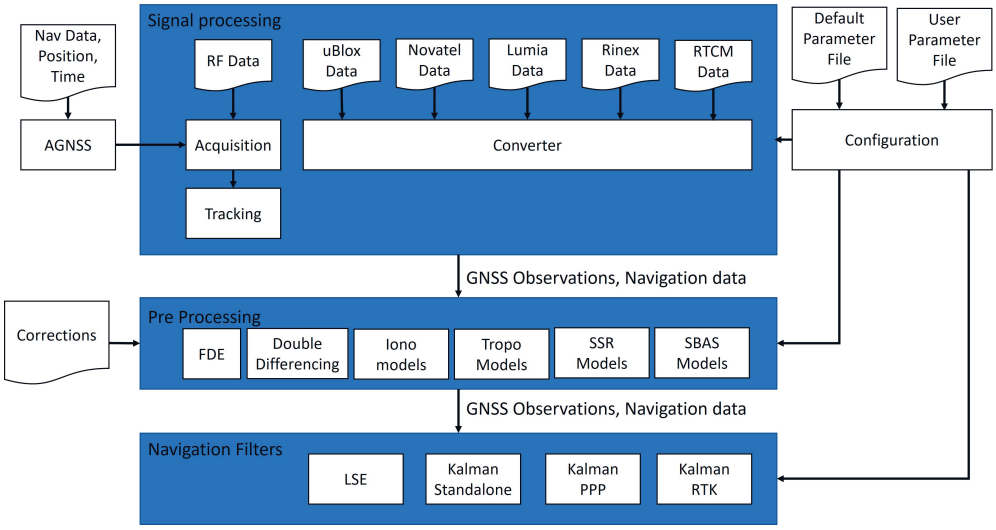

5.3.1 RF Data

The original SDR developed by Borre was designed to work with RF Data from one specific front end developed by Nottingham Scientific Limited (NSL) [Nor05]. The frequency plan, i.e., the central frequency, sampling rate, bandwidth, real or imaginary data and number of bits per sample was determined by this front end and the receiver could not use other types of RF Data. This was changed in FGI-GSRx and all the parameters defining the RF data can be easily configured and many different types of front ends have been used. The original NSL front end could only receive the L1 frequency with a bandwidth of four MHz, so it was not possible to receive other signals than GPS L1 and Galileo E1. The Fraunhofer front end [Rüg14] that was used in [Söd23] for example was configured to use a center frequency of 1.58375 GHz, bandwidth of 54 MHz and sample size of four bits I and four bits Q. When RF Data is used as input the receivers signal processing part will process that to produce GNSS Observables. The signal processing unit consist of an acquisition unit and a tracking unit.

5.3.2 Supported Signals

Initially the receiver had support for the GPS L1 and Galileo E1B signals, but several other signals have been added later. Support for the Galileo E1C was added early on together with support for the Beidou B1 and B2 signals. GLONASS L1 support has also been added and for dual frequency support GPS L5 and Galileo E5b was added. There is also support for the GPS E5 AltBoc signal, but only in the navigation filter, not in the signal processing. In [Tho16] finally the support for the IRNSS L5 frequency was added. A special case was made for the research done in [Söd23] when the support for the E1A PRS signal was added. Adding new signals in FGI-GSRx is straight forward, but if the processing algorithms are different, they also need to implemented.

5.3.3 Multi GNSS Signal Acquisition

The acquisition algorithms for the GPS L1 C/A and Galileo E1 OS signals are a simple Fast Fourier Transform (FFT)-based parallel code phase search. For Beidou signals the secondary NH code requires a slightly modified approach described in [Bhu14]. Common for all signals is that the width of the search window, the number of coherent and non-coherent integration rounds, and signal thresholds are all configurable parameters. In unaided acquisition mode the full frequency range is searched and in aided acquisition mode only one frequency bin is used. All configuration parameters can be set for both aided and unaided modes. For the Galileo E1 OS signal the data bit is four ms long and if we use longer coherent integration times there is a risk that the data bit might flip. This is managed so that we search also over all possible combinations of data bits and use four, eight or 12 ms of coherent integration. The output of the acquisition stage is stored into a file that can be used later if the user wants to bypass the acquisition stage.

5.3.4 Multi GNSS Signal Tracking

FGI-GSRx has implemented tracking channels in Matlab providing a unique possibility for configuration of correlator fingers. The normal configuration for most signals is to use three fingers for tracking and one finger for estimating the noise level,

but the user can specify any number of fingers with any finger spacing if needed. This is especially valuable for developing more advanced tracking algorithms for high order BOC signals [Söd23] or for developing multipath mitigation algorithms. For tracking the BOC(15,2.5) signal the receiver can use either a BOC(15,2.5) modulated replica or a code only replica. If only the code is used the result will be a BPSK like correlation peak on either side of the center frequency (upper and lower sidelobe). This is shown in figure 5.2

Figure 5.2 BOC(15,2.5) signal correlated with a BOC(15,2.5) signal and with only the code (generating an upper and a lower BPSK like correlation peak

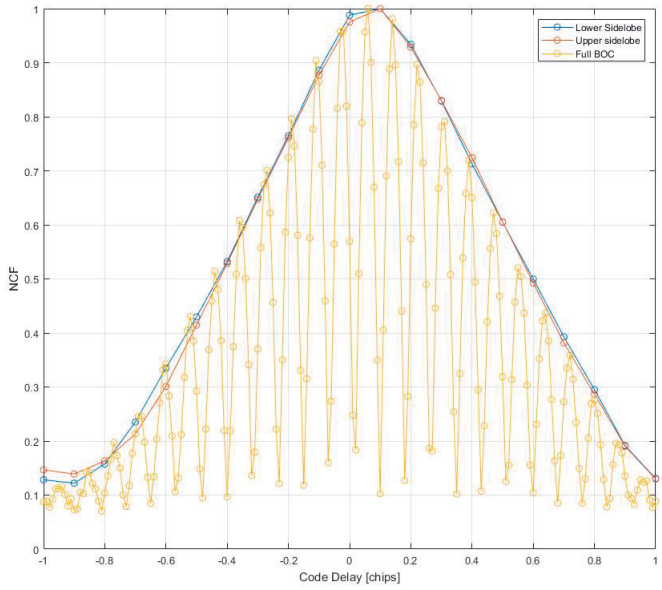

As described in section 3.2.4 a tracking channel also includes discriminators and loop filters for tracking code, carrier frequency and carrier phase. In FGI-GSRx each of these logical units are defined as a type and each type may have multiple states it can be in. A state is defined as a function or model and an update rate of that function. In addition to the states of the different types there is also a tracking state that consists of a set of states for each type. This is all illustrated in figure 5.3

This architecture allows for easy switching between different types of discriminators and filters depending on the signal we are tracking, the signal power, the signal environment, or any other factor that might require a different configuration.

Figure 5.3 Track states

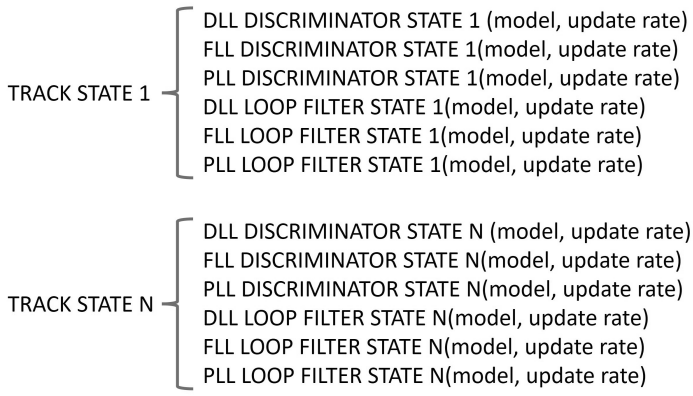

The signal tracking unit in FGI-GSRx will output track data containing the raw observables from the signal tracking including the signal strength, carrier frequency and phase, transmission time, code epoch and phase. The track data also include lock status bits, correlator finger outputs, sample counter etc. This track data will be converted in the obs unit into GNSS observations that contain Doppler frequency, pseudo ranges and carrier phase ranges and a lot of other related information.

The signal tracking in each channel is always aligned to the data bit edge as soon as it is detected to allow for maximum coherent integration times. Since the traveling time of the signals are different for different satellites it means that the track data is not synchronized between the channels. In order to achieve synchronization, we therefore need to adjust the transmission time for each channel to a common baseband sample before calculating the pseudo ranges. This operation is illustrated in figure 5.4

Since the transmission time for each channel is in system time, i.e., for GPS signals in GPS time and for Galileo signals in Galileo time, we also need to estimate the receiver time t_{rx} as a vector with the different system times as is shown in equation 5.1

$$\mathbf{t_{rx}} = \begin{bmatrix} t_{rx}^{G} \\ t_{rx}^{E} \\ t_{rx}^{B} \end{bmatrix} \tag{5.1}$$

where t_{rx}^{G} is the receiver time in the GPS time domain, t_{rx}^{E} is the receiver time

Figure 5.4 Transmission time alignment for all channels

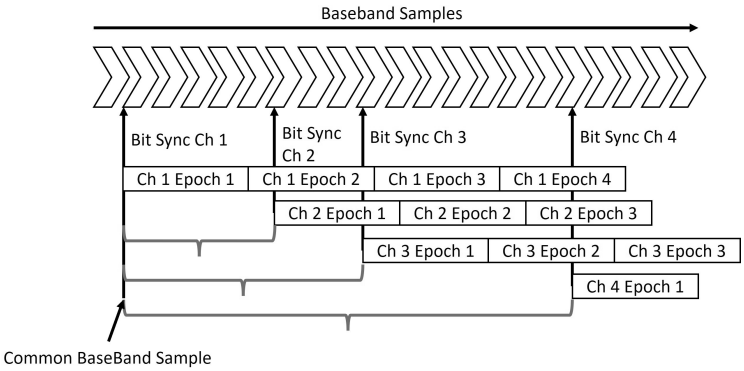

in the Galileo time domain, and t_{rx}^{B} is the receiver time in the Beidou time domain. We can then formulate the pseudo ranges ρ_i^k by selecting the correct receiver time estimate for each satellite signal shown in equation 5.2

$$\rho_i^k = \left(t_{rx}^k - t_{sv}^i\right) \tag{5.2}$$

where i is the index for the satellite signal and k is the index for the system. The output of the tracking stage is also stored into a file that can be used later if the user wants to bypass the acquisition and tracking stage.

5.3.5 GNSS Observations

If the receiver is configured to use RF Data, the GNSS Observations will be generated by the signal processing stage described in the previous section. Later on support for other types of observations has been added to the receiver. The supported formats in the FGI-GSRx are Novatel binary format, uBlox binary format, proprietary binary format from the Nokia Lumia Mobile Phone, RINEX 3 Observation files and RTCM 3 observation messages. Observations from these sources are converted into the same generic observation format used in the FGI-GSRx so that the PVT solution could be made receiver agnostic. When other data than RF Data is used the acquisition and tracking stages are bi-passed and the data is processed in a converter block instead. This is illustrated in figure 5.1

5.3.6 Navigation Data

When the FGI-GSRx is configured to use an RF Data file the navigation data is obtained from the tracking part in the receiver. The sign of the correlator prompt finger is then copied into a ring buffer and the buffer is correlated with the known frame preamble from every system. When the preamble is found in the data buffer the raw data bits can be extracted from the buffer and processed. For GPS only a parity check is needed before the actual decoding, but for Galileo we need to do the de-interleaving and Viterbi decoding first. The decoded data bits then contain the transmission time for each channel and this time stamp can be linked to a unique baseband sample counter.

Navigation data can also be provided using RINEX 2 or RINEX 3 navigation files, or it can be decoded from a uBlox or Novatel receiver. In these cases, the signal processing in FGI-GSRx is not used. Regardless of the source of the navigation data it is always converted into a generic format for ephemeris data that is also kept as similar as possible between different constellations.

5.3.7 Assisted GNSS

Assisted GNSS functionality was added to the receiver so that it was possible to provide position, time, and ephemeris information upfront and FGI-GSRx used this information to set the width of the search window, the number of coherent and non-coherent integration rounds, and signal thresholds for the acquisition stage. Using this aided acquisition the time to obtain a first position solution could be reduced significantly when using RF data files.

5.3.8 SBAS

Support for EGNOS corrections was also added to the receiver. These corrections are provided to the receiver in binary files that can be retrieved from the EGNOS Data Access Service (EDAS) service for example. Pseudo Range corrections, clock corrections and ionospheric grid corrections are supported.

5.3.9 DGNSS and RTK

Support for a differential code and differential phase solution is also included in the receiver. These solutions use data from two hardware receivers or a hardware receiver and a base station to calculate double difference observations and the Kalman Filter matrices are configured for a differential solution. Base Station data is typically provided in the RTCM format. For RTK the lambda method [De 96] is used to search for the ambiguities in RTK. The RTK feature was used for the paper [Kir15].

5.3.10 PPP Solution

In [Söd16b] a PPP solution was needed and therefore support for multiple formats of PPP corrections was added to FGI-GSRx. The primary format was RTCM-SSR including orbit and clock corrections, code biases and ionospheric corrections [Sch12]. For comparison support for post-processing formats like precise clock and orbit files was also added. To use these post-processing formats a model for correction between satellite center of mass and satellite phase center was also implemented. For the PVT solution states for the tropospheric wet delay and ambiguity states were added to the Kalman Filter.

5.3.11 Other

For ionospheric corrections we have already mentioned SBAS and RTCM-SSR, but FGI-GSRx can also use IONEX files, the NeQuick Model or the Klobuchar model for modelling and correcting for the ionospheric error. The selection of model is done using the configuration system described in more detail in the next chapter.

For the troposphere the Saastamoinen model [Saa72] is used for the hydrostatic zenith delay and a Niell function or the model from Collins [Col97] is used as a mapping function. For the wet delay the function from Mendes [Men98] is used for the zenith wet delay and the function from Niell [Nie96; Nie00] is used as a mapping function.

The FGI-GSRx also includes a statistical analysis feature that can calculate all the significant performance numbers based on the output of the processing. A typical output includes the parameters listed in table 5.3.

Table 5.3 Statistical output from FGI-GSRx

Total Number of processed Epochs
East, North and Up offsets from reference position
Horizontal 50% and 95% limits
Horizontal RMS deviation
Horizontal Standard deviation
Horizontal Max deviation for solutions
Vertical 50% and 95% limits
Vertical RMS deviation
Vertical Standard deviation
Vertical Max deviation for solutions

These parameters are provided for all solutions, i.e., LSE, Kalman, and PPP if enabled.

Several different types of FDE algorithms have also been developed for FGI-GSRx and based on these both Horizontal and Vertical protection limits are calculated [Inn16].

5.3.12 Receiver configuration

To allow for the receiver to be used in multiple research projects and with all the different types of data and features it was essential to implement a versatile configuration system. Changing parameter values and adding new parameters allows researchers to develop and test algorithms independently without impacting what other researchers are doing with the same code base.

FGI-GSRx includes a parameter system based on text files. Just by simply adding lines and values new parameters can be added to the receiver and testing with different parameter values is very easy. Default parameter values are provided in a default parameter file and a user can have multiple personal parameter files that contain only the parameter with changed values, or any new parameters used only in new algorithms for example. So, changing and adding parameters for development purposes do not require any changes to the actual receiver code.

5.3.13 Position, time and velocity solutions

Some general information on various navigation filters was presented already in section 3.2.9 and in the FGI-GSRx we actually have multiple filters that can be run in parallel. For the standalone solution we have a LSE and a Kalman Filter running. The Kalman filter is initialized when we have a good solution from the LSE. The two filters are otherwise independent of each other and both solutions can be extracted. For the PPP solution the same Kalman filter is used with additional states. RTK and DGNSS uses the same filters as the standalone, but the matrices are adapted to use double differences instead of conventional observations.

For a multi constellation receiver it is good to mention that we now have one clock offset per constellation instead of only one common clock offset as is the case in equations 3.36 and 3.41. The state vector then becomes

$$\mathbf{x} = \begin{bmatrix} \Delta x \\ \Delta y \\ \Delta z \\ c\Delta t_{rx}^{G} \\ c\Delta t_{rx}^{E} \\ c\Delta t_{rx}^{B} \end{bmatrix} \tag{5.3}$$

if we have GPS, Galileo and Beidou observations. Δt_{rx}^{k} is here the receiver clock offset for constellation k. Adding more constellations just means we also need to add clock offsets for those. The time solution then becomes a vector

$$\mathbf{t_{rx}^{true}} = \begin{bmatrix} t_{rx}^{G} - c\Delta t_{rx}^{G} \\ t_{rx}^{E} - c\Delta t_{rx}^{E} \\ t_{rx}^{B} - cd\Delta t_{rx}^{B} \end{bmatrix} \tag{5.4}$$

giving us the true time t_{rx}^{true} in all time domains. For the PPP solution the vectors and matrices are slightly more complicated. The state vector includes the three position states, the three velocity states, a clock bias and drift for each constellation, one or two optional tropospheric states and the ambiguity states for all the observations. The state transition matrix then assumes that the predicted position is the

initial position extrapolated with the velocity and the velocity is assumed to be the same.

5.4 Snapshot Receiver

In the paper [Söd23] the FGI-GSRx Matlab receiver was modified to some extent in order to provide a snapshot functionality. A snapshot receiver works with short pieces of data, typically 1 - 100 ms, and processes these using open loop tracking. Tracking in open loop mode means that instead of continuously filtering the discriminator outputs and controlling the correlators using loop filters we simply need to find the code phase, carrier frequency and carrier phase that minimize the discriminator functions for one particular snapshot. The small amount of data also means that no navigation data can be decoded from the snapshot. Instead, the support for RINEX Nav files and Assisted GNSS in FGI-GSRx was used to obtain orbit and clock information for the satellites.

There is also a significant difference in obtaining the position in a snapshot receiver since there is typically no transmission time available. The data is simply too short to contain any navigation data. This means that navigation data must be provided from external sources and that the transmission times of the signals are unknown. In a snapshot receiver the receiver time and transmission times therefore need to be solved iteratively by minimizing the residuals of the observations. For this the LSE filter was used since there is no real benefit from the Kalman filter since only a single position solution is calculated for one snapshot.

The snapshot receiver was used to process the PRS signal, which uses a so-called long code. For such codes FFT based parallel code phase search in the FGI-GSRx could not be used. Instead, a serial search approach was implemented. The main differences between the snapshot version of FGI-GSRx and FGI-GSRx itself is listed in table 5.4

Table 5.4 Snapshot receiver operation

Normal Operation	Snapshot Operation
Data Decoding from I/Q data	Navigation data from RINEX nav files
Kalman Filter	Iterative LSE Solution
Parallel FFT code phase search	Serial Search for PRS signal
Closed loop tracking	Open loop tracking

6 CONCLUSION

The main objectives of this thesis were to assess the impact of the evolution of GNSS technology on the performance and design of consumer grade GNSS receivers. In the objectives in chapter one five different main questions were presented:

1. How should a receiver be designed to allow for maximum flexibility when it comes to new signals and methods?
2. What is the impact of having more satellite navigation systems and signals available?
3. What kind of new receiver algorithms are needed to process new signals?
4. What will the impact be of more accurate observations from high frequency codes?
5. How well does methods like RTK and PPP work in consumer grade receivers?

The first question is addressed in Publication I [Söd08] and Publication II [Söd16a]. Already with only GPS signals present 15 years ago the author has shown in Publication I [Söd08] that there are options to the pure hardware-based receiver allowing for reducing the hardware cost by utilizing existing application processors to run the signal processing software on. Publication I [Söd08] also clearly show that the performance of such a software receiver is matching the performance of hardware receivers even if the memory usage and CPU load are reduced significantly.

A software-based approach allows for maximum configurability and unlimited number of channels and a design for such a software receiver is then presented in more detail in Publication II [Söd16a]. The design is such that the addition of new signals and modulations is straightforward, and it can be used even as a snapshot receiver as is shown in Publication V [Söd23].

In chapter 2 the author describes the evolution of GNSS in detail and the increasing number of constellations and signals as well as introduction of more complex

signal modulations and longer codes becomes very clear. To support all these new signals, it will result in a larger silicon area and higher price for ASIC's and therefore the benefits of a software defined receiver increases significantly. The second question is then addressed in Publication II [Söd16a] where it is shown that the increased number of signals and constellation improves both availability and accuracy of the receiver, especially in urban canyon environment where signal blockage is significant. In severe urban canyons, the position error for GPS only can be more than ten times bigger, and the fix availability can be less than half of the availability for a multi-GNSS solution.

The third research question is addressed in Publication III [Bhu14] and Publication IV [Tho16] where some more details on the support of Beidou and IRNSS signals is provided. Additional challenges dealing with the NH modulation of the Beidou signal in the acquisition stage of the receiver is presented in Publication III [Bhu14]. This is also a good example of how easy it is in a software defined receiver to add support for a new signal compared to making a new ASIC. The addition of support for the IRNSS L5 signal in the SDR is presented in Publication IV [Tho16].

The fourth research question is addressed in Publication V [Söd23], where the benefits from the modern codes and modulation have clearly been shown. Here the authors present the performance of a snapshot receiver when utilizing the high order BOC modulated Galileo PRS signal. The paper also presents new algorithms optimized for long signal acquisition and tracking. It is shown that by using these new methods with a high order BOC signal the accuracy improves by a factor five.

Chapter 4 in this thesis presents the challenges and benefits with carrier based positioning methods like RTK and PPP. Such methods have traditionally been used only with geodetic grade receivers and often in post-processing mode, but today they are becoming much more common also in consumer grade receivers with the increasing amount of correctional service provider, significantly improved measurement quality and increased number of signals. Especially the introduction of dual frequency receivers into the consumer segment have been an enabler of PPP and RTK methods.

The fifth research question is addressed in Publications VI [Kir15] and Publication VII [Söd16b], where the performance of RTK on consumer grade receivers and the quality of PPP-SSR correction from the FinnRef network in is addressed.

The results and conclusions presented in this thesis clearly indicate that there has

been a significant performance improvement in accuracy and availability of a solution in consumer grade GNSS receivers during the last two decades. This improvement is partly due to the introduction of more signals as well as the introduction of new modern modulation techniques. This development has enabled the introduction of carrier phase positioning methods like PPP and RTK further improving especially the accuracy of the receivers.

The thesis show that it is essential that the receiver itself is adapted to make use of all the above-mentioned new signals. This means that the architecture of consumer grade receivers is significantly more complex than two decades ago. Constantly developing new generation of ASICs with more and more features has become an expensive exercise for many companies and the software defined receiver would in many cases be a much better choice. Still, in order to design the architecture of such a modern receiver remain challenging but is essential in order to accommodate for more and more new signals.

6.1 Future Work

Future work includes more detailed studies on modern signals and how to use these in the best way. There are still a lot of new algorithms that needs to be investigated for optimal signal processing of these signals and there is a lot of research needed for designing the logic to use these signals in the navigation filters. The availability of a third frequency in mass market receivers is not yet there, but it will eventually come and thus also algorithm utilizing three and even four signals are also important for the future of these receivers and clearly a topic for future research. The use of a third frequency in PPP and RTK has a significant impact on improving atmospheric estimation and making ambiguity fixing faster and is also an interesting topic for future work. A part of the new signals is the new concept of pilot signals that could be used for increasing the sensitivity of the receivers. Finally, it would be valuable to investigate the quality of new open PPP-SSR services including CLAS and HAS and how they would impact the performance of consumer grade receivers.

REFERENCES

[Agg20] Aggrey, J. , Bisnath, S. , Naciri, N. et al. Multi-GNSS precise point positioning with next-generation smartphone measurements. *Journal of Spatial Science* 65.1 (2020), 79–98.

[Ary15] Arya, K. C. , Bhatt, B. , Adhikari, S. et al. Design of a Rectangular Microstrip Patch Antenna for GNSS/GPS System. *International Journal of Engineering Research & Technology* 4.4 (2015).

[Asc72] Asche, G. P. Omega system of global navigation. *International Hydrographic Review* 50.1 (1972), 87–99.

[Avi07] Avila-Rodriguez, J-A. , Hein, G.W., Wallner, S. et al. The MBOC modulation: the final touch to the Galileo frequency and signal plan. *Proceedings of the 20th International Technical Meeting of the Satellite Division of The Institute of Navigation*. FortWorth, TX, 2007, 1515–1529.

[Avi06] Avila-Rodriguez, J-A. , Wallner, S., Hein, G.W. et al. CBOC : an implementation of MBOC. *1rst CNES-ESA Workshop on Galileo Signals and Signal Processing* (Oct. 2006).

[Bag16] Baggen, H. u-blox adds Galileo support for GNSS modules. *ElektorMag* (Jan. 2016). URL: `https://www.elektormagazine.com/news/u-blox-adds-galileo-support-for-gnss-modules` (visited on 07/27/2023).

[Ban16] Banville, S. and van Diggelen, F. Precise positioning using raw GPS measurements from Android smartphones. *GPS world* 27.11 (2016), 43–48.

[Bar53] Barker, R. H. Group Synchronizing of Binary Digital Systems. *Communication Theory* (1953), 273–287.

[Ben99] Benefon. *Annual report 1999*. 1999. URL: https://web.lib.aalto.fi/fi/old/yrityspalvelin/pdf/1999/Ebenefon1999.pdf (visited on 07/27/2023).

[Ber52] Bergstrand, E. Distance measuring by means of modulated light. *Bulletin Géodésique* 24.1 (1952), 243–249.

[Bet01] Betz, J. W. Binary Offset Carrier Modulations for Radionavigation. *Navigation: Journal of The Institute of Navigation* 48.4 (2001), 227–246. DOI: 10.1002/j.2161-4296.2001.tb00247.x.

[Bet06] Betz, J. W. , Blanco, M.A. , Cahn, C.R. et al. Description of the L1C signal. *Proceedings of the 19th International Technical Meeting of the Satellite Division of The Institute of Navigation*. FortWorth, TX, 2006, 2080–2091.

[Bhu14] Bhuiyan, M. Z. H. , Söderholm, S. , Thombre, S. et al. Overcoming the Challenges of BeiDou Receiver Implementation. *Sensors* 2014 (Nov. 2014), 22082–22098. DOI: 10.3390/s141122082.

[Bla91] Blanchard, W. Air Navigation Systems Chapter 4. Hyperbolic Airborne Radio Navigation Aids – A Navigator's View of their History and Development. *The Journal of Navigation* 44.3 (1991).

[Bla15] Blanchard, W. The Genesis of the Decca Navigator System. *Journal of Navigation* 68.2 (2015), 219–237. DOI: 10.1017/S0373463314000666.

[Bor07] Borre K., Akos D.M., Bertelsen N. et al. *A software-defined GPS and Galileo receiver*. Birkhäuser Verlag GmbH, Boston, 2007. ISBN: 978-0-8176-4390-4.

[Bos80] Bossler J. D. , Goad C. C. and Bender P. L. Using the Global Positioning System (GPS) for geodetic positioning. *Bulletin géodésique* 54 (1980), 553–563.

[Chi20] China satellite Navigation Office. *BeiDou Navigation Satellite System Signal In Space Interface Control Document*. 2020. URL: http://en.beidou.gov.cn/SYSTEMS/ICD/ (visited on 08/05/2023).

[Col97] Collins, J. P. and Langley, R. B. *A Tropospheric Delay Model for the User of the Wide Area Augmentation System*. 1997. URL: http://gauss.gge.unb.ca/papers.pdf/waas.tropo.oct96.pdf (visited on 08/05/2023).

[Coo98] Coordination Scientific Information Center. *GLONASS Interface Control Document*. 1998. URL: https://www.unavco.org/help/glossary/docs/ICD_GLONASS_4.0_(1998)_en.pdf (visited on 08/05/2023).

[Dal86] Daly, P. and Perry, G. E. Recent Developments with the Soviet Union's VHF Satellite Navigation System. *Space Communication and Broadcasting* 44 (1986), 51–61.

[Dan98] Danchik, R. J. An Overview of Transit Development. *Johns Hopkins APL Technical Digest* 19.1 (1998), 18–26.

[Dar19] Darugna, F. , Wübbena, J.B., Ito, A. et al. RTK and PPP-RTK using smartphones: From short-base-line to long-baseline applications. *Proceedings ION GNSS 2019* (2019), 3932–3945.

[Dau89] Daumas, M. *Scientific Instruments of the Seventeenth and Eighteenth Centuries and Their Makers*. London: Portman Books, 1989. ISBN: 978-0713407273.

[De 96] De Jonge, P. and Tiberius, C. The LAMBDA method for integer ambiguity estimation: implementation aspects. *Delft Geodetic Computing Centre LGR Series* 12 (1996).

[De 07] De Wilde, W. , Boon, F. , Sleewaegen, J-M. et al. More Compass points. Tracking China's MEO satellite on a hardware receiver. *Inside GNSS* July/August (2007), 44–48.

[Dia30] Diamond, H. and Dunmore, F. W. A Radio System for Blind Landing of Aircraft in Fog. *Proceedings of the National Academy of Sciences* 16 (1930), 678–685.

[Dic59] Dickinson, W. T. Engineering Evaluation of the LORAN C Navigation System. *The Journal of Navigation* (1959).

[ESA20] ESA. *Tracking the solar cycle, NOAA*. 2020. URL: https://www.esa.int/ESA_Multimedia/Images/2020/10/Tracking_the_solar_cycle_NOAA (visited on 08/05/2023).

[Eur16] European Commission. *Ionospheric Correction Algorithm for Galileo single frequency users*. 2016. URL: https://www.gsc-europa.eu/sites/default/files/sites/all/files/Galileo_Ionospheric_Model.pdf (visited on 11/25/2021).

[Eur21] European Commission. *Signal-In-Space Interface Control Document*. 2021. URL: https://www.gsc-europa.eu/sites/default/files/sites/all/files/Galileo_OS_SIS_ICD_v2.0.pdf (visited on 08/05/2023).

[Eur20] European GNSS Agency. *Galileo High Accuracy Service (HAS)*. 2020. URL: https://www.gsc-europa.eu/sites/default/files/sites/all/files/Galileo_HAS_Info_Note.pdf (visited on 08/05/2023).

[EUS22] EUSPA. *EUSPA EO and GNSS Market Report*. 2022. URL: https://www.euspa.europa.eu/sites/default/files/uploads/euspa_market_report_2022.pdf (visited on 07/26/2023).

[EUS23] EUSPA. *Galileo: putting the smart into smartphones*. 2023. URL: https://www.euspa.europa.eu/newsroom/news/galileo-putting-smart-smartphones (visited on 07/26/2023).

[EWD11] EWDN. Swedish satellite data provider prefers GLONASS to GPS. *East-West Digital News (https://www.ewdn.com/)* April 12 (2011).

[Flo21] Flores, A. *NAVSTAR GPS Space Segment/Navigation User Interfaces*. 2021. URL: https://www.gps.gov/technical/icwg/IS-GPS-200M.pdf (visited on 08/05/2023).

[Fri33] Frisius, G. Libellus de locorum describendum ratione. *Cosmographica* (1533).

[Gar05] Gardner, F. M. *Phaselock techniques*. Hoboke, New Jersey, USA: John Wiley and Sons, Inc., 2005. ISBN: 978-0-471-43063-6.

[Gat06] Gatti, G. , Garutti, A. , Mandorlo, G. et al. The GIOVE-A Satellite: From Design to in-orbit Commissioning. *Proceedings ION GNSS 2006* (2006), 2542–2547.

[Ge 08] Ge, M. , Gendt, G. , Rothacher, M. et al. Resolution of GPS carrier-phase ambiguities in precise point positioning (PPP) with daily observations. *Journal of geodesy* 82.7 (2008), 389–399.

[Geo20] Geo++. *Geo++®State Space Representation Format (SSRZ)*. 2020. URL: https://www.geopp.de/wp-content/uploads/2020/09/gpp_ssrz_v1_0.pdf (visited on 08/05/2023).

[Gib11] Gibbs, B. P. *Advanced Kalman Filtering, Least-Squares and Modeling*. Hoboke, New Jersey, USA: John Wiley and Sons, Inc., 2011. ISBN: 978-0-470-89004-2.

[Gol67] Gold, R. Optimal binary sequences for spread spectrum multiplexing. *IEEE Transactions on Information Theory (Correspondence)* IT-13 (4) (1967), 619–621. DOI: 10.1109/TIT.1967.1054048.

[Gre06] Grelier, T. , Ries, L. and Issler, J-L. New Spectral Measurements of GNSS Signals. *Proceedings of the Institute of Navigation National Technical Meeting* (2006), 82–91.

[Gur89] Gurtner, W. and Mader, G. and MacArthur, D. A Common Exchange Format for GPS Data. *Proceedings of the Fifth International Geodetic Symposium on Satellite Systems* (1989), 917ff.

[Ham50] Hamming, R. W. Error Detecting and Error Correcting Codes. *Bell System Technical Journal* 29.2 (1950), 147–160. DOI: 10.1002/j.1538-7305.1950.tb00463.x.

[Har87] Harley, J. B. and Woodward, D. *The History of Cartography, Volume 1*. 1427 E. 60th Street Chicago, IL 60637 USA: University of Chicago Press, 1987.

[Hef72] Hefley, G. *The Development of LORAN-C Navigation and Timing*. Boulder, Colorado, USA: U.S. Depatment of Commerce, Natinal Bureau of Standards, 1972.

[Hei06] Hein, G. W., Avila-Rodriguez, J.-A. , Wallner, S. et al. MBOC: the new optimized spreading modulation recommended for GALILEO L1 OS and GPS L1C. *Inside GNSS* 4 (Jan. 2006), 883–892. DOI: 10.1109/PLANS.2006.1650688.

[Hex21a] Hexagon. *RINEX Download*. 2021. URL: https://hxgnsmartnet.com/en-gb/services/rinex-download (visited on 08/05/2023).

[Hex21b] Hexagon. *TerraStar Correction Services*. 2021. URL: https://novatel.com/products/gps-gnss-correction-services/terrastar-correction-services (visited on 08/05/2023).

[Hil16] Hilla, S. *The Extended Standard Product 3 Orbit Format (SP3-d)*. 2016. URL: https://gssc.esa.int/wp-content/uploads/2018/07/sp3d.pdf (visited on 08/05/2023).

[Hof92] Hofmann-Wellenhof, B. , Lichtenegger, H. and Collins, J. *Global Positioning System*. Vienna: Springer, 1992. ISBN: 978-3-211-82364-4.

[IGS21a] IGS. *IGS RTS Products*. 2021. URL: https://igs.org/rts/products/ (visited on 08/05/2023).

[IGS21b] IGS. *International GNSS Service*. 2021. URL: https://igs.org (visited on 08/05/2023).

[Ind17] Indian Space Research Organization. *Signal In Space ICD for Standard Positioning Service*. 2017. URL: https://www.isro.gov.in/sites/default/files/irnss_sps_icd_version1.1-2017.pdf (visited on 08/05/2023).

[Inn16] Innac, A. , Bhuiyan, M. Z. H. , Söderholm, S. et al. Reliability testing for multiple GNSS measurement outlier detection. *2016 European Navigation Conference*. 2016, 1–8. DOI: 10.1109/EURONAV.2016.7530540.

[Ins11] Inside GNSS. Qualcomm Adds GLONASS Capability to Chipsets. *Inside GNSS* June 6 (2011).

[Int16a] International Earth Rotation and reference Systems Service. *Solution (Software/technique) INdependent EXchange Format Version 2.02*. 2016. URL: https://www.iers.org/IERS/EN/Organization/AnalysisCoordinator/SinexFormat/sinex.html (visited on 08/05/2023).

[Int16b] International Telecommunication Union. *ITU Radio Regulations*. 2016. URL: https://www.itu.int (visited on 08/05/2023).

[Int16c] International Telecommunication Union. *ITU Radio Regulations*. 2016. URL: https://www.itu.int (visited on 08/05/2023).

[Int22] International Telecommunication Union. 2022. URL: https://www.itu.int (visited on 08/05/2023).

[Jul07] Julien, O. , Macabiau, C. , Issler, J-L. et al. Two for One - Tracking Galileo CBOC Signal with TMBOC. *Inside GNSS* Sping (2007), 50–57.

[Kap17] Kaplan, E.D. and Hegarty, C.J. *Understanding GPS/GNSS Principles and Applications*. Artech, 2017. ISBN: 978-1-63081-058-0.

[Kas66] Kasami, T. *Weight Distribution Formula for Some Class of Cyclic Codes*. Tech. rep. Coordinated Science Laboratory, University of Illinois at Urbana-Champaign, 1966.

[Kir15] Kirkko-Jaakkola, M. , Söderholm, S., Honkala, S. et al. Low-Cost Precise Positioning Using a National GNSS Network. *Proceedings of the ION GNSS+ 2015* (2015), 2570–2577.

[Klo87] Klobuchar, J.A. Ionospheric Time-Delay Algorithms for Single-Frequency GPS Users. *IEEE Transactions on Aerospace and Electronic Systems* 3 (1987), 325–331.

[Kuu05] Kuusniemi, H. User-Level Reliability and Quality Monitoring in Satellite-Based Personal Navigation. PhD thesis. P.O. Box 527, FIN-33101 Tampere, Finland: Tampere University of Technology, 2005. ISBN: 952-15-1426-4.

[Les08] Lestarquit, L. , Artaud, G. and Issler, J-L. AltBOC for Dummies or Everything You Always Wanted to Know About AltBOC. *Proceedings of the 21st International Technical Meeting of the Satellite Division of The Institute of Navigation*. Sept. 2008.

[Li 23] Li, X. , Barriot, J-P., Lou, Y., et al. Towards Millimeter-Level Accuracy in GNSS-Based Space Geodesy: A Review of Error Budget for GNSS Precise Point Positioning. *Surveys in Geophysics* 2023/05/13 (2023).

[Lo 06] Lo, S. , Chen, A. , Enge, P. et al. Images and Spectral Signatures of the new GNSS Signals. *Inside GNSS* May/June (2006), 46–56.

[Loh06] Lohan, E.S. ,Lakhzouri, A. and Renfors, M. Binary-offset-carrier modulation techniques with applications in satellite navigation systems. *Wireless Communications and Mobile Computing* 7 (2006), 767–779.

[Lu 10] Lu M. QMBOC modulation and its multiplexing techniques. 2010. URL: `https://api.semanticscholar.org/CorpusID:113068267`.

[Maj17] Majithiya, P. , Khatri, K. , Bera, S.C. et al. Future Space Service of NavIC (IRNSS) Constellation. *Inside GNSS* July/August (2017), 40–45.

[Mal90] Malys, S. and Jensen, P. A. Geodetic point positioning with GPS carrier beat phase data from the CASA UNO experiment. *Geophysical Research Letters* 17.5 (1990), 651–654.

[Men98] Mendes, V.B. and Langley, R.B. Tropospheric zenith delay prediction accuracy for airborne gps high-precision positioning. *Proceedings of The Institute of Navigation 54th Annual Meeting* (1998), 337–347.

[Mer20] Merwe, J. van der, Zubizarreta, X., Rubino, D. et al. Position Solution Sensitivity for Snapshot Receivers. *2020 International Conference on Localization and GNSS (ICL-GNSS)* (June 2020). DOI: 10.1109/ICL-GNSS49876.2020.9115574.

[Mis06] Misra, P. and Enge, P. *Global Positioning System: Signals, Measurements, and Performance*. 2nd edition. Ganga-Jamuna Press, Lincoln MA, 2006.

[Moe09] Moernaut, G. J. K. and Orban, D. GNSS Antennas. An introduction to Bandwidth, Gain Paterns, Polarization and All That. *GPS World* (2009), 42–48.

[NAS21] NASA. *NASA's archive of Space Geodesy data*. 2021. URL: https://cddis.nasa.gov/ (visited on 08/05/2023).

[Nat21a] National land Survey of Finland. *FinnRef DGNSS service*. 2021. URL: https://www.maanmittauslaitos.fi/en/finpos/dgnss (visited on 08/05/2023).

[Nat21b] National land Survey of Finland. *RINEX Service*. 2021. URL: https://www.maanmittauslaitos.fi/en/finpos/rinex (visited on 08/05/2023).

[Nie96] Niell, A.E. Global mapping functions for the atmosphere delay at radio wavelengths. *J Geophys Res* 101.B2 (1996), 3227–3246.

[Nie00] Niell, A.E. Improved atmospheric mapping functions for VLBI and GPS. *Earth Planets Space* 52 (2000), 699–702.

[Nor05] Normark, P-L. and Ståhlberg, C. Hybrid GPS/Galileo Real Time Software Receiver. *Proceedings of ION GNSS 2005* (Sept. 2005), 1906–1913.

[Orb09] Orban, D. and Moernaut, G.J.K. *The Basics of Patch Antennas*. 2009. URL: https://www.orbanmicrowave.com/gps (visited on 08/05/2023).

[Pac20] Pacione, R. and Douša, J. *SINEX*. 2020. URL: https://files.igs.org/pub/data/format/sinex_tro_v2.00.pdf (visited on 08/05/2023).

[Pan12] Panther, G. Patch Antennas for the New GNSS. *GPS World* (2012).

[Par79] Parkinson, B. W. The global positioning system (navstar). *Bulletin géodésique* 53 (1979), 89–108.

[Pír06] Píriz, R. , Fernández, V. , Auz, A. et al. The Galileo System Test Bed V2 for Orbit and Clock Modeling. *Proceedings ION GNSS 2006* (2006), 549–562.

[Qua11] Qualcomm. *Qualcomm Enhances Mobile Location Performance by Utilizing GPS and GLONASS Satellite Networks for Greater Location Accuracy*. 2011. URL: https://investor.qualcomm.com/news-events/press-releases/detail/177/qualcomm-enhances-mobile-location-performance-by-utilizing (visited on 07/27/2023).

[Qua16] Qualcomm. *Qualcomm announced in June 2016 that they will add support for Galileo to their Snapdragon processors*. 2016. URL: https://d1io3yog0oux5.cloudfront.net/_4af90b54e4cc62eca32840b588ceb7aa/qualcomm/news/2016-06-21_Qualcomm_Announces_Broad_Support_for_Galileo_792.pdf (visited on 07/27/2023).

[Qua21a] Quasi Zenith Satellite System Navigation Service. *Quasi Zenith Satellite System Interface Specification Satellite Positioning, Navigation and Timing Service*. 2021. URL: https://qzss.go.jp/en/technical/download/pdf/ps-is-

qzss/is-qzss-pnt-004.pdf?t=1637860652984 (visited on 08/05/2023).

[Qua21b] Quasi-Zenith Satellite System Services Inc. *Quasi-Zenith Satellite System Interface Specification Centimeter Level Augmentation Service*. 2021. URL: https://qzss.go.jp/en/technical/ps-is-qzss/is_qzss_l6_004_agree.html (visited on 08/05/2023).

[Ray17] Ray, J. and Gurtner, W. *RINEX Extensions to Handle Clock Information*. 2017. URL: https://files.igs.org/pub/data/format/rinex_clock302.txt (visited on 08/05/2023).

[Rob19] Robustelli, U. , Baiocchi, V. and Pugliano, G. Assessment of Dual Frequency GNSS Observations from a Xiaomi Mi 8 Android Smartphone and Positioning Performance Analysis. *Electronics* 8 (2019), 91.

[Rom20] Romero, I. (ed). *The Receiver Independent Exchange Format*. 2020. URL: https://files.igs.org/pub/data/format/rinex305.pdf?_ga=2.44456743.20921313.1637862087-363049383.1637862087 (visited on 08/01/2023).

[Rot10] Rothacher, M. and Schmid, R. *ANTEX format description*. 2010. URL: https://files.igs.org/pub/data/format/antex14.txt (visited on 08/01/2023).

[RTC20] RTCM Special Committee no. 104. *RTCM 10403.3, Differential GNSS (Global Navigation Satellite Systems) Services*. 2020. URL: https://rtcm.myshopify.com/collections/differential-global-navigation-satellite-dgnss-standards/products/differential-gnss-package-both-of-the-current-standards-10402-3-and-10403-2 (visited on 08/01/2023).

[Rüg14] Rügamer, A. , Förster, F. , Stahl, M.et al. Features and applications of the adaptable flexiband USB3.0 front-end. *Proceedings of ION GNSS 2014* (Sept. 2014), 330–362.

[Rus06] Rushanan, J. J. Weil Sequences: A Family of Binary Sequences with Good Correlation Properties. *2006 IEEE International Symposium on Information Theory*. 2006, 1648–1652. DOI: 10.1109/ISIT.2006.261556.

[Rus07] Rushanan, J. J. The Spreading and Overlay Codes for the L1C Signal. *NAVIGATION* 54.1 (2007), 43–51. DOI: https://doi.org/10.1002/j.2161-4296.2007.tb00394.x.

[RX 12] RX Networks. *Truepoint.io*. 2012. URL: https://www.rxnetworks.com/truepoint.io#!PPP-RTK (visited on 08/01/2023).

[Saa72] Saastamoinen, J. Atmospheric Correction for the Troposphere and Stratosphere in Radio Ranging of Satellites. *The Use of Artificial Satellites for Geodesy*. Ed. by B. H. C. S. W. Henriksen A. Mancini. Vol. 15. Geophysical Monograph Series. Washington, D.C.: AGU, 1972, 247–251.

[Sch16] Schaer, S. *SINEX BIAS—Solution (Software/technique) INdependent EXchange Format for GNSS Biases Version 1.00*. 2016. URL: http://ftp.aiub.unibe.ch/bcwg/format/draft/sinex_bias_100_dec07.pdf (visited on 08/01/2023).

[Sch89] Schaer, S., Gurtner, W. and Feltens, J. *IONEX: The IONosphere Map EXchange Format Version 1.1*. 1989. URL: http://ftp.aiub.unibe.ch/ionex/draft/ionex11.pdf (visited on 08/01/2023).

[Sch12] Schmitz, M. *RTCM State Space Representation Messages, Status and Plans*. 2012. URL: https://www.geopp.de/pdf/gpp_ppprtk12_msg_f.pdf (visited on 08/01/2023).

[Sch00] Schüler, T. On Ground-Based GPS Tropospheric Delay Estimation. An optional note. PhD thesis. Werner-Heisenberg-Weg 39, D-85577 Neubiberg: Universität der Bundeswehr München, Oct. 2000.

[Sco69] Scott, R. E. Study and Evaluation of the Omega Navigation System for transoceanic navigation by civil aviation. *FAARD* 39 (1969).

[Sim06] Simsky, A. , Sleewaegen, J-M. , Hollreiser, M. et al. Performance Assessment of Galileo Ranging Signals Transmitted by GSTB-V2 Satellites. *Proceedings ION GNSS 2006* (2006), 1547–1559.

[Sle12] Sleewaegen J.M., Simsky, A., De Wilde, W. et al. Demystifying GLONASS interfrequency carrier-phase biases. *Inside GNSS* 7.3 (2012), 57–61.

[Söd05] Söderholm, S. GPS L1 Carrier Phase Double Difference Solution Using Low Cost Receivers. *Proceedings of the 18th ITM of the Satellite Division of The Institute of Navigation* (2005), 376–380.

[Söd16a] Söderholm, S. , Bhuiyan, M. Z. H. , Thombre, S. et al. A multi-GNSS software-defined receiver: design, implementation, and performance benefits. *Annals of Telecommunications* 71.7-8 (2016), 399–410.

[Söd08] Söderholm, S. , Jokitalo, T., Kaisti, K. et al. Smart positioning with Fastrax's software GPS receiver solution. *Proceedings of the 21st International Technical Meeting of the Satellite Division of The Institute of Navigation (ION GNSS 2008)*. Savannah, GA, 2008, 1193–1200.

[Söd16b] Söderholm, S. , Koivula, H. , Kuusniemi, H. et al. Performance assessment of single frequency Precise Point Positioning using the SSR model from the Finnish National GNSS Network. *European Journal of Navigation* 14.4 (2016), 39–44.

[Söd23] Söderholm, S., Nurmi, J. , Berg, A., and Kuusniemi, H. Optimal Signal Processing of the Galileo PRS signal in a snapshot receiver. (2023).

[Spo89] Spofford, P. R. and Remondi, B. W. *The National Geodetic Survey Standard GPS Format SP3*. 1989. URL: `https://files.igs.org/pub/data/format/sp3_docu.txt` (visited on 08/05/2023).

[Teu14] Teunissen, P.J.G. and Khodabandeh, A. Review and principles of PPP-RTK methods. *Journal of Geodesy* (Nov. 2014), 1–24. DOI: 10.1007/s00190-014-0771-3.

[Teu17] Teunissen, P.J.G. and Montenbruck, O. (Eds.) *Springer Handbook of Global Navigation Satellite Systems*. Cham, Switzerland: Springer International Publishing, 2017, 967–982.

[The99] The Council of The European Union. *Council Resolution of 19 July 1999 on the involvement of Europe in a new generation of satellite navigation services -Galileo- Definition phase*. Tech. rep. The Council of The European Union, 1999.

[Tho16] Thombre, S., Bhuiyan, M. Z. H.,Söderholm, S. et al. A Software Multi-GNSS Receiver Implementation for the Indian Regional Navigation Satellite System. *IETE Journal of Research* 62.2 (2016), 246–256. ISSN: 0377-2063. DOI: 10.1080/03772063.2015.1093968.

[Tri21] Trimble. *Positioning Services*. 2021. URL: https://positioningservices.trimble.com/services/ (visited on 08/05/2023).

[u-B21a] u-Blox. *NEO-D9S series*. 2021. URL: https://www.u-blox.com/en/product/neo-d9s-series (visited on 08/05/2023).

[u-B21b] u-Blox. *Secure Position Augmentation for Real-Time Navigation (SPARTN) Interface Control Document*. 2021. URL: https://www.spartnformat.org/wp-content/uploads/210928_SPARTN_v2.0.1.pdf (visited on 08/05/2023).

[Wad57] Wadley, T. L. The Tellurometer System of Distance Measurement. *Empire Survey Review* (1957), 100–110.

[Wat71] Watson, D.W. and Wright, H.E. *Radio Direction Finding*. Marconi series covering advances in radio and radar. Van Nostrand-Reinhold, 1971. ISBN: 9780442092276. URL: https://books.google.fi/books?id=Sg0fAQAAIAAJ.

[Wüb05] Wübbena, G., Schmitz, M. and Bagge, A. PPP-RTK: Precise Point Positioning Using State-Space Representation in RTK Networks. *Proceedings of ION GNSS 2005* (Sept. 2005), 2584–2594.

[Xia02] Xiao, B., Zhang, K., Grenfell, R. et al. Handheld GPS –Today and Tomorrow. *FIG XXII International Congress* (Apr. 2002). URL: http://fp-hid-1076751.testsider.dk/resources/proceedings/fig_proceedings/fig_2002/Ts5-13/TS5_13_xiao_zhang_etal.pdf.

[Yeg18] Yegin, K. *Antennas and Front-End in GNSS*. Intechopen, 2018. ISBN: 978-1-78923-214-1. DOI: 10.5772/intechopen.74971.

[Zie59] Zierler, N. Linear recurring sequences. *J. SI A M 7* (1959). DOI: 10.1109/TIT.1967.1054048.

[Zum97] Zumberge, J.F. , Heflin, M.B. , Jefferson, D.C. et al. Precise Point Positioning for the Efficient And Robust Analysis of GPS Data from Large Networks. *Journal of Geophysical Research* 102 (Apr. 1997). DOI: 10.1029/96JB03860.

PUBLICATIONS

PUBLICATION

I

Smart positioning with Fastrax's software GPS receiver solution

S. Söderholm, T. Jokitalo, K. Kaisti, H. Kuusniemi and H. Naukkarinen

*Proceedings of the 21st International Technical Meeting of the Satellite Division of The Institute of Navigation*2008, 1193–1200

Smart Positioning with Fastrax's Software GPS Receiver Solution

S. Söderholm, T. Jokitalo, K. Kaisti, H. Kuusniemi, H. Naukkarinen
Fastrax Ltd, Finland

BIOGRAPHIES

Mr. Stefan Söderholm is the Chief Research Officer at Fastrax Ltd. since 2000. He received his M.Sc. degree from Åbo Akademi University, department of Experimental Physics, in 1991 and his Licentiate degree from University of Turku, Department of Applied Physics, in 1996. Since then he has been working with FT spectroscopy before joining Fastrax in 2000. At Fastrax Stefan first started developing signal processing algorithms and later also implemented RAIM algorithms and kalman filters for the current generation of Fastrax's GPS receivers. The last 4 years Stefan has been leading the SW R&D team at Fastrax.

Mr. Timo Jokitalo received his M.Sc degree in 1994 at Helsinki University of Technology, Department of Engineering Physics and Mathematics. Before joining Fastrax in 2002, he worked on space related embedded and data processing software, and also on indoor pseudolite-based navigation. Since 2002 he has been a senior SW engineer in Fastrax's R&D team. He has been in charge of developing the navigation algorithms and embedded system software for Fastrax's current generation of standalone receivers and acquisition and correlation algorithms for the software GPS solution.

Mr. Kim Kaisti, co-founder of Fastrax, received his M.Sc. from Helsinki University of Technology in 1993, department of Electrical Engineering. Prior to Fastrax Kim worked during 1993-1999 with GPS in Vaisala Ltd. where he and the other co-founders developed a codeless GPS solution for weather balloon applications. At Fastrax Kim is currently a member of the Board and engaged in partnership activities.

Dr. Heidi Kuusniemi (born Sandström) received her M.Sc. and Doctor of Technology degrees from Tampere University of Technology, Finland, in 2002 and 2005, respectively. Her doctoral studies on reliability and quality monitoring in personal satellite navigation were partly conducted at the Department of Geomatics Engineering at the University of Calgary, Canada. Since October 2005, she has been working in research and development at Fastrax Ltd., Finland, where her current interests include high sensitivity GNSS and various reliability enhancement techniques.

Ms. Hanna Naukkarinen (born Immonen) received her M.Sc degree in April 2003 at Helsinki University of Technology, Department of Electrical and Communications Engineering. Before joining Fastrax in 2003 as a field application engineer, she worked at VTT Technical Research Center of Finland with ozone monitoring instruments. At the end of 2007, she joined Fastrax's R&D software team where her focus has been on GPS tracking and performance testing.

Fastrax Ltd., www.fastraxgps.com, is the provider of industry-leading receivers and software solutions for optimal utilization of GPS (Global Positioning System) and other GNSS location services (Global Navigation Satellite Systems). Headquartered in Finland and founded in 1999, the company is privately owned and backed by leading venture capital investors.

ABSTRACT

Fastrax introduces a new, software-based GPS receiver solution enabling more cost-effective GPS applications. The solution consists of a GPS RF module together with the complete signal processing and navigation software and is targeted mainly for platforms where the total CPU performance is in the range of a few hundred MIPS (Million Instructions Per Second). This software based approach for GPS reduces the bill-of-material to <3$ and yet achieves state-of-the-art GPS performance equivalent to stand alone GPS receivers. With a cold start sensitivity of –144 dBm and a navigation sensitivity of –163 dBm the presented software GPS solution can match any existing solution on the market. The Fastrax software GPS approach also includes a wide range of navigation enhancing features in all stages from acquisition to navigation.

This paper presents the Fastrax Software GPS receiver: the functionality, architecture, flexibility with parameters, system features, interfaces, extendibility to an accelerated version, and performance. To demonstrate the performance of the Fastrax Software GPS solution, test examples focusing on the CPU load, navigation accuracy, sensitivity, and cold/hot start characteristics are provided. The relatively low requirements for processing power and memory usage make the Fastrax Software GPS receiver a feasible and attractive alternative even for less powerful processor platforms at a low cost.

INTRODUCTION

A traditional GPS receiver consists of an antenna, an RF front-end and a baseband IC. The RF front-end converts the RF signal into a digital IF signal to be processed by the baseband IC. The baseband IC typically consists of an application processor, some memory, and dedicated HW modules for communication (UART, SPI) and signal processing (correlators, acquisition engine). All the power consuming operations of satellite acquisition and tracking, measuring satellite-to-user distances (pseudoranges), decoding the navigation data to retrieve the satellite ephemerides, and calculating the user position are done in the baseband IC. Figure 1 presents the tasks done in the baseband IC of a typical GPS receiver.

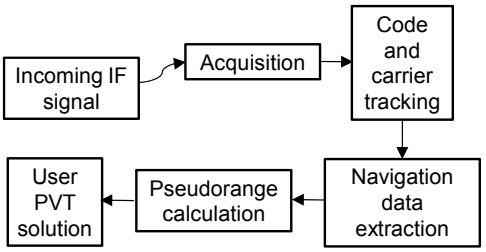

Figure 1. Typical GPS receiver tasks.

In addition to the traditional GPS receiver described above, there are also solutions on the market that reduce the size and price of the receiver hardware by moving parts of the software onto the host CPU. In such approaches, typically only the acquisition and tracking tasks are running on the GPS baseband IC, and the navigation algorithms are run on the host CPU. These approaches are usually referred to as measurement front-end receivers.

Modern PC's and mobile devices have powerful CPUs and lots of memory. With a CPU that is capable of executing instructions at a rate of a few hundred MHz, it is possible to implement most of the GPS baseband functionality in software, as opposed to a classic GPS receiver, which contains a dedicated baseband chip. This allows for considerable reductions in cost. In addition, implementing the baseband functionality in software allows the implementation of new capabilities in software, for example to benefit from the upcoming modernized GPS or Galileo signals. In contrast, a traditional hardware receiver will need to be replaced to implement the reception of new signals. The Fastrax software GPS receiver solution is also designed so that it can be accelerated by moving all or parts of the correlation tasks to hardware and therefore saving in required processing power.

Figure 2 illustrates the different GPS receiver approaches discussed above. The right-hand side of the picture represents the traditional standalone GPS receiver, which is the most costly solution and which requires the lowest amount of MIPS on the host CPU. A slightly less expensive option is the GPS measurement front-end followed by an accelerated software GPS approach and finally the full software GPS solution. Figure 3 presents some of the possible application platforms for a software GPS approach.

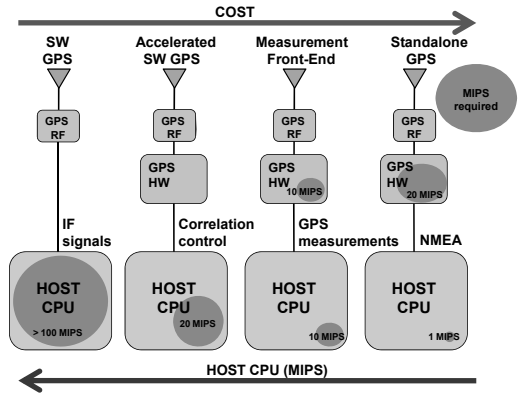

Figure 2. Different GPS receiver approaches.

Figure 3. Target software GPS end-user applications (cameras, smart phones, personal navigation devices and laptops).

FASTRAX SOFTWARE GPS RECEIVER

Fastrax Software GPS receiver (Figure 4) provides enhanced tracking and positioning capabilities resulting in short TTFFs and high sensitivity. No further hardware beyond an RF front-end is required. The achieved performance is equivalent to any traditional GPS receiver.

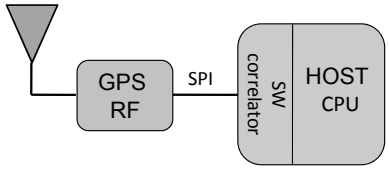

Figure 4. Fastrax Software GPS receiver.

Background
The software is based on the highly successful iSuite 3 embedded software architecture used in the family of iTrax receivers. Currently, iSuite is the only environment available for multiple GPS chipset platforms. The iSuite software has been very aggressively optimised for an extremely small CPU and memory footprint and is designed to be easily portable for all parts that do not directly depend on the GPS chipset. This unique flexibility and portability of the iSuite software has allowed significant reuse of the software as-is. This has made it easy to keep the CPU and memory usage very low also in the Fastrax Software GPS.

The reuse of all applicable parts of iSuite 3 ensures that the same high sensitivity and state-of-the-art performance that have been available for over 5 years in standalone GPS receivers are available also in the software GPS receiver. In addition, the larger quantity of CPU and memory on the new platforms has also allowed the introduction of new algorithms for improved tracking and navigation performance. Many of these algorithms have been developed during iSuite development, but have remained out of reach on standalone module platforms because of their extremely limited CPU and memory.

The iSuite performance and features have been widely demonstrated also in recent-year ION conference proceedings [1, 2, 3, 4, 5 and 6].

Software Design
The parts of the software that are newly developed for the software GPS receiver are those which are performed by hardware modules on a traditional GPS receiver, most notably the acquisition and correlation. These functions are also the ones typically requiring the most CPU and memory in software GPS receivers. The acquisition and tracking architectures of the iSuite software were originally designed for ultra low power consumption. In a software GPS receiver the same features of the architecture contribute towards a low CPU usage. In Fastrax's receiver the architecture and the underlying libraries, including the FFT and correlation libraries, have been heavily optimized and are configurable to obtain the best performance on different platforms, for example depending on the availability of a hardware floating point unit. Figure 5 shows the overall Fastrax Software GPS receiver architecture including the core functions of acquisition and correlation as well as navigation and various control and support features.

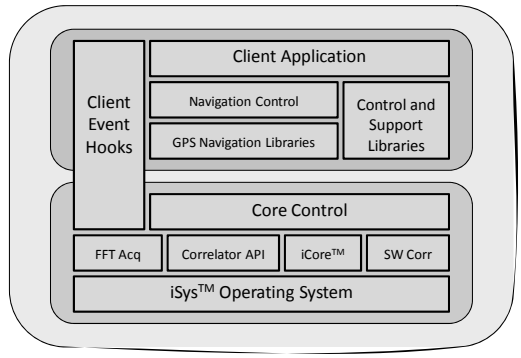

Figure 5. Fastrax Software GPS architecture.

The Fastrax Software GPS receiver currently provides two interfaces, a virtual serial port utilizing standard NMEA protocol, and a TCP/IP interface utilizing the proprietary binary iTalk protocol. The iTalk messages give access to data from all stages of a GPS receiver including information e.g. from the tracking loops, carrier phase and pseudorange measurements, and navigation quality indicators. The software is also capable of logging data to files for later processing, either as IF data or as iTalk archives containing among other information the raw phase measurements and decoded navigation data. This enables a powerful debugging and development environment, which is one of the key advantages of a software GPS receiver.

The modular software architecture allows flexibility when fitting the software GPS receiver to a particular application. For example, the receiver can easily be adapted to function as an ordinary executable, which can be started by the user, or as a system service which is started by the operating system during the system startup.

RF Module
The hardware needed for the Fastrax Software GPS receiver is available as a convenient SMD module, the IT900. It is especially designed to be used together with Fastrax's GPS software package. The module is based on the SiGe SE4120S RF chip and it contains all the other required components for a complete stand-alone RF front-end, including an LNA, SAW filter, TCXO and passive components. The size of the module is only 8x8 mm. The output data from the module is provided to the host CPU over an SPI interface. The module supports an active or a passive antenna. It has also support for both GPS and Galileo frequencies.

Resource Requirements
The CPU consumption for the Fastrax Software GPS receiver in continuous navigation is in the low hundreds

of MIPS, and the memory required is a few megabytes. The exact numbers depend on the configuration of the acquisition, tracking and navigation software. With a suitable software configuration and good signal conditions, the average CPU usage in continuous navigation can be as low as 100 MIPS for the whole Software GPS. The major part of this is consumed by the acquisition and tracking parts, with the navigation software and the support functionality taking only about 10 MIPS on an ARM platform. There is also a trade off between memory consumption and CPU usage, with the lowest memory usage being approximately 500 kb. This very small CPU and memory usage demonstrates that software GPS has become a feasible alternative for also less powerful processor platforms.

Accelerated Software GPS

Fastrax's unique software GPS receiver architecture also enables the use of hardware accelerators on platforms that do not have the processing power to run a full software GPS receiver. The Fastrax Accelerated Software GPS (Figure 6) reduces the CPU load by performing the correlation process on hardware. The correlation process can be integrated either in the RF front-end chip or in the host processor and this makes the Fastrax Accelerated Software GPS receiver especially attractive for devices using low-end or mid-end host processors with a limited clock frequency (200-300 MHz). For those platforms Fastrax offers a hardware based correlator IP solution to relax the CPU load for the correlation process. The IP is available as RTL for silicon integration purposes. It can easily be integrated into the RF chip or the host processor. The correlator IP reduces the CPU load for signal tracking with a factor of 10/channel.

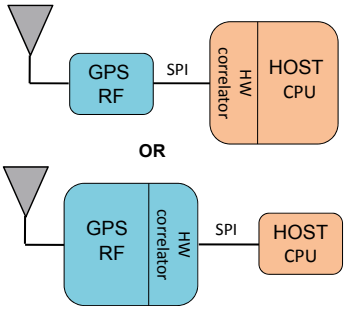

Figure 6. Fastrax Accelerated Software GPS receiver.

Portability

To ease the deployment in different kinds of devices, the Fastrax Software GPS and Accelerated Software GPS are configurable by parameters to obtain the best performance on every platform, depending on processing power and memory available.

The software has so far been ported to x86 and ARM processors and the Windows, Windows CE and Linux operating systems. Due to the high level of portability in the original iSuite architecture design, porting the software to a new OS and/or HW platform is straightforward.

Table 1 presents the key features of the Fastrax Software GPS solution. Unaided acquisition sensitivity is as low as -144 dBm and tracking sensitivity is -163 dBm. The average TTFF in hot starts is 0.55 s while 33.5 s in cold starts. In addition, Table 1 shows the typical processing loads in MIPS for different modes. Figure 7 presents the graphical user interface for the Fastrax Software GPS. The tabbed user interface enables monitoring the signal power levels, form of the correlation peak for each PRN, IF signal spectra, and azimuth and elevation in addition to the navigation PVT solution.

Software Key Features	
Unaided acquisition sensitivity	-144 dBm
Tracking sensitivity	-163 dBm
TTFF (hot start)	0.55 sec
TTFF (cold start)	33.5 sec
Output formats	NMEA, iTalk
Processing load (acquisition)	22-225 MIPS
Processing load - tracking	
Good signal visibility	2.5 MIPS / ch
Urban canyon environment	20 MIPS / ch
Full processing power	25 MIPS / ch

Table 1. The Fastrax Software GPS receiver: key features.

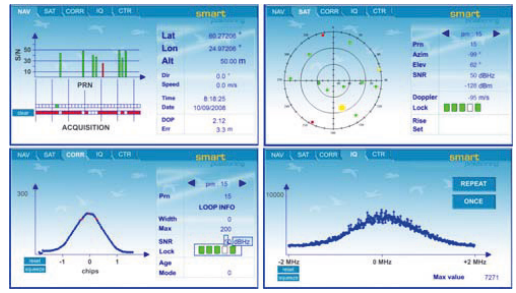

Figure 7. Screenshot of the graphical user interface for the Fastrax Software GPS.

TEST RESULTS

In the following, the performance of the Fastrax Software GPS receiver is presented.

The test platform in the tests described below was a 900 MHz ASUS Eee PC. By running a benchmarking program which processed amounts of data similar to the software GPS, it was estimated that the Eee platform is capable of executing such software at roughly 400 MIPS, which is in line with the 400 MHz bus speed of the Eee.

In the CPU load tests described below, the MIPS values are based on this estimate.

Urban-Canyon Automotive Test

First, the performance is demonstrated in an urban canyon automotive test. The test was performed in downtown Dallas, Texas, USA, which is a very challenging environment for GPS because of the tall skyscrapers that surround the streets. Figure 8 shows the ground plot in a northing-easting coordinate frame where the origin is the starting point of the test. Figure 11 presents the same result in Google Earth [7]. Figure 12 presents the same view at an oblique angle, showing how severely the tall buildings obstruct the line-of-sight to the GPS satellites. The software GPS receiver still has very reliable performance in the test, as seen in Figure 9 which presents the cross-track error. The maximum error in the urban canyon was only 33 meters, and the median cross-track error only 7 meters. Figure 10 shows the number of satellites used in the position solution, demonstrating the good measurement availability.

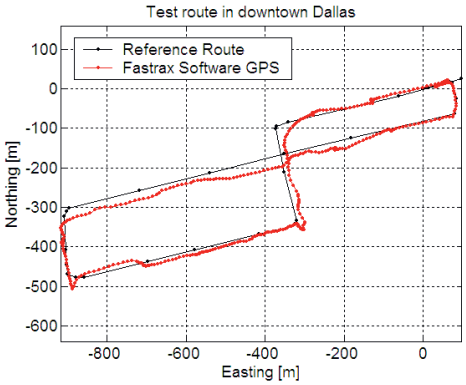

Figure 8. Test route in Dallas downtown: Fastrax Software GPS Receiver.

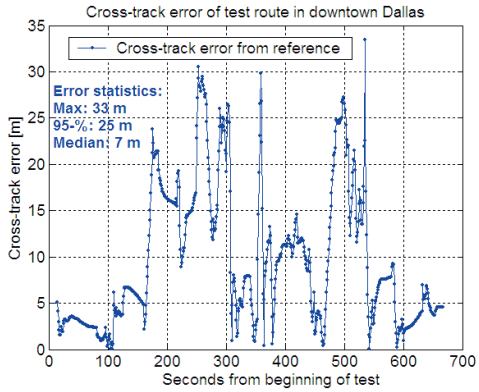

Figure 9. Cross-track error during test.

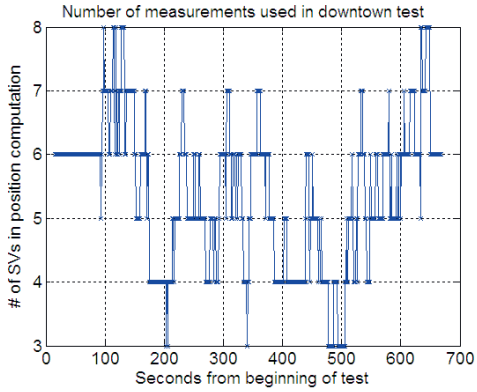

Figure 10. Number of measurements used in position computation.

Figure 11. Automotive test result in Google Earth.

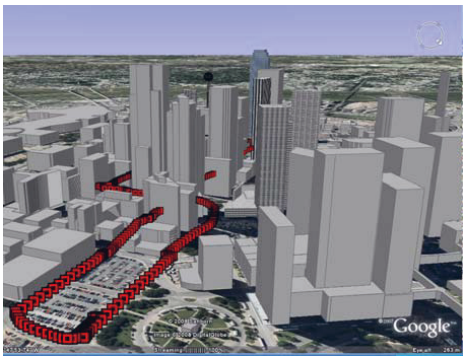

Figure 12. Test route from a different angle in Google Earth to demonstrate the tall buildings.

CPU Load – Tracking

Acquisition is usually active only during the first seconds of navigation until a navigation solution is obtained. After obtaining the navigation solution, most of the CPU consumption occurs in the software correlators. The other parts of the software GPS, including the navigation algorithms, usually consume about 5% of the CPU. Figure 13 presents the CPU usage of the correlators in the Dallas

test route, as a percentage of the total available CPU capability. The peak CPU load was 38%. During the beginning of the test run, the acquisition used about 80% of the CPU. From the typical CPU consumption of the correlators, 25%, it can be estimated that the correlating process consumes currently about 100 MIPS.

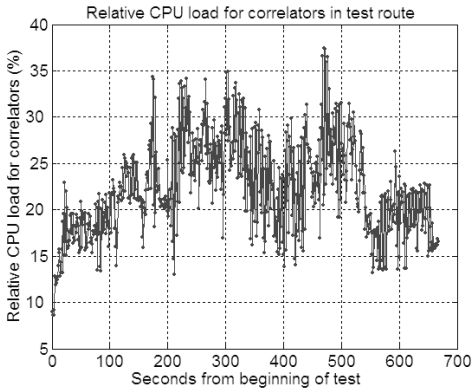

Figure 13. Percentage of CPU used by the correlators in the downtown Dallas test.

CPU Load - Acquisition

Acquiring the GPS signals using an FFT in a Software GPS receiver is often one of the most CPU intensive tasks. However, once the data needed for the acquisition are properly time stamped, the processing of the data does not need to occur in real time. The handover to the tracking can still be done even a few seconds after the sampling, as long as the acquisition process compensates for the Doppler shifts. This means that it is possible to acquire signals also with less powerful processors by increasing the acquisition duration. The high cost of the acquisition process means that the acquisition algorithms must be carefully managed; otherwise the CPU resources will be consumed completely by acquisition and will block other more critical tasks. The acquisition of Fastrax's Software GPS can be easily configured by specifying an approximate acquisition CPU quota, which the acquisition algorithms try to follow. Measurements of the effect of a varying acquisition CPU quota on the search time and CPU load are shown in Table 2, which shows the duration of a single satellite acquisition at nominal signal level. The first rows of table 2 show that at the maximum quota, the acquisition process used all the available CPU. This would eventually lead to a lag in the position output. Therefore, in our solutions we typically use an acquisition quota of 25%, which is a compromise providing acceptable acquisition times and CPU loads.

Relative CPU Quota for Acq	Search time / SV (sec)	Acq CPU load (MIPS)
Max	0.09	225
50 %	0.30	225
25 %	0.58	100
10 %	1.38	40
5 %	2.80	22

Table 2. Search time and average CPU load for different acquisition configurations. Signals were at –130 dBm.

Hot Start

Hot start performance was tested using a Spirent GSS6560 GPS signal simulator [8]. A static scenario with 10 visible satellites was used and the output signal level was calibrated so that the signal level at the input of the receiver was at the nominal level of –130 dBm. The receiver was first allowed to decode all available satellite ephemerides. After this the receiver was stopped, started again after a delay of 4 seconds, allowed to navigate for 10 seconds and then stopped again. The results are shown in Table 3. The average hot TTFF was as low as 0.55 seconds.

Average TTFF (sec)	0.55
Min TTFF (sec)	0.12
Max TTFF (sec)	2.33
Average 2D position error / First Fix (m)	9.15
Max 2D position error / First Fix (m)	16.8

Table 3. Hot start TTFF and first fix position errors.

Cold Start

Cold start tests were performed using the same scenario as was used for hot start testing. In a cold start, however, the receiver is not allowed to have any prior information available in memory. Results are shown in Table 4. Average cold start TTFF is 33.45 seconds. In a cold start situation, the factor that most affects the TTFF is the need to decode the ephemerides. The position error of the first fix in a cold start is typically smaller than in the hot start, since by the time the ephemerides are decoded, the tracker has had more time to stabilize from any inaccuracies in the acquisition.

Average TTFF (sec)	33.45
Min TTFF (sec)	24.18
Max TTFF (sec)	41.02
Average 2D position error / First Fix (m)	1.31
Max 2D position error / First Fix (m)	2.78

Table 4. Cold start TTFF and first fix position errors.

Tracking Sensitivity

The tracking and navigation sensitivity was measured using the Spirent GSS6560 GPS signal simulator. A static scenario with 11 visible satellites was used and the output signal level was calibrated so that the signal level at the input of the receiver was –130 dBm, -150 dBm, -155 dBm, and –160 dBm respectively. The signals were lost from track at -163 dBm. The average 2D error for each

test was calculated over a period of 5 minutes and the results are listed in Table 5.

Signal level (dBm)	2D error (m)
-130	0.82
-150	2.13
-155	41.6
-160	83.6

Table 5. Average 2D error as a function of signal level at the receiver.

Data Decoding Sensitivity

When acquiring a position fix when the ephemerides are not available, the data decoding sensitivity is the limiting factor for obtaining the position. The data decoding sensitivity was measured using the same signal simulator and scenario as mentioned above. The signal level was gradually dropped and the number of successfully decoded GPS subframe words was calculated. The results are shown in Figure 14.

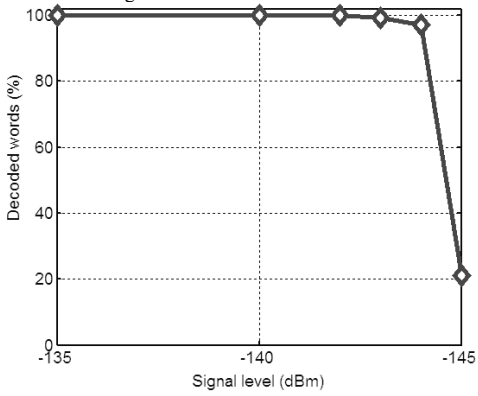

Figure 14. Percentage of successfully decoded subframe words as a function of signal level.

As can be seen from Figure 14 the data decoding capability drops rapidly around -145 dBm, which is considered to be the data decoding sensitivity. This is also considered the unaided acquisition sensitivity because below this level the decoding of the ephemerides would take unacceptably long,

IF Data Analysis

An additional benefit in a software GPS receiver is that the uncorrelated input signal is readily available and can be used for various analyses. As an example, Figure 15 shows a frequency plot of the raw baseband signal, showing a narrowband interference at about 400 kHz originating from a nearby poorly shielded computer. Similar interference peaks are seen near many PC's, caused by a 30 MHz frequency whose 52nd harmonic coincides with the GPS band.

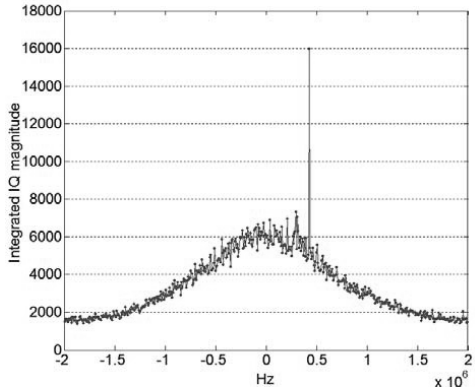

Figure 15. Iq spectrum showing narrowband interference.

The correlation results are also much more easily analyzable than in traditional hardware receivers. Figure 16 shows the form of a correlation peak corrupted by multipath. In this case the signal has been integrated for 500 milliseconds.

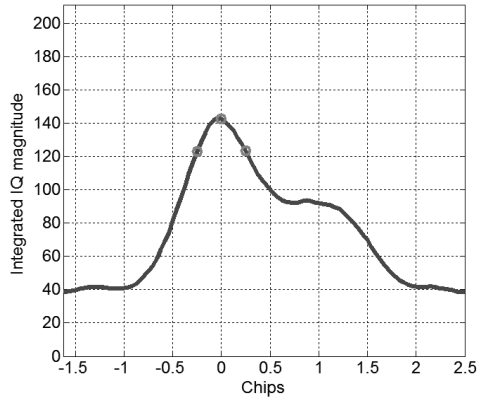

Figure 16. A correlation peak with multipath, integrated over 500 ms.

CONCLUSIONS

This paper presented the Fastrax Software GPS solution. The relatively small requirements for processing power and memory usage make the Fastrax Software GPS receiver a feasible alternative even for less powerful processor platforms with a low cost. The attractive features of the Fastrax Software GPS solution were widely demonstrated: its software architecture, extendibility to an accelerated software GPS version, adjustable resource requirements, and excellent navigation and sensitivity performance.

Even with the software GPS becoming a feasible approach in more and more applications, there will still be a market for traditional GPS receivers in applications where the main concern is the very low power consumption. In parallel to finalizing the software GPS offerings into commercially available OEM products, Fastrax continues its advanced GPS receiver development by further improving its industry-leading range of programmable hardware-based GPS receivers.

For more information, see *www.fastraxgps.com*.

REFERENCES

[1] S. Söderholm, T. Juhola, T. Saarnimo, V. Karttunen, T. Toivanen, Fastrax Ltd., "Indoor Navigation Using a GPS Receiver", Proc. ION GNSS 2001, Sept. 2001, pp. 1479-1486.

[2] S. Söderholm, Fastrax Ltd., Timo Jokitalo, Space Systems Finland Ltd., "Synchronized Pseudolites – The Key To Indoor Navigation", Proc. ION GNSS 2002, Sept. 2002, pp. 226-230.

[3] S. Söderholm, Fastrax Ltd., "GPS L1 Carrier Phase Double Difference Solution Using Low Cost Receivers", Proc. ION GNSS 2005, Sept. 2005, pp. 376-380.

[4] K. Högström, H. Kuusniemi, S. Söderholm, M. Räty, T. Ylhäinen, S. Kakarlapudi, Fastrax Ltd., "The iSuiteTM MP, a True MultiPlatform Development Environment", Proc. ION GNSS 2006, Sept. 2006, pp. 259-266.

[5] H. Kuusniemi, T. Jokitalo, S. Söderholm, S. Kakarlapudi, Fastrax Ltd., "Obtaining a Faster and More Accurate First Position Fix in Poor Signal Environments", Proc. ION GNSS 2007, Sept. 2007, pp.1351-1358.

[6] T. Jokitalo, H. Kuusniemi, S. Söderholm, S. Kakarlapudi, Fastrax Ltd., "Performance Assessment of Almanac Navigation", Proc. ION GNSS 2007, Sept. 2007, pp.1405-1412.

[7] Google Earth, URL: http://earth.google.com/

[8] Spirent Federal Systems, The GSS6560 Simulator Datasheet, URL: www.spirent.com/documents/3445.pdf

PUBLICATION II

A multi-GNSS software-defined receiver: design, implementation, and performance benefits

S. Söderholm, M. Z. H. Bhuiyan, S. Thombre, L. Ruotsalainen and H. Kuusniemi

Annals of Telecommunications 71.(2016), 399–410

Ann. Telecommun. (2016) 71:399–410
DOI 10.1007/s12243-016-0518-7

A multi-GNSS software-defined receiver: design, implementation, and performance benefits

Stefan Söderholm[1] · Mohammad Zahidul H. Bhuiyan[1] · Sarang Thombre[1] · Laura Ruotsalainen[1] · Heidi Kuusniemi[1]

Received: 19 May 2015 / Accepted: 28 April 2016 / Published online: 18 May 2016

Abstract Global navigation satellite systems (GNSSs) have been experiencing a rapid growth in recent years with the inclusion of Galileo and BeiDou navigation satellite systems. The existing GPS and GLONASS systems are also being modernized to better serve the current challenging applications under harsh signal conditions. Therefore, the research and development of GNSS receivers have been experiencing a new upsurge in view of multi-GNSS constellations. In this article, a multi-GNSS receiver design is presented in various processing stages for three different GNSS systems, namely, GPS, Galileo, and the Chinese BeiDou navigation satellite system (BDS). The developed multi-GNSS software-defined receiver performance is analyzed with real static data and utilizing a hardware signal simulator. The performance analysis is carried out for each individual system, and it is then compared against each possible multi-GNSS combination. The true multi-GNSS benefits are also highlighted via an urban scenario test carried out with the hardware signal simulator. In open sky tests, the horizontal 50 % error is approximately 3 m for GPS only, 1.8 to 2.8 m for combinations of any two systems, and 1.4 m when using GPS, Galileo, and BDS satellites. The vertical 50 % error reduces from 4.6 to 3.9 when using all the three systems compared to GPS only. In severe urban canyons, the position error for GPS only can be more than ten times larger, and the solution availability can be less than half of the availability for a multi-GNSS solution.

✉ Stefan Söderholm
stefan.soderholm@nls.fi

[1] Department of Navigation and Positioning, Finnish Geospatial Research Institute, National Land Survey, Geodeetinrinne 2, FIN-02430 Kirkkonummi, Finland

Keywords Multi-GNSS · BeiDou · Galileo · Software receiver · SDR · Performance analysis · Receiver architecture

1 Introduction

The United States Department of Defense (DoD) Navigation System using Timing And Ranging (NAVSTAR) global positioning system (GPS) [1] was declared fully operational in 1995 and has since then evolved to being the de facto standard for satellite navigation systems. GLObalnaja NAvigatsionnaja Sputnikovaja Sistema (GLONASS) was developed in parallel with GPS, but was allowed to deteriorate drastically. Today, its value can hardly be overestimated since it offers an almost complete constellation of modern satellites, and it is also truly global. Unfortunately, still today, it only offers frequency division multiple access (FDMA) modulated signals [2], and thus, a relatively large bandwidth is required to receive all the signals. The European Galileo system is currently in its initial operation capability (IOC) phase with 12 satellites in orbit. The last two satellites were launched in December 2015, and two additional satellites are planned to be launched in May 2016. Two of the satellites that have been launched are on wrong orbits [3]. Though initially planned to be available already in 2010 [4], initial Galileo services are scheduled now to begin within the next year, and Galileo will become a truly global system by the end of this decade [5]. The BDS [6] consists of a mixed space constellation that has, when fully operational, five geostationary Earth orbit (GEO), twenty seven medium Earth orbit (MEO), and three inclined geo-synchronous satellite orbit (IGSO) satellites. The ground tracks of all BDS satellites are shown in Fig. 1. The GEO satellites are operating in orbit at an altitude of 35,786 km and positioned at 58.75° E, 80° E, 110.5° E, 140° E, and 160° E, respectively. The MEO

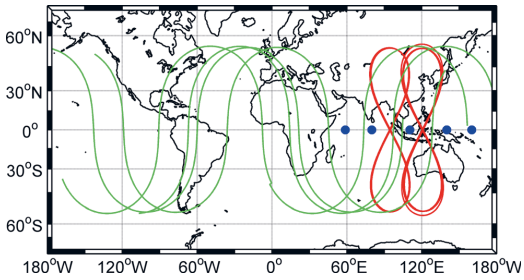

Fig. 1 Ground track of BDS satellites. GEO = *blue dots*, IGSO = *red*, MEO = *green*

satellites are operating in orbit at an altitude of 21,528 km with an inclination of 55° to the equatorial plane, whereas the IGSO satellites are operating in orbit at an altitude of 35,786 km with an inclination of 55° to the equatorial plane.

As of March 2015, the BDS has five GEO, five IGSO, and four MEO satellites [7]. These satellites broadcast navigation signals and messages within three frequency bands (termed as B1 in 1561.098 MHz, B2 in 1207.14 MHz, and B3 in 1268.52 MHz) using code division multiple access modulation (CDMA). As of now, the interface control document (ICD) was released only for B1 and B2 frequencies [6]. Considering the civilian CDMA only-modulated signals on the L1 band offered by three different systems, i.e., GPS, Galileo, and BDS, there is currently a total of 50 satellites orbiting around the world [8]. The minimum number of visible satellites in any place on earth during a 24-h period in February 2015 from these three systems is shown in Fig. 2.

Other regional systems like quasi zenith satellite system (QZSS), Indian regional navigation satellite system (IRNSS), GPS aided augmented navigation (GAGAN), and space-based augmentation system (SBAS) in general offer only a few additional satellites, and the satellites are often targeted to improve performance for well-defined areas rather than globally.

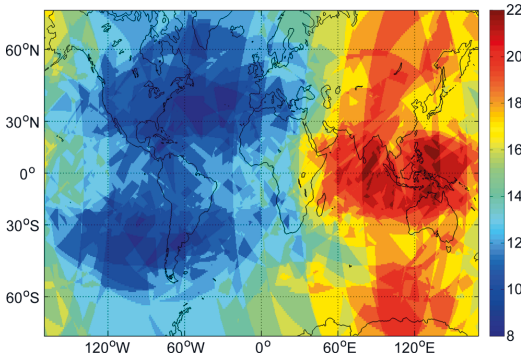

Fig. 2 Example of minimum number of GPS + Galileo + BDS satellites combined visible on Earth during a 24-h period in February 2015

The development of modern software-defined receivers (SDR) for GNSS signals can be considered to have initiated with the dissertation work by Akos [9] at the University of Colorado. He presented the design and the architecture of a GPS/Galileo SDR receiver in Matlab with test results for GPS signals. Later, this receiver was converted into a real-time receiver implemented in C, the gpSrx [10, 11]. The Matlab version of the receiver was later documented as a book edited by Borre et al. [12]. The documented receiver was capable of performing all steps from signal acquisition to navigation utilizing GPS and Galileo signals. One of the co-authors of Dennis Akos [10, 11] later founded a company named NordNav Technologies, that developed the R30, a commercial 24 channel real-time SDR for L1 band capable of receiving GPS and Galileo E1 signals [13, 14].

The group at the University of Calgary also developed their own SDR that was first presented in 2004 [15]. At that time, it supported only GPS signals and utilized a front end called the GPS signal tap made by Accord Inc. The Institute of Geodesy and Navigation at the University FAF Munich was also one of the forerunners of GNSS SDR development with its own SDR named as ipexSR [16], which is a real-time SDR for a personal computer (PC) platform running in Windows operating system (OS). The receiver was capable of receiving three GPS frequencies in L1, L2, and L5 bands in addition to the signals broadcasted from Galileo's test satellites GIOVE A and GIOVE B. Several groups also presented their contribution on the development of multi-frequency SDRs for GPS and Galileo during the last decade [17–21].

Later at the end of the last decade when the GLONASS signals again provided a reliable complementary system to GPS, several research groups around the world started working on integrating GPS and GLONASS. A group in Italy [22] presented a solution with the universal software radio peripheral (USRP) front end where they sampled wide bandwidth data and divided the data into separate channels for GPS and GLONASS using two down converters. They presented a performance analysis for combined GPS and GLONASS observations. In [23], Ferreira presented a GPS/Galileo/GLONASS SDR with a major emphasis on the configurability of the receiver. The focus of the paper was on the developed hardware designed for sampling the data from the front end and streaming it over the Ethernet to the computer where the signal processing was done in software. GPS + Galileo signal compatibility was shown, but no GLONASS signals were acquired successfully. Also, the presented architecture was not designed to simultaneously receive GLONASS and GPS/Galileo signals. In general, there has not been much literature published with details on the architecture of a multi-frequency multi-GNSS SDR from the viewpoints of implementation and scalability with respect to the growing number of global/regional satellite navigation systems. To this end, the authors in this paper present a highly scalable and configurable multi-

frequency multi-GNSS SDR architecture that has been under continuous implementation for the last two years at Finnish Geospatial Research Institute (FGI), Finland.

The most apparent advantage of a multi-GNSS receiver is the availability of a greater number of signals than before. The increased number of observations will increase robustness and availability of the position solution as well as offer a better accuracy for the user in certain scenarios. In open sky conditions, this advantage is often not obvious. But especially in urban canyons, where the user is surrounded by high buildings, the total number of available satellites becomes a critical factor. Another perhaps less apparent advantage is the robustness against interference when multiple frequencies are considered from multi-GNSS. A good overview of different kinds of GNSS interference and the options to mitigate them was well described in [24–29].

In this paper, we will first present the design of the implemented multi-GNSS software-defined receiver, then show the experimental results, and finally end with conclusions and future work. The design includes the description of the data flow and functional blocks in the receiver. Three features—the parameter system, assisted GNSS, and multi-correlator tracking—are described in more detail. Next, a description is given of how the acquisition, tracking, data decoding, and positioning can be implemented in a multi-GNSS receiver. The tracking architecture is described in detail together with how the position, velocity, and time are obtained in a multi-GNSS receiver. The time differences between the GNSS systems are indicated with some experimental results. Results from an open sky test case and a simulated urban canyon test case using a GNSS signal simulator are presented in the "Experimental results" section. The focus of the test cases is to compare the performance of a multi-GNSS solution with a GPS-only solution.

2 Multi-GNSS receiver design

A software-defined multi-GNSS receiver platform, named as FGI-GSRx, has been developed at FGI during the past years. The FGI-GSRx multi-GNSS receiver is mainly a Matlab-based research platform for the analysis and validation of novel algorithms for an optimized GNSS navigation performance. The first version of FGI-GSRx was based on an open-source software receiver platform developed by Borre et al. [12]. Since the receiver by Borre et al. was not originally designed for multi-GNSS operation, the authors have been modifying this receiver significantly to support more GNSS systems simultaneously and to make the receiver more configurable.

The receiver is implemented in Matlab and thus provides a unique and easy-to-use platform for the various research projects at FGI. The receiver is designed for post-processing operation, and it does not support real-time operation. The receiver architecture has been designed so that the intermediate data from acquisition and tracking can be saved, and the processing can be started from any pre-saved data file. A block diagram of the receiver is shown in Fig. 3.

User parameters are read from the file system together with optional receiver independent exchange format (RINEX) navigation files [30] for assisted GNSS functionality. The parameters specify how the processing of the intermediate frequency (IF) data that has been logged before with the radio frequency (RF) front end will be processed. If requested by the user, the acquisition is executed using the IF data stored in the file system, and the results are stored to the memory on the computer. Optionally, already stored acquisition data can be retrieved from the file system, and the acquisition is bypassed. The result is the same regardless of which approach the user takes; the acquisition output is passed on to the tracking stage.

The same options are available for tracking. Either we process the logged IF data and store the output to the file system or we use already processed data from the file system. The result from tracking is then passed on to navigation.

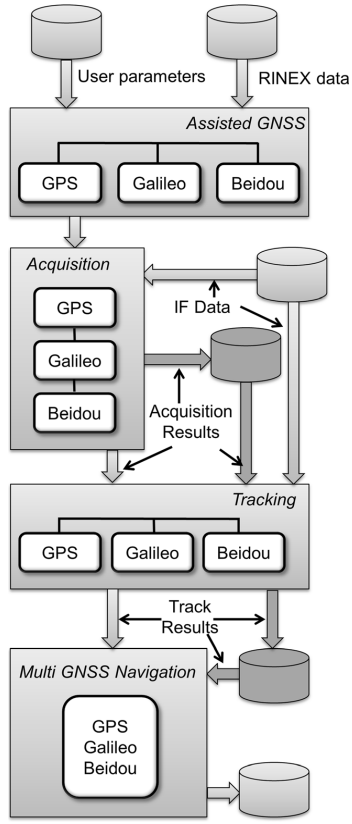

Fig. 3 Functional blocks in the FGI-GSRx receiver. The parts in *red* indicate the option to use pre-stored output from acquisition and tracking

2.1 Parameter system

Modifying parameters and configuring the receiver is one of the most relevant parts of a receiver intended for research. The goal is to enable all researchers to independently develop and test new algorithms in tracking, acquisition, and navigation. In the FGI-GSRx, we have implemented a parametric system based on text files. This approach makes it very easy to test different algorithms with many different data sets quickly and in a way that can be easily reproduced later. All default values are in a default parameter file, and each user can have multiple personal parameter files containing only parameters that differ from the default values. Therefore, changing and adding parameters for development purposes do not require any changes to the actual receiver code.

2.2 Assisted GNSS

To aid the acquisition process, an assisted GNSS functionality has been added to the receiver. The approximate user position, time, and receiver intermediate frequency for each front end can be provided as input parameters to the receiver. In addition, the ephemeris assistance can be provided either in the RINEX navigation file format [30] or previously saved already decoded broadcast ephemeris files. Utilizing this information, we can estimate the Doppler frequencies of each visible satellite and narrow our frequency search window to speed up the acquisition process.

2.3 Multi-GNSS acquisition

Some suitable algorithms for GNSS signal acquisition can be found in [31] and [32]. At the moment, the acquisition in the FGI-GSRx is done for one GNSS system at a time. Part of the future work is to investigate how signals from different systems should be prioritized at the acquisition stage. The basic algorithm for the acquisition of the GPS and Galileo signals is the same [11], where a fast Fourier transform (FFT)-based parallel code phase search is utilized. The implemented acquisition algorithms to acquire BDS MEO, GEO, and IGSO satellites are discussed in detail in [33] and [34].

The search window, number of coherent and non-coherent integration rounds, and signal thresholds are all configurable parameters. Two different acquisition modes exist, an unaided and an aided acquisition. In the aided mode, only one frequency bin is used, and the threshold can be set separately.

For the Galileo E1 data/pilot channel, both the spreading code and the data bit are 4-ms long so if we want to do longer coherent integrations than 4 ms, we need to take into account the possibility that a bit transition may occur between any two consecutive epochs. In the FGI-GSRx, we can use 8- and 12-ms coherent integration, and we can then search over all combinations of data-bits. For example, for 8-ms coherent integration, the two data-bits may take any of the following values [+1; +1], [−1; +1], [+1; −1], and [−1; −1].

2.4 Multi-GNSS tracking

Not many good tracking architectures have been presented for GNSS signals in literature. A good architecture can however be found in [35]. Similarly, in the FGI-GSRx presented herein, after acquisition has been completed for all systems, bit edge detection is performed for each satellite signal, and each signal with a detected bit edge will be assigned to a specific tracking channel. Tracking is then initiated with a correlation interval of code length duration for each individual system (i.e., 1 ms for GPS and BDS, 4 ms for Galileo), as shown in Fig. 4.

The tracking of GPS and BDS is done for every ms of data, whereas the Galileo signals are processed only for every 4 ms of data due to the different lengths of one code epoch. The actual amount of data read from the file is adjusted for each epoch based on the true code frequency so that we always aim to process exactly one code epoch. Essentially, we are trying to keep the code phase as close to zero as possible.

The tracking architecture has been designed to be highly configurable with good support for different tracking modes. Each logical unit, such as the discriminators, loop filters, etc., is separated into its own functions. Each logical unit is linked to a certain type; for example, GPS_FREQ_LOOP is used as the frequency-locked loop (FLL) of GPS. Each type can also be in many different states; for example, FREQ_LOOP_PULL_1 can be used in the initial stage of carrier tracking with update rate of 1 ms. Each state also has a predefined update rate. An example of states, types, and functions is shown in Table 1.

As can be seen from Table 1, one type can refer to many different functions and update rates, but each function and update rate is linked to only one state. Depending on what state that type is in, one specific function will be executed at one specific rate. When the state of a type changes, another function will be executed or the update rate will change. With this approach, we can easily switch between, for example, different kinds of discriminator or loop filter and manage the update rate of those functions. Utilizing this kind of an approach, we can easily accommodate for loop pull in, high sensitivity or high dynamic states of the tracking without the risk of unmanageable code.

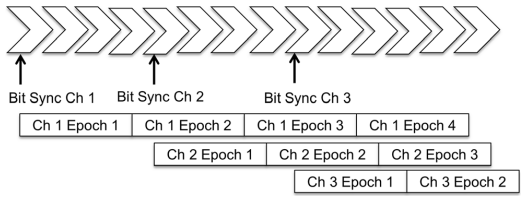

Fig. 4 Tracking is synchronized to the bit edge for each channel

Table 1 Example of how state, function, and type are related

Type:	GPS_FLL_DISCR		GPS_FREQ_LOOP		GPS_DLL_DISCR	
State:	Function	Rate (ms)	Function	Rate (ms)	Function	Rate (ms)
FLL_DISCR_1	mulFreqDiscrim	1				
FLL_DISCR_5	mulFreqDiscrim	5				
FLL_DISCR_20	mulFreqDiscrim	20				
FREQ_LOOP_PULL_1			gpsFreqLoopPullIn	1		
FREQ_LOOP_TRACK_1			gpsFreqLoop	1		
FREQ_LOOP_TRACK_20			gpsFreqLoop	20		
DLL_DISCR_1					mulCodeDiscrim	1
DLL_DISCR_5					mulCodeDiscrim	5
DLL_DISCR_20					mulCodeDiscrim	20

Tracking states are defined as a set of states

2.5 Multi-correlator tracking

In the default configuration, only three correlator fingers are used for tracking and one finger for monitoring the noise level. The finger spacing is configurable, and the default value is 0.25 chips. The FGI-GSRx has a feature called multi-correlator tracking where the user can specify the number of fingers used, fingers' spacing, and the output rate. This feature is intended for analyzing the channel characteristics in more detail. A typical multi-correlation output for a code delay window of ±2 chips is shown in Fig. 5.

2.6 Data decoding

The sign of the prompt finger is copied into the data decoding buffer, and when the buffer is full, the FGI-GSRx correlates the incoming bit stream with the up-sampled data frame preamble for the respective system. After successful correlation, the start of a data frame is found, and the raw data-bits can be extracted from the signal. The GPS bits are passed through a parity check, and the Galileo bits are de-interleaved and passed through a Viterbi decoder. The final decoded data contains the transmission time for the beginning of the data frame for each channel. Since we know at what sample the data frame started, we can link the transmission time for each signal to a specific sample count.

2.7 Position, time, and velocity solution

The position, time, and velocity can be calculated after tracking has been completed successfully. The input is the decoded data and the measurements for each channel from the tracking engine. The measurements from each channel are aligned with the bit edge of that channel. In order to have synchronized measurements, we need to realign our observations from the tracking. The decoded data frame in each channel n will provide the transmission time, T_n, for the sample, S_n, that the receiver acquired at the beginning of the frame. In order to obtain synchronization, we have to extrapolate the transmission time for all channels to one common sample, S_0 as shown in Fig. 6.

The measured transmission times for all channels T_n' refer to the same sample S_0 in our incoming data. It is worth noting here that since these transmission times are extrapolated from the time stamp in the data frames for each channel, they are in different time domains, namely Galileo standard time (GST), BDS system time (BDT), and GPS time depending on what signal occupies that channel.

To obtain the initial receiver time estimate, $\boldsymbol{T_{rx}}$, at sample S_0, we assume that the signal with the shortest traveling distance for each system has traveled for 80 ms. The accuracy of this receiver time estimate is not critical for the position solution, and our time solution will give us the final accurate receiver time. The estimated receiver time is a vector with three components:

$$T_{\mathrm{rx}} = \begin{bmatrix} T_{\mathrm{rx}}^{G} \\ T_{\mathrm{rx}}^{E} \\ T_{\mathrm{rx}}^{B} \end{bmatrix} \tag{1}$$

i.e., the estimated receiver time in GST, BDT, and GPS time for the same sample S_0. The pseudo-ranges ${\rho_n}^k$ can then be calculated as

$$\rho_n^k = \left(T_{\mathrm{rx}}^k - T_n'\right) * c \tag{2}$$

where n is the channel index, k the system index (GPS, Galileo, or BDS), and c is the speed of light.

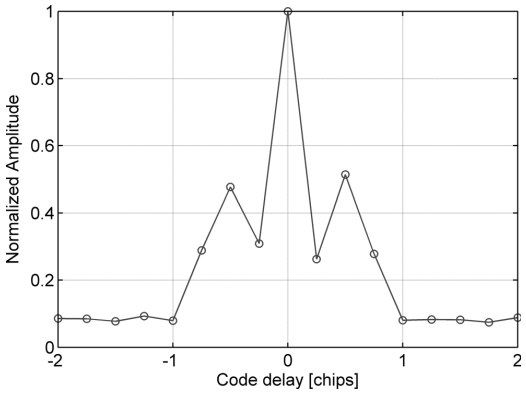

Fig. 5 Example of Galileo E1 signal correlation peak with 17 fingers with 0.25 chip spacing (*dots*). *Blue line* is an interpolation to illustrate the peak. Data have been integrated over 200 ms

2.7.1 Position solution

Using an a priori estimate for the user position, **Pos** = $[x_0 y_0 z_0]$, and the decoded ephemeris, we can calculate the satellite positions and the predicted range between the user and each satellite, r_i^k, and form the observation matrix with the observed values minus the predicted ones

$$\Delta\rho = \begin{bmatrix} \rho_1^G - r_1^G \\ \vdots \\ \rho_n^G - r_n^G \\ \rho_1^E - r_1^E \\ \vdots \\ \rho_m^E - r_m^E \\ \rho_1^B - r_1^B \\ \vdots \\ \rho_k^B - r_k^B \end{bmatrix} \quad (3)$$

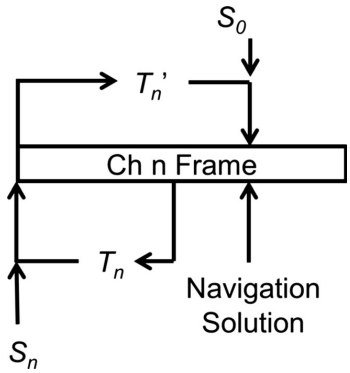

Fig. 6 Transmission time for channel n, T_n, is extrapolated to the sample at which we will calculate our navigation solution. Note here that the T_n' is channel-specific and system-dependent

The observation vector is identical regardless of the number of systems we have. For the geometry matrix **H** containing the directional cosines, we need to add one clock term for each enabled system. One row in **H** can be therefore written as

$$H_{i,j} = \begin{bmatrix} \Delta x_i^j / r_i^j & \Delta y_i^j / r_i^j & \Delta z_i^j / r_i^j & \begin{cases} 1, & j = G \\ 0, & j \neq G \end{cases} & \begin{cases} 1, & j = E \\ 0, & j \neq E \end{cases} & \begin{cases} 1, & j = B \\ 0, & j \neq B \end{cases} \end{bmatrix} \quad (4)$$

where Δx, Δy, and Δz are the differences between the satellite coordinates and the a priori user coordinates, r is the range to the satellite, and the prefixes i indicate satellite number and suffixes j indicate satellite system (G—GPS, E—Galileo, and B—BDS). To obtain the updates to the a priori user position, **ΔPos**, we need to solve a set or normal equations

$$\Delta\rho = H\Delta\mathrm{Pos} + \Delta\varepsilon_\rho \quad (5)$$

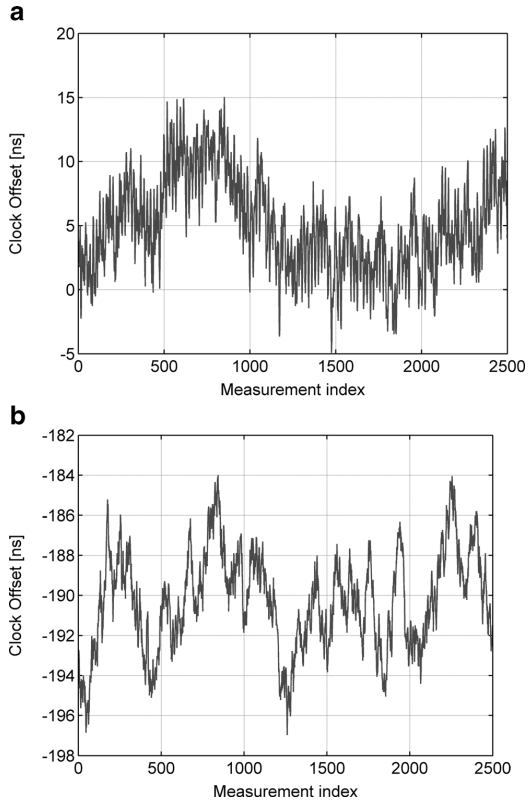

Fig. 7 **a** GPS—Galileo clock offset in ns. **b** GPS—BDS clock offset in ns. The leap second difference between GPS and BDS of 14 s has been removed

Table 2 Configurations for NSL front ends

Properties	MAX2769B	MAX2112
Center frequency (MHz)	1561.098	1575.42
3-dB bandwidth (MHz)	~4.2	~6.6
Max sampling frequency (MHz)	40	30
Reference frequency (MHz)	26	26
Received signal	BDS B1	GPS L1, Galileo E1

where $\Delta\varepsilon_\rho$ is assumed to be a zero mean residual vector. The least squares solution to (5) can be written as

$$\Delta\mathrm{Pos} = \left(H^T H\right)^{-1} H^T \Delta\rho \tag{6}$$

The solution in the multi-GNSS case can then be written as

$$\Delta\mathrm{Pos} = \begin{bmatrix} \Delta x & \Delta y & \Delta z & c\Delta t^G & c\Delta t^E & c\Delta t^B \end{bmatrix} \tag{7}$$

where Δt are the clock offsets for the three systems and c is the speed of light. When the a priori user estimate has been corrected by the output of (7), we repeat the steps (3) to (7) until the change in the estimate is sufficiently small.

2.7.2 Time solution

We start by aligning all the measurements to one single sample count, S_0, in the original data file (see Fig. 6), and then, we assume that the receiver time at this sample is T_{rx}. Note that the measurements from all systems are aligned to the same sample count, but the receiver time is a vector (1), with the time in each system separately. The navigation solution will provide us with the clock offset, Δt, for each system (7), and we can accurately determine the true time for that particular sample count in each system's time domain by correcting the initial estimate with Δt

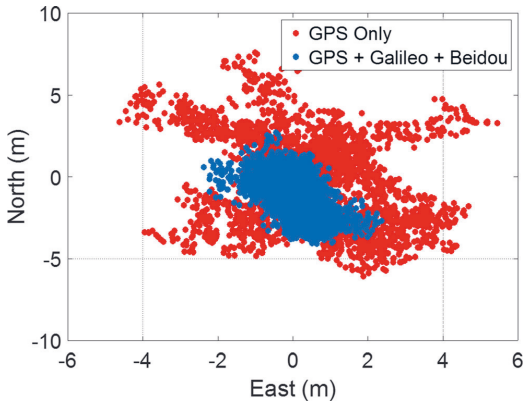

Fig. 8 Ground plot of GPS (6 satellites) solution versus GPS + Galileo + BDS (14 satellites)

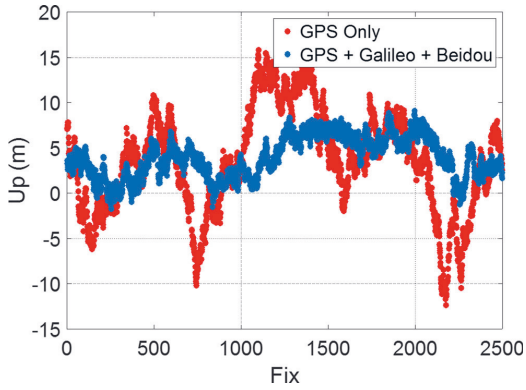

Fig. 9 Altitude error of GPS (6 satellites) solution versus GPS + Galileo + BDS (14 satellites)

$$T_{\mathrm{rx}}^{\mathrm{true}} = \begin{bmatrix} T_{rx}^G - \Delta t^G \\ T_{rx}^E - \Delta t^E \\ T_{rx}^B - \Delta t^B \end{bmatrix} \tag{8}$$

The GPS time is semi-synchronized to coordinated universal time (UTC) time in such a way that the time difference is defined as

$$\mathrm{UTC} - \mathrm{GPS\ time} = -\mathrm{leap}_G + C_0 \tag{9}$$

where leap_G is the number of leap seconds specified for a particular time and date. At the time of writing, the number of leap seconds for GPS was 16. The value of the constant C_0 is continuously monitored by the GPS ground segment, and parameters for a UTC model are broadcasted as a part of the GPS almanacs. The value of C_0 is targeted to be less than 1 μs, but it is typically less than 100 ns.

GST is defined in a very similar fashion

$$\mathrm{UTC} - \mathrm{GST} = -\mathrm{leap}_E + C_1 \tag{10}$$

The number of leap seconds is the same for Galileo as for GPS and the difference between C_0 and C_1 is typically less than 50 ns. BDS time is defined as

$$\mathrm{UTC} - \mathrm{BDT} = -\mathrm{leap}_B + C_2 \tag{11}$$

The value of the constant C_2 is kept less than 100 ns, and for BDS the number of leap seconds is 2. An example of time domain differences is shown in Fig. 7a, b.

As is shown in Fig. 7b, the difference between the two constants C_0 and C_2 for this test was 190 ns.

2.7.3 Velocity solution

The velocity solution is calculated similarly as the position solution. The observation matrix is in this case the difference

Table 3 Horizontal statistics for various combinations of GNSS

Configuration	Nr. of solutions	Nr. of sat	50 % error (m)	East offset (m)	North offset (m)	StDev (m)	Max error (m)	HDOP
GPS	2500	6	2.98	0.48	−0.06	1.51	7.67	2.25
Galileo	2500	4	4.31	0.7	−4.05	2.25	11.56	2.31
BDS	2500	4	3.41	−0.14	−2.9	1.96	9.52	4.77
GPS + Galileo	2500	10	1.78	0.41	−1.28	1.24	6.18	1.44
GPS + BDS	2500	10	2.28	−0.4	−0.26	1.26	6.42	1.8
Galileo + BDS	2500	8	2.78	−0.02	−2.57	1.3	6.62	1.94
GPS + Galileo + BDS	2500	14	1.38	0.04	−1.2	0.93	4.16	1.34

between the measured Doppler frequency obtained directly from the phase lock loop (PLL) and the theoretical Doppler calculated from the a priori user velocity and the satellite ephemeris. The geometry matrix **H** (4) is the same as for the position calculation, and the solution is obtained using (5)–(7). Instead of obtaining a position solution, we obtain a velocity solution as

$$\Delta\mathrm{Vel} = \left[\Delta v_x \quad \Delta v_y \quad \Delta v_z \quad {}^{c}/_{L_G}\Delta f^{G} \quad {}^{c}/_{L_E}\Delta f^{E} \quad {}^{c}/_{L_B}\Delta f^{B} \right] \tag{12}$$

where c is the speed of light, L is the center frequency for each system, and Δf is the frequency offset from the nominal intermediate frequency. After iteration, we obtain the true user velocity and the frequency offsets for each system.

At the end of the processing, some additional operations such as coordinate transformations, time corrections, and satellite elevation and azimuth angles are calculated. The satellite elevation is used after the initial position estimate to omit satellites below a user defined cutoff angle. The update rate for the navigation is defined by the user. The default rate is every 20 ms, i.e. 50 Hz.

3 Experimental results

Data was logged with the Nottingham Scientific Limited (NSL) Stereo Software GNSS front end [36]. One of its front ends uses the Maxim MAX2769B radio chip, and the other one uses the Maxim MAX2112 radio chip. The key configuration parameters for these radios are listed in Table 2.

3.1 Static open sky test with live data

The first test with the multi-GNSS FGI-GSRx receiver was carried out with the roof antenna signal at FGI in Kirkkonummi, Finland. The antenna used in the test was the G5Ant-3AT1 active antenna by Antcom [37]. A suitable time for the test was selected so that a minimum of four satellites were visible from all the three systems; 100 s of data was logged, and the position was calculated at a rate of 50 Hz. The ground plot is shown in Fig. 8. The altitude variations for the GPS-only and multi-GNSS solutions are also shown in Fig. 9.

Additional analysis was performed with the various combinations of satellite systems, and the performance metrics are presented in Tables 3 and 4. Even if BDS and Galileo only can add four satellites each to the multi-GNSS solution, we can still clearly see from the figures and the tables that the accuracy is better for a multi-GNSS solution compared to a GPS-only solution with this particular data set. The offsets vary somewhat for the three systems in both the horizontal and the vertical directions (East, North, and Up offsets). This is partly due to the fact that we have used default values for the ionospheric corrections. The same default parameters were used for all the systems, but the remaining errors in the observations affect the systems differently due to the different

Table 4 Vertical statistics for various combinations of GNSS

Configuration	Nr. of solutions	Nr. of sat	50 % error (m)	Up offset (m)	StDev (m)	Max error (m)	VDOP
GPS	2500	6	4.6	3.49	3.78	15.81	2.41
Galileo	2500	4	2.49	0.68	2.15	11.22	3.32
BDS	2500	4	9.77	9.63	5.05	22.65	2.85
GPS + Galileo	2500	10	3.31	2.73	2.31	10.63	1.71
GPS + BDS	2500	10	3.43	3.56	3.07	11.22	1.47
Galileo + BDS	2500	8	6.5	6.56	1.45	11.73	1.76
GPS + Galileo + BDS	2500	14	3.9	3.93	2.21	9.11	1.27

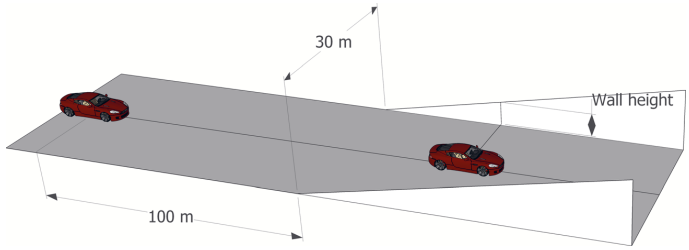

Fig. 10 Urban canyon for simulator test

horizontal dilution of precision (HDOP) and vertical dilution of precision (VDOP) values.

The horizontal 50 % error is approximately 3 m for GPS only and 1.4 m when using the additional Galileo and BDS satellites. We see an improvement even if the actual position offsets, especially in the north direction, are somewhat bigger for BDS and Galileo compared to that of GPS. If we look at the standard deviation with respect to mean position and the maximum error, we also clearly see an improvement by adding the observations from Galileo and BDS.

For the vertical component (Table 4), the offset is relatively large for the BDS-only solution, which is most likely due to the geometry. This affects the vertical offset of the multi-GNSS solution. However, all other statistical values improve in the same way as for the horizontal values. When looking at the Figs. 9 and 10, the improvement in both the horizontal and in the vertical component is clearly visible when we used a multi-GNSS solution.

3.2 Urban canyon test

The advantages of using multiple GNSSs in a receiver become more apparent in urban canyon and other blocked signal environments. Unfortunately, due to the very few Galileo satellites and the limited number of BDS satellites visible in northern Europe, it would be very difficult to obtain any conclusive results using live signals. Therefore, we used instead a GNSS signal simulator capable of producing all the signals of interest (GPS, Galileo, and BDS). The simulator does not have any urban canyon capability. Hence, we generated such a scenario instead by artificially blocking out non-visible satellites. The simulator that was used was a Spectracom GSG 6 [38] with default satellite orbit data resulting in full constellation for all the three systems.

The urban canyon was generated by introducing identical walls of specific height on both sides of the receiver. The height of the walls was increased with a rate of 1 m for every 10 m, and for the first 100 m, there were no walls at all. The dimensions of the generated urban canyon are shown in Fig. 10.

As can be seen from Fig. 10, the user started at a distance of 100 m from the urban canyon and driving at a speed of 10 m/s quickly entered the canyon where the walls on both sides are continuously becoming higher with a rate of 1 m/s. The elevation angle of the top of the walls was calculated for each azimuthal angle, and any satellite that was blocked by a wall was disregarded from the navigation solution. The test is repeated for eight different directions of the canyon.

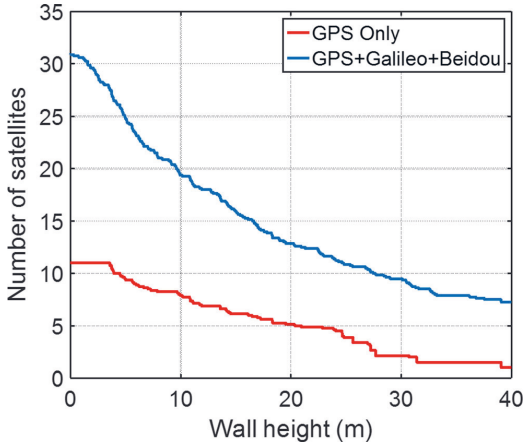

Fig. 11 Average number of satellites for GPS (*red*) and GPS + Galileo + BDS (*blue*)

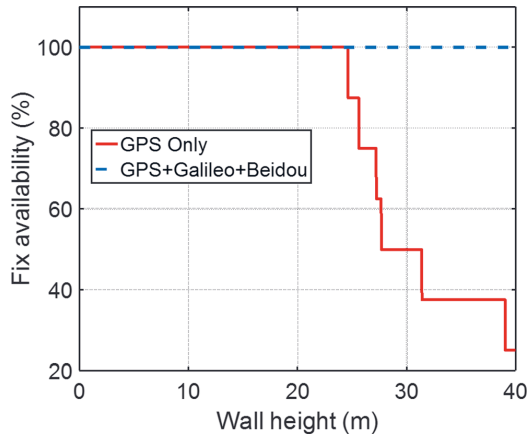

Fig. 12 Fix availability for GPS (*red*) and GPS + Galileo + BDS (*blue*)

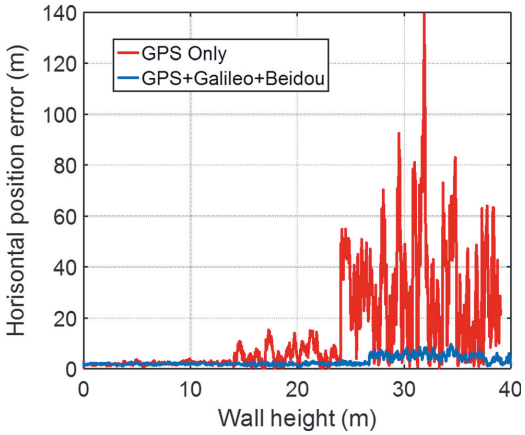

Fig. 13 Horizontal position error for urban canyon with azimuth of 225°

The result is that the number of available satellites becomes less and less and eventually the position will be lost. When fewer satellites are available the geometry becomes worse, affecting the quality of the position. Two options are compared, GPS only and GPS + BDS + Galileo. The average number of satellites over all for eight directions is shown in Fig. 11. The fix availability as a function of the height of the urban canyon wall is shown for GPS only and GPS + BDS + Galileo in Fig. 12.

Besides the low number of satellite visibility and the inevitable low number of navigation solution, i.e., "fix" availability for a GPS-only solution, the performance of the receiver will be worse when using GPS-only signals. The horizontal position errors for the two cases are shown in Figs. 13 and 14.

In the 225° case (Fig. 14), the GPS-only solution managed to maintain a position solution almost until the walls became 40-m high, but the position errors became larger than 100 m.

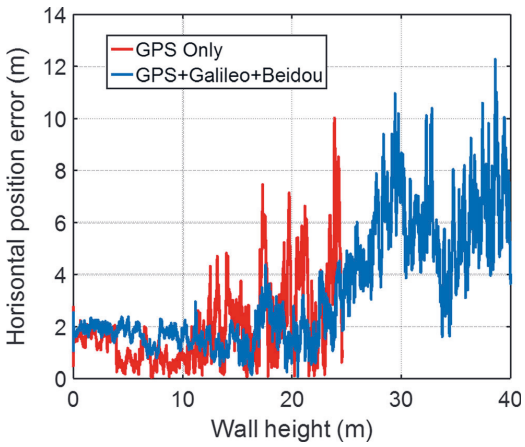

Fig. 14 Horizontal position error for urban canyon with azimuth of 315°

In the 315° case, the GPS-only solution lost its position fixes already much earlier, and the accuracy was degraded.

4 Conclusions

The new Matlab-based multi-GNSS software-defined receiver architecture developed at the Finnish Geospatial Research Institute was presented in this paper. The design of the receiver was described in detail in various processing stages and the impacts of this design when supporting multiple systems were explained. Finally, experimental results were presented where it was distinctively shown that the use of multiple systems simultaneously will result in improved performance, namely availability and accuracy, both in open sky conditions and in urban canyon environments. In the open sky tests, the horizontal 50 % error is approximately 3 m for GPS only, 1.8 to 2.8 m for combinations of any two systems, and 1.4 m when using GPS, Galileo, and BDS satellites. The vertical 50 % error reduces from 4.6 to 3.9 when using all the three systems compared to GPS only. In severe urban canyons, the position error for GPS only can be more than ten times bigger, and the fix availability can be less than half of the availability for a multi-GNSS solution.

Further development of the multi-GNSS receiver is planned, and the following main features will be developed in near future:

- Work on adding support for GLONASS signals has already been started, and this will continue until we have successfully added the fourth system to our receiver.
- A search unit that will contain the logic on how to optimize the search for signals from multiple systems. Some novel algorithms will be developed in this area.
- A Kalman navigation filter to replace the least square estimator (LSE) solution. The LSE solution will in the future be used for initialization only.
- Development of novel multi-GNSS receiver autonomous integrity monitoring (RAIM) algorithms for error detection and exclusion for mass-market-grade receivers.
- A fully integrated multi-GNSS tracking engine with support for all GNSS signals including advanced mode switching techniques. Switching between modes optimized for high dynamic tracking or high sensitivity tracking will improve the overall performance of the receiver significantly.
- In the current implementation, navigation is initiated only after tracking has completed. The plan is to perform navigation for each new measurement from the track engine. This will resemble a more real-time operation, and it will enable feedback from the navigation to the tracking. This makes it possible to integrate any deeply coupled inertial navigation system (INS) algorithm into the receiver.

Acknowledgments This research has been conducted within the projects DETERJAM (Detection analysis and risk management of satellite navigation jamming) funded by the Scientific Advisory Board for Defence of the Finnish Ministry of Defence and the Finnish Geodetic Institute/Finnish Geospatial Research Institute, Finland, and FINCOMPASS, funded by the Finnish Technology Agency TEKES with the Finnish Geodetic Institute/Finnish Geospatial Research Institute, Nokia Corporation, Roger-GPS Ltd., and Vaisala Ltd.

References

1. Global Positioning Systems Directorate (2012). Systems engineering & integration interface specification. http://www.gps.gov/technical/icwg/IS-GPS-200G.pdf. Accessed 6 May 2015
2. Russian Institute of Space Device Engineering (2008). GLONASS interface control document ed. 5.1. http://www.spacecorp.ru/upload/iblock/1c4/cgs-aaixymyt%205.1%20ENG%20v%202014.02.18w.pdf. Accessed 5 May 2015
3. European Space Agency (2015). Galileo satellites—status update. http://www.esa.int/Our_Activities/Navigation/Galileo_satellites_status_update. Accessed 2 May 2016
4. Pagny R, Dardelet J-C, Chenebault J (2005) From EGNOS to Galileo: a European vision of satellite-based radio navigation. Ann Telecommun 60(3):357–375. doi:10.1007/BF03219825
5. European Union (2014) European GNSS open service. http://ec.europa.eu/enterprise/policies/satnav/pubconsult-2/files/galileo_os_sis_icd_v1-2-3_short_version270614_en.pdf. Accessed 5 May 2015
6. China Satellite Navigation Office (2013) BeiDou navigation satellite system signal in space interface control document version 2.0. http://www.beidou.gov.cn/attach/2013/12/26/20131226b8a6182fa73a4ab3a5f107f762283712.pdf. Accessed 5 May 2015
7. Min L, Lizhong Q, Qile Z, Jing G, Xing S, Xiaotao L (2014) Precise point positioning with the BeiDou navigation satellite system. Sensors 14:927–943. doi:10.3390/s140100927
8. Montenbruck O, Steigenberger P, Khachikyan R, Weber G, Langley RB, Mervart L, Hugentobler U (2014) IGS-MGEX, preparing the ground for multi-constellation GNSS science. Inside GNSS, Jan/Feb. 42–49
9. Akos DM (1997) A software radio approach to global navigation satellite system receiver design. A dissertation for the degree Doctor of Philosophy presented to The Faculty of the Fritz J. and Dolores H. R., College of Engineering and Technology, Ohio University
10. Akos DM, Normark PL, Hansson A, Rosenlind A, Ståhlberg C, Svensson F (2001) Global positioning system software receiver (GPSrx) implementation in low cost/power programmable processors. In: Proceedings of ION 2001, September 11–14, 2851–2858, Salt Lake
11. Akos DM, Normark PL, Hansson A, Rosenlind A (2001) Real-time GPS software radio receiver. In: Proceedings of ION 2001, September 11–14, 809–816, Salt Lake City
12. Borre K, Akos DM, Bertelsen N, Rinder P, Jensen SH (2007) A software-defined GPS and Galileo receiver: a single-frequency approach. Birkhäuser Verlag GmbH, Boston
13. Normark PL, Macgougan G, Stahlberg C (2004) GNSS software receivers—a disruptive technology. In: Proceedings of GNSS Symposium, Tokyo
14. Normark PL, Christian S (2005) Hybrid GPS/Galileo real time software receiver. In: Proceedings of the 18th International Technical Meeting of the Satellite Division of The Institute of Navigation, September 13–16, 1906–1913, Long Beach
15. Ma C, Lachapelle G, Cannon ME (2004) Implementation of a software GPS receiver. In Proceedings of ION GNSS 17th International Technical Meeting of the Satellite Division, September 21–24, 956–970, Long Beach
16. Stöber C, Anghileri M, Ayaz AS, Dötterböck D, Krämer I, Kropp V, Won JH, Eissfeller B, Güixens DS, Pany T (2010) ipexSR: a real-time multi-frequency software GNSS receiver. In: 52nd International Symposium ELMAR-2010, 15–17 September, Zadar
17. Jovancevic A, Brown A, Ganguly S, Goda J, Kirchner M, Zigic S (2003) Real-time dual frequency software receiver. In: Proceedings of ION GNSS 16th International Technical Meeting of the Satellite Division, September 9–12, 2572–2583, Portland
18. Ledvina BM, Psiaki ML, Sheinfeld DJ, Cerruti AP, Powell SP, Kintner PM (2004) A real-time GPS Civilian L1/L2 software receiver. In Proceedings of ION GNSS 17th International Technical Meeting of the Satellite Division, September 21–24, 986–1005, Long Beach
19. Pany T, Förster F, Eissfeller B (2004) Real-time processing and multipath mitigation of high-bandwidth L1/L2 GPS signals with a PC-based software receiver. In: Proceedings of ION GNSS 17th International Technical Meeting of the Satellite Division, September 21–24, 971–985, Long Beach
20. Chen YH, Juang JC, De Lorenzo DS, Seo J, Lo S, Enge P, Akos DM (2011) Real-time dual-frequency (L1/L5) GPS/WAAS software receiver. In: Proceedings of the 24th International Technical Meeting of The Satellite Division of the Institute of Navigation, September 19–23, 767–774, Portland
21. Juang J-C, Tsai C-T, Chen Y-H (2013) Development of a PC-based software receiver for the reception of Beidou navigation satellite signals. J Navig 66(5):701–718
22. Viola S, Mascolo M, Madonna P, Sfarzo L, Leonardi M (2012) Design and implementation of a single-frequency L1 multi constellation GPS/EGNOS/GLONASS SDR receiver with NIORAIM FDE integrity. In: Proceedings of the 25th International Technical Meeting of the Satellite Division of the Institute of Navigation, September 17–21, 2968–2977, Nashville
23. Ferreira PMLM (2012). GPS/Galileo/GLONASS software defined signal receiver. M.Sc. Dissertation, Universidade Téchnica de Lisboa
24. Casabona M, Rosen M (1999) Discussion of GPS anti-jam technology. GPS Solutions 2(3):18–23
25. Bhuiyan MZH, Kuusniemi H, Söderholm S, Airos E (2014) The impact of interference on GNSS receiver observables—a running digital sum based simple jammer detector. Radioeng J 23(3):898–906
26. Jones M (2011) The civilian battlefield-protecting GNSS receivers from interference and jamming, inside GNSS magazine, March/April, 40–49
27. Kraus T, Bauernfeind R, Eissfeller B (2011) Survey of in-car jammers—analysis and modeling of the RF signals and IF samples (suitable for active signal cancellation). In: Proceedings of the 24th International Technical Meeting of the Satellite Division of the Institute of Navigation, September 19–23, 430–435, Portland
28. Mitch RH, Dougherty RC, Psiaki ML, Powell SP, O'hanlon BW, Bhatti JA, Humphreys TE (2011) Signal characteristics of civil GPS jammers. In: Proceedings of the 24th International Technical Meeting of the Satellite Division of the Institute of Navigation, September 19–23, 1907–1919, Portland
29. Jiang Z, Ma C, Lachapelle G (2004) Mitigation of narrow-band interference on software receivers based on spectrum analysis. In: Proceedings of ION GNSS 17th International Technical

Meeting of the Satellite Division, September 21–24, 144–155, Long Beach
30. Gurtner W, Estey L (2009) RINEX—the receiver independent exchange format, version 3.00. ftp://igscb.jpl.nasa.gov/pub/data/format/rinex300.pdf. Accessed 5 May 2015
31. Sagiraju PK, Raju GSV, Akopian D (2008) Fast acquisition implementation for high sensitivity global positioning systems receivers based on joint and reduced space search. IET Radar Sonar Navig 2(5):376–387
32. Juang JC, Chen YH (2010) Global navigation satellite system signal acquisition using multi-bit code and a multi-layer acquisition strategy. IET Radar Sonar Navig 4(5):673–684
33. Bhuiyan MZH, Söderholm S, Thombre S, Ruotsalainen L, Kuusniemi H (2014) Overcoming the challenges of BeiDou receiver implementation. Sensors 14:22082–22098
34. Bhuiyan MZH, Söderholm S, Thombre S, Ruotsalainen L, Kuusniemi H (2014) Implementation of a software-defined BeiDou receiver. In: Chinese Satellite Navigation Conference Proceedings: Volume I, Lecture Notes in Electrical Engineering, 751–762, Vol. 303, ISSN 1876–1100, Springer
35. Borio D, Lachapelle G (2009) A non-coherent architecture for GNSS digital tracking loops. Ann Telecommun 2009(64):601–614. doi:10.1007/s12243-009-0114-1
36. Nottingham Scientific Limited. NSL stereo datasheet. http://www.nsl.eu.com/datasheets/stereo.pdf. Accessed on 10 Jan 2014
37. Antcom Corporation (2014) G5 L1/L2 glonass + L1/L2 GPS + Omnistar antennas for ground, avionics, marines, buoy and deepsea applications. http://www.antcom.com/documents/catalogs/G5_Antennas_L1L2GLonass_Plus_L1L2GPS_Omnistar.pdf. Accessed 5 May 2015
38. Spectracom (2014) GSG-6 SERIES. Multi-channel, multi-frequency advanced GNSS simulator. http://www.spectracomcorp.com/ProductsServices/GPSSimulation/Multi-FrequencyGPSSimulator. Accessed 5 May 2015

PUBLICATION

III

Overcoming the challenges of BeiDou receiver implementation

M. Z. H. Bhuiyan, S. Söderholm, S. T. L. Ruotsalainen and H. Kuusniemi

Sensors 14.(2014), 22082–22098

Sensors **2014**, *14*, 22082-22098; doi:10.3390/s141122082

OPEN ACCESS

sensors

ISSN 1424-8220

www.mdpi.com/journal/sensors

Article

Overcoming the Challenges of BeiDou Receiver Implementation

Mohammad Zahidul H. Bhuiyan *, Stefan Söderholm, Sarang Thombre, Laura Ruotsalainen and Heidi Kuusniemi

Department of Navigation and Positioning, Finnish Geodetic Institute, 02430 Kirkkonummi, Finland; E-Mails: stefan.soderholm@fgi.fi (S.S.); sarang.thombre@fgi.fi (S.T.); laura.ruotsalainen@fgi.fi (L.R.); heidi.kuusniemi@fgi.fi (H.K.)

* Author to whom correspondence should be addressed; E-Mail: zahidul.bhuiyan@fgi.fi; Tel.: +358-50-3726-569; Fax: +358-92-9555-211.

External Editor: Assefa M. Melesse

Received: 26 August 2014; in revised form: 26 September 2014 / Accepted: 12 November 2014 / Published: 21 November 2014

Abstract: Global Navigation Satellite System (GNSS)-based positioning is experiencing rapid changes. The existing GPS and the GLONASS systems are being modernized to better serve the current challenging applications under harsh signal conditions. These modernizations include increasing the number of transmission frequencies and changes to the signal components. In addition, the Chinese BeiDou Navigation Satellite system (BDS) and the European Galileo are currently under development for global operation. Therefore, in view of these new upcoming systems the research and development of GNSS receivers has been experiencing a new upsurge. In this article, the authors discuss the main functionalities of a GNSS receiver in view of BDS. While describing the main functionalities of a software-defined BeiDou receiver, the authors also highlight the similarities and differences between the signal characteristics of the BeiDou B1 open service signal and the legacy GPS L1 C/A signal, as in general they both exhibit similar characteristics. In addition, the authors implement a novel acquisition technique for long coherent integration in the presence of NH code modulation in BeiDou D1 signal. Furthermore, a simple phase-preserved coherent integration based acquisition scheme is implemented for BeiDou GEO satellite acquisition. Apart from the above BeiDou-specific implementations, a novel Carrier-to-Noise-density ratio estimation technique is also implemented in the software receiver, which does not necessarily require bit synchronization prior to estimation. Finally, the authors present a BeiDou-only position fix with the implemented software-defined

BeiDou receiver considering all three satellite constellations from BDS. In addition, a true multi-GNSS position fix with GPS and BDS systems is also presented while comparing their performances for a static stand-alone code phase-based positioning.

Keywords: BeiDou Navigation Satellite system; acquisition; tracking; software-defined receiver; multi-GNSS

1. Introduction

The Chinese BeiDou Navigation Satellite system (BDS) has a mixed space constellation that will have, when fully deployed, five Geostationary Earth Orbit (GEO) satellites, twenty-seven MEO satellites and three Inclined Geosynchronous Satellite Orbit (IGSO) satellites. The GEO satellites are operating in orbit at an altitude of 35,786 kilometers and positioned at 58.75°E, 80°E, 110.5°E, 140°E and 160°E, respectively. The MEO satellites are operating in orbit at an altitude of 21,528 km and an inclination of 55° to the equatorial plane. The IGSO satellites are operating in orbit at an altitude of 35,786 km and an inclination of 55° to the equatorial plane. These satellites broadcast navigation signals and messages within three frequency bands. The BDS has been in development for more than a decade, and it is estimated to be operational with global coverage at the latest in 2020 [1,2]. The BeiDou satellites transmit ranging signals based on Code Division Multiple Access (CDMA) principle, like GPS and Galileo. The mixed constellation structure of BeiDou results in better observation geometry for positioning and orbit determination compared to current GPS and GLONASS, and future Galileo, especially in China and neighboring regions. The BeiDou system has already started contributing to the multi-GNSS benefits where increased accuracy, availability and integrity are possible when utilizing interoperable GNSS [3].

The characteristics of BeiDou B1I (B1 In-phase) signal can be compared with GPS L1 signal in order to realize the similarities and differences between the two systems. Both the civilian signals from these two systems have similar characteristics in general, for example, the periods of their spreading codes are both 1 millisecond (ms) long, and the coordinate systems and the navigation message structures are almost the same with minor differences [4,5]. This eventually means that many algorithms that are implemented for the GPS receiver can be readily available to the BeiDou receiver without any major modification. But to improve the positioning performance, the modern GNSS signals, including BeiDou and the GPS L5, introduce a second layer of modulation between the navigation data and the PRN code chips, known as Neumann-Hoffman (NH) code modulation. This ultimately improves the data bit rate of the modern GNSS signals.

The legacy GPS L1 C/A signal has a data bit rate of 50 bits per second (bps), which means that 1 bit data lasts for 20 ms (*i.e.*, the PRN code cycle repeats 20 times for each data bit). The data bit rate of BeiDou D2 signal is 500 bps, which means that 1 bit of data lasts for only 2 ms (*i.e.*, two spreading code cycles). The data bit rate of BeiDou D1 signals is originally 50 bps, but after modulation by NH code, the data bit rate becomes 1 kbps, so compared to the GPS signal, the data bit rate of the BeiDou signal increases significantly. Particularly, the NH code modulated D1 signal has 1 kbps data bit rate which makes data bit transition possible within the data bit boundary. The use of NH code and the resultant

increase in the data bit rate has pros and cons. On the positive side, the NH code can boost the ability of anti-narrowband interference and improve the cross-correlation property of satellite signals and the bit synchronization [6]; whereas on the negative side, the existence of NH code makes the acquisition and tracking of the modernized GNSS signals more challenging [7–12]. The acquisition and tracking challenges in BDS will be discussed in more detail in Sections 2.1 and 2.2, respectively.

The use of a software-defined GNSS receiver is highly appreciated for its flexibility, re-configurability and diversity. These unique characteristics of a software-defined receiver make it possible to develop and then to validate new algorithms for optimizing the receiver performance at a low cost [13]. A number of software-defined receivers have already been developed for GNSS signal reception and processing [13–17]. Most of these receivers are capable of processing GPS, GLONASS and Galileo signals. Recently, a PC-based BeiDou software receiver was introduced in [18] albeit with limited algorithmic details on how to acquire, track and process a NH code modulated BeiDou signal. Therefore, in this paper, the authors discuss the implementation issues of a software-defined BeiDou receiver considering the challenges introduced by the existence of NH code modulation in case of BeiDou D1 signal and the higher data rate in case of BeiDou D2 signal.

The rest of this paper is organized as follows: Section 2 discusses the main functionalities of a software-defined GNSS receiver in view of BDS. In Section 3, a live data collection scenario, front-end configurations and positioning results are presented and discussed. Finally, conclusions and future work are discussed in Section 4.

2. Software-Defined GNSS Receiver

A GNSS software-defined receiver consists of three major components: RF front-end unit, a signal processing unit, and a navigation processing unit. The RF front-end module is responsible for signal amplification, noise filtering, down-conversion, automatic gain control, and analogue-to-digital conversion. The front-end module converts the received analog data to digital Intermediate Frequency (IF) data at a rate which is several times more than the code chipping rate. A 26 MHz sampling frequency is used to generate the raw digitized IF samples in all the experimented cases of this work.

The digital IF data are then processed by a signal processing unit whose main responsibilities include signal acquisition, code and carrier tracking and data demodulation. The demodulated data and the resulting pseudorange measurements are then utilized by a navigation processing unit in order to offer a Position, Velocity and Timing (PVT) solution, along with some other relevant information. The software-defined receiver differs from a conventional receiver in the sense that the functions of the processing and navigation units, including correlation/tracking and navigation tasks, are delivered by software, leading to a more flexible design with potential savings in cost and power.

A software-defined GNSS receiver platform, named as FGI-GSRx (Version 2), has been developed in Finnish Geodetic Institute for the analysis and validation of novel algorithms for an optimized GNSS navigation performance. The basic version of FGI-GSRx is based on an open-source software receiver platform [13], and it has been adapted to be BeiDou-compatible with a dual-frequency front-end from Nottingham Scientific Limited (NSL) [18]. The NSL front-end, ‘stereo v2’ is used to capture the BeiDou data. The stereo front-end configuration is presented in Table 1. The BeiDou B1I signal spectrum, time-domain plot and bin distribution of the digitized IF samples are shown in Figure 1.

Figure 1. BeiDou signal spectrum (**Top**); time-domain plot (**Bottom-left**); and bin distribution (**Bottom-right**) of the digitized IF samples.

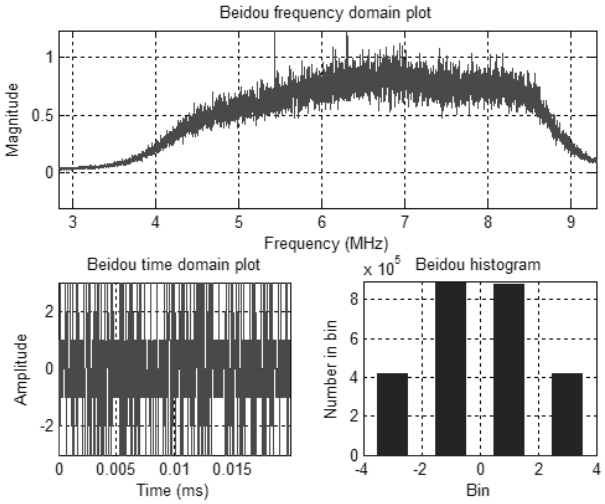

Table 1. NSL stereo v2 front-End configuration for BeiDou B1I signal reception.

Parameter	Value
Intermediate Frequency	6.5 MHz
Front-end Bandwidth	4.2 MHz
Sampling Frequency	26 MHz
Number of Quantization bits	2 bits

2.1. BeiDou Signal Acquisition

The main task at the signal acquisition stage is to determine which of the satellites are visible to the user and then, to coarsely estimate the carrier Doppler and the code phase of those visible satellites. Generally speaking, signal acquisition is a three dimensional search, where the satellite PRN number, the carrier Doppler and the code phase are coarsely estimated. An FFT-based signal acquisition technique is implemented in the software receiver.

2.1.1. BeiDou IGSO and MEO Satellites Acquisition

The traditional coherent acquisition techniques used for GPS L1 C/A signal acquisition cannot directly be applied to acquire BeiDou D1 signal transmitted from IGSO and MEO satellites due to the presence of NH code modulation. The presence of NH code modulation on top of navigation data bits increases the final data bit rate from 50 bps to 1 kHz. Therefore, the sign changes for BeiDou D1 signal occur more frequently than that of a GPS L1 C/A signal due to the presence of NH code. This eventually means that an acquisition scheme for BeiDou D1 signal with more than 1 ms coherent integration period may appear dangerous, if sign information is not consistently preserved. In view of this sign transition problem, a novel acquisition technique is implemented for BeiDou D1 signal that preserves the total useful signal energy in the presence of a sign transition, and hence, makes a correct acquisition decision

on the presence of the satellite, and its carrier Doppler and the corresponding code phase. The working principle of the novel BeiDou D1 acquisition technique, first introduced in [9], is also depicted in the following.

Step 1: For a coherent integration period of T_{coh} ms, a (T_{coh} × 1000 =) X_{bit} number of NH code bits is selected first. For example, for a coherent integration period of 5 ms, the first 5 bits of NH code, *i.e.*, [−1 −1 −1 −1 −1] can be selected. Also, a long incoming BeiDou signal of (T_{coh} + 19) ms is required to carry out the FFT-based acquisition. In case of T_{coh} = 5 ms, the acquisition metric will be consisted of 24 ms long incoming signal.

Step 2: The frequency resolution is chosen such that the frequency bin size is less than (2/3) × T_{coh}, where T_{coh} is the coherent integration time. In case of a 5 ms integration time, the frequency bin size should be less than or equal to 133.33 Hz.

Step 3: The chosen X_{bit} long NH code sequence is then multiplied with the locally generated BeiDou PRN codes in order to form an X_{bit} long NH-code-modulated-PRN-code-cycle.

Step 4: An FFT-based correlation is then performed on each T_{coh} ms blocks of incoming BeiDou signal with the locally generated X_{bit} long NH-code-modulated-PRN-code-cycles (*i.e.*, the output of Step 3 with an incoming signal index increment of 1. An example on how the incoming BeiDou D1 signal is structured for acquisition is shown in Figure 2 below for a coherent integration period of T_{coh} = 5 ms.

Step 5: As the NH code length is 20 bits, there are altogether 20 chunks of correlation matrices with all possible code delay and carrier Doppler combinations for a specific BeiDou satellite. The winning index is the one which has the maximum correlation peak as shown in Figure 3. Therefore, this winning NH index can be used for detecting the presence of the satellite, along with the estimation of the carrier Doppler and the code phase via a pre-detection threshold computed against a certain probability of false alarm.

Figure 2. 24 ms long incoming BeiDou signal is structured into 20 chunks of 5 ms long block with an index increment of 1.

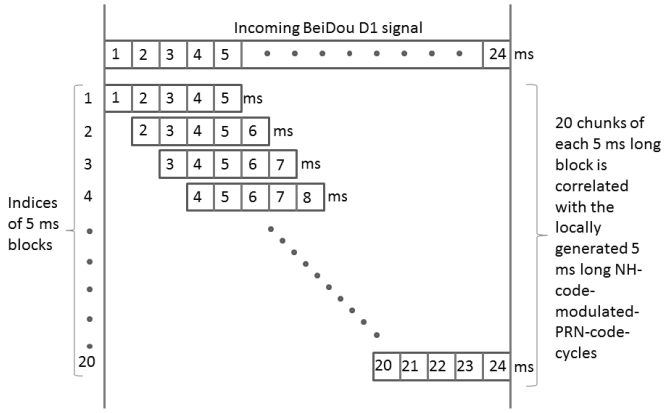

Figure 3. Acquisition correlation peaks for different NH indices.

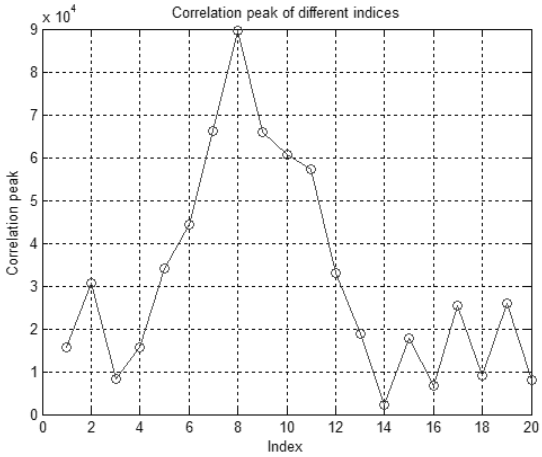

2.1.2. BeiDou GEO Satellites Acquisition

In case of BeiDou GEO satellites which transmit D2 navigation signal, there is no NH code modulation on top of the data bits. But, D2 signal has a data bit rate of 500 bps, meaning that each data bit will last for 2 ms. Therefore, the bit transition in case of BeiDou D2 signal may occur after every 2 ms unlike the GPS L1 C/A signal, where the bit transition may occur only after 20 ms. In view of this much frequent sign transition occurrences, a similar strategy like D1 signal acquisition technique is implemented for BeiDou D2 signal. The implementation strategy for D2 signal acquisition is described in the following.

Step 1: The chosen number of coherent integration summation should be even (*i.e.*, multiple of 2 due to the bit interval duration of D2 signal).

Step 2: For a coherent integration period of T_{coh} ms (which is chosen as even), a $(((T_{coh})/2) \times 1000 =)$ X_{bit} number of data bits is selected first. For example, for a coherent integration period of 4 ms, the number of data bits, $X_{bit} = 2$. In case of $X_{bit} = 2$, all possible combinations for incoming data bits will be $2^{X_{bit}} = 4$. Therefore, there will be four possibilities for incoming received data bits, which are: [+1 +1], [+1 −1], [−1 +1], and [+1 +1].

Step 3: The frequency resolution is chosen such that the frequency bin size is less than $(2/3) \times T_{coh}$, where T_{coh} is the coherent integration time. In case of a 4 ms integration time, the frequency bin size should be less than or equal to 166.67 Hz.

Step 4: Each of the $2^{X_{bit}}$ data-bit set is then multiplied with the locally generated BeiDou PRN codes in order to form a T_{coh} ms long data-modulated-PRN-code-cycles. It is important to note here that while forming the data-modulated-PRN-code-cycles, the data bits are hold such that they match the locally generated PRN code chip rate. In other words, the data bits are hold such that 1 data bit lasts for 2 ms, as is the case for BeiDou D2 signal.

Step 5: An FFT-based correlation is then performed on each of the possible $2^{X_{bit}}$ data-bit combinations of the incoming BeiDou signal with the locally generated T_{coh} ms long data-modulated-PRN-code-cycles (*i.e.*, the output of Step 4).

Step 6: As the data-bit set length is $2^{X_{bit}}$, there will be altogether $2^{X_{bit}}$ chunks of correlation matrices with all possible code delay and carrier Doppler combinations for a specific BeiDou GEO satellite. The winning index is the one which has the maximum correlation peak, and therefore, it can then be used for detecting the presence of the satellite, along with the estimation of the carrier Doppler and the code phase via a pre-detection threshold computed against a certain probability of false alarm.

The resultant acquisition metric after utilizing the above two acquisition strategies for BeiDou IGSO/MEO and GEO satellites is shown in Figure 4. BeiDou PRNs 05 (GEO); 07, 09, 10 (IGSO); 11, 13, 14 (MEO) were acquired successfully, which were in view with 10^0 or more elevation angle at the time of data collection in Finnish Geodetic Institute, Finland.

Figure 4. Acquisition metric for BeiDou GEO, IGSO and MEO satellites.

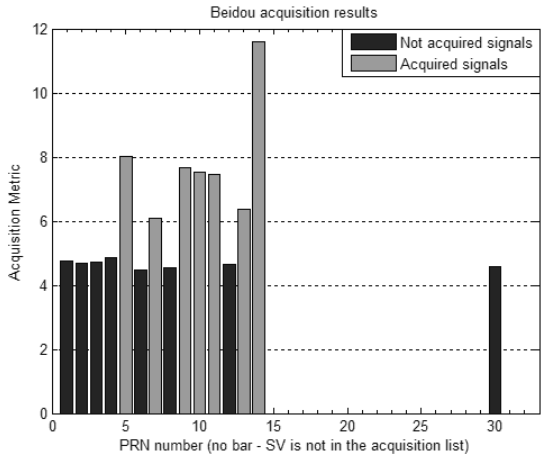

2.2. BeiDou Signal Tracking

The acquisition approaches mentioned earlier in Section 2.1 provide the initial estimates of the carrier Doppler and the code offset. After the acquisition, the control will be handed over to the tracking loops to track the variations of carrier phase and code offset due to the line of sight movement between the satellites and the receiver.

2.2.1. Carrier Tracking

The main objective of signal tracking is to wipe off the code and the carrier. The carrier tracking loop synchronizes the carrier frequency and phase with that of the incoming signal. One of the most commonly used frequency discriminator in a conventional GPS Frequency Locked Loop (FLL) is a four-quadrant arctangent discriminator. This discriminator is optimal at high and low C/N_0 with a wide frequency pull-in range and it offers a linear relationship between the discriminator output and the real frequency error. This discriminator can not only enhance the robustness of signal tracking but also tolerate large acquisition frequency errors coming from the acquisition. But, this four-quadrant arctangent discriminator is sensitive to data bit transition, meaning that two adjacent integration samples

should be within the same data bit interval. In case of legacy GPS L1 signal, the data bit transition may occur only after every 20 ms offering a low data bit rate. Due to the low data bit rate, the GPS receiver can meet this condition in most occasions. Therefore, the probability that the data bit transition affects the discriminator is relatively small (less than or equal to 5%), and the four-quadrant arctangent discriminator based FLL can work correctly [19]. However, in case of BeiDou D1 or any modern GNSS signals with an extra tier of modulation on top of data bits, the bit transition usually occurs rather quickly, and therefore, the four-quadrant arctangent discriminator based FLL is not an appropriate choice for BeiDou D1 signal tracking. The same observation is true for BeiDou D2, where the data bit lasts for only 2 ms, with a maximum probability of data bit transition of 50%. Therefore, the BeiDou receiver should choose an FLL discriminator that is insensitive to data bit transition. In view of this particular situation, a two-quadrant arctangent discriminator is implemented in the software receiver, which is first proposed in [8]. The implemented two-quadrant arctangent discriminator is insensitive to data bit transition, but it has reduced tolerance of frequency uncertainty coming from the acquisition stage. It was shown in [8] that the frequency uncertainty tolerance is reduced by half, as compared to the conventional four-quadrant arctangent discriminator. This restriction in frequency uncertainty can be overcome by proper selection of coherent integration time (*i.e.*, frequency bin size) at the acquisition stage. The signal tracking is switched from FLL to a costas Phase Locked Loop (PLL), once the FLL is locked.

2.2.2. Code Tracking

The code tracking loop or Delay Locked Loop (DLL) synchronizes the code phase of the local replica with the incoming signal. A Narrow Correlator (NC) discriminator [20] is implemented in the software receiver as a conventional DLL with early and prompt correlator spacing of 0.1 chips. Figure 5 below shows the tracking status of BeiDou PRN 14 for a 60 s long data.

Figure 5. Channel tracking status for PRN 14.

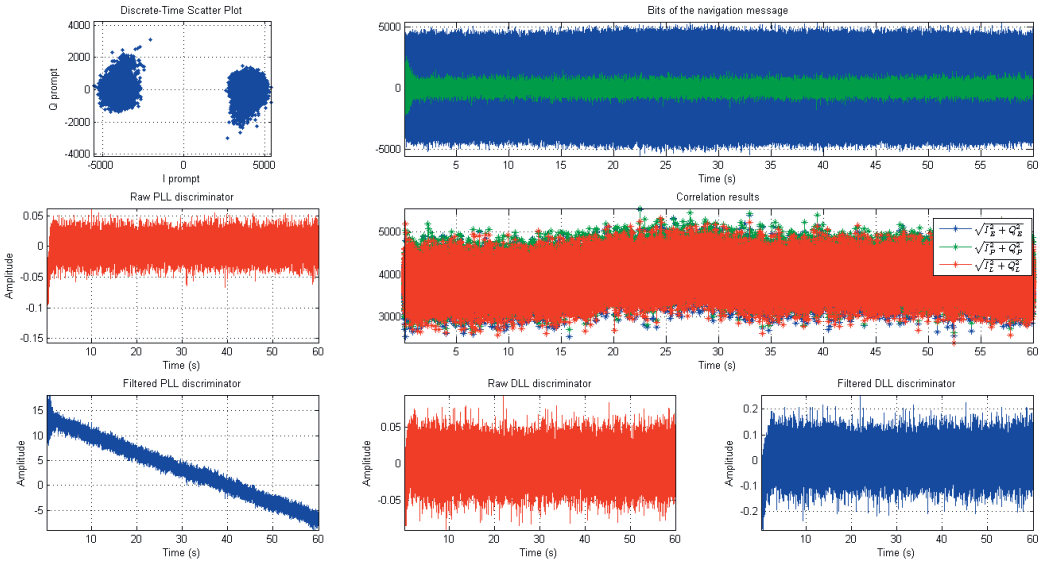

2.3. Bit Boundary Detection

Once the BeiDou receiver keeps tracking the carrier phase and the code offset of the incoming signal, the next phase is to detect the bit boundary and then to wipe off the NH code. The purpose of bit boundary detection is to avoid integration across a data bit-edge which might cause errors in the navigation message detection. Algorithms for the bit boundary detection can be found in [16,21,22]. The Histogram Method, for instance, senses the bit sign changes and keeps a statistic of their position. But this approach will not work with the BeiDou D1 signal due to the presence of NH code. The sign changes in this code within the data bit boundary would in fact be detected as data bit changes affecting the statistics that this method uses for the bit boundary detection. On the other hand, as the data bits are now modulated with the NH code, a simple correlation of the incoming NH code modulated data with the locally generated NH code can then be used to estimate the bit edge. The index with a maximum correlation peak of 20 will be perfectly aligned with the NH code, and it can then be used as the bit boundary index. In case of BeiDou D2 signal, a histogram-based approach is implemented for D2 bit edge detection.

2.4. Carrier-to-Noise Density Ratio (C/N_0) Estimation

The Carrier-to-Noise density ratio (C/N_0) for the GPS receivers is often calculated based on the Narrow-band Wide-band Power Ratio (NWPR) of the received signal [21]. If this C/N_0 estimation technique is used, the NH code (in case of D1 navigation signal) must have to be wiped off before the narrowband power is calculated. Otherwise, the narrowband power calculation will be erroneous due to the presence of bit transition within the 20 ms bit boundary. In case of D2 navigation signal, the narrowband power computation may not be accurate enough since the data bit duration for D2 signal is only 2 ms, which is 10 times less than GPS L1 C/A or BeiDou D1 data bit duration. In view of this particular issue, a new C/N_0 estimation technique based on the Signal-to-Noise Power Ratio (SNPR) is implemented in the FGI-GSRx software receiver. The implementation scheme is unique in the sense that the noise power is computed from the tracking channel itself through a +2 chips distant correlator from the prompt correlator. The properties of the Gold codes (both GPS L1 and BeiDou B1 signals are Gold codes) suggests that any auto-correlation with the same Gold codes outside ±1 chip delay from the prompt correlator should either be zero or very close to zero due to the limiting length of the Gold codes itself. A fair choice of +2 chips early correlation index is preferred here, as this correlation index (+2 chips with respect to prompt correlator) will have no impact from the multipath which usually comes as a delay in the late side of the correlation. The implementation scheme for SNPR-based C/N_0 estimation technique is mentioned in the following.

Step 1: An estimate of the noise power μ_N is obtained first by correlating the incoming signal with the locally generated PRN (Pseudo Random Noise) code with a correlator which is +2 chips early from the prompt correlation index.

Step 2: The signal power $\mu_{S,N}$ is computed from the prompt correlation between the incoming signal and the locally generated PRN code after each code integration period T_{coh} (*i.e.*, 1 ms for GPS L1 or BeiDou B1).

Step 3: Signal-to-Noise Power Ratio (*SNPR*), after each code epoch period, can be written as follows:

$$SNPR_i = \frac{\mu_{S_i}}{\mu_{N_i}} = \frac{\mu_{S,N_i} - \mu_{N_i}}{\mu_{N_i}} \quad (1)$$

Step 4: Finally, Carrier-to-Noise-density ratio, C/N_0 can be derived as:

$$C/N_{0_i}\Big|_{dB-Hz} = \left|10\log_{10}\left(\frac{SNPR_i}{T_{coh}}\right)\right| \quad (2)$$

Figure 6 shows the C/N_0 of the tracked BeiDou satellites. As shown in the figure, PRN 14 has the highest C/N_0 (~48 dB-Hz) and PRN 5 has the lowest C/N_0 (~39 dB-Hz) depending on their elevation angles with respect to the receiver at the time of data collection. The performance evaluation of SNPR-based C/N_0 estimation technique with respect to the traditional NWPR-based technique for BeiDou B1 signal is presented in [23].

Figure 6. C/N_0 for the tracked BeiDou satellites.

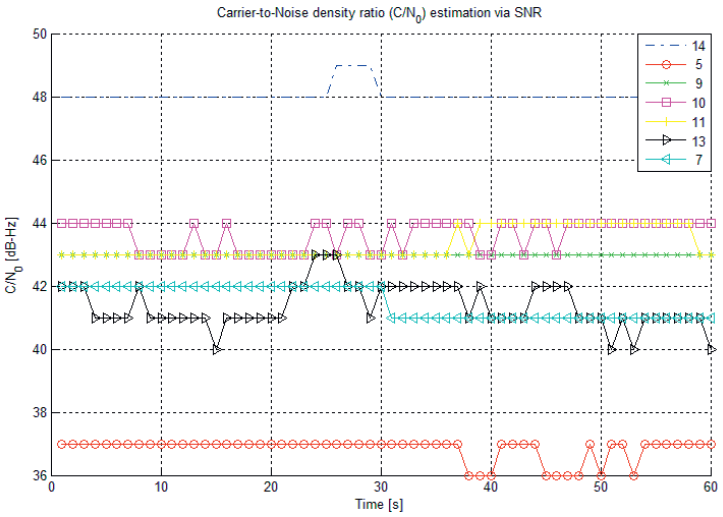

2.5. Navigation Solution

At the navigation message decoding phase, the first step is to detect the sub-frame preambles on the demodulated data. The BeiDou navigation message has both error correction coding and data interleaving. The error correction is performed by the Bose, Chaudhuri, and Hocquenghem (BCH 15,11,1) codes, which are capable of correcting one-bit error within every block of 15 bits. The decoding process can be illustrated by the flowchart shown in Figure 7. It is important to mention here that the BCH decoding and deinterleaving mechanism is same for both (D1 and D2) navigation messages, and the first word of every sub-frame, the first 15 bits are not BCH encoded. Only the next 11 bits are encoded and hence, this word consists of 26 information bits and four parity bits. Also, data interleaving is not performed in this word. Therefore, the first word of every sub-frame has to be processed differently at the decoding

stage within the receiver. After successfully decoding the navigation message, a receiver position can be calculated via a least-square method with at least four visible satellites with decoded ephemerides.

Figure 7. Flowchart illustrating the decoding procedure of BeiDou navigation message.

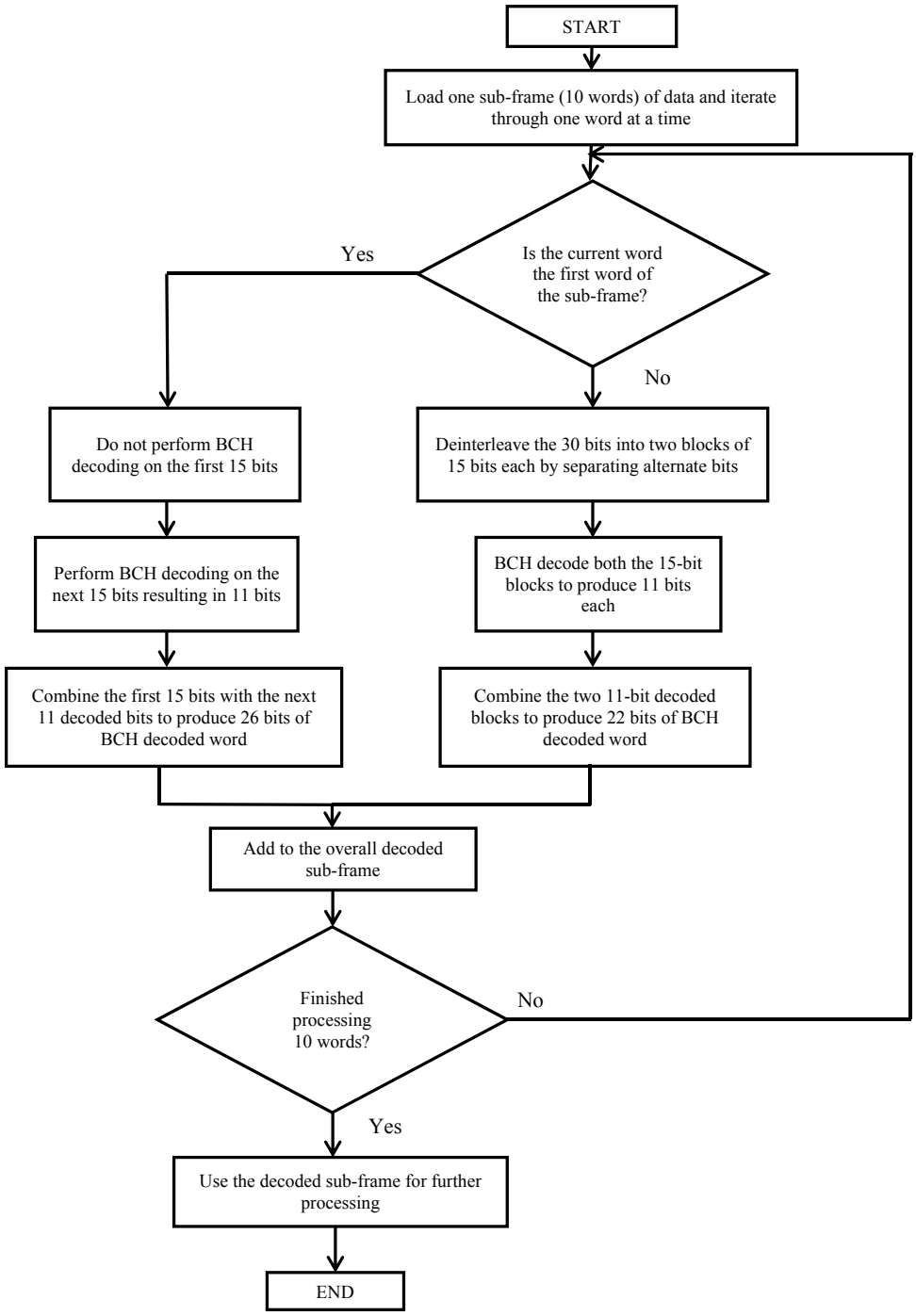

3. Live Data Collection and Result Analysis

A dual-frequency front-end from NSL is used to capture the real GNSS data. Among the two front-ends, the maxim 2769B front-end [24] is configured to receive BeiDou B1I signal at 1561.098 MHz, and the maxim 2112 front-end is configured to receive GPS L1 C/A signal at 1575.42 MHz, as mentioned in Table 2. The BeiDou B1I signal spectrum, time-domain plot and bin distribution of the digitized IF samples were already shown in Figure 1 of Section 2.

Table 2. NSL stereo v2 front-end configurations.

Parameter	Max2769B Front-End	Max2112 Front-End
Received signal	BeiDou	GPS
Intermediate Frequency	6.5 MHz	0 MHz
Front-end Bandwidth	4.2 MHz	6.6 MHz
Sampling Frequency	26 MHz	26 MHz
Number of Quantization bits	2 bits	2 bits

The GNSS data was collected on 31th January at around 9:30 AM UTC time at a static position with a roof antenna in Finnish Geodetic Institute, Kirkkonummi, Finland. The data was collected for about 60 s. The sky-plot for BeiDou constellation at the time of data collection is shown in Figure 8. There are one GEO satellite (PRN 05), three IGSO satellites (PRNs 7, 9, 10), and three MEO (PRNs 11, 13 and 14) satellites available at the moment of data collection. The FGI-GSRx receiver can acquire, track and compute a navigation solution with all the visible BeiDou satellites. The stand-alone positioning results with BDS are presented first followed by GPS-only and multi-GNSS positioning results with BeiDou and GPS.

Figure 8. Sky-plot of BeiDou satellite navigation system at UTC time 9:30 AM at Finnish Geodetic Institute with an elevation cut-off angle of 10^0.

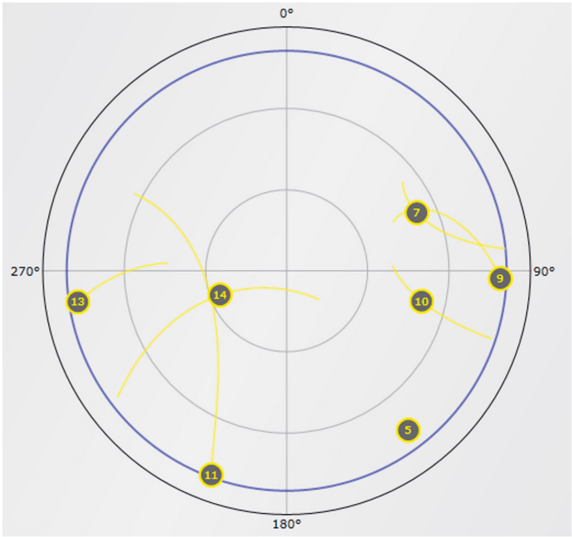

The horizontal error scatter plot and the position error variations in ENU frame are shown in Figures 9 and 10, respectively for BeiDou-only position fix. The 95% Circular Error Probable (CEP) for BeiDou-only horizontal position fix is within 3.76 m. The BeiDou-only position fix is also shown in Google Earth in Figure 11.

Figure 9. Horizontal error scatter plot.

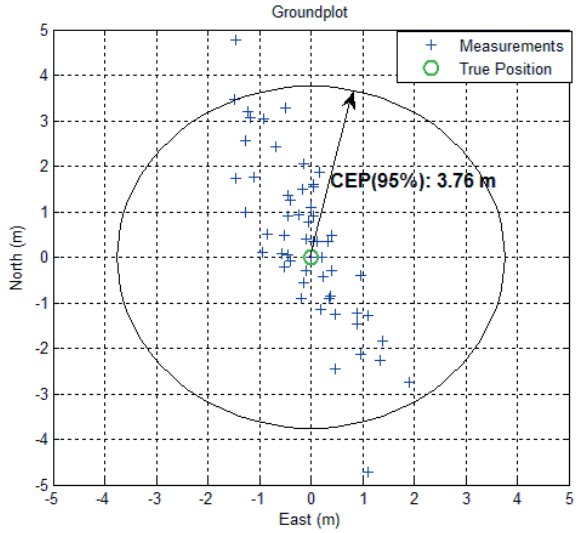

Figure 10. Position error variations with respect to true position in ENU frame.

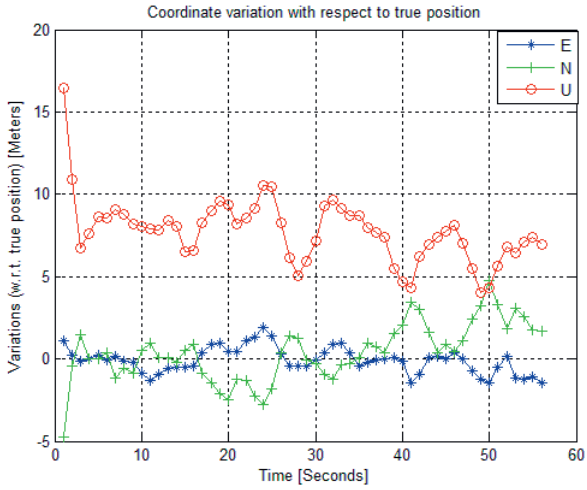

The position error statistics for BeiDou, GPS, and multi-GNSS solutions are finally presented in Table 3. The error statistics were computed for a stand-alone code-phase based position solution. The broadcasted Klobuchar ionospheric model parameters are utilized to calculate the ionospheric corrections. The position error statistics were computed with respect to the true known position. The 3D RMS errors for BeiDou and GPS are 8.24 m and 2.80 m, respectively. The error contribution for BeiDou

is coming from the vertical component, which is partly due to the fact that four out of seven satellites are low elevated, and hence, the broadcast ionospheric corrections are less accurate with those noisy measurements. Both BeiDou and GPS have comparable horizontal accuracy, whereas GPS outperforms BeiDou in terms of 3D RMS. In case of Multi-GNSS position fix, only the best two BeiDou satellites with the highest elevation angles were considered along with the eight GPS satellites for position computation. The improvement in 3D RMS is really minor with two extra measurements, but the improvement in PDOP is really significant. This eventually means that the multi-GNSS benefits will be more noticeable in harsh GNSS environment than in normal outdoor scenarios with good satellite visibility. In addition to that, the multi-GNSS can certainly offer higher reliability with the addition of new satellites from different constellations.

Figure 11. Position fix with BeiDou Satellite Navigation System in Google Earth.

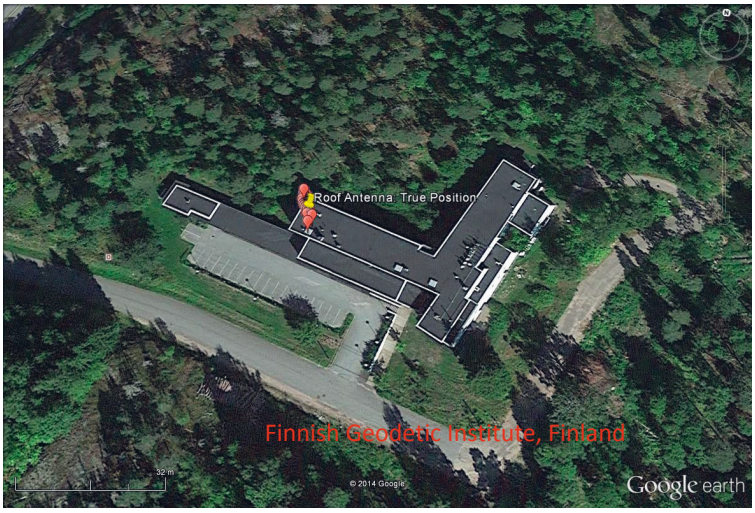

Table 3. Position error statistics with respect to true position.

	BeiDou				**GPS**				**Multi-GNSS**			
	East	**North**	**Up**	**3D**	**East**	**North**	**Up**	**3D**	**East**	**North**	**Up**	**3D**
RMS	0.77	1.78	8.0	8.24	1.19	1.77	1.82	2.80	1.0	1.76	1.88	2.77
PDOP	2.05				1.87				1.81			

4. Conclusions

The main functionalities of a software-defined BeiDou B1 receiver were presented, while highlighting the similarities and differences of BeiDou B1 signal with the existing GPS L1 C/A signal. A novel acquisition scheme for long coherent integration in the presence of NH code was presented and implemented for acquiring BeiDou IGSO and MEO satellites. Furthermore, a similar phase-preserved acquisition scheme was implemented for BeiDou GEO satellites acquisition. Real GNSS data was collected with a dual frequency front-end, which is then processed with the implemented software-defined GNSS receiver. The positioning results were presented for different GNSS

constellations for a static scenario with 60 s long dataset. It was shown that the BeiDou has comparable positioning performance with that of GPS, provided that both the systems have somewhat similar DOP values. A true multi-GNSS positioning results were also computed with GPS and BeiDou systems. The true benefits of multi-GNSS will be more noticeable in harsh GNSS environment with obstructed sky view. The future work includes investigating the performance of a multi-GNSS software-defined receiver in harsh multipath environments (*i.e.*, in urban canyons), as well as developing a Receiver Autonomous Integrity Monitoring (RAIM) system considering the signal quality of individual satellites from different GNSS constellations.

Acknowledgments

This research has been conducted within the Detection analysis, and risk management of satellite navigation jamming (DETERJAM) project funded by the Scientific Advisory Board for Defence of the Finnish Ministry of Defence and the Finnish Geodetic Institute, Finland and the FINCOMPASS project, funded by the Finnish Technology Agency TEKES with the Finnish Geodetic Institute, Microsoft Corporation, Roger-GPS Ltd., and Vaisala Ltd.

Author Contributions

Mohammad Zahidul H. Bhuiyan developed the BeiDou part of the multi-frequency multi-system FGI-GSRx software-defined GNSS receiver including the novel acquisition schemes mentioned in the manuscript. He also wrote most part of the manuscript. The co-authors contributed on writing some part of the manuscript and helped during the phase of data collection and data analysis.

Conflicts of Interest

The authors declare no conflict of interest.

References

1. Li, M.; Qu, L.; Zhao, Q.; Guo, J.; Su, X.; Li, X. Precise Point Positioning with the BeiDou Navigation Satellite System. *Sensors* **2014**, *14*, 927–943.
2. Xu, A.; Xu, Z.; Ge, M.; Xu, X.; Zhu, H.; Sui, X. Estimating Zenith Tropospheric Delays from BeiDou Navigation Satellite System Observations. *Sensors* **2013**, *13*, 4514–4526.
3. Nadarajah, N.; Teunissen, P.J.G.; Raziq, N. BeiDou Inter-Satellite-Type Bias Evaluation and Calibration for Mixed Receiver Attitude Determination. *Sensors* **2013**, *13*, 9435–9463.
4. China Satellite Navigation Office, BeiDou Navigation Satellite System Signal in Space Interface Control Document Open Service Signal (Version 2.0). Available online: http://en.beidou.gov.cn/index.html (accessed on 18 June 2014).
5. Global Positioning Systems Directorate, IS-GPS-200H Navstar GPS space segment/Navigation User Interfaces. Available online: http://www.gps.gov/technical/icwg/ (accessed on 4 June 2014).
6. Zou, D.; Deng, Z.; Huang, J.; Liu, H.; Yang, L. A study of Neuman Hoffman codes for GNSS application. In Proceedings of Wireless Communications, Networking and Mobile Computing, Beijing, China, 24–26 September 2009.

7. Mongrédien, C.; Lachapelle, G.; Cannon, M.E. Testing GPS L5 Acquisition and Tracking algorithms using a hardware simulator. In Proceedings of ION GNSS, Fort Worth, TX, USA, 26–29 September 2006; pp. 2901–2913.
8. Yan, K.; Zhang, H.; Zhang, T.; Xu, L.; Niu, X. Analysis and Verification to the Effects of NH Code for Beidou Signal Acquisition and Tracking. In Proceedings of the 26th International Technical Meeting of the Satellite Division of the Institute of Navigation (ION GNSS+ 2013), Nashville, TN, USA, 16–20 September 2013; pp. 107–113.
9. Bhuiyan, M.Z.H.; Söderholm, S.; Thombre, S.; Ruotsalainen, L.; Kuusniemi, H. Implementation of a Software-Defined BeiDou Receiver. In *Chinese Satellite Navigation Conference Proceedings: Volume I, Lecture Notes in Electrical Engineering*; Springer: Berlin, Germany, 2014; Volume 303, pp. 751–762.
10. Hegarty, C.; Tran, M.; Van Dierendonck, A.J. Acquisition Algorithms for the GPS L5 Signal. In Proceedings of the 16th International Technical Meeting of the Satellite Division of the Institute of Navigation, Portland, OR, USA, 9–12 September 2003; pp. 165–177.
11. Zheng, B.; Lachapelle, G. Acquisition Schemes for a GPS L5 Software Receiver. In Proceedings of ION GNSS, Long Beach, CA, USA, 21–24 September 2004; pp. 1035–1040.
12. Yang, C.; Hegarty, C.; Tran, M. Acquisition of the GPS L5 Signal using Coherent Combining of L5 and Q5. In Proceedings of the 17th International Technical Meeting of the Satellite Division of the Institute of Navigation, Long Beach, CA, USA, 21–24 September 2004; pp. 2184–2195.
13. Borre, K.; Akos, D.M.; Bertelsen, N.; Rinder, P.; Jensen, S.H. *A Software-defined GPS and Galileo Receiver: A Single-Frequency Approach*, 1st ed.; Birkhäuser Verlag GmbH: Boston, MA, USA, 2007.
14. Principe, F.; Bacci, G.; Giannetti, F; Luise, M. Software-Defined Radio Technologies for GNSS Receivers: A Tutorial Approach to a Simple Design and Implementation. *Int. J. Navig. Obs.* **2011**, doi:10.1155/2011/979815.
15. Tsui, J. *Fundamentals of Global Positioning System Receivers: A Software Approach*; John-Wiley & Sons: New York, NY, USA, 2000.
16. Ma, C.; Lachapelle, G.; Cannon, M.E. Implementation of a software GPS receiver. In Proceedings of ION GNSS, Long Beach, CA, USA, 21–24 2004; pp. 21–24.
17. Normark, P.L.; Christian, S. Hybrid GPS/Galileo Real Time Software Receiver. In Proceedings of the 18th International Technical Meeting of the Satellite Division of The Institute of Navigation, Long Beach, CA, USA, 13–16 September 2005; pp. 1906–1913.
18. Juanga, J.C.; Tsaia, C.T.; Chena, Y.H. Development of a PC-Based Software Receiver for the Reception of Beidou Navigation Satellite Signals. *J. Navig.* **2013**, *66*, 701–718.
19. Bhuiyan, M.Z.H.; Söderholm, S.; Thombre, S.; Ruotsalainen, L.; Jaakkola, M.K.; Kuusniemi, H. Performance Evaluation of Carrier-to-Noise Density Ratio Estimation Techniques for BeiDou B1 Signal. In Proceedings of Ubiquitous Positioning, Indoor Navigation and Location-Based Services Conference, TX, USA, 20–21 November 2014.
20. Nottingham Scientific Limited. Available online: http://www.nsl.eu.com/datasheets/stereo.pdf (accessed on 10 November 2013).
21. Kaplan, E.D. *Understanding GPS—Principles and Applications*, 2nd ed.; Artech House Publishers: Boston, MA, USA, 2006.

22. Van Dierendonck, A.J.; Fenton, P.; Ford, T. Theory and Performance of Narrow Correlator Spacing in a GPS Receiver. *Navig. J. Inst. Navig.* **1992**, *39*, 265–283.
23. Parkinson, B.W.; Spilker, J.J. *Global Positioning System: Theory and Applications*; American Institute of Aeronautics: Washington, BC, USA, 1996; pp. 390–394.
24. Ziedan, N.I.; Garrison, J. Bit Synchronization and Doppler Frequency Removal at very Low Carrier to Noise Ratio Using a Combination of the Viterbi Algorithm with an Extended Kalman Filter. In Proceedings of ION GPS/GNSS, Portland, OR, USA, 9–12 September, 2003.

PUBLICATION

IV

Investigating the Indian regional navigation satellite system using a software multi-GNSS receiver in Europe

S. Thombre, S. Söderholm, M. Z. H. Bhuiyan and M. Kirkko-Jaakkola

*Proceedings of 2015 European Navigation Conference*2015, 22082–22098

Investigating the Indian Regional Navigation Satellite System using a Software Multi-GNSS Receiver in Europe

Conference Paper · April 2015

CITATION
1

READS
1,222

6 authors, including:

Sarang Thombre
Finnish Geospatial Research Institute
38 PUBLICATIONS **273** CITATIONS
SEE PROFILE

Stefan Söderholm
Finnish Geodetic Institute
37 PUBLICATIONS **305** CITATIONS
SEE PROFILE

Mohammad Zahidul H. Bhuiyan
Finnish Geospatial Research Institute
55 PUBLICATIONS **586** CITATIONS
SEE PROFILE

Laura Ruotsalainen
University of Helsinki
66 PUBLICATIONS **530** CITATIONS
SEE PROFILE

INVESTIGATING THE INDIAN REGIONAL NAVIGATION SATELLITE SYSTEM USING A SOFTWARE MULTI-GNSS RECEIVER IN EUROPE

Sarang Thombre[(1)], Stefan Söderholm[(1)], Mohammad Zahidul Hasan Bhuiyan[(2)], Martti Kirkko-Jaakkola[(1)], Laura Ruotsalainen[(1)], Heidi Kuusniemi[(1)]

Finnish Geospatial Research Institute FGI,
Geodeetinrinne 2, FI-02430 Masala, Finland.
[(1)]firstname.lastname@nls.fi
[(2)]zahidul.bhuiyan@nls.fi

ABSTRACT

The Indian Regional Navigation Satellite System (IRNSS) is currently under development with approximately half of the total planned satellites deployed in space. The Department of Navigation and Positioning of the Finnish Geospatial Research Institute (FGI) has been an early adopter of this system in Europe through the development of its software multi-frequency multi-GNSS receiver, called FGI-GSRx. This paper presents the results of the first comprehensive study in Finland, if not in Europe, about the IRNSS system using the FGI-GSRx receiver. Following a brief description of the IRNSS system, the paper presents the receiver architecture, including the acquisition and tracking engines, position computation and its results. IRNSS satellites can be beneficial in augmenting other satellite systems over North and East Europe. These benefits are expected to grow as more IRNSS satellites are deployed in space in the future. Therefore, the impact of these results is interesting to the positioning, navigation and timing (PNT) community even outside the intended service area of IRNSS. It has been observed that there is very sparse literature available in the research domain that describes in detail the implementation of a software receiver for IRNSS signals. This paper bridges this gap by presenting a unified and consolidated framework for the design, implementation, and validation of the entire receiver chain for the IRNSS L5 signal.

INTRODUCTION

The FGI-GSRx receiver has been used for the analysis and validation of novel algorithms for optimized navigation performance [1], [2]. The basic version of FGI-GSRx is based on an open-source software receiver platform [3], and is now expanded and compatible with Galileo, GPS, GLONASS, BeiDou (B1 & B2 frequencies) and all the currently available IRNSS satellites (GEO/IGSO) for a truly multi-GNSS, multi-frequency architecture. It is also capable of offering an IRNSS-only navigation fix when at least 4 satellites are in view [4]. The goal of this receiver development is to provide European industry and society with new knowledge about the Indian navigation system and its benefits, as well as introduce novel approaches for multi-GNSS positioning. This study has enabled IRNSS L5 (center frequency at 1176.45 MHz) capability to be implemented in the FGI-GSRx receiver, demonstrating that IRNSS signals might be very useful in augmenting GPS and Galileo service in northern and eastern Europe. There has been previous research work on IRNSS [5], [6]. However, a comprehensive description of the receiver implementation is still missing, a gap which this paper hopes to fill.

This paper begins with an introduction to IRNSS followed by a description of the overall architecture of the FGI-GSRx software receiver including optimum parameters of the antenna and radio front-end used to capture and digitize the L5 frequency signals. This is followed by a brief description of the acquisition engine. The following Section of the paper describes the implementation of an innovative, flexible and modular state-based tracking architecture for the IRNSS signals using a Frequency Locked Loop (FLL), Phase Locked Loop (PLL), and Delay Locked Loop (DLL). A tracking table holds a list of functions to perform under each tracking state. The carrier tracking can progressively and regressively transition between different states, for example initial FLL-only 'Pull-in' state followed by a more stable FLL-assisted-PLL 'Tracking' state or vice-versa, as it satisfies the transition criteria. More states, for example a high sensitivity state, can be added simply by adding rows with modified parameters to the tracking table. Also described is the implementation of a combined bit-edge detection and lock detection stage. Optimum loop filter implementation parameters for the IRNSS L5 signal tracking are presented. The final part of the paper describes briefly the IRNSS navigation data structure and the corresponding positioning engine of the software receiver. The Results section describes the IRNSS satellite acquisition and tracking results. The positioning results in a multi-GNSS scenario are already described in [4] and hence not reprinted here.

FUNDAMENTALS OF IRNSS

The Indian Regional Navigation Satellite System is an independent system operated by the Indian Space Research Organization [7]. The signal in space interface control document was released in September 2014 [15], and contains descriptive figures of its system architecture, satellite constellation, frequency spectrum, signal structure, modulation scheme and contents of the navigation payload. IRNSS consists of a Space Segment, a Ground Segment and a User Segment. The Space Segment will eventually consist of seven satellites, 4 in geostationary (GEO) and 3 in inclined geosynchronous (IGSO) orbits. The three GEO satellites are positioned over 32.5º E, 83º E, and 131.5º E respectively, while the four IGSO satellites over longitudes of 55º E and 111.75º E respectively. Three of the total seven satellites are already in space with the first being launched on 1 July, 2013 [8] and the fourth planned to be launched in Spring 2015 (expected launch date of 09 March was deferred due to an anomaly in one of the onboard telemetry transmitters [9]).

The Ground Segment consists of the IRNSS Navigation Centre (INC) which monitors and controls the overall system, along with IRNSS Network Timing Centre for accurate time reference. The satellite positions and orbits in space are monitored using the CDMA Ranging and Laser Ranging stations, while their navigation data is updated using the Telemetry Tracking & Control (TT&C) and Navigation Uplink Centres which are a part of the Spacecraft Control Facility (SCF). The performance and integrity of the satellites is monitored by the IRNSS Range and Integrity Monitoring Stations (IRIMS). Intermodule communication is facilitated through the Data Communication Network.

IRNSS offers two services to users: Open Service also called Standard Positioning Service (SPS) which is free of cost and utilizes unencrypted signals, and Restricted Service which utilizes signal encryption and is restricted to authorized users. Signals are offered on two frequency bands: L5 (centered at 1176.45 MHz with bandwidth of 24 MHz) and S (centered at 2492.028 MHz with bandwidth of 16.5 MHz). Henceforth, we consider only L5 SPS for simplicity. IRNSS signals are right hand circularly polarized (RHCP), and the received power on ground (L5 SPS) using an ideally matched RHCP 0 dBi receiver antenna is between -154.0 dBm and -159.0 dBm. The SPS signal uses Code Division Multiple Access (CDMA) modulation with Binary Phase Shift Keying (BPSK(1)). The navigation data rate is 50 Hz and pseudorandom noise (PRN) code rate is 1.023 MHz with duration 1 ms. The navigation data is modulo-2 added with the pseudorandom noise (PRN) code sequence followed by modulation with the radio frequency (RF) carrier at the L5 frequency.

Fig. 1 shows the sky-plot of the visible IRNSS and GPS satellites overhead the FGI campus on 31 March, 2015 at 07:30 Finland Time (courtesy of the Orbitron tool [10]). As can be observed, all three currently available IRNSS satellites (IRNSS – 1A, 1B, and 1C) are visible in the South-East corner of the sky (IRNSS-1D was launched on March 28, 2015 [17] and hence not included yet in the receiver results).

FGI-GSRX RECEIVER ASSEMBLY

The block diagram of the FGI-GSRx receiver assembly is shown in [4]. It consists of the radio front-end which receives the RF signals from the sky and converts them into digital samples after analog pre-processing in real-time. These samples at a lower intermediate frequency (IF) are stored in memory for later post-processing. The post-processing module consists of the FGI-GSRx software receiver where the samples are processed in the Acquisition, Tracking, and Positioning engines. The user is able to modify the operational parameters and settings of the software receiver through an external text file, represented as “Parameters and Settings.”

RADIO FRONT-END

The radio front-end consists of an Antcom active L1/L2/L5 antenna [11] capable of receiving GLONASS, GPS, and satellite-based augmentation signals from a roof-top location in combination with a highly configurable dual-frequency GNSS RF front-end, called Stereo V2 [12] to capture and store GNSS signals in digitized format for post-processing by the FGI-GSRx software receiver platform. Table 1 describes the technical specifications of the collected RF (sampled) data for the GPS L1 and IRNSS L5 signals.

SATELLITE ACQUISITION

The IRNSS SPS PRN code is generated by the modulo-2 sum of two time-synchronized 10-bit maximum length feedback shift registers, called G1 and G2, with different generator polynomials [7]. The generator polynomial for register G1 is $X^{10} + X^3 + 1$, and for G2 is $X^{10} + X^9 + X^8 + X^6 + X^3 + X^2 + 1$. Each satellite has a unique initial sequence

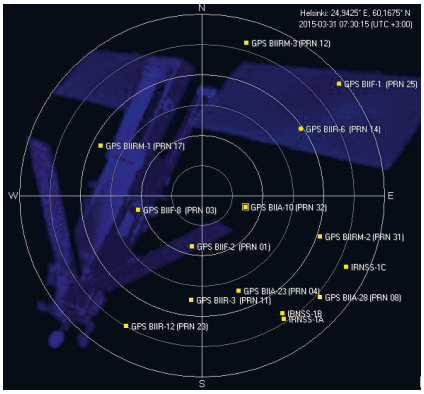

Fig. 1 Sky plot of IRNSS and GPS satellites over Helsinki Finland on March 31, 2015 at 07:30 am.

Table 1. Specifications of the sampled RF data

	L1 band	L5 band
Intermediate Frequency	6.39 MHz	353 Hz
RF Front-end Bandwidth	4.2 MHz	10.9 MHz
Sampling Frequency	26 MHz	26 MHz
Number of Quantization Bits	3	3 + 3
Data Type	Real	Complex (I/Q)

for register G2, which provides its particular chip delay. The acquisition engine performs parallel code phase search [3], [13] using fast Fourier transform (FFT)-based acquisition to locate visible satellites and record coarse estimates of their respective Doppler frequency and code phase values to initialize the individual tracking loops. The search window, number of coherent and non-coherent integration rounds and signal thresholds are all configurable parameters. For the IRNSS signal, one code epoch is 1 ms long and the data bit is 20 epoch's long, or approximately 20 ms, which determines the limit for the amount of coherent integrations.

The daily time window during which all three available IRNSS satellites are visible at an acceptable elevation in Finland is quite short (approx. 1 hr) and usually occurs in the late afternoon or early morning. This situation is expected to improve with the launch of the GEO satellite planned to be placed over longitude 32.5º E. Additionally, it would be interesting to investigate the visibility (and test acquisition) in Finland of the satellites planned to be placed over the more Eastern longitudes.

SATELLITE TRACKING

Components of the Tracking Loops

One scalar tracking loop — a frequency locked loop (FLL)-assisted phase locked loop (FLL-assisted-PLL) for carrier signal tracking, and delay locked loop (DLL) for PRN code tracking — is assigned to each visible satellite identified from the acquisition engine. The overall block schematic of the scalar tracking loop is shown in Fig. 2. Upon completion of the acquisition stage, the results are handed over to initialize the individual tracking loops, and additional variables are defined and initialized. Next, the raw IF data file is reopened for reading the pre-defined block-size of sampled IRNSS L5 data. This constitutes the raw signal into the carrier demodulation mixer. The other input to this mixer is from the local carrier frequency generator. The raw input signal and the local carrier signal can be mathematically represented as in (1) and (2) respectively.

$$R(k) = \sqrt{2A}\, C(k)D(k)Cos(2\pi f_{IF} + \emptyset_r) + n_r(k) \quad (1)$$

$$L(k) = \exp(i * (2\pi f_{C_{Local}} t_k + \delta_{C_\varphi})) \quad (2)$$

where the k denotes a sample index, A is the amplitude component, C is the pseudorandom noise (PRN) code, D is the navigation data, f_{IF} is the true IF of the raw signal, $f_{C_{Local}}$ is the local generated carrier frequency, $\emptyset_r$ represents the initial phase of the raw signal, n_r represents the noise component in the two signals, t_k is the sampled time-base and δ_{C_φ} represents the remainder/residual carrier phase from the previous tracking epoch, if any. Receiver and satellite motion, and non-idealities of the receiver clock result in residual frequency and phase components. These terms are estimated by the frequency and phase discriminators, while the noise in these estimations is suppressed by the loop filters.

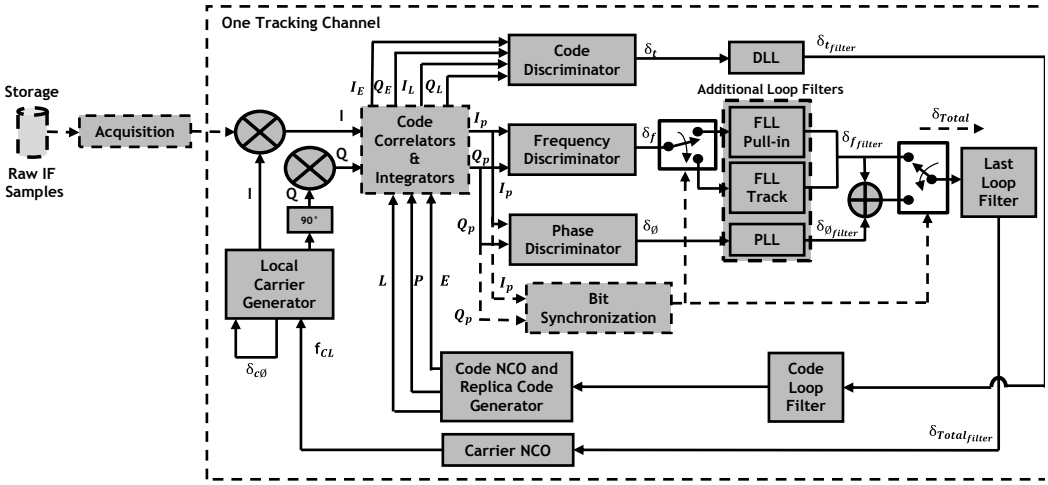

Fig. 2 Block schematic of the scalar tracking loop for one channel of the FGI-GSRx receiver

A complex mixing process results in real (I) and imaginary (Q) components, which are provided to the code correlation and integration blocks (code demodulation). In normal tracking mode, FGI-GSRx receiver's code correlation tracking mechanism uses a 1 ms integration interval. The actual amount of data read from the sampled data file is adjusted for each epoch based on the true code frequency so that the aim is always to process exactly one code epoch. The goal is to keep the remaining code phase error from the DLL discriminator as close to zero as possible. The complex signal at this point in the signal processing chain can be represented by (3) and (4).

$$I(k) = \sqrt{2A}\, D(k) Cos\big(2\pi f_D + \delta_\varphi\big) + n_I(k) \tag{3}$$

$$Q(k) = \sqrt{2A}\, D(k) Sin\big(2\pi f_D + \delta_\varphi\big) + n_Q(k) \tag{4}$$

where f_D is the Doppler frequency, δ_φ is the carrier phase error, and n_I and n_Q are the noise terms in the two signal branches. The residual frequency, phase and delay from the input signal after the carrier and code correlators are estimated in the frequency, phase and delay discriminators respectively. The implementation of these discriminators is based on 2-quadrant atan-discriminator [16] for frequency, traditional Costas loop two-quadrant arctangent discriminator for phase and Non-coherent Early-Minus-Late Normalized discriminator for code delay [14].

Typically, a Numerically Controlled Oscillator (NCO) is employed as an integrator, and hence a first-order low pass filter and local phase generator. However, an NCO alone may not be enough to sustain the high inconsistency in the error estimates. Therefore, additional loop filters are employed. The combination of the NCO, last loop filter and the additional loop filters offers a third-order filtering capability in the overall phase tracking loop, and a second-order filtering in the overall frequency tracking loop, effectively resulting in a second-order FLL assisted third-order PLL. The optimum values for loop gain (G_L), damping ratio (ξ) and noise bandwidth (B_n) for the filter implementations are given in Table 2.

Tracking States

FLL-only with a wide loop filter bandwidth is more efficient in the 'pull-in' stage of carrier tracking to enable faster convergence to the actual Doppler frequency. In this condition, the tracking transitions into a more stable 'tracking' state of operation, where the PLL is more dominant and it continues to track the precise phase of the carrier signal. However, the FLL is still operational, albeit with a smaller loop filter bandwidth, which enables very low noise tracking performance. If the frequency errors increase beyond a pre-defined threshold, the loop re-enters the 'pull-in' state, and the FLL with the wider bandwidth loop filter takes over, attempting to bring the loop back into the 'tracking' state of operation. Thus, this FLL assisted PLL mechanism ensures a very robust carrier tracking performance, especially under conditions of moderate dynamic stress.

Table 2. Optimum parameter values for IRNSS tracking loop

Filter Position	Damping Ratio (ζ)	Loop Gain (G_L)	Loop Noise BW (B_n), Hz
FLL in Pull-in Mode	0.7	1.5	200
FLL Track Mode	0.7	1.5	5
PLL	0.7	0.1	5
Last Loop Filter	0.7	0.1	15
DLL	0.7	-	1

The decision to transition from the pull-in to tracking state is made upon successful bit synchronization, which is possible only when the receiver is tracking the carrier frequency with sufficient accuracy. The bit edges start to be detected successfully when the pull-in stage has the frequency and phase errors small enough for the navigation data bits to be successfully decoded. If at any instant the frequency and phase errors reach unsustainable levels, the probability of data decoding starts to degrade, which in turn causes a loss in bit synchronization. The tracking reenters the more robust 'pull-in' mode, and the process repeats.

Within one state, the tracking loops use parameters that can be very different from other states. Also, different channels of the receiver can be in different tracking states at any instant. This allows the tracking loops to be independent and modular, making it possible to include more states quite easily. For example, the channel may transition to a high-sensitivity state, which can be activated when the Carrier to Noise Ratio (C/N_0) degrades below a pre-defined threshold. In this state the tracking interval may be increased beyond the traditional 1 ms to improve weak signal tracking. Another state can be defined for high-dynamics scenarios, where traditional FLL- and PLL-based tracking schemes may prove to be over-damped. Each channel may transition freely from one tracking state to another depending upon the prevalent signal and environmental conditions.

Table-based Tracking Architecture

In order to accommodate the diversity of tracking states and also to ensure that new states can be introduced without significant modification to existing software code, a table-based tracking architecture is adopted which improves its modularity and flexibility. An example of the tracking table is shown in Table 3. A separate function (column 1) is used to define the operation of each processing unit within the tracking engine, for example correlator, integrator, discriminator, loop filter etc. Each function is then assigned to a functionality group (column 2). Therefore, one functionality group may contain more than one function which perform a similar operation albeit using different input parameters depending upon the tracking state (column 3) the channel is currently in.

The final column of the tracking table denotes the tracking epoch (in ms), which also denotes the coherent pre-detection integration time for the tracking engine. Under normal (moderate to strong signal conditions) the tracking loop uses 1ms of PIT. A high-sensitivity (HS) state can be easily included by adding additional rows to the tracking table for every function with 20 in the last column. This will allow the functions to be implemented every 20 ms instead of every 1 ms. With this approach the tracking engine can easily switch between for example, different kinds of discriminators or loop filters and manage the update rate of those functions. Furthermore, utilizing this kind of approach the tracking can easily accommodate for loop pull in, high sensitivity or high-dynamic states without the risk of unmanageable code.

Multi correlator code tracking

In the traditional code tracking mechanism only three correlators are used for tracking producing the Early, Prompt, and Late correlator results (called 'fingers'). The time spacing between the adjacent correlators is configurable in the FGI-GSRx receiver and the default value is 0.25 chips for GPS and IRNSS. The receiver also has a feature called multi-Correlator tracking where the user can specify the number of fingers used, time spacing between the fingers, and correlator update rate. This feature is intended for analyzing shape of the correlator peak in more detail and it does not interfere with the actual satellite tracking.

NAVIGATION DATA DECODING AND POSITION COMPUTATION

The IRNSS navigation data structure and contents are described in the ICD [7]. Out of the four Sub Frames comprising one Master Frame, Sub Frame 1 and 2 (containing primary navigation parameters) are sufficient to decode the most

Table 3. Example tracking table

Functions	Functionality Group	Tracking State	Tracking Epoch (ms)
⋮	⋮	⋮	⋮
Frequency_Accumulator	FREQUENCY_ACCUMULATOR	Tracking	1
Frequency_Accumulator_HS	FREQUENCY_ACCUMULATOR	High Sensitivity	20
Frequency_Discriminator	FREQUENCY_DISCRIMINATOR	Tracking	1
Frequency_Discriminator_HS	FREQUENCY_DISCRIMINATOR	High Sensitivity	20
FLL_LoopFilter_PullIn	FLL_LOOP_FILTER	Pull-in	1
FLL_LoopFilter_Tracking	FLL_LOOP_FILTER	Tracking	1
FLL_LoopFilter_HS	FLL_LOOP_FILTER	High Sensitivity	20
FLL_Additional_LoopFilter	FLL_LOOP_FILTER	High Dynamics	1
⋮	⋮	⋮	⋮

necessary parameters for obtaining a positioning solution. Sub Frame 3 and 4 contain secondary navigation parameters such as, ionosphere correction coefficients, earth observation parameters, differential corrections, and text messages. Fig. 3 shows a flow diagram for the process of decoding the IRNSS navigation payload. The number of bits processed at every stage is shown alongside. After decoding the navigation payload the resulting parameters enter the main loop for navigation computation, which is performed using the traditional Weighted Least Squares (WLS) technique. The product of this final stage is structured data sets containing observations, satellite information and a navigation solution for all measurement epochs. The primary inputs to this stage are the results from track engine, list of Channels with ephemeris data available, receiver configuration parameters, and ephemeris data from IRNSS.

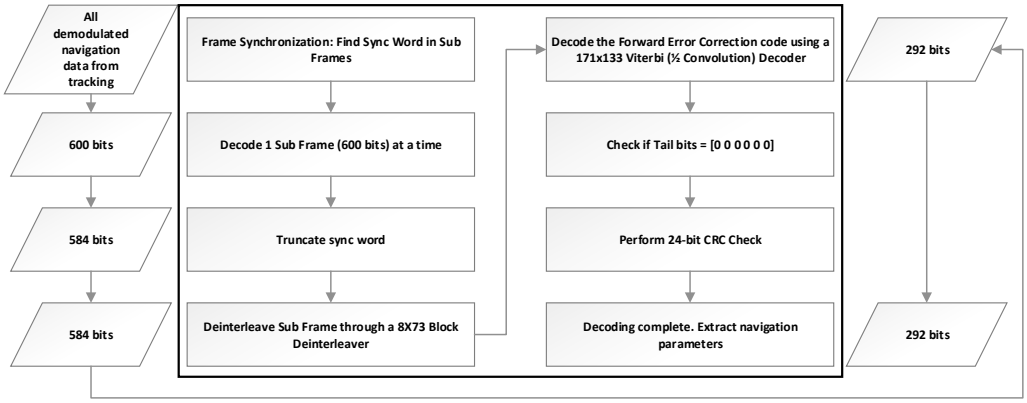

Fig. 3 Flow diagram for decoding the IRNSS navigation payload

RESULTS

The preliminary results of IRNSS-based positioning in a multi-GNSS scenario with GPS satellites have been demonstrated in [4], and hence not reprinted in this paper. Here we show the results of IRNSS satellite acquisition and its tracking performance. Fig. 4a and 4b show the acquisition peak for IRNSS-1B (PRN 2) and the acquisition results for all IRNSS satellites, while Fig. 5 shows the tracking performance of IRNSS-1A (PRN 1).

From these results, it can be observed that the FGI-GSRx receiver successfully acquires and tracks the IRNSS satellites. Additionally, at the moment of data-capture IRNSS-1B was at a higher elevation, hence its acquisition result is the strongest. However, the acquisition result is low compared to that of visible GPS satellites for example, which may climb to higher elevations at Helsinki's northern latitudes.

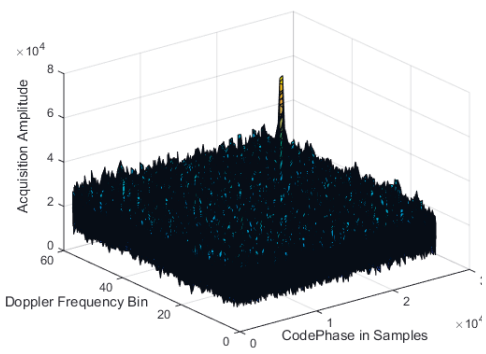

Fig. 4a Acquisition peak for IRNSS 1B (PRN 2)

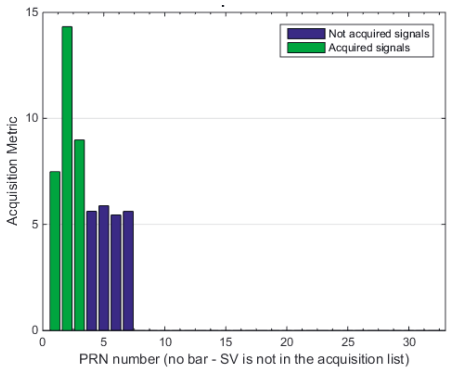

Fig. 4b Acquisition result for all IRNSS satellites per the skyplot of Fig. 1

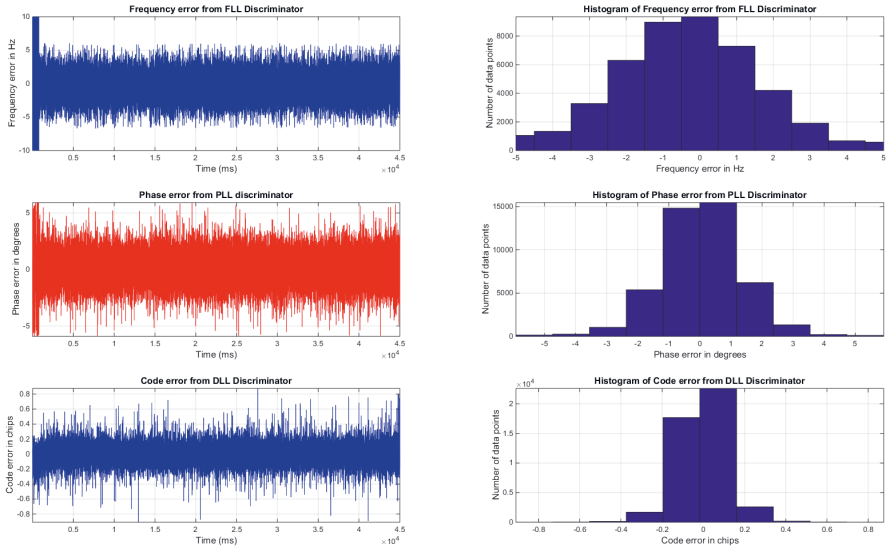

Fig. 5 IRNSS 1A (PRN 1) satellite tracking performance

The tracking results show the performance of the carrier and code tracking loops with regards to their residual errors. The results are distinguishable between the 'pull-in' and 'tracking' phases, clearly showing the instant of transition between them. On average, the frequency residual in the FLL is within ±5 Hz, phase residual is within ±2 degrees and code residual is within ±0.2 chips. The plots on the right show the histogram distribution of the residual errors.

CONCLUSION

This paper demonstrates the FGI-GSRx receiver operation in acquiring, tracking and using available IRNSS satellites in positioning in South Finland. Salient features of the IRNSS system have been studied and its benefits in positioning in a region outside its core coverage area have been demonstrated. Results from IRNSS satellite acquisition and tracking have been demonstrated. These results also show that IRNSS satellites may also be used to supplement Galileo in North and East Europe until sufficient Galileo satellites are available to provide a Galileo-only positioning solution. These benefits are expected to improve in the future as the IRNSS constellation itself achieves full deployment.

ACKNOWLEDGEMENT

This research has been conducted within the Detection Analysis, and Risk Management of Satellite Navigation Jamming (DETERJAM) project funded by the Scientific Advisory Board for Defense of the Finnish Ministry of Defense and the Finnish Geodetic Institute, Finland, and the FINCOMPASS project, funded by the Finnish Technology Agency TEKES with the Finnish Geodetic Institute, Microsoft Corporation, Roger-GPS Ltd., and Vaisala Ltd.

REFERENCES

[1] M. Z. H. Bhuiyan, S. Söderholm, S. Thombre, L. Ruotsalainen, H. Kuusniemi, "Implementation of a Software-defined BeiDou Receiver", Proceedings of the Chinese Satellite Navigation Conference, Nanjing, China, May 2014.

[2] M. Z. H. Bhuiyan, H. Kuusniemi, S. Söderholm, S. Thombre, L. Ruotsalainen, "Tracking the BeiDou Satellites with a Software-defined Receiver", Geospatial World Magazine, April 2014.

[3] K. Borre, D. Akos, N. Bertelsen, P. Rinder, S. Jensen, "A software-defined GPS and Galileo receiver: a single-frequency approach", 1st ed. Applied And Numerical Harmonic Analysis, Birkhäuser Verlag GmbH, Boston, USA, 2007.

[4] S. Thombre, M. Z. H. Bhuiyan, S. Söderholm, M. Kirkko-Jaakkola, L. Ruotsalainen, H. Kuusniemi, "Tracking IRNSS Satellites For Multi-GNSS Positioning in Finland", InsideGNSS, November/December, 2014.

[5] V. G. Rao, "Proposed LOS Fast TTFF Signal Design for IRNSS", Ph.D. Thesis, University of Calgary, January 2013, available at: http://www.ucalgary.ca/engo_webdocs/GL/01.20370_VyasRao.pdf, last accessed: 18.3.2015

[6] S. Thoelert, O. Montenbruck, M. Meurer, "IRNSS-1A: signal and clock characterization of the Indian regional navigation system", GPS Solutions, 01/2014; DOI: 10.1007/s10291-013-0351-7

[7] Indian Regional Navigation Satellite System Signal In Space ICD for Standard Positioning Service (Version 1.0, ISRO-IRNSS-ICD-SPS-1.0), Indian Space Research Organization, June 2014, available at: http://irnss.isro.gov.in/, last access: 18.3.2015.

[8] W. Graham, "Indian PSLV lofts IRNSS-1C satellite", October 15, 2014, available at: http://www.nasaspaceflight.com/2014/10/indian-pslv-irnss-1c-satellite/, last accessed: 18.3.2015

[9] Press Trust of India, "India's fourth Navigation Satellite IRNSS-1D satellite launch deferred due to anomaly", The Economic Times, March, 2015, available at: http://economictimes.indiatimes.com/news/science/indias-fourth-navigation-satellite-irnss-1d-satellite-launch-deferred-due-to-anomaly/articleshow/46454438.cms, last accessed 18.3.2015

[10] S. Stoff, "Orbitron - Satellite Tracking System", available at: http://www.stoff.pl/, last accessed: 18.3.2015

[11] Antcom's G5 Antenna, Active L1/L2 Glonass + L1/L2 GPS + OmniStar Antenna, P/N: G5Ant-3AT1, available at: http://гнссплюс.рф/uploads/catalog/misc/100/G5_Antennas_L1L2GLonass_Plus_L1L2GPS_Omnistar.pdf

[12] Nottingham Scientific Limited (2013) Delivering Reliable and Robust GNSS, available online (retrieved on 10 November, 2013): http://www.nsl.eu.com/datasheets/stereo.pdf

[13] C. Ma, G. Lachapelle, and M.E. Cannon, "Implementation of a Software GPS Receiver", Proceedings of ION GNSS 2004 (Session A3), Long Beach, CA, September 21-24, 2004, available at: http://plan.geomatics.ucalgary.ca/papers/04gnss_ion_cmaetal.pdf, last accessed: 18.3.2015

[14] E. D. Kaplan, C. J. Hegarty (Eds.), "Understanding GPS: Principles and Applications", Artech House, 2nd Edition, 2006, ISBN 1580538959, 9781580538954

[15] "IRNSS Signal in Space ICD Released", GPSWorld, September 25, 2014, available at: http://gpsworld.com/irnss-signal-in-space-icd-released/, last accessed: 19.3.2015

[16] K. Yan, H. Zhang, T. Zhang, L. Xu, X. Niu, "Analysis and Verification to the Effects of NH Code for Beidou Signal Acquisition and Tracking," Proceedings of the 26th International Technical Meeting of The Satellite Division of the Institute of Navigation (ION GNSS+ 2013), Nashville, TN, September 2013, pp. 107-113.

[17] First Post, "India successfully launches its fourth navigational satellite IRNSS-1D", available at: http://www.firstpost.com/india/india-successfully-launches-fourth-navigational-satellite-irnss-1d-2178235.html, last accessed: 30 March, 2015.

PUBLICATION

V

Optimal Signal processing of the Galileo PRS Signal In a Snapshot Receiver

S. Söderholm, J. Nurmi, A. Berg and H. Kuusniemi

IEEE Sensors Journal (2023). Submitted

PUBLICATION VI

Low-cost precise positioning using a national GNSS network

M. Kirkko-Jaakkola, S. Söderholm, S. Honkala, H. Koivula and S. Nyberg

Proceedings of the 28th International Technical Meeting of the Satellite Division of The Institute of Navigation 2015, 2570–2577

Low-Cost Precise Positioning Using a National GNSS Network

Martti Kirkko-Jaakkola, Stefan Söderholm, Salomon Honkala, Hannu Koivula, Sonja Nyberg, and Heidi Kuusniemi
Finnish Geospatial Research Institute (FGI), National Land Survey of Finland

BIOGRAPHY

Martti Kirkko-Jaakkola is a Senior Research Scientist at the Finnish Geospatial Research Institute (FGI), National Land Survey of Finland. He received his M.Sc. (Tech.) and D.Sc. (Tech.) degrees from Tampere University of Technology, Finland, in 2008 and 2013, respectively. His research interests include precise GNSS positioning and inertial navigation using low-cost equipment.

Stefan Söderholm is a Senior Research Scientist and a research group leader at FGI. He received his M.Sc. degree from Åbo Akademi University, Finland, and the Licentiate degree from University of Turku, Finland. Before joining FGI he was the head of R&D at Fastrax Ltd. and a project manager at U-Blox AG. Currently he is working on improving the performance of consumer grade GNSS receivers.

Salomon Honkala is an Assistant Researcher at FGI. He holds a B.Sc. (Tech.) in electrical engineering from Aalto University, Espoo, Finland, and is finishing an M.Sc. (Tech.) degree at Aalto University. His current research interests include software GNSS receivers and GNSS signal processing.

Hannu Koivula is a Senior Research Scientist and the leader of the Reference systems research group at FGI. He received his M.Sc. (Tech.) and Lic.Sc. (Tech.) degrees from Helsinki University of Technology, Finland, in 1994 and 2007, respectively. His current research interests include the usability of GNSS in deforming coordinate frames and the metrology (traceability) of GNSS measurements.

Sonja Nyberg is a Research Scientist at FGI. She received her M.Sc. (Tech.) degree from Helsinki University of Technology, Finland, in 2009. She has been analysing the FinnRef data for the maintenance of national coordinate systems as well as operating the FinnRef positioning services.

Heidi Kuusniemi is a Professor and the Director of the Department of Navigation and Positioning at FGI. She is also an Adjunct Professor at Aalto University and Tampere University of Technology, Finland, and the President of the Nordic Institute of Navigation. Her research interests cover various aspects of GNSS and sensor fusion for seamless indoor/outdoor positioning.

ABSTRACT

This article presents an implementation of Real-Time Kinematics (RTK) using a low-cost GNSS receiver and a sparse countrywide reference station network. Furthermore, we assess the feasibility of implementing RTK on a smartphone by comparing the raw GNSS measurements of a commercial smartphone's internal GNSS receiver with a commercial off-the-shelf (COTS) low-cost GNSS receiver. The RTK implementation presented in this paper utilizes the Finnish national GNSS network FinnRef as the RTK base station, either in single-base or network RTK mode; although the main purpose of FinnRef is to maintain the national coordinate system, it is also capable of delivering DGNSS and network RTK data over the NTRIP protocol.

The test results show that despite the sparseness of FinnRef, a horizontal position accuracy of 0.5 meters or better was achieved for more than 90 % of the time with the COTS receiver both in a dynamic single-base test and in a network RTK experiment using GPS signals only. Obtaining such a positoning performance with low-cost and small-size devices is expected to be useful in various applications, particularly in the field of intelligent transportation systems. Furthermore, the results indicate that the smartphone's GNSS measurements are less precise than those of the COTS receiver and suffer from frequent outliers, making them less favorable for use in precise positioning applications as such.

INTRODUCTION

Current consumer-grade GNSS solutions routinely offer a positioning accuracy in the order of 5 meters, and satellite-based augmentation systems (SBAS) such as WAAS and EGNOS can be used to improve the accuracy to the order of 1 m. However, this is not adequate for all use cases; in particular, intelligent transportation systems (ITS) require a better positioning performance. For instance, a horizontal accuracy of 0.5 meters would be needed in order to reliably identify the lane on which a vehicle is driving. As another example, maintaining inventory of, e.g., machines and road signs would benefit from sub-meter accuracy. In addition to the sub-optimal accuracy, the visibility of geostationary augmentation satellites cannot be guaranteed at high latitudes.

Sub-meter or even sub-decimeter positioning accuracies can be attained with a relatively good reliability in real time if a dual-frequency GNSS receiver and a physical or virtual base station are available. However, such receivers and virtual base station services are currently too expensive to gain popularity in the mass market. In recent years it has been demonstrated that comparable accuracies can be attained without a base station using real-time precise correction data [1], but the typical drawback of this approach, usually referred to as precise point positioning (PPP), is a long convergence time. In contrast, differential methods utilizing raw base station observations, such as real-time kinematics (RTK), converge much faster.

This paper presents new results from the P3-Service (Public Precise Positioning) project [2] whose goal is to achieve a horizontal positioning accuracy of 0.5 meters using low-cost equipment. The project hinges on the utilization of the Finnish national GNSS network FinnRef which has been recently modernized [3]. With inter-station baselines in the order of 200 km, the FinnRef network is relatively sparse in comparison with commercial RTK networks. This makes the modeling of atmospheric errors challenging, especially from a single-frequency user's perspective. However, the purpose of FinnRef is to maintain the national coordinate system and to offer a half-meter positioning accuracy, not to compete with commercial RTK networks.

Implementing precise positioning on low-cost GNSS receivers has been an active research topic for years, and recent research projects related to P3-Service exists. Guo et al. [4] described a precise positioning service developed for China. The service is based on proprietary correction data formats and can achieve a lane-level accuracy for ITS applications. Lovas et al. [5] investigated the use of SBAS signals and RTK on ITS. Pesyna et al. [6] investigated the performance of the GNSS antenna of a smartphone by connecting the antenna to an external radio frontend and processing the signals using a software GNSS receiver, concluding that integer ambiguity resolution was possible even though the signals were received by the smartphone antenna.

The contribution of this paper is twofold. First, we show that the goal of achieving a horizontal RTK accuracy of 0.5 meters is feasible with a low-cost GNSS receiver using standard RTCM data formats [7] even with a sparse GNSS network and without ambiguity resolution at the receiver. Then, we present raw GNSS pseudorange and carrier phase measurement data from the actual internal GNSS receiver of a commercial smartphone (Nokia Lumia 1520) and assess its suitability for precise positioning applications. The paper is organized as follows. First, the basics of RTK positioning are reviewed. Then, the FinnRef network is presented in more detail, after which experimental results are presented.

REAL-TIME KINEMATIC POSITIONING

RTK is a method of *relative* positioning, i.e., it can only resolve the user's location with respect to a known reference point. The three-dimensional vector from the reference (base station) to the user, often referred to as the *rover*, is called the *baseline* and constitutes the unknowns to be estimated, along with the carrier phase ambiguities. The key to the high precision in RTK is to mitigate measurement errors by forming measurement differences where the errors are significantly decreased or canceled out totally. In the following sections, we first describe the double difference model which RTK hinges on, and then outline the RTK processing workflow. Finally, we briefly describe the concept of network RTK.

Differential Measurements

Let us model the carrier phase measurement ϕ to satellite i in units of meters as

$$\phi_i = \|\mathbf{p} - \mathbf{p}_i - \delta\mathbf{p}_i\| + c\,(\delta t - \delta t_i) - I_i + T_i + \lambda N_i + \varepsilon_i \quad (1)$$

where $\mathbf{p}$ and $\mathbf{p}_i$ are the positions of the user and satellite i, respectively, and $\delta\mathbf{p}_i$ denotes the error in the broadcast satellite position; δt and δt_i are the clock biases of the receiver and the satellite, respectively; c is the speed of light; I_i and T_i are the ionospheric and tropospheric delays for satellite i, respectively; λ denotes the signal wavelength and N_i is the carrier phase cycle ambiguity; and finally, ε_i contains all unmodeled error sources, such as measurement noise, multipath, antenna phase center variations, etc. Note that the cycle ambiguity N_i contains fractional phase biases caused both in the satellite and in the receiver and, therefore, is *not* an integer by nature.

We assume that the noise term ε_i can be modeled as an uncorrelated zero-mean random variable having a Gaussian distribution. The pseudorange measurement can be modeled in a way similar to (1), with the differences being the sign of the ionospheric delay I_i (the carrier wave is subject to a phase advance, i.e., a negative delay, in the dispersive ionosphere while the ranging code modulation is subject to a group delay of equal magnitude), the absence of the ambiguity term N_i, and the variance of the noise ε_i.

Now suppose that a base station exists close to the user and that the base station is equipped with a GNSS receiver that makes measurements perfectly synchronized with the user's receiver. Then, we can form the receiver–receiver carrier phase single difference $\Delta\phi_i$ as

$$\begin{aligned}\Delta\phi_i &= \phi_i^{\text{user}} - \phi_i^{\text{base}} \\ &= \|\mathbf{b}+\mathbf{r}-\mathbf{p}_i\| - \|\mathbf{r}-\mathbf{p}_i\| + \Delta\delta t + \lambda\Delta N_i + \Delta\varepsilon_i\end{aligned} \tag{2}$$

where the new terms $\mathbf{b}$ and $\mathbf{r}$ denote the baseline and the position of the base station, respectively. Satellite clock errors have been canceled out and atmospheric errors have been mitigated; the amount of residual atmospheric errors depends on the length of the baseline. Also note that the difference essentially cancels out satellite ephemeris errors. The receiver clock bias and the cycle ambiguity were redefined as the differences of those of the two receivers; note that single-differenced cycle ambiguity ΔN_i is still not an integer because of receiver-dependent fractional phase biases. Assuming that the measurement noise variance is equal for both receivers, the variance of the differenced noise term $\Delta\varepsilon_i$ is twice as large as the non-differenced measurement variance.

In order to cancel out the receiver clock biases and the rest of the fractional phase biases, compute the difference of the single differences to satellites i and j, widely known as the *double difference*:

$$\begin{aligned}\Delta\phi_{i-j} =& \Delta\phi_i - \Delta\phi_j \\ =& \|\mathbf{b}+\mathbf{r}-\mathbf{p}_i\| - \|\mathbf{r}-\mathbf{p}_i\| - \|\mathbf{b}+\mathbf{r}-\mathbf{p}_j\| + \|\mathbf{r}-\mathbf{p}_j\| \\ &+ \lambda\Delta N_{i-j} + \Delta\varepsilon_{i-j}.\end{aligned} \tag{3}$$

The only remaining unknowns are the baseline and the cycle ambiguity which is now free of fractional biases; note that this *integer ambiguity* is constant in time as long as both receivers maintain a phase lock on the signal. The variance of the noise term is again doubled, therefore, the standard deviation of the double difference noise is twice the standard deviation of the noise in the original, non-differenced observable (1).

RTK Workflow

The process of baseline estimation in RTK consists of three main steps:

1. Float solution: use double-differenced pseudoranges and carrier phases to estimate the baseline $\mathbf{b}$ and the ambiguities ΔN_{i-j} without any integer constraints
2. Ambiguity resolution
3. Fixed solution: if the ambiguity resolution succeeded, substitute the integer-valued estimates to the carrier phase double differences to obtain a precise baseline estimate.

Typically, the float solution is filtered using an Extended Kalman Filter (EKF). This way, a covariance estimate is obtained for the float ambiguity estimates. During the float estimation process, cycle slip detection and other quality control methods are applied. Moreover, if the rover receiver's measurements are not synchronized with the base station, the measurements are interpolated to a common time tag to satisfy the underlying assumption of (2).

The ambiguity resolution step involves solving an integer programming problem. Nowadays, the most popular ambiguity resolution method is LAMBDA [8] which implements integer least squares, i.e., finds the integer vector that is closest to the float ambiguity estimate in terms of the Euclidian norm weighted by the inverse of the covariance of the float ambiguities. Acceptance of rejectance of the ambiguities is based on some kind of a test. Often, the ratio of the residuals of the two closest integer vectors is compared to a fixed threshold; however, more sophisticated statistical tests exist, e.g., [9]. If accepted, the fixed baseline solution can be computed by conditioning the float estimate on the integers [8].

Network RTK

Since the double-differencing approach assumes that the user is located so close to the base station that residual atmospheric (and other) errors are negligible, the admissible baseline lengths are very short; for instance, it is often stated that single-frequency systems are limited to baselines of a few kilometers [10] because they cannot directly estimate the ionospheric errors; dual-frequency systems can successfully resolve the ambiguities with somewhat longer baselines.

Network RTK [11] is a technique to avoid the baseline length limitation by utilizing multiple base stations. Having such a network makes it possible to model the atmo-

spheric errors over the entire area of the network and use the model to compensate for the double-differencing residuals at the user's location. Currently, three network RTK approaches have been standardized: Flächenkorrekturparameter (FKP), Master–Auxiliary Concept (MAC), and non-physical reference station [7]. In FKP and MAC, the network provides the user with error models that are applied to the base station's measurements by the user; in contrast, in the non-physical reference station approach, the network sends the user artificial GNSS measurements that would be made by a base station in his or her vicinity.

In terms of computational load, FKP and MAC impose the burden of computing the corrections on the user's side whereas the creation of a non-physical reference station is entirely carried out on the network server side. In this article, we choose to use the non-physical reference station approach because from an RTK processing flow point of view, the algorithms are no different from those of single-base RTK.

THE FINNISH NATIONAL GNSS NETWORK FINNREF

The FinnRef GNSS network was modernized between 2012 and 2014 for the maintenance of the national coordinate system; the network is shown in Fig. 1. A typical station was set up on solid bedrock on the top of a three-meter-high steel grid mast with a narrowed top [3]. Any surrounding trees were felled to approximately ten degrees from the antenna level to ensure good visibility to the satellites. The station data have shown very low near-field effects, which confirms a successful station configuration.

The positioning services offered by FinnRef are based on the GNSMART software developed by Geo++ GmbH, Germany. GNSS data from 20 reference stations are transferred in real time to the processing center where the errors affecting the positioning at the reference stations are modeled. Then, real-time observation and correction data are available for users via the NTRIP protocol in various RTCM formats. Freely available DGNSS pseudorange corrections may be either received from a single station or tailored for the user's location through error modeling of the network, which enables a 0.5 m static positioning accuracy with adequate GIS receivers.

More precise network RTK corrections intended for carrier phase measurements, i.e., Pseudo-Reference Station (PRS), MAC, and FKP, are currently available for test users only. Our initial tests have shown that network RTK with better than 5 cm (95 %) accuracy and high fixing rate is possible even with this sparse reference network (see Fig. 1) when high-end dual-frequency GNSS receivers are used.

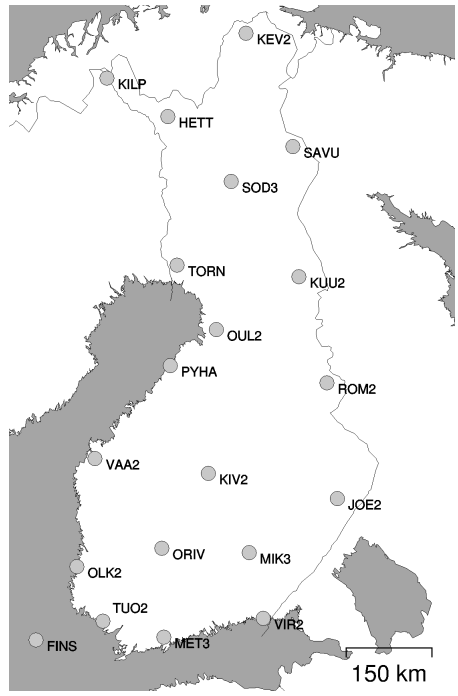

Figure 1. The FinnRef permanent GNSS network

FinnRef also supports state-space representation (SSR) error models for PPP. Although SSR is still under development as an RTCM standard, it is available because we are running a tailored version of GNSMART offered for the P3-Service project by Geo++ GmbH.

TEST RESULTS

In this section, we present field test results for single-frequency RTK using FinnRef as the base station. First, a single physical FinnRef station is used as the base; then, another experiment is carried out with the base station information retrieved in the form of network RTK. Finally, we analyze the raw GNSS measurements, i.e., pseudorange and carrier phase, obtained from the positioning module of a real commercial smartphone to assess the feasibility of RTK on a cell phone.

Test Equipment

The positioning performance was evaluated with a post-processing test setup where a consumer-grade U-Blox EVK-6T GNSS receiver and a geodetic-grade dual-frequency No-

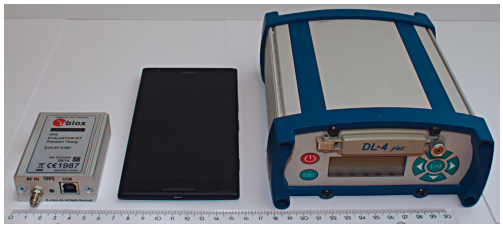

Figure 2. GNSS receivers used in the tests: U-Blox EVK-6T (left), Nokia Lumia 1520 smartphone (middle), and NovAtel DL-4 plus (right)

vAtel DL-4 plus GPS receiver were connected to the same antenna through a signal splitter; the purpose of the NovAtel receiver was to provide a reference position solution. FinnRef data were logged on site over NTRIP using a cellular network connection. Note that the accuracy of the reference position obtained this way depends on the quality of the RTK network data, but its error can be assumed to be negligible in comparison with the low-cost single-frequency solution.

The smartphone measurements were made by a Nokia Lumia 1520 running a custom firmware, courtesy of Microsoft Mobile, that allows access to the raw GNSS measurements from the phone's internal GNSS receiver (Qualcomm integrated receiver). The three receivers used in the tests are shown in Fig. 2. Satellites below 10° elevation were ignored in the RTK computations in each test, and ambiguity validation was based on the residual ratio test with threshold value 3. Furthermore, only GPS signals were considered because the U-Blox receiver has no GLONASS support.

Single-Base RTK Test

In the single-base test, the antenna was mounted on the roof of a vehicle driving back and forth on a short road, see Fig. 3a. The test site was located 2.7 kilometers from a physical FinnRef station which was used as the RTK base station. The resulting position errors are shown in Fig. 3b. The curves are partly discontinuous because of two reasons. First, the RTCM stream reception seemed to suffer from occasional outages and, therefore, the base station observations were missing for certain epochs (see Fig. 3c. Second, there were a handful of epochs where the reference dual-frequency solution was float-level only; these epochs were ignored in the analysis.

In 92.6 % of the epochs where an ambiguity-fixed reference solution was available, the horizontal positioning accuracy was better than 0.5 meters, and it seems evident

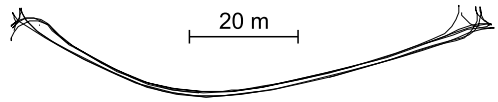

(a) Reference trajectory from dual-frequency receiver

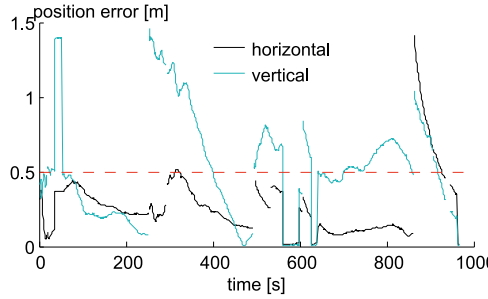

(b) Resulting position estimation errors using the U-Blox receiver

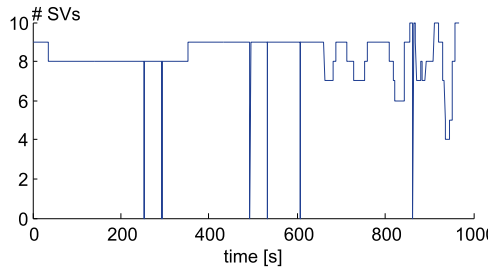

(c) Number of satellites used in the U-Blox RTK solution

Figure 3. Dynamic single-base RTK field test results

that significant a part of the estimates with error exceeding the goal were caused by error accumulation during a data gap. Moreover, in 7.3 % of all epochs, the ambiguities were accepted by the residual ratio test. The same figure also shows the absolute vertical position errors even though they are not of primary interest in the P3-Service project; it can be seen that the vertical has a larger variance but stays below one meter for most of the time.

Network RTK Test

The network RTK performance was tested in a static scenario with the closest physical base station being located approximately 63 kilometers from the rover receiver. The network corrections were delivered in the PRS representation, and data were logged for 20 minutes at a rate of 1 Hz.

The resulting horizontal position errors, as referred to the

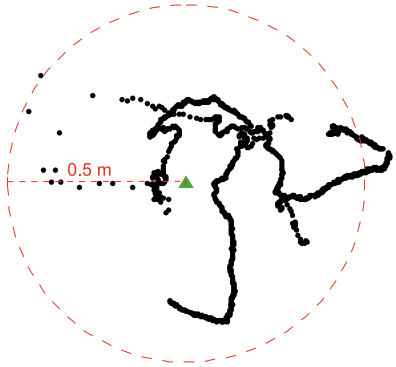

(a) Horizontal position estimation results; the green triangle marks the reference position solution

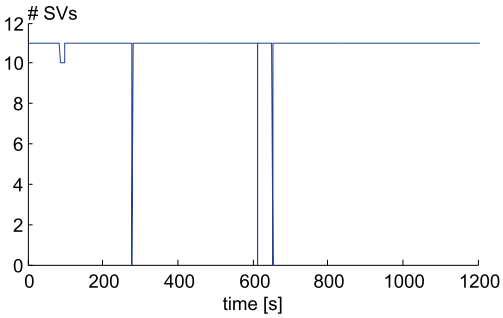

(b) Number of satellites used in the RTK solution

Figure 4. Static network RTK field test results using the U-Blox receiver

average of the dual-frequency solution, are shown in Fig. 4. The dashed red circle with radius 0.5 meters centered at the reference location (green triangle) contains 90.4 % of the position estimates. Ambiguity fixing did not succeed in this test, which is not surprising given the long distance to the nearest physical base stations: When using non-physical reference stations, the users are expected to perform (residual) ionospheric error estimation—the network cannot be assumed to construct perfect atmospheric models. For instance, the PRS concept utilized by FinnRef attempts to enforce receiver-level residual error estimation by creating the non-physical reference station nominally 5 kilometers away from the receiver [12]. However, it is well known that only multi-frequency receivers can observe the ionospheric errors directly; therefore, single-frequency users should not expect to obtain the same performance with non-physical reference station as when using a physical base station even if the virtual baseline is short.

Smartphone Test

As smartphones in general do not have connectors for external GNSS antennas, a rigorous zero-baseline test cannot be conducted to measure the noise levels. Thus, to assess the measurement quality of the phone's internal GNSS receiver, the test setup was as follows. Again, a physical FinnRef station was used as the base station for double differencing (baseline approx. 930 m), and a Lumia phone and a U-Blox receiver's patch antenna were stationary next to each other (distance approximately 30 cm) for 20 minutes. The exact baseline between the antenna base centers was not known.

The measurement noise levels were estimated as follows. First, double-differenced measurements were computed for both the smartphone and the U-Blox receiver with respect to the FinnRef station; the base station's measurement noise can be expected to be negligible in comparison with the low-cost receivers. Then in order to cancel biases such as integer ambiguities, triple differences were computed by differencing consecutive double differences over time. Finally, a linear polynomial was fitted to each measurement channel and subtracted from the triple differences in order to obtain zero-mean residuals. Note that the noise variance of the differenced measurements is larger than that of the original measurements; this amplification was not compensated for, and thus, the residuals do not directly represent the measurement noise.

The distributions of the resulting triple difference residuals for all channels are shown in Fig. 5. Note that the histograms are truncated, i.e., the minimum and maximum bins have no lower and upper bound, respectively. It can be seen that for both observables, the smartphone measurements are much less precise. In particular, the smartphone pseudorange noise is in the order of tens of meters, but the pseudorange residuals cannot be regarded as directly comparable because it is likely that the receivers are applying different types of filtering on the pseudoranges. Notwithstanding, the smartphone's histograms are heavy-tailed as opposed to the U-Blox: both the smartphone's pseudorange and carrier phase distributions have distinctive minimum and maximum bins, indicating a substantial amount of outliers (or cycle slips in the case of carrier phase) in the data.

Fig. 6a demonstrates how the quality of the measurements reflected in Fig. 5—note that the noise level analysis excludes many factors such as the antenna phase center variations—translates to the position domain. The measurement noise variances of the EKF were set to reflect the precison of each receiver, but otherwise, the processing parameters were identical. It can be seen that the variations in the smartphone's float estimates are much larger than the

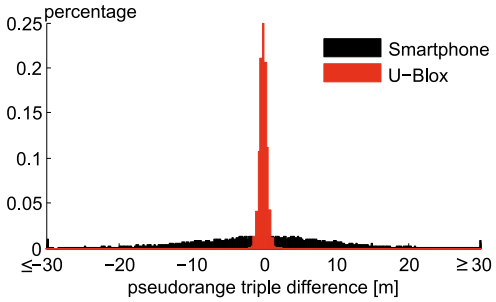

(a) Pseudorange

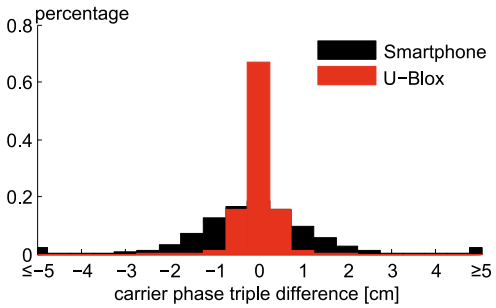

(b) Carrier phase

Figure 5. Noise level comparison of U-Blox and the smartphone. Constant biases and linear slopes were eliminated from the triple differences before computing the histograms, and the bin counts were normalized by the total sample count

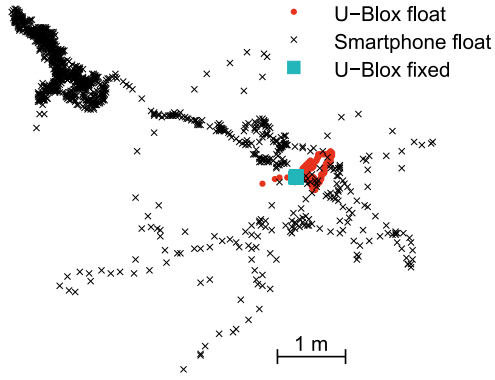

(a) Horizontal position estimation results

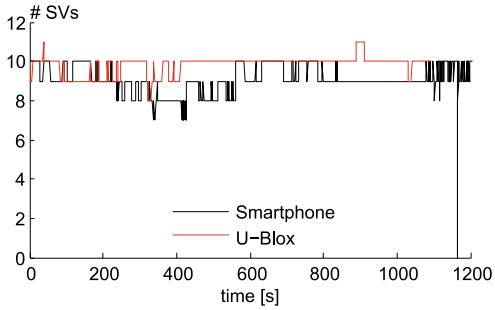

(b) Number of satellites used in the RTK solution

Figure 6. Comparison of RTK results with smartphone and U-Blox

distance between the smartphone and the U-Blox' antenna. In contrast, the U-Blox solution is less scattered and good enough for ambiguity fixing; also note that it made use of more satellites as shown in Fig. 6b.

CONCLUSIONS AND FUTURE WORK

This paper presented results from the P3-Service project where the goal is to achieve a 0.5 m horizontal position accuracy in Finland using a low-cost GNSS receiver and the national GNSS network FinnRef. It was seen that the goal could be met for 90 % of the time using a U-Blox GNSS receiver both in a short-baseline kinematic test and in a static network RTK test 63 km away from the nearest physical base station. It is noteworthy that integer ambiguity fixing was not necessary to achieve this performance; however, successful ambiguity resolution is expected to improve the accuracy by an order of magnitude. Furthermore, the accuracy was achieved despite the sparsity of FinnRef.

Moreover, we compared the raw GNSS pseudorange and carrier phase measurements of the internal GNSS receiver of a commercial smartphone (Nokia Lumia 1520) with those of the U-Blox receiver. It was seen that the smartphone measurements are noisy and suffer from a significant amount of outliers in comparison with the U-Blox. The difference in measurement quality becomes evident by computing the RTK solutions: the U-Blox was precise enough to allow ambiguity fixing while the smartphone-based float RTK solution suffered from meter-level errors.

The results presented in this paper were based on GPS only. An obvious way to improving the performance would be to increase the amount of satellites used by incorporating GLONASS, BeiDou, and Galileo measurements into the RTK processing. In particular, a large amount of observations would help to exclude the frequent outliers and cycle slips in the smartphone data, which might be a door opener for high-precision mobile positioning; it has been shown that the quality of a smartphone's GNSS antenna alone does not prevent ambiguity fixing [6]. A horizontal accuracy of

0.5 meters for small and low-cost devices would be useful in several applications, e.g., inventory management and various ITS use cases such as detecting the lane or parking slot occupied by the vehicle.

An important objective for P3-Service is to use the RTK solution to initialize a PPP filter. The concept has earlier been shown to be feasible [13]; however, in P3-Service, the purpose is to use SSR ionosphere corrections from the network instead of combining the pseudorange and carrier phase measurement to cancel the ionospheric error. SSR correction data [7] for PPP need not be updated as frequently as base station measurements for RTK, therefore, using PPP instead of RTK would decrease the necessary communications bandwidth and, on the other hand, make the system more robust against temporary network connection outages.

ACKNOWLEDGMENTS

This research has been conducted within the project P3-Service (Public Precise Positioning) funded by Destia Oy, Fastroi Oy, Hohto Labs Oy, Indagon Oy, TeliaSonera Finland Oyj, Microsoft Mobile, Space Systems Finland Oy, Semel Oy, VR Track Oy, the Finnish Technology Agency TEKES, and the Finnish Geospatial Research Institute.

REFERENCES

[1] J. Geng, F. N. Teferle, X. Meng, and A. H. Dodson, "Towards PPP-RTK: Ambiguity resolution in real-time precise point positioning," *Advances in Space Research*, vol. 47, no. 10, pp. 1664–1673, May 2011.

[2] M. Kirkko-Jaakkola, J. Saarimäki, S. Söderholm, R. Guinness, L. Ruotsalainen, H. Kuusniemi, H. Koivula, T. Mattila, and S. Nyberg, "P3: A public precise positioning service based on a national GNSS network," in *Proc. International Conference on Localization and GNSS (ICL-GNSS)*, Helsinki, Finland, June 2014.

[3] H. Koivula, J. Kuokkanen, S. Marila, T. Tenhunen, P. Häkli, U. Kallio, S. Nyberg, and M. Poutanen, "Finnish permanent GNSS network: From dual-frequency GPS to multi-satellite GNSS," in *Proc. 2nd International Conference and Exhibition on Ubiquitous Positioning, Indoor Navigation and Location-Based Service*, Helsinki, Finland, Oct. 2012.

[4] C. Guo, W. Guo, G. Cao, and H. Dong, "A lane-level LBS system for vehicle network with high-precision BDS/GPS positioning," *Computational Intelligence and Neuroscience*, 2015.

[5] T. Lovas, A. Wieczynski, M. Baczynska, A. Perski, I. Kertesz, A. Berenyi, A. Barsi, and A. Beeharee, "Positioning for next generation intelligent transport systems services in SafeTRIP," in *Proc. ASPRS Annual Conference*, Milwaukee, WI, May 2011.

[6] K. M. Pesyna, Jr., R. W. Heath, Jr., and T. E. Humphreys, "Centimeter positioning with a smartphone-quality GNSS antenna," in *Proc. 27th International Technical Meeting of The Satellite Division of the Institute of Navigation (ION GNSS+ 2014)*, Tampa, FL, Sept. 2014, pp. 1568–1577.

[7] *Differential GNSS (Global Navigation Satellite Systems) Services – Version 3*, RTCM Std. 10 403.2, Nov. 2013, with Amendments 1 and 2.

[8] P. de Jonge and C. Tiberius, "The LAMBDA method for integer ambiguity estimation: implementation aspects," Delft Geodetic Computing Centre, Delft, The Netherlands, LGR-Series 12, Aug. 1996.

[9] S. Verhagen and P. J. G. Teunissen, "The ratio test for future GNSS ambiguity resolution," *GPS Solutions*, vol. 17, no. 4, pp. 535–548, Oct. 2013.

[10] S. Verhagen, P. J. G. Teunissen, and D. Odijk, "The future of single-frequency integer ambiguity resolution," in *VII Hotine-Marussi Symposium on Mathematical Geodesy*, ser. International Association of Geodesy Symposia, N. Sneeuw, P. Novák, M. Crespi, and F. Sansò, Eds. Berlin/Heidelberg, Germany: Springer, 2012, vol. 137, pp. 33–38.

[11] U. Vollath, H. Landau, X. Chen, K. Doucet, and C. Pagels, "Network RTK versus single base RTK – understanding the error characteristics," in *Proc. 15th International Technical Meeting of the Satellite Division of The Institute of Navigation (ION GPS 2002)*, Portland, OR, Sept. 2002, pp. 2774–2781.

[12] G. Wübbena, M. Schmitz, and A. Bagge, "PPP-RTK: Precise point positioning using state-space representation in RTK networks," in *Proc. 18th International Technical Meeting of the Satellite Division of The Institute of Navigation (ION GNSS 2005)*, Long Beach, CA, Sept. 2005, pp. 2584–2594.

[13] S. Carcanague, O. Julien, W. Vigneau, and C. Macabiau, "Undifferenced ambiguity resolution applied to RTK," in *Proc. 24th International Technical Meeting of The Satellite Division of the Institute of Navigation (ION GNSS 2011)*, Portland, OR, Sept. 2011, pp. 663–678.

PUBLICATION VII

Performance assessment of single frequency Precise Point Positioning using the SSR model from the Finnish National GNSS Network

S. Söderholm, H. Koivula, H. Kuusniemi, S. Lahtinen and M. Kirkko-Jaakkola

European Journal of Navigation 14.(2016), 39–40

Performance assessment of single frequency Precise Point Positioning using the SSR model from the Finnish National GNSS Network

Stefan Söderholm [1]*, Hannu Koivula[2], Heidi Kuusniemi[1], Sonja Lahtinen[2], Martti Kirkko-Jaakkola[1]

[1]Department of Navigation and Positioning, Finnish Geospatial Research Institute,

National Land Survey, Geodeetinrinne 2, FIN-02430 Kirkkonummi, Finland

[2]Department of Geodesy and Geodynamic, Finnish Geospatial Research Institute,

National Land Survey, Geodeetinrinne 2, FIN-02430 Kirkkonummi, Finland

* Author to whom correspondence should be addressed; E-Mail: stefan.soderholm@nls.fi; Tel.: +358-40-5443757; Fax: +358-9-29555-211.

Abstract

The Finnish National GNSS Network, *FinnRef*, was established and is operated by the Finnish Geospatial Research Institute (FGI). The data provided by *FinnRef* include a State Space Representation (SSR) model of GNSS (Global Navigation Satellite System) observation errors that can be used in Precise Point Positioning (PPP) solutions. In this work the main objective has been to assess the performance of this SSR model for single frequency PPP. For the purpose of this, software has been developed with supports for such a model and a PPP solution. Data has been logged and analyzed from all *FinnRef* stations. Results show that the SSR model available from FinnRef can reduce the positioning error in GNSS receivers to less than 10 cm in optimal conditions. This would indicate that Precise Point Positioning with a State Space Representation model of the GNSS errors is a promising method in applications such as Intelligent Transport Systems, precision farming, machine control, etc.

Introduction

PPP is a common name for many technology flavors in GNSS positioning where the basic idea is to improve the accuracy by eliminating known errors neglected in the standard positioning method. The GNSS observation errors can be obtained from many different sources - there are both real

time and post processing applications that use PPP. In addition, PPP can be done using both single and dual frequency receivers. The number of GNSS errors corrected for depends on the accuracy requirements and may differ between applications. The type of errors and the typical size of these errors are listed in Table 1

Table 1. Typical GNSS error budget

Error Source	Typical size (m)
Ionosphere	5
Satellite Orbit	2.5
Satellite Clock	1.5
Signal offsets	1
Troposphere	0.5
Site displacement	0.3

The error values are assuming we use all the available broadcast information from the satellites themselves and a standard tropospheric model in the receiver. Local errors from receiver noise and multipath effects are not considered here, but they are typically in the order of 1 meter in total under good signal conditions.

The by far most dominant error in GNSS observations is the ionospheric delay. In a standalone receiver the ionospheric error is corrected using broadcasted models like the Klobuchar model (Klobuchar, 1987) or the NeQuick (Di Giovanni and Radicella, 1990). The performance of these two models was compared by (Somieski 2007). Broadcast models typically correct for only 50-60 % of the error and other better internal ionospheric models have been presented by (Ruan 2013; Choy2011). SBAS (Satellite Based Augmentation System) can provide more precise ionospheric models with a precision allowing for decimeter-level position (Wanninger, et al., 2012; Carcanague 2011). For post processing applications, ionospheric TEC (total electron content) maps can be obtained from sources like the IGS (international GNSS service) for example (Ruan 2013; Beran, 2008; Muellerschoen, et al., 2004). The JPL (Jet Propulsion Laboratory) also provides similar kind of data (Muellerschoen 2004; Gao 2006) and the Center for Orbital Determination in Europe (CODE) provides a GIM (Global Ionopsheric Model) (Le 2004; Le 2006; Ovstedal 2002; Bree 2012). If no models are available it is possible to estimate the delay as a part of the actual solution (Ruan 2013; Carcanague 2011; Lu 2011) or we can construct ionospheric free observations. For a single frequency receiver the GRAPHIC observable (Group and Phase Ionosphere Calibration (Yunck, 1996; Beran, 2008; Laurichesse, et al., 2009; Ruan 2013; Carcanague 2011; Cai 2013) takes advantage of the fact that the group delay in range observable and the carrier phase advance have the same magnitude but are opposite in sign and this can be used to remove the first order

ionospheric delay. A comparison between different external and internal ionospheric models have been provided in several papers (Ovstedal 2002; Somieski 2007; Chen 2005).

The IGS and other similar sources also provide precise satellite clock and orbit information reducing these errors significantly. A complete guide to the different products offered by IGS is given by (Kouba 2009; Marel 2012). The JPL has similar products available and a comparison between the two is given by (Chen 2004). In the work by (Bree 2012) accurate satellite clock and orbit estimates were taken from the Real Time Clock Estimation (RETICLE) service developed by the German Space Operations Center.

The troposphere is usually modelled in the receiver since it is a relatively slowly changing component and can be modelled relatively accurate. A good overview of the impact and models of the troposphere is given in the thesis (Kleijer 2004).

In a State Space Representation (SSR) all of the above mentioned errors are included (Wabbena 2005) and in this work we have adapted an SSR-PPP post processing approach where we have not taken into account site displacement errors. The SSR model is obtained from the Finnish Permanent GNSS network FinnRef.

In this paper we will first present the tools used in this work, then present test results and end with conclusions. The tools section describes the FinnRef network and the Matlab software that was used for this work.

Tools and methods

FinnRef network

The Finnish National GNSS Network (Koivula et al, 2012) – *FinnRef* – was established and is operated by FGI (Finnish Geospatial Research Institute). Each station has been installed with a high-end (geodetic class) GNSS receiver that is capable of tracking multiple GNSS constellations (GPS, GLONASS, Galileo and BeiDou). Additionally, a wireless or fixed broadband Internet connection has also been installed at each station for real-time data transmission. The network tracks the GNSS satellites continuously and the GNSS data of the network is made available in real-time. There are a total of 20 stations with an average inter-station distance of 200 km, shown in Figure 1.

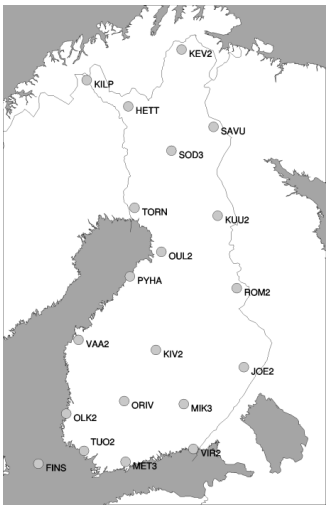

Figure 1. The National GNSS infrastructure – *the FinnRef Network*

The FinnRef data processing component connects to the FinnRef data streams and calculates an SSM (State Space Model) from the observation. The SSM is represented by a SSR (State Space Representation) of the error components in the observations and transmitted to the users using GNSMART software by Geo++. The SSR are made available over a standard NTrip (Networked Transport of RTCM via Internet Protocol) interface utilizing the RTCM 3.x protocol. The RTCM messages offered by this interface are listed in Table 2

Table 2. Supported RCM 3.x messages

RTCM Message Id	Content
1004	Extended L1&L2 GPS RTK Observables
1005	Stationary RTK Reference Station ARP
1012	Extended L1&L2 GLONASS RTK Observables
1019	GPS Ephemerides
1057	SSR GPS Orbit Correction Message
1058	SSR GPS Clock Correction Message
1059	SSR GPS Satellite Code Bias Message
1062	SSR GPS High Rate Clock Correction
1264	SSR Ionosphere VTEC Spherical Harmonics Message
1265	SSR GPS Satellite Phase Bias Message
Proprietary 4090	SSR Ionosphere STEC Polynomial Message

The 1004 and 1012 messages are observation data from the station, the 1019 contains the GPS ephemeris information and the 1057-4090 messages are SSR messages.

The GSRx receiver

A software-defined GNSS receiver platform, named as FGI-GSRx, has been developed by FGI in several previous projects for the analysis and validation of novel algorithms for optimized GNSS navigation performance. The receiver is implemented in Matlab and thus provides a unique and easy-to-use platform for the various research projects at FGI. The receiver is designed for post-processing operation and does not yet support real time operation. In this work we have developed new features and integrated them into the FGI-GSRx. The main new features that have been developed are support for several new GNSS observation formats, support for the SSR model, Kalman filter for the PPP solution and new tropospheric models. The support for all the RTCM SSR messages and the algorithms needed to calculate the OSR (observation space corrections) from the SSR model parameters have been integrated into the FGI-GSRx. The data flow for the SSR data is shown in Figure 3.

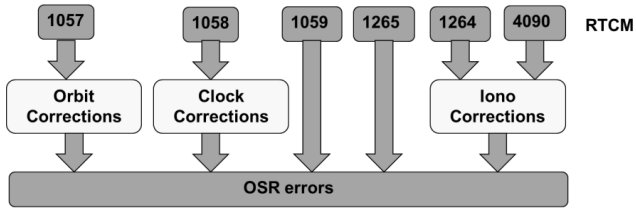

Figure 3. Data flow for SSR data.

The new observation data formats that have been added are listed in Table 3

Table 3. New observation data formats supported in the GSRx

RTCM 1004 messages
Mobile Phone observations (Lumia Phone)
uBlox binary protocol
uBlox FGI specified data format
Rinex observation files

The RINEX observation format enables us to use geodetic grade receivers as references (produces RINEX files). The support for the RTCM 1004 message containing the observations for a Finnref station (real or virtual) enables us also to test using those. All the above mentioned formats are handled in the receiver so that they are converted into the FGI-GSRx default format using unique conversion functions. After this conversion the observations can be corrected by the OSR corrections before passed on to the Multi-GNSS Navigation block. The complete data flow is shown in Figure 4.

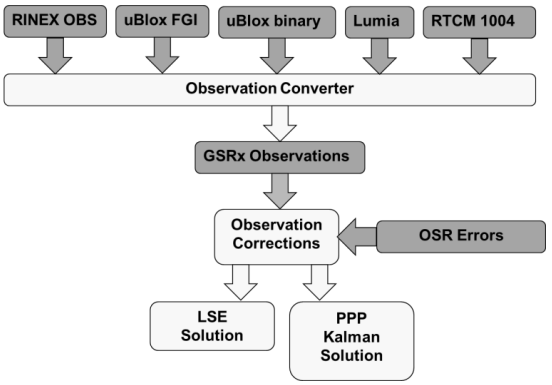

Figure 4. Data flow for observation data

The tropospheric corrections are not currently available from the Finnref. Therefore some new tropospheric models have been added to the GSRx and a tropospheric state is also added to the PPP Kalman filter. The actual PPP solution is calculated both with an LSE (Least Squares Estimation) and a Kalman filter using the corrected code and carrier phase observations.

Results and discussion

To verify that the SSR model is working and that the performance is as good as expected we made a 24-hour zero baseline tests using the data directly from the FinnRef stations. The stations are equipped with geodetic grade Javad Delta-G3T GNSS receivers and calibrated Javad Choke Ring antennas so measurement quality is very good. An nTrip connection was opened from each of the 20 stations in Finland and the RTCM messages 1004, 1005 and 1019 were received and stored. The observations from the 1004 message were passed on to our navigation filter and the reference station position from message 1005 was used as the true position. The GPS ephemeris data was obtained from the 1019 message. For the SSR model we open an additional nTrip connection to a stream containing the RTCM messages 1057, 1058, 1059, 1264, 1265 and 4090. Data was logged for 20 min periods each 30 minutes during a total time of 24 hours. A single-frequency positioning solution was calculated for each epoch applying the SSR model from FinnRef. The result from one 20 min period is shown in Figure 5.

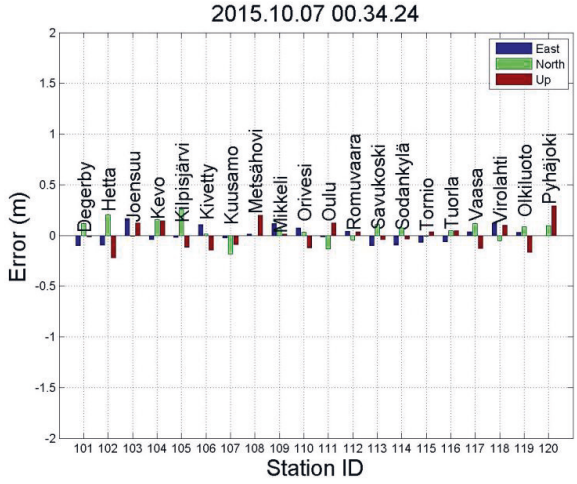

Figure 5. Bar plot of errors at all FinnRef Stations

Average errors for all FinnRef stations over a period of 24 hours is shown in Table 3.

Table 3. Average errors for all FinnRef stations.

Station	East(m)	North(m)	Up(m)
Degerby	0.015	-0.025	0.137
Hetta	-0.108	0.058	-0.286
Joensuu	-0.002	0.031	-0.226
Kevo	-0.056	0.062	-0.120
Kilpisjärvi	-0.103	0.018	-0.548
Kivetty	0.021	-0.008	-0.196
Kuusamo	-0.102	0.021	-0.449
Metsähovi	0.012	0.031	0.021
Mikkeli	0.020	-0.012	-0.205
Olkiluoto	0.013	-0.041	0.116
Orivesi	0.000	-0.018	-0.066
Oulu	-0.047	0.028	-0.012
Pyhäjoki	-0.032	-0.004	0.106
Romuvaara	-0.032	0.054	-0.374
Savukoski	-0.082	0.137	-0.195
Sodankylä	-0.113	0.135	-0.011
Tornio	-0.064	0.091	0.202
Tuorla	0.020	-0.012	0.084
Vaasa	-0.016	-0.017	0.041
Virolahti	-0.024	0.008	-0.090

The maximum error in the East direction is 11.3 cm (Sodankylä) and in the North direction 13.7 cm (Savukoski). In the Up direction the error is slightly larger as was expected and the maximum error is 54.8 cm (Kilpisjärvi). The remaining error especially in the Up direction is likely due to site displacement and a non-optimal tropospheric model.

Conclusions

A single-frequency precise point positioning solution using the SSR model from the Finnish National GNSS Network was presented in this paper. The Finnref network and the SSR model available from this network were described in detail together with the software architecture developed for this work. Finally, experimental results were presented where it was distinctively shown that the SSR model effectively eliminates the GNSS errors. The obtained accuracy was better than 15 cm in the horizontal direction and no more than 55 cm in the vertical direction. Further work includes testing with receivers within the network and implementing models for site displacement errors.

Acknowledgement

The work presented in this paper has been conducted as a part of the P3-Service project (www.p3-service.net, Development of a Mobile Public Precise Positioning Service Based on the National GNSS Network) The project was co-funded by Tekes, FGI, Microsoft Mobile, TeliaSonera, VR Track, Destia, Indagon, Space Systems Finland, Semel, Fastroi, Hohto Labs. Its duration was 27 months starting from August 2013 to the end of November 2015.

References

Cai, C., Liu, Z., Luo, X. (2013), Single-frequency Ionosphere-free Precise Point Positioning Using Combined GPS and GLONASS Observations, Journal of Navigation 66(3) 2013, pp. 417-434

Carcanague S. (2013), Low-cost GPS/GLONASS Precise Positioning Algorithm in Constrained Environment, phD thesis, Institut National Polytechnique de Toulouse (INP Toulouse), 2013

Klobuchar, J., 1987. Ionospheric Time-Delay Algorithms for Single-Frequency GPS Users. IEEE Transactions on Aerospace and Electronic Systems (3), pp. 325-331.
Di Giovanni, G. and Radicella, S. M., 1990. An analytical model of the electron density pro_le in the ionosphere. Advances in Space Research. 10(11), pp. 27-30.

Somieski, A., Favey, E., Buergi, C. (2007., Evaluation and Comparison of Different Methods of Ionospheric Delay Mitigation for Further Galileo Mass Market receivers, Proceedings of ION GNSS 2007, Forth Worth, TX, 2007.

Ruan, R., Wu, X., Feng, L. (2013), Comparison of observation models and ionospheric elimination approaches for single frequency precise point positioning, Geomatics and Information Science of Wuhan University 38(9) 2013, pp. 1023-1028

Choy, S. (2011), High accuracy precise point positioning using a single frequency GPS receiver, Journal of Applied Geodesy 5(2) 2011, pp. 59-69

Wanninger, L., & Hesselbarth, A. (2012). SBAS Based Single and Dual Frequency Precise Point Positioning. Proceedings of ION GNSS 2012, September 17-21, 2012, Nashville Convention Center, Nashville, Tennessee.

Carcanague, S., Julien, O., Vigneau, W., Macabiau, C. (2011), Undifferenced ambiguity resolution applied to RTK. ION GNSS 2011, 24th International Technical Meeting of The Satellite Division of the Institute of Navigation, Sep 2011, Portland, United States. Pp 663-668

Ruan, R., Wu, X., Feng, L. (2013), Comparison of observation models and ionospheric elimination approaches for single frequency precise point positioning, Geomatics and Information Science of Wuhan University 38(9) 2013, pp. 1023-1028

Beran, T. (2008). Single-Frequency, Single-Receiver Terrestrial and Spaceborne Point Positioning. Ph.D. dissertation, Department of Geodesy and Geomatics Engineering, Technical Report

Muellerschoen, R. J., Iijima, B., Meyer, R., Bar-Seve, Y., & Accad, E. (2004). Real-Time Point- Positioning Performance Evaluation of Single-Frequency Receivers Using NASA's Global Differential GPS System. ION GNSS 17th International Technical Meeting of the Satellite Division.

Gao, Y., Zhang, Y., Chen, K. (2006), Development of a Real-Time Single-Frequency Precise Point Positioning System and Test Results Proceedings of the 19th ION GNSS International Technical Meeting of the Satellited Division, September 26-29, Forth Worth, TX, 2006, 2297-2303

Le A.Q. (2004), Achieving decimetre accuracy with single frequency standalone gps positioning. In: Proceedings of the ION GNSS 17th International Technical Meeting of the Satellite Division, 21–24 Sept. 2004, Long Beach, pp 1881– 1892

Le A.Q., Teunissen P.J.G. (2006), Optimal Recursive least-squares filtering of GPS pseudorange measurements. VI Hotine-Marussi Symposium on Theoretical and Computational Geodesy, IAG Symposium, Wuhan, China, 29 May - 2 June, 2006, pp. 166-172

Ovstedal, O. (2002), Absolute Positioning with Single-Frequency GPS Receivers
GPS Solutions, **2002***, 5: No. 4*, 33-44

Bree, R.J.P. van, Tiberius, C.C.J.M. (2012), Real Time Single Frequency Precise Point Positioning – accuracy assessment. GPS Solutions. DOI 10.1007/s10291-011- 0228-6.

Lu, C., Tan, Y., Zhou, L. (2011), Adaptive Kalman filter based navigation algorithm for single-frequency precise point positioning, Beijing Daxue Xuebao (Ziran Kexue Ban)/Acta Scientiarum Naturalium Universitatis Pekinensis Volume 47, Issue 4, July 2011, Pages 587-592

Yunck, T.P. (1996), Orbit Determination. In Parkinson & Spilker, Jr. (Eds.), Global positioning systems: Theory and applications. Progress in Astronautics and Aeronautics, Volume 163, American Institute of Aeronautics and Astronautics, Inc.

Laurichesse, D., Mercier, F., Berthias, J., Broca, P., & Cerri, L. (2009). Integer Ambiguity Resolution on Undifferenced GPS Phase Measurements and its Application to PPP and Satellite Precise Orbit Determination. Navigation, Journal of the institute of Navigation, Vol. 56, N° 2, Summer 2009.

Chen, K., Gao, Y. (2005), Real-Time Precise Point Positioning Using Single Frequency Data", Proceedings of ION GNSS 2005, Long Beach, California, September 13-16, 2005.

Kouba, J., (2009), A Guide to using international GPS service (IGS) products. Online publication at IGS website http://igscb.jpl.nasa.gov/components/usage.html

Marel, van der H., de Bakker, P.F. (2012), Single versus Dual-Frequency Precise Point Positioning Inside GNSS, 2012, July/August, 30-35

Chen, K. (2004). Real-Time Precise Point Positioning and Its Potential Applications. Proceedings of ION GNSS 2004, Long Beach, California, September 21-24, 2004.

Kleijer, F. (2004), Troposphere delay modeling and filtering for precise GPS leveling. Ph.D thesis. Mathematical Geodesy and Positioning, Delft University of Technology

Wabbena, Gerhard, Schmitz, Martin, Bagge, Andreas, "PPP-RTK: Precise Point Positioning Using State-Space Representation in RTK Networks," Proceedings of the 18th International Technical Meeting of the Satellite Division of The Institute of Navigation (ION GNSS 2005), Long Beach, CA, September 2005, pp. 2584-2594.

Koivula, H., J. Kuokkanen, S. Marila, T. Tenhunen, P. Häkli, U. Kallio, S. Nyberg, and M. Poutanen (2012), Finnish Permanent GNSS Network, From dual-frequency GPS to multi-satellite GNSS, in Proceedings of the 2nd International Conference on Ubiquitous Positioning, Indoor Navigation, and Location Based Services, UPINLBS 2012, Helsinki, Finland, 3-4 October 2012, IEEE Xplore, 5 p.